NASA Technical Memorandum 104628

Tectonics and Volcanism of East Africa as Seen Using Remote Sensing Imagery

Duncan John Hutt

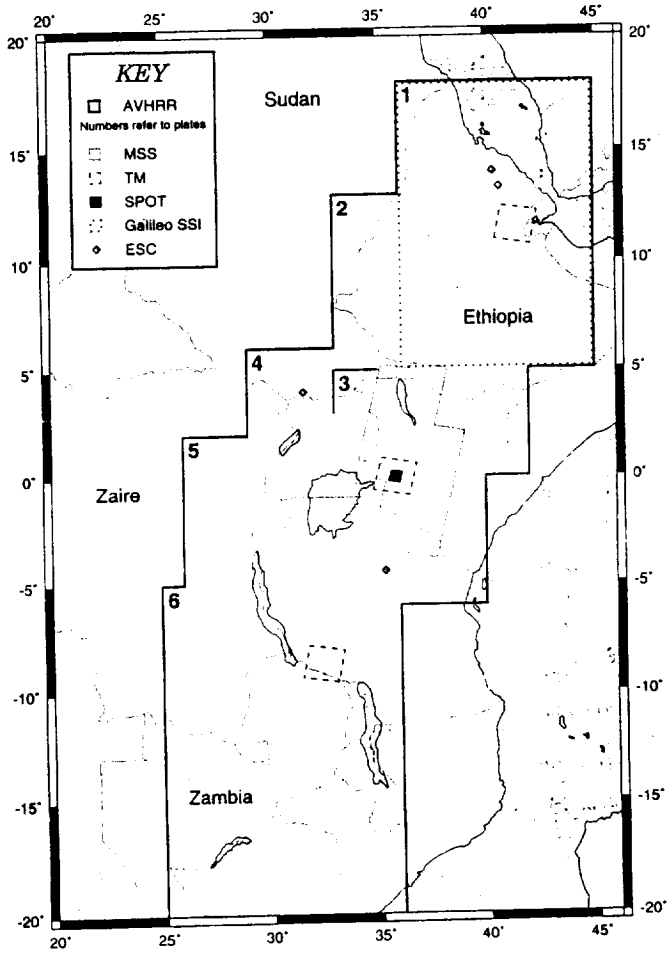

FEBRUARY 1996

foreword

This report is issued by the Laboratory of Terrestrial Physics, NASA Goddard Space Flight Center, Greenbelt, MD 20771. It represents a significant effort of this Laboratory, over the last few years, in the study of the East African Rift -- the most geologically active area of the Earth -- using various types of remote sensing imagery, and should serve as a guide for many other remote sensing studies of this area. Dr. Hutt spent two months during each of three years in residence at Goddard working with the Goddard group. Appreciation is extended to Marathon Oil which provided support for this work through a grant to J. Heirtzler.

This work represents a large part of Dr. Hutt's thesis submitted for the degree of Doctor of Philosophy at The University of Newcastle upon Tyne. Communications should be addressed to Duncan J. Hutt (e-mail: n08hk%rift@newcastle.ac.uk) or to J. R. Heirtzler (e-mail: jamesh@ltpmail.gsfc.nasa.gov) at Goddard Space Flight Center, Code 920.

NASA Technical Memorandum 104628

Tectonics and Volcanism of East Africa as Seen Using Remote Sensing Imagery

Duncan John Hutt
The University of Newcastle
Newcastle, England

National Aeronautics and
Space Administration

Goddard Space Flight Center
Greenbelt, Maryland 20771

1996

ACKNOWLEDGEMENTS

I would like to thank Prof. J Mitchell for allowing me to study in the Department of Physics at Newcastle and Dr J. Heirtzler for making it possible to spend a number of months at NASA GSFC. I would also like to thank Dr Heirtzler for suggesting the project and jointly supervising it with Prof. R. Girdler.

Data for my project was provided by NASA GSFC, Laboratory for Terrestrial Physics; The DMAAC Browse facility (NASA GSFC), Dr D. Harding, Dr P. Geissler and Dr R. Nusbaum. Topography data was provided by the USGS.

Those deserving acknowledgement at NASA GSFC are too numerous to mention but the patient help and advice of Dr J. Frawley was invaluable as was the assistence in locating imagery and in using the computer system given by P. Masouoka. Advice on the use of day and night AVHRR imagery was provided by Dr H. Blodget and help with Landsat TM was given by Dr D. Harding. Thanks also to all those who made my stay the USA a pleasant experience.

I would like to thank all my friends and colleagues in Newcastle who have given valuable advice and much needed moral support throughout the project. I would also like to thank my parents for their support throughout the last four years.

Finally I would like to extend my special thanks to Marathon Oil who funded the project and Dr B. Bosworth who persuaded them to do so. Thanks also to the Universities Space Research Association who organised my visits to NASA.

CONTENTS

ABSTRACT

The East African Rift System was first recognised at the end of the 19th century. The rift system extends from the Dead Sea area in the north to Mozambique in the south. The continental section of the East African Rift System is made up of the eastern and western branches. The Afar region of Ethiopia and Eritrea is a triple junction of the Red Sea, Gulf of Aden and Ethiopia section of the eastern branch. The eastern branch extends south from Afar through Ethiopia and Kenya and dies out in northern Tanzania. The western branch is characterised by the finger like rift valley Lakes including; Mobutu, Tanganyika, Rukwa and Malawi. There are a number of suggested southwesterly rifts propagating from the western branch. These include the Upemba Lakes region, Lake Mweru and the Luangwa Valley.

Few studies of the East African Rift have looked at the entire continental section and no consistent map existed. The use of Advanced Very High Resolution Radiometer (AVHRR) satellite data, with a resolution of about 1.1 km, has made this possible. Lineaments of East Africa have been mapped using AVHRR scenes and local comparisons have been made with lineaments mapped from other imagery. These other imagery include; Landsat Multi-spectral Scanner (MSS) & Thematic Mapper (TM), Satellite Probatoire Pour l'Observation de la Terre (SPOT) and Electronic Still Camera (ESC) data. It has also been possible to consider these other types of remote sensing imagery for their potential in mapping local rift features. Additionally data-sets of earthquake epicentres and volcano locations cover the whole of East Africa and are used in association with the remote sensing data.

Sections of the rift system are considered in detail using AVHRR imagery, earthquake epicentres, volcano locations and other types of satellite data. These studies largely confirm previous understanding of the regions but also provide some additional information and confirmation of suggested features. The presence of a boundary graben on the western flank of Afar is highlighted and a similar structure on the southern flank appears likely. A dextral offset of the Ethiopia rift at about 8.5°N is seen. The existence of a 'leaky' transform type structure in northern Tanzania appears to be confirmed by the AVHRR, earthquake, volcano and other satellite data-sets. The presence of Southwestern rifts branching off the western branch are also clearly visible. Use of day and night AVHRR data has highlighted more lineaments on the ancient cratons than are seen from day scenes.

The greatest potential of using AVHRR is for considering large scale features, such as the East African Rift System, in their entirety. The AVHRR interpretations have largely been able to delineate the rift system well though also show trending associated with older rifts or mobile belts. The directional trends of lineaments over the whole of East Africa is approximately NE-SW indicating an average extension direction of NW-SW, assuming most faulting is normal.

CHAPTER 1

Introduction

1.1 Aims

This project uses relatively low resolution satellite imagery to study and map the East African Rift System. The aims are twofold; firstly, to discover whether low resolution imagery has a role to play in studies of geology and tectonics and secondly to produce an overview map of the East African Rift System based on a single and consistent technique for mapping. The imagery used for this purpose was Advanced Very High Resolution Radiometer (AVHRR) imagery from the National Oceanographic and Atmospheric Administration (NOAA) series of weather satellites. The nominal resolution is 1.1 km in its local area coverage (LAC) mode of data acquisition (cf. 70m resolution for Landsat Multi-spectral Scanner (MSS) and 30m for Landsat Thematic Mapper (TM) data).

Using relatively inexpensive imagery, in terms of cost of data and computing power, has further reaching consequences than making a task cheaper and 'easier'. If low resolution data can prove valuable and adequate for many uses, such as tectonics and vegetation studies, it can and should be developed. Current research is, for the most part, attempting to develop higher and higher resolution data as the philosophy follows the idea that the more you can see the better the image. However, if the resultant data are too expensive for most users and if the acquisition rate of imagery outstrips the capability to process and use the data then its value is severely reduced. AVHRR was designed for meteorological studies but its potential in other fields needs assessing. The determination of the value of such data is useful when considering the future development of Earth observation as well as in developing sensors for interplanetary exploration.

The rationale behind the use of AVHRR data was that it provides a regional rather than a local coverage for a given amount of data. More than 100 Landsat scenes would be required to cover the East African Rift System, each would need processing, data storage and interpretation. Three out of the seven Landsat TM bands require 120 Mb of disk space per scene and processing requires at least twice this. Thus, to cover the entire rift system would require an enormous amount of disk, or tape, storage space and much computer intensive processing. AVHRR data, on the other hand, can cover the entire rift system, and the surrounding areas, with the equivalent data of about three TM scenes. Disk space, computer processing requirements and interpretation are therefore reduced

markedly. Also of potential value in the use of AVHRR is the facility to study the rift system on a regional scale rather than in isolated, local, sections.

The use of AVHRR data alone would give rise to a number of uncertainties as to the nature of the mapped features. Therefore a certain amount of correlation with other imagery is necessary; this has been carried out for selected localities throughout the region. A mosaic of Landsat MSS scenes was available for the Kenya sector of the rift system which was able to provide a reasonably large areal coverage for correlation with AVHRR. Additionally a single Landsat TM scene was used to cover part of the MSS mosaic and a Satellite Probatoire Pour l'Observation de la Terre (SPOT) scene covered part of the TM image. In other areas single TM scenes have been used and elsewhere Electronic Still Camera (ESC) images have been compared with TM data. Thus, while different imagery was used to compare with, and control the AVHRR interpretation an inevitable result has been the assessment of the values of various types of higher resolution imagery.

At the other end of the scale it is also important to look at AVHRR data as compared to lower resolution imagery as this allows the AVHRR scenes to be assessed within the range of available imagery. For this purpose a Solid State Imaging (SSI) scene, acquired by the Galileo spacecraft, covering the Afar area has been used.

In addition to the satellite imagery there are a number of other data-sets available for East Africa. A systematic study of all geophysical data is beyond the scope of this study but the recognition of faults and lineaments is facilitated by the using topography and earthquake epicentres. Volcano locations can also provide some insight into the rift processes, these like lineaments can be recognised from the higher resolution satellite imagery and are, therefore, also considered.

1.2 A Brief History of Exploration in East Africa

"The African continent, fenced by an unbroken line of coast,... has ever been to the outer world a land of mystery and fables. The want of precise topographical notices has heaped hypothesis upon hypothesis; in fact no part of the inhabitable globe has given rise to theories and reports so marvellous, so contradictory, and so erroneous, as the central and equatorial regions, the heart of the great peninsula."

So wrote captain R.F. Burton (1859) after his expedition to the 'Lake regions of Central Equatorial Africa'. The theories, based largely upon guesswork and partly on word from Arab traders, included a vast desert extending throughout the interior of the continent; an immense mountain plateau; and a huge inland sea forming the sources of all the great African rivers.

Few European travellers had ventured further than the coastline until the middle of the nineteenth century. Portuguese tradesmen had punctuated the coast with bases for their voyages to the east but had rarely, if at all, explored beyond the relative safety of the coastal strip. A few incursions into western Africa had been made by Rodriguez Graca [1843 - 1847] but little progress was made in the east until 1847. In that year the Church Missionary Society of Great Britain set up a mission at Mombassa under Krapf and Rebmann. From their station they made short but significant steps into the country. In 1848 Rebmann discovered Kilimanjaro and further explored the regions around: in 1849 Krapf caught a glimpse of Mount Kenya.

The names of Livingstone, Stanley and Burton have always been synonymous with exploration in Africa and indeed it was these three, along with their respective teams, who made the first major documented excursions deep into the interior of the continent.

Travelling through Africa held many problems for the first explorers: disease, terrain and attacks by natives all made the going tough. One description of the roads given by Burton (1859) sums up the tortuousness of the land they were trying to cross:

"... near Ujiji the roads are truly vile, combining all the disadvantages of bog and swamp, river and rivulet, thorn-bush and jungle, towering grasses, steep inclines, riddled surface and broken ground."

Livingstone's first major journey into the heart of the continent started in 1849. This journey was embarked upon from the south and involved the crossing of the Kalahari. The aim of this expedition was to find a location to set up a mission but the Kalahari and Lake Ngami were not promising. Hence, Livingstone continued north and in 1851 came upon 'a glorious river' - the Zambesi. After an excursion to the Atlantic coast and back Livingstone followed the Zambesi to the sea at Quilimane: he now saw the Zambesi as an ideal route into the interior. He managed to persuade the British government to spend £5000 on an expedition to explore the Zambesi Valley, a project that was to last from 1858-1863. Most of Livingstone's accounts give topological details of the land he crossed and the majority of the scientific input he made, along with most of his

contemporaries, is concerned with the natural history and anthropology of the area. Only rarely are geological factors noted as in the coal seams on the banks of the lower Shire River.

By 1866 Livingstone had embarked on another journey. This time he used the River Rovuma as his line into the continent. This journey broke into the 'Lake regions' of the area. His route took him past Lakes Malawi (Nyassa), Bangweulu, Mweru and by 1869 Livingstone was at Ujiji, on the shores of Lake Tanganyika.

Meanwhile Burton and Grant, during their expedition of 1857-1859 (Burton, 1859), had reached Lake Tanganyika and had reached the southern shores of Lake Victoria, thus locating the source of the Nile, a task that had troubled explorers for hundreds of years.

Stanley is probably most famous for his meeting with Livingstone at Ujiji in 1871, yet he had made many excursions through "The Dark Continent" and in 1875-6 was the first explorer to circumnavigate, and map, Lake Victoria (Anon, 1876).

These early explorers had described the land they crossed in great detail. From their accounts we have cross sections (mainly from Zanzibar westwards) into the continent. Some geological samples were collected and altitude information was collected at every opportunity. However, despite these efforts, and some minor reference to basic geology, little information of the geology of the area can be gleaned until the late 1870s. Indeed Thomson (1880) starts his account with the words:

" Though many travellers have now penetrated almost every part of Central Africa, and described the main geographical features, yet their accounts have been singularly barren in any reliable geological details."

Unfortunately Thomson's best intentions to "remedy this want" were thwarted by the death of the expedition leader, thus causing Thomson to take over the position. Thomson's journey took him from the coast to Lake Malawi (Nyassa) to Lake Tanganyika. The account (Thomson, 1880) is generally not very specific though hints at various features. A "great fault" is pointed to, as forming the boundaries of Lakes Malawi and Tanganyika. The noting of both east and west flanking faults to Lake Tanganyika essentially points to the existence of a rift valley, though this is not specified. The predominance of metamorphic and igneous rocks is also mentioned as well as the existence of large areas of red sandstones, presumably from the Karoo (Permian) or the overlying Red Bed rocks. Also noteworthy is Thomson's description of volcanic cones at

the north end of Lake Malawi. Their perfect shapes led Thomson (1880) to state that "They must have arisen in comparatively recent times."

Exploration in what is now known as the Kenya rift was surprisingly limited as most expeditions seem to have entered east Africa from the south. Rebmann and Krapf had seen Kilimanjaro and Mt. Kenya in 1848 and 1849 respectively but, except for an excursion into this region by Baron von der Decken in the early 1860s, no further exploration of the region was carried out until 1883. In that year Fischer broke into the rift valley near Mt. Meru. In the same year Thomson explored the rift valley further north and was finally able to confirm the sighting of Mt. Kenya from 34 years earlier.

In 1887-88 Count Teleki and Lieut. von Höhnel made, what is generally regarded as, the most important expedition into what was then British East Africa. They reached further north than anyone before, into the Lake Turkana region, and carefully mapped what they found. The map they produced, along with rock samples, sketches and notes enabled the geology and topography of the region to be reasonably well mapped for the first time.

Suess (1891) pieced together much of the work of these early explorers and geologists to put together a remarkable first step towards the understanding of the geology and tectonics of this section of the African Continent. He mapped the rift system using the accounts of visitors to the area and using their altitude determinations and geological samples. To him, rifting and the mountain chains around were additional evidence for his preferred model of the Earth. His model, and one which became widely accepted for many years, was that of a shrinking Earth, the mountains and rifts being the wrinkled skin of the planet.

With the use of satellite remote sensing techniques it now seems remarkable that only 150 years ago little was known about the interior of the African continent. The expeditions relied on 'primitive' techniques of transport and location and documented what was seen around them and what was guessed or interpolated to lie beyond. Now we are able to look down on the continent from satellites passing over the area almost continually. The images they provide can 'see' things as small as 10m in size and can be used to locate villages, tracks, fires and even which crops are being grown where. Those first tentative steps into the continent now seem to hold little relevance in today's world, the maps they produced have long been superseded and the information about tribes and peoples no longer holds true in the post colonial Africa of today. Yet without the perseverance of those first explorers the interior of Africa may still have remained an unknown corner of the world.

1.3 African Topography

The topography of East Africa can give some insight into the location of rift valleys and other related features. The best digital data-set of topography that was available until 1994 was the 5 minute resolution Etopo-5. Two new topography data-sets are now available; Terrainbase and Terrain-30. Terrainbase is a 5 minute resolution replacement of Etopo-5 while Terrain-30 has a 30 second resolution.

Terrainbase has been compiled from spot heights and selected points along contours of the 1: 1 000 000 U.S. Defense Mapping Agency (DMA) Operational Navigation Chart (ONC) series. The Australia National University Digital Elevation Model interpolation program was used to generate a 5 minute gridded dataset from these point data (Hutchinson, 1989).

Three sources have been used to compile the Terrain-30 topography. A Digital Chart of the World (DCW) was made by the DMA from the ONC series; this DCW was used with point elevations and hydrology data. The three data-sets were combined and run through the Australia National University Digital Elevation Model program to produce the resultant Digital Elevation Model (DEM) (USGS, 1994).

Figure 1.1 (Frawley, pers. comm.) shows the topography of Africa using the Terrainbase data, shown illuminated from the east. The topography of the continent clearly indicates the location of the East African Rift System from the Afar triangle (at about 42°E, 12°N) south to Mozambique (at about 35°E, 20°S). Much of East Africa is characterised by uplifted regions with an axial rift valley. To the west the Congo basin (apx. 20°E, 0°N) and the Kalahari (apx. 20°E, 22°S) are seen as lower-lying and less rugged terrain.

1.4 African Seismicity

The teleseismicity of African for the period of 1 January 1964 to 31 May 1993 is shown in figure 1.2. For this period the western branch has been much more seismically active than its eastern counterpart. The largest earthquake recorded had a magnitude of M_S = 7.4, and occurred in the Rukwa region in 1910 (Ambraseys, 1991a). Within the eastern branch one event measuring M_S = 6.9 was recorded at Subukia in 1928 (Ambraseys, 1991b). The majority of teleseismic events listed by the ISC are in the M_S = 3 to 5 range. More recently, in 1990, a M_S = 7.2 event occurred in southern Sudan (Girdler & McConnell, 1994).

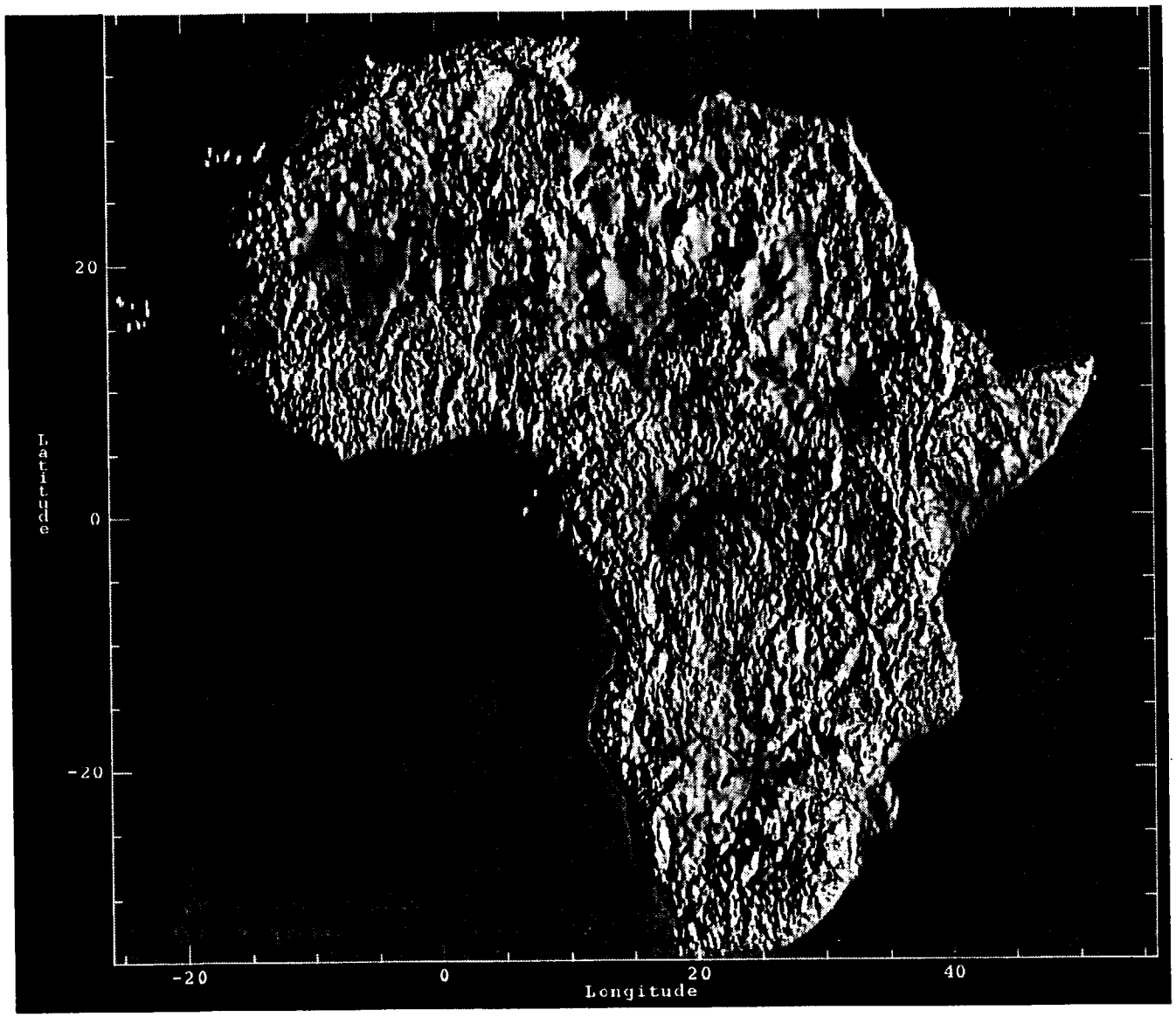

Fig. 1.1. Topography of Africa. Terrainbase topography data illuminated from the east. From Frawley (pers. comm.)

Earthquake Epicentres (1964-1991)

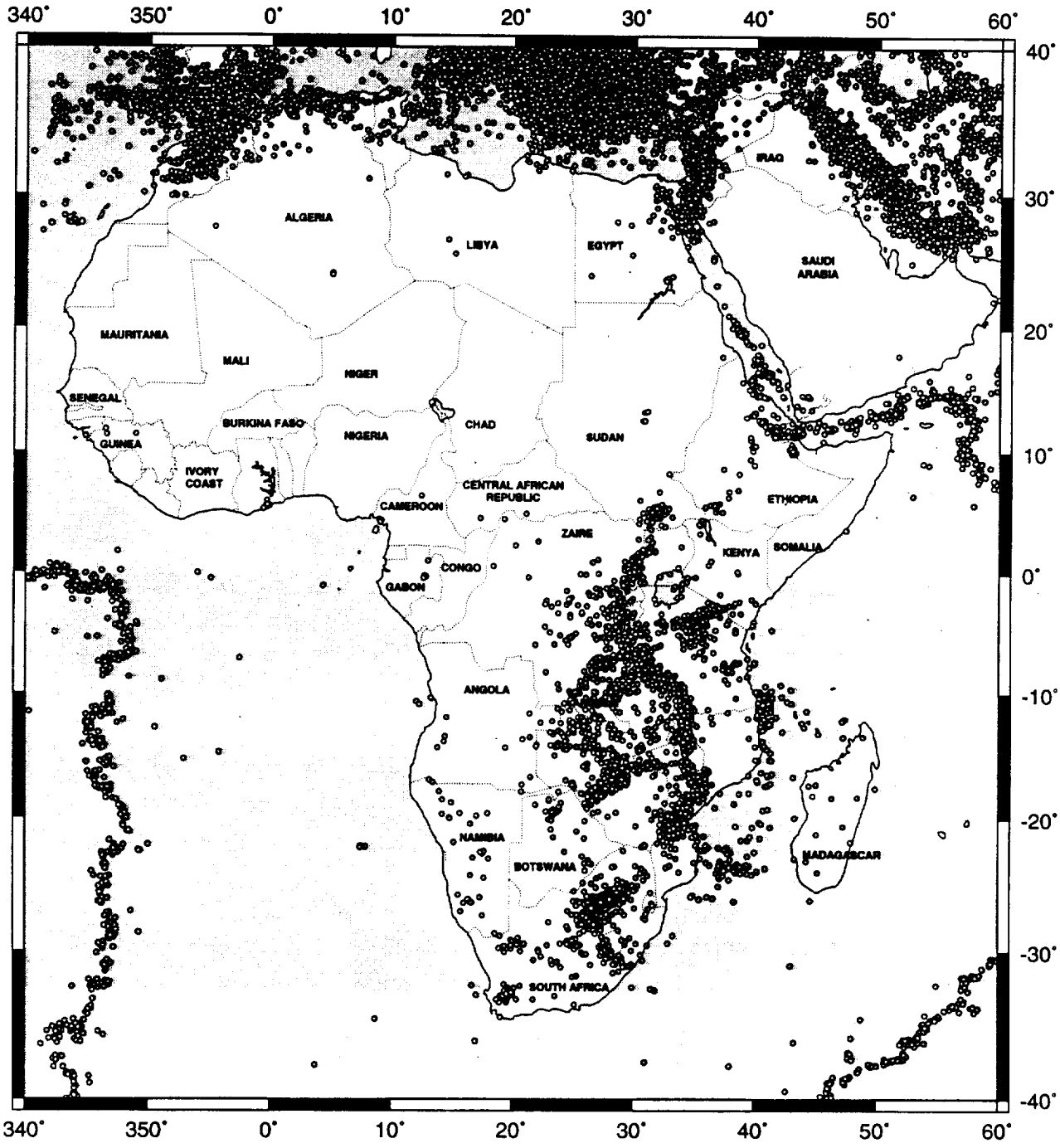

Fig 1.2. ISC determined epicentres of Africa (1 January 1964 to 31 May 1991)

1.4.1 Data Availability

Since January 1964 the World-Wide Standard Seismograph Net, WWSSN, and other nets have been used to record earthquakes. The International Seismological Centre (ISC) uses the data acquired from these networks, and from an increasing number of local networks, to produce the definitive epicentral location. The locations are usually accurate to within 10 km depending on the event magnitude and station distribution. The difficulty in obtaining some of the available data means that the ISC determinations are always about 2 years behind the present. For more recent events preliminary determinations by the National Earthquake Information Service (NEIS) are used. Figure 1.3 shows all available data for East Africa (1904 to 15th April 1993): prime estimates, listed as such by the ISC, have been used where an event is recorded by more than one agency. Figure 1.4 shows the larger events for East Africa.

Prior to 1964 the recording and location of earthquakes fell to various individuals and agencies, The events used here are from Gutenberg & Richter (1954) for 1906 - 1954; The International Seismological Summary for 1913 - 1963; and the Bureau Central International de Séismologie for 1950 - 1963. The lack of any integrated seismograph network and the scarcity of stations in many regions meant that location accuracy was often poor. Many events in east Africa, before 1935, are quoted to the nearest degree or half degree (about 110 - 55 km). The usefulness of these early events is thus as an overview of seismicity only, and not for cause and effect studies of the seismicity. The annual frequency of recorded earthquakes in East Africa is given in figure 1.5.

1.4.2 Seismicity in the East African Rift

The larger earthquakes that have occurred in East Africa, between 1964 and 1993, are shown in figure 1.4. Figure 1.4A shows the location of earthquakes with $m_b \geq 6.0$, of which there are 9 recorded up to May 1991 by the ISC and two by the NEIS, between May 1991 and April 1993. Figure 1.4B gives all the events where $m_b \geq 5.0$. Of the 11 events larger than magnitude 6, three occurred in Afar, two in southern Sudan, three along the western branch and one in northern Tanzania. The earthquakes with a magnitude of 5 or greater appear to be more representative of rifting than when all events are considered. Including only events of this size eliminates any weighting associated with local and temporary seismic networks as events of this size are seen regardless of global location.

Earthquake Epicentres (1904 - 1993)

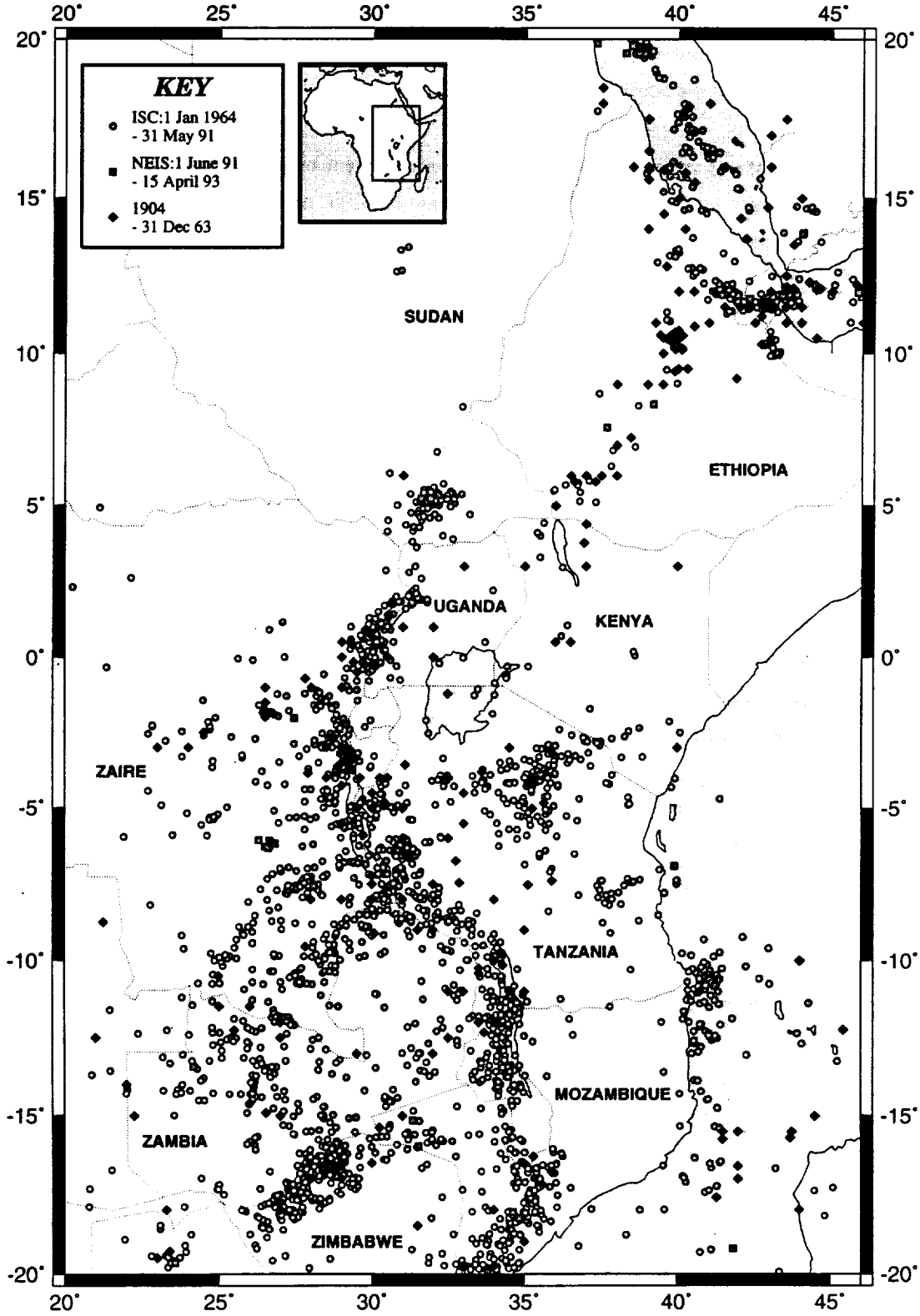

Fig. 1.3. Earthquake epicentres for East Africa. All available prime estimates (ISC) from 1904 through to 15th April 1993.

Large East African Earthquakes

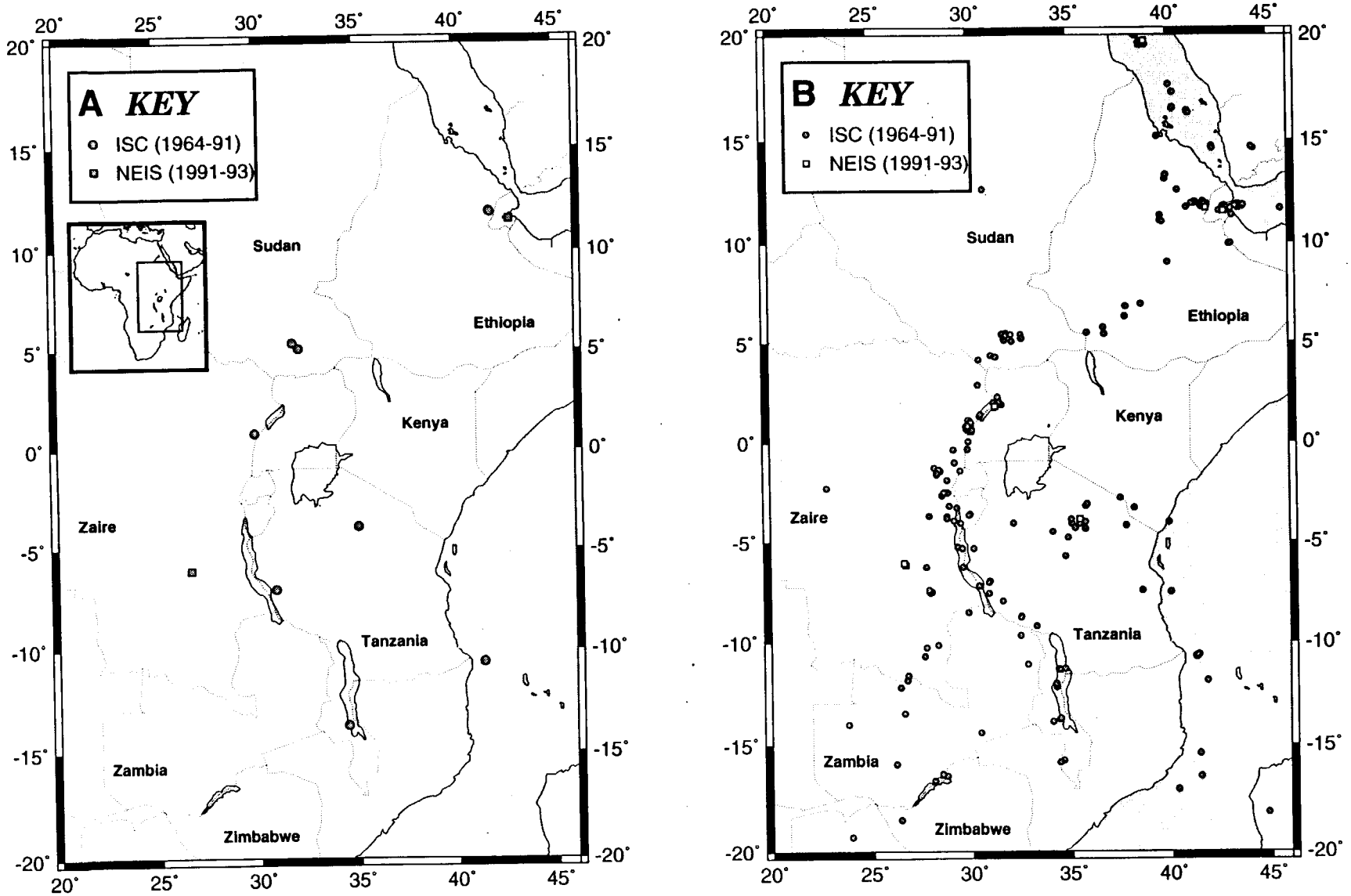

Fig. 1.4. ISC and NEIS determined earthquake epicentres of east African from January 1964 to April 1993: A. Magnitude > 6, B. Magnitude > 5

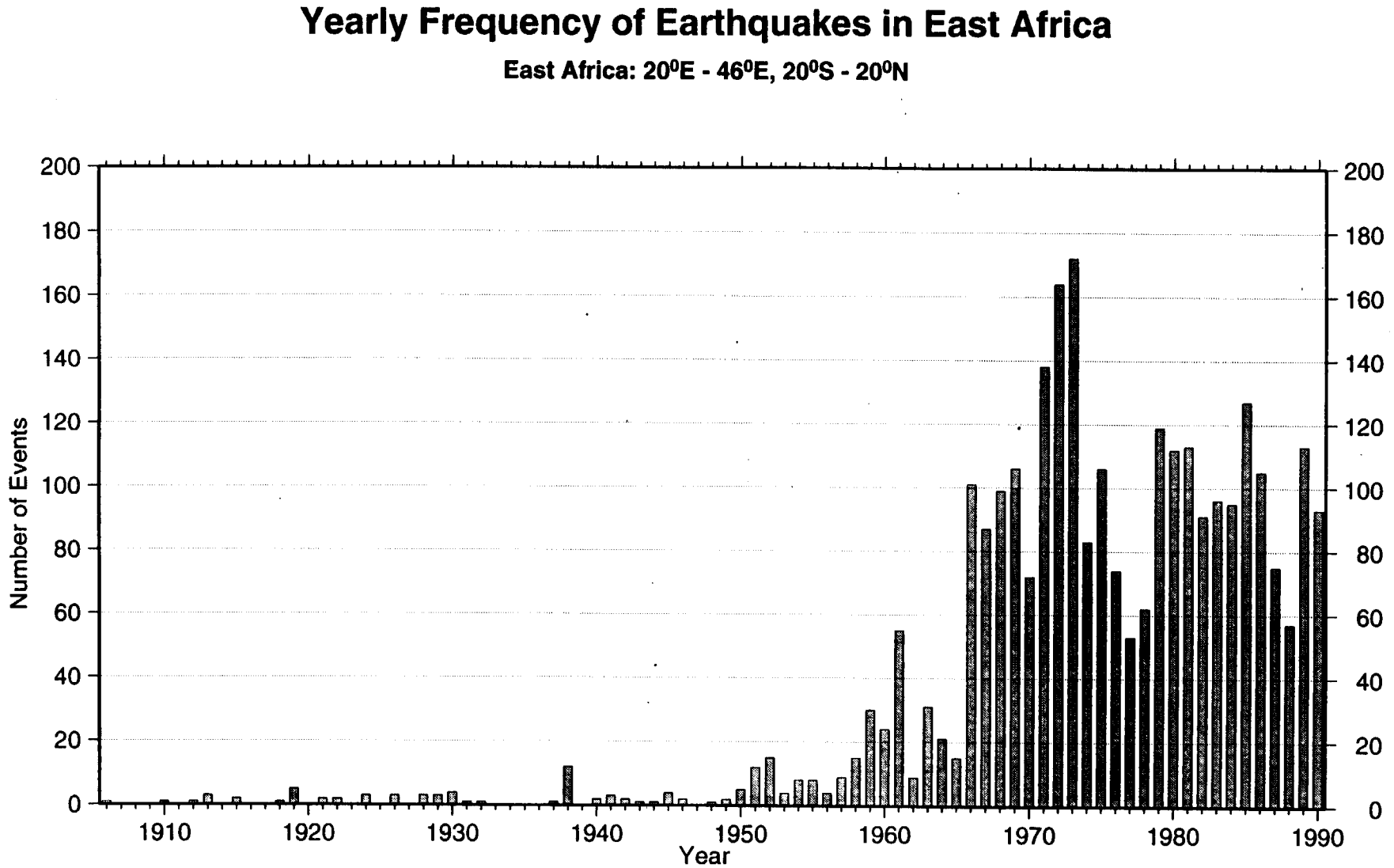

Fig. 1.5. Yearly frequency of earthquakes in East Africa, prime estimates from various agencies.

The seismically active section of the western branch extends from southern Sudan, north of Lake Mobutu (Albert), along the line of rift lakes to the south of Lake Malawi. There are several side branches of seismicity running in a southwesterly direction from the main rift zone, figure 1.3. The first of these branches includes the Upemba Lakes region; the second runs from the southern end of Lake Tanganyika through the Lake Mweru and Lake Mweru-Wantipa area and the third follows the Luangwa Valley from the north end of Lake Malawi as far as the Zambesi River and Lake Kariba. These zones are considered in section 1.7 and are thought, by Rosendahl (1987), to be pre-Tertiary (Karoo) rifting zones. Only the Mweru trend is picked up from events where $m_b \geq 5.0$, figure 1.4.

The termination of the western branch in the north was usually considered to be where it reached the Aswa lineament (e.g. Rosendahl, 1987) though the actual role of the lineament has always been doubtful. Rosendahl (1987) and Chorowicz (1983) have suggested that the Aswa lineament acts as a transfer zone in much the same way as the Rukwa rift further south, though there is little evidence for activity along the lineament itself. In 1991 an earthquake swarm occurred in southern Sudan, around the town of Juba. This led Girdler & McConnell (1994) to propose an extension of the rift further north, to about 6°N.

Taking seismicity alone there is evidence for rift extension north along the valley of the Nile and also southwest along the Upemba, Mweru and Luangwa zones. However, seismic activity cannot prove these extension hypotheses over the arguments for reactivation and settling of older rifts, thought the magnitude of the events in southern Sudan and southwest of Lake Mweru would tend to suggest some form of contemporary tectonic process occurring in the area. Evidence from seismic activity covers too short a time-frame to be used to draw sweeping conclusions as to the full extent and nature of rifting, indeed, looking at the teleseismicity alone would draw one to the conclusion that the Kenya rift does not exist.

The Ethiopia rift exhibits considerably less seismicity than the western branch, as seen on figure 1.3, but when only the larger events, figure 1.4, are shown it becomes more equal in epicentre density with other parts of the rift system. With events where $m_b \geq 5.0$ all sections of the rift system appear to exhibit similar levels of seismicity. The exception to this is the Kenya rift.

The Kenya rift is teleseismically quiet except south of line of earthquakes in Northern Tanzania which corresponds to the Kilimanjaro, Meru line of volcanoes (see section 5.7).

Despite the lack of teleseismicity, possibly due to the short period of data acquisition, microseismicity is common and has been the basis for a number of studies in the region (e.g. Tongue *et al*, 1992). This microseismic activity indicates a continuing process of low energy release within the rift at depths generally less than 10 km (Bosworth *et al*, 1992). The study carried out by Tongue *et al* (1992) drew on microseismicity ($M_L < 3$) seen in the Kenya rift up to 1992. The results show that activity is largely confined to three main sections of the rift and is associated with hydrothermal and volcanic activity. The three main regions are: southern Lake Turkana and the Sugata valley (about 1.8° - 3.4°N); the Kavirondo rift; and the Lake Bogoria region at about 0.1°N, 36.2°E. Some scattered activity also occurs on the eastern flank of the rift in regions of recent volcanic activity (Tongue *et al*, 1992).

Microseismic activity has also been studied in many sections of the western branch (e.g. Rykounov *et al*, 1972, Zana *et al*, 1989). Regions of microseismicity have been observed around the Ruwenzori massif (Rykounov *et al*, 1972) and around Lake Kivu (Zana *et al*, 1989). The studies carried out by Zana *et al* (1989) showed swarms of microseismic events to the west of the rift valley.

Earthquake studies have been able to provide some information on the stress regime along the rift system. In recent times borehole breakout data have added to the available stress information and the alignment of Quaternary volcanic vents has also been used to study the current and palaeo-stress field in east Africa. Bosworth *et al* (1992) concluded that the present orientations of the least horizontal stress, S_{hmin}, is roughly radial about the Afar triple junction. This gives an approximately NW - SE orientation in Kenya and N - S in Sudan. Evidence for the palaeo-stress direction gives an almost E - W orientation for Kenya in the pre-mid Quaternary. Zoback (1992) estimated the magnitude of $S_{hmax} - S_{hmin}$ for East Africa, from the rotations of the principal stresses in the rift, as being about 14 MPa.

Figure 1.6 shows the available fault plane solutions for earthquakes in East Africa, from various sources. Figure 1.6A shows solutions based on first motions while figure 1.6B show the mechanisms based on moment tensors. Within the region of the continental rift the majority of these solutions show predominantly normal fault mechanisms while in Afar and the Red Sea strike slip mechanisms are more common. The extension direction shown by the focal mechanisms of normal faults within the rift is generally perpendicular to the section of the rift in which the event occurred.

Fault Plane Solutions for East Africa

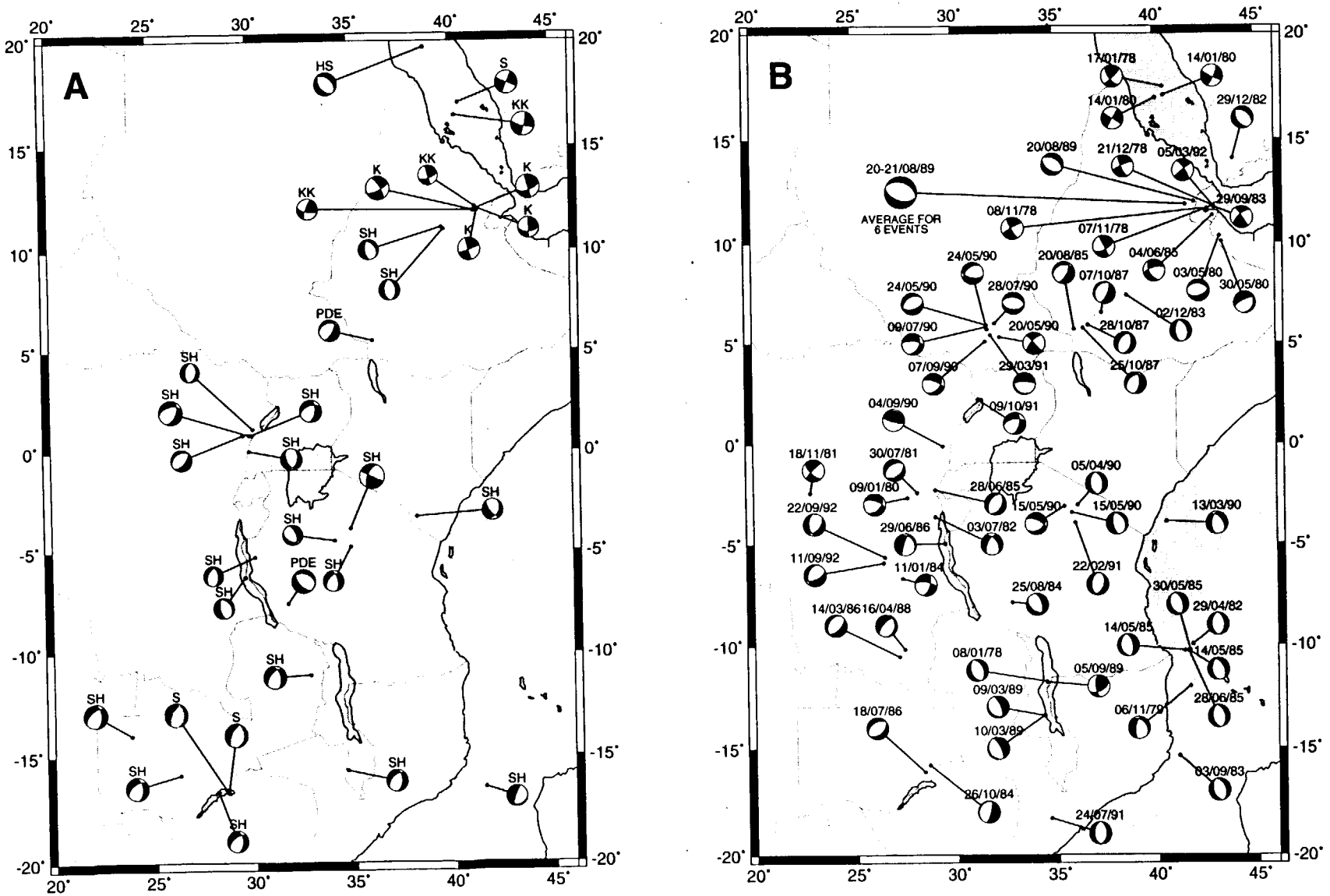

Fig. 1.6. Fault plane solutions for East African earthquakes: A. S, Sykes (1967); SH, Shudofsky (1985); K, Kebede (1989); KK, Kebede & Kulhanek (1991); PDE, Preliminary determinations; HS, Huang & Soloman (1987). B Moment tensor solutions from Dzeiwonski et al (1983 etc.).

Yearly Frequency of Earthquakes in East Africa

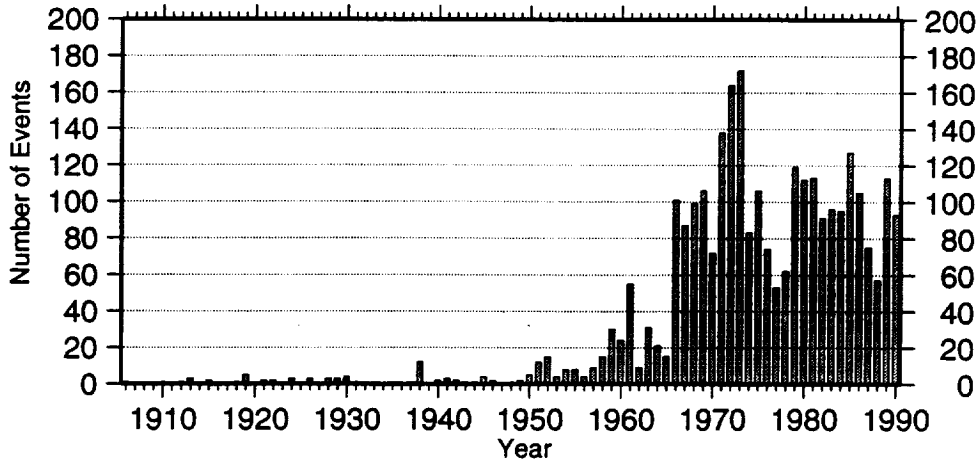

A: East Africa: 20^{0}E - 46^{0}E, 20^{0}S - 20^{0}N

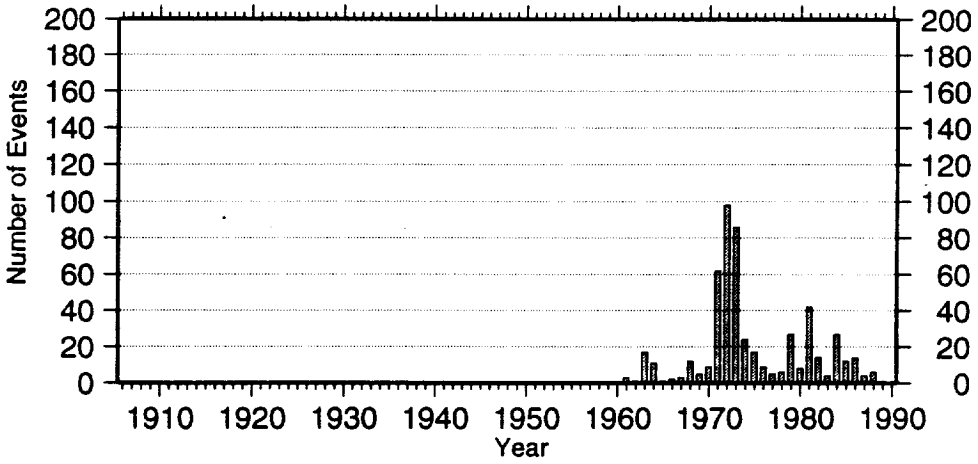

B: Lake Kariba: 25^{0}E - 30^{0}E, 20^{0}S - 15^{0}S

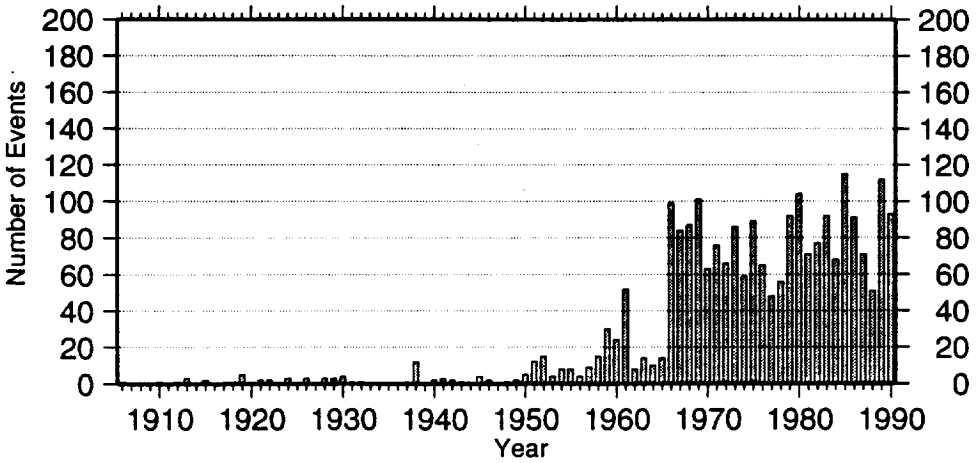

C: East Africa (A) - Lake Kariba (B)

Fig. 1.7. Yearly frequency of earthquakes in East Africa, prime estimates from various agencies.

Man-made engineering projects can give rise to anomalous bursts of seismicity. One such example is the Lake Kariba dam. The filling of Lake Kariba started in 1958 and was completed in 1963, the seismicity increased in the region to a maximum during September 1963 (Fairhead & Girdler, 1971). To investigate this, a local network was set up in 1971 around the lake. Thus, a large number of earthquakes suddenly appear in the ISC catalogue in and after 1971, See figures 1.7A, B and C. Many of the Kariba events occurred on reactivated faults. It would appear, from this, that the dam loading induced earthquakes after its completion. This illustrates the use of local networks in specialist studies.

1.5 Cenozoic Rifting and Volcanism

1.5.1 The East African Rift System

The 'East African Rift System' extends from the Dead Sea, through the Red Sea then from Ethiopia to Malawi. In the Afar region of Ethiopia, Djibouti and Eritrea the continental section of the East African Rift System joins with the Red Sea and Gulf of Aden rifts, figure 1.8. From Afar the rift tracks south-westerly through Ethiopia then south through Kenya. In equatorial regions the rift is split into the western and eastern branches, the eastern through Kenya and the western through Lakes Mobutu (Albert), Edward, Kivu and Tanganyika. While the eastern branch all but dies out in northern Tanzania, the western branch is offset through Lake Rukwa to continue south through Lake Malawi. It was first recognised as being of geological significance towards the end of the nineteenth century when reports from expeditions told of a great valley cutting through the continent.

As early as 1880 Thomson had hinted at a fault bounded valley for Lake Tanganyika. In 1891 Suess published his understanding of the region based entirely on accounts from explorers in the region, such as Thomson and von Höhnel. This account covers the entire system, figure 1.9A, from the Dead Sea (Todtes Meer) in the north and through the Red Sea (Rothes Meer) and Afar; from here a line indicates the eastern branch of the rift from Afar, through Ethiopia and Lake Turkana (Rudolf See) thence southwards to Lake Manyara (Manjara See). The western branch is essentially shown only as far as the lakes extend, from Lake Mobutu (Albert See) to Lake Malawi (Nyassa See). Two regions are considered in more detail, the Dead Sea and the Kenya rift zone. The Kenya rift zone is based on a survey by von Höhnel and clearly shows the trend of the rift valley from Lake

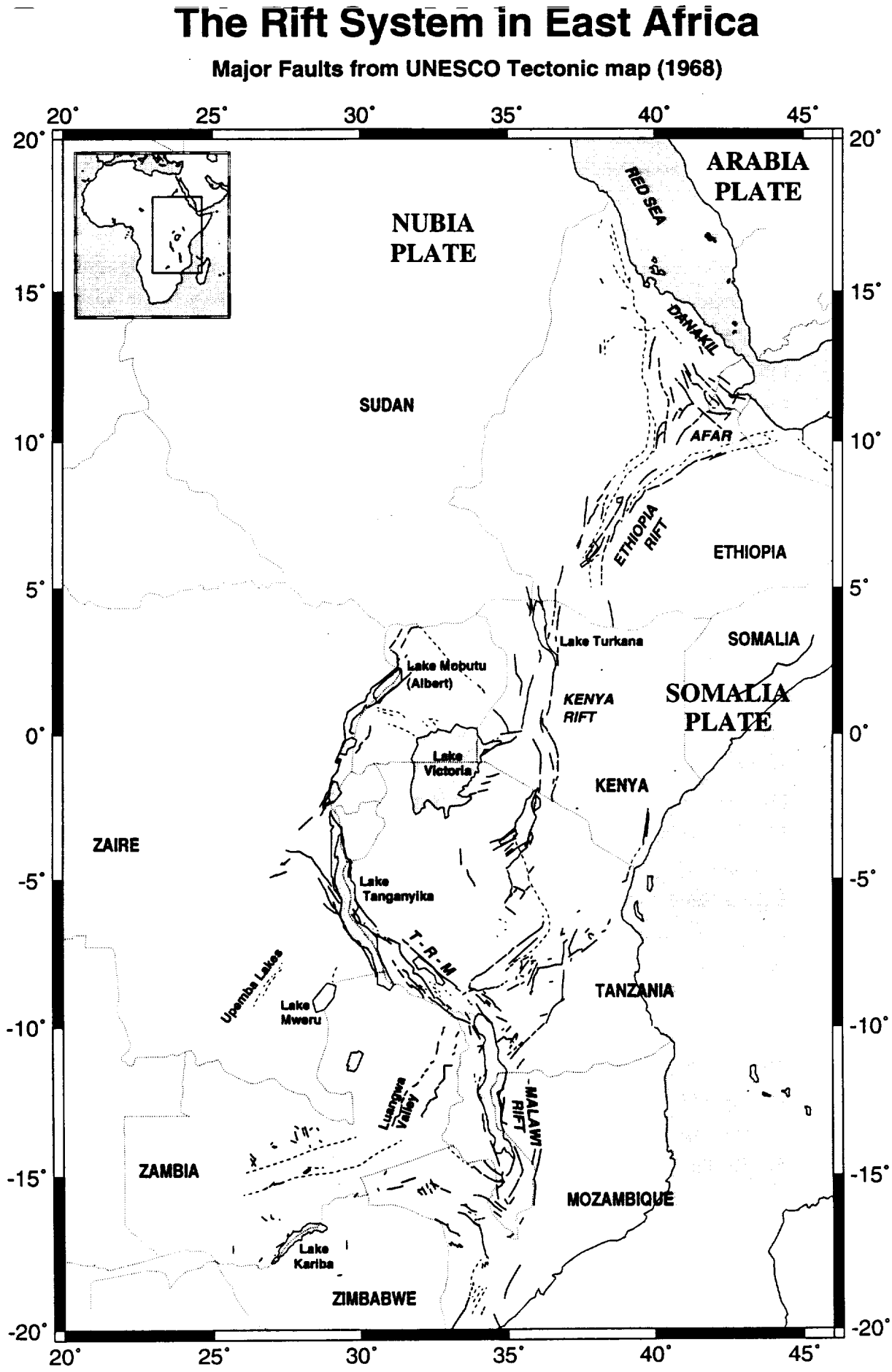

Fig 1.8. The continental section of the east African rift system.

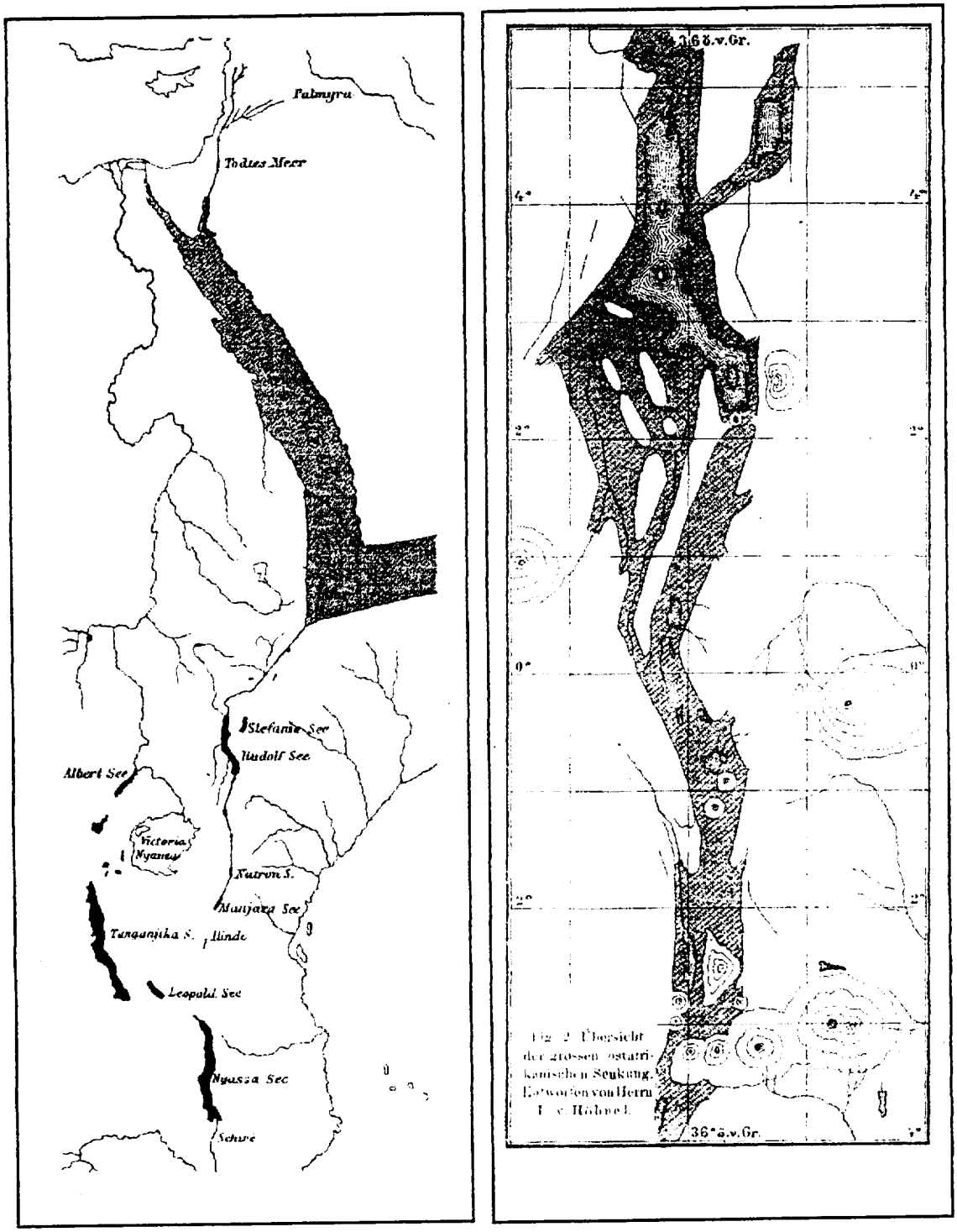

A The East African Rift System **B. The Kenya Rift**

Fig 1.9. The East African Rift System and Kenya Rift as known in 1891, from Suess (1891)

Turkana to Kilimanjaro, figure 1.9B. The inclusion of the Ethiopian section is of particular interest as at the time (1891) no European had visited this region.

In 1896 Gregory's *The Great Rift Valley* was published. This account adds to the work of Suess as far as the Kenyan sector of the rift is concerned. However, it is not until 1921 that Gregory's work on the area is brought together in *The Rift Valleys and Geology of East Africa*: in this Gregory discusses, and maps, the entire rift system of East Africa. The map, figure 1.10, is particularly notable in its completeness, including many sectors that were not generally recognised until many years later.

Ideas as to the process of formation of the rift system abounded. Willis (1936) proposed a compressional regime for the rift formation suggesting that the rift valleys were a feature of the broad uplift caused by arching due to compression. Gregory, and many others, supported the hypothesis that tension had caused the 'keystone' to drop out of the pre-existing arches. Willis further argued that the rift valley was bounded by reverse faults and that later slumping of the valley walls had caused the present shape. Bullard (1936) supported this compressional theory with interpretation of gravity data in the area.

In 1912 Wegener proposed the ideas of continental drift, yet the relevance to the continental portion of the East African Rift System was not noted until the discovery of the world's mid ocean ridge system and the wide acceptance of the ideas of plate tectonics. The realisation that the rifting in East African was linked to the plate boundaries gave new impetus to the studies of the rift. The East African Rift System provided a relatively accessible laboratory for rift studies.

By the end of the 1960s the ideas of plate tectonics were largely developed. Convection cells are generally accepted as the driving force. However, despite the advances in understanding since Wegener's time, problems still remain in the realisation of the precise processes that drive the plates. Of particular interest are the processes surrounding the formation of new oceans from the initiation of rifting such as in East Africa to the onset of sea-floor spreading as in the Red Sea.

The two branches of the East African Rift System are significantly different in their morphology and activity. The western branch is seismically active, with separate volcanic centres, and consists of a series of deep, lake filled, troughs. In contrast, the eastern branch has widespread volcanic activity, low levels of seismicity, and has few large and deep lakes.

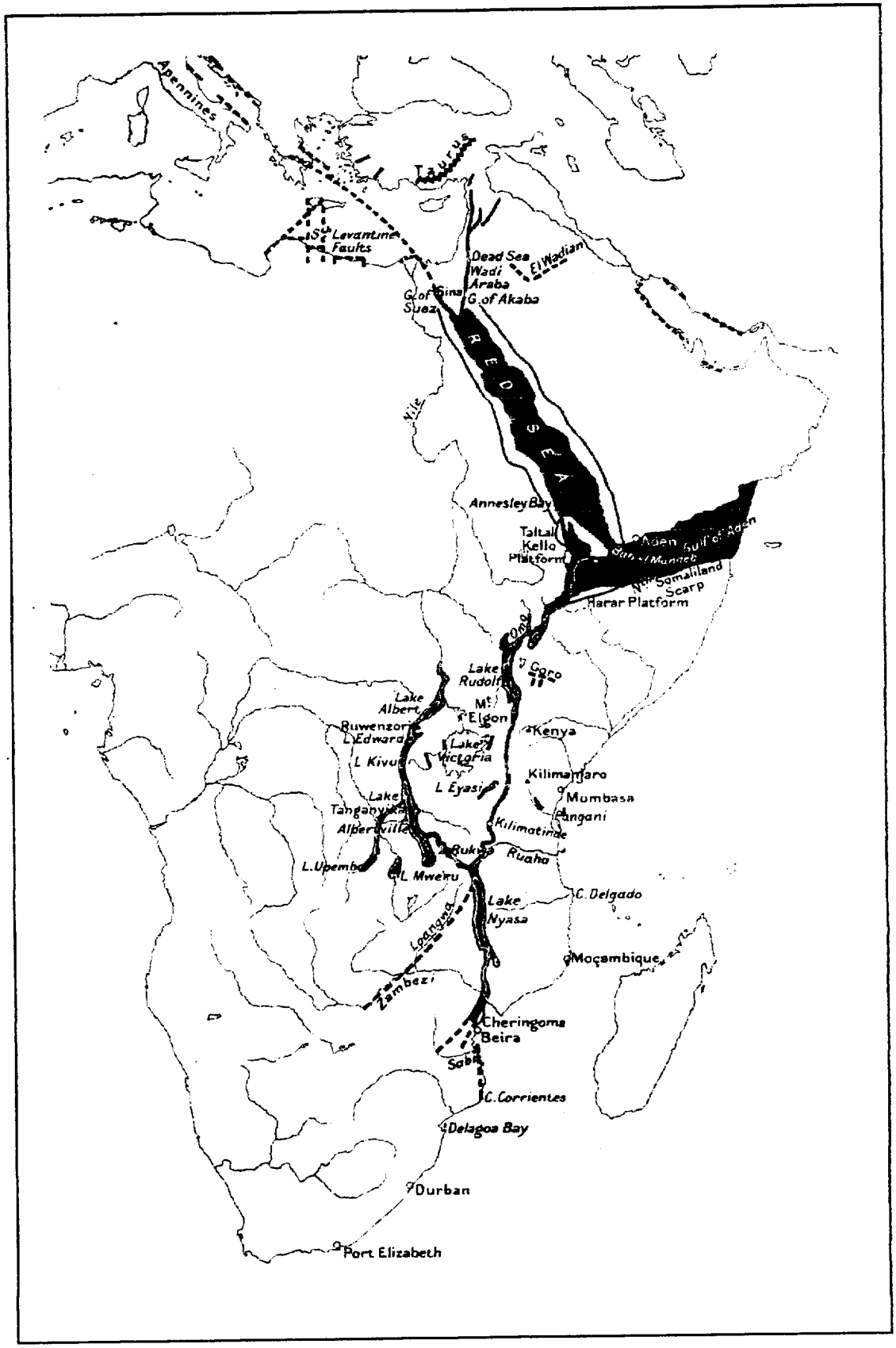

Fig. 1.10. The East African Rift System as seen by Gregory (1921)

The western branch is characterised by deep troughs filled with Pliocene and Quaternary sediments. These troughs are extremely deep, typically 3-5 km of sediments is found beneath Lakes Tanganyika and Malawi, which are themselves about 1.5 and 0.7 km deep respectively (e.g. Delvaux, 1992). Lake Rukwa is shallow, only about 13 m deep, but the basin it occupies has up to 12 km of sediments (Rosendahl *et al*, 1992). Tertiary volcanism is observed in four isolated provinces, Toro-Ankole, Virunga, Kivu and Rungwe; (Delvaux, 1992). The dates assigned to the initiation of volcanism in Kivu are about 12 Ma (Ebinger, 1989b) while in Rungwe the start is thought to be about 7 Ma (Ebinger *et al*, 1989).

The eastern branch, while exhibiting the classical graben or alternating half graben morphology, differs from its western counterpart in being extensively filled by igneous extrusives, basalts and trachytes. Excluding Lake Turkana all the rift valley lakes are small and shallow and many are highly alkaline, soda lakes. The earliest recognisable rift structures are mid-Tertiary and the first extensive rift faulting, in Kenya, is thought to date from the early Miocene (Baker & Wohlenberg, 1971). Volcanoes exist in an axial line down the rift and are also located away from the rift itself on the western and eastern flanks.

The presence of older rift structures and mobile belts makes dating the onset of rifting in the East African Rift System extremely difficult. Extensive igneous flows in the eastern branch also make the task of dating problematic. As mentioned above, the first recognisable faulting in the eastern branch is mid-Tertiary but this does not discount the possibilities that older structures are obscured or that these mid-Tertiary structures may have been initiated in an older rift structure. In the western branch the Lupa fault which bounds Lake Rukwa to its north-east is Karoo (Permian) in age with reactivation in the Tertiary (7 Ma) up to the present. Thus exact dating of the onset of the East African Rift System is not possible though the majority of the features associated with it are 20 Ma or younger.

1.5.2 Volcanism

In contrast to the locations of earthquake epicentres, volcanoes are more common in the eastern than in the western branch of the East African Rift System. Figure 1.11 shows the location of volcanoes for east Africa, pre-Holocene volcanoes are shown in figure

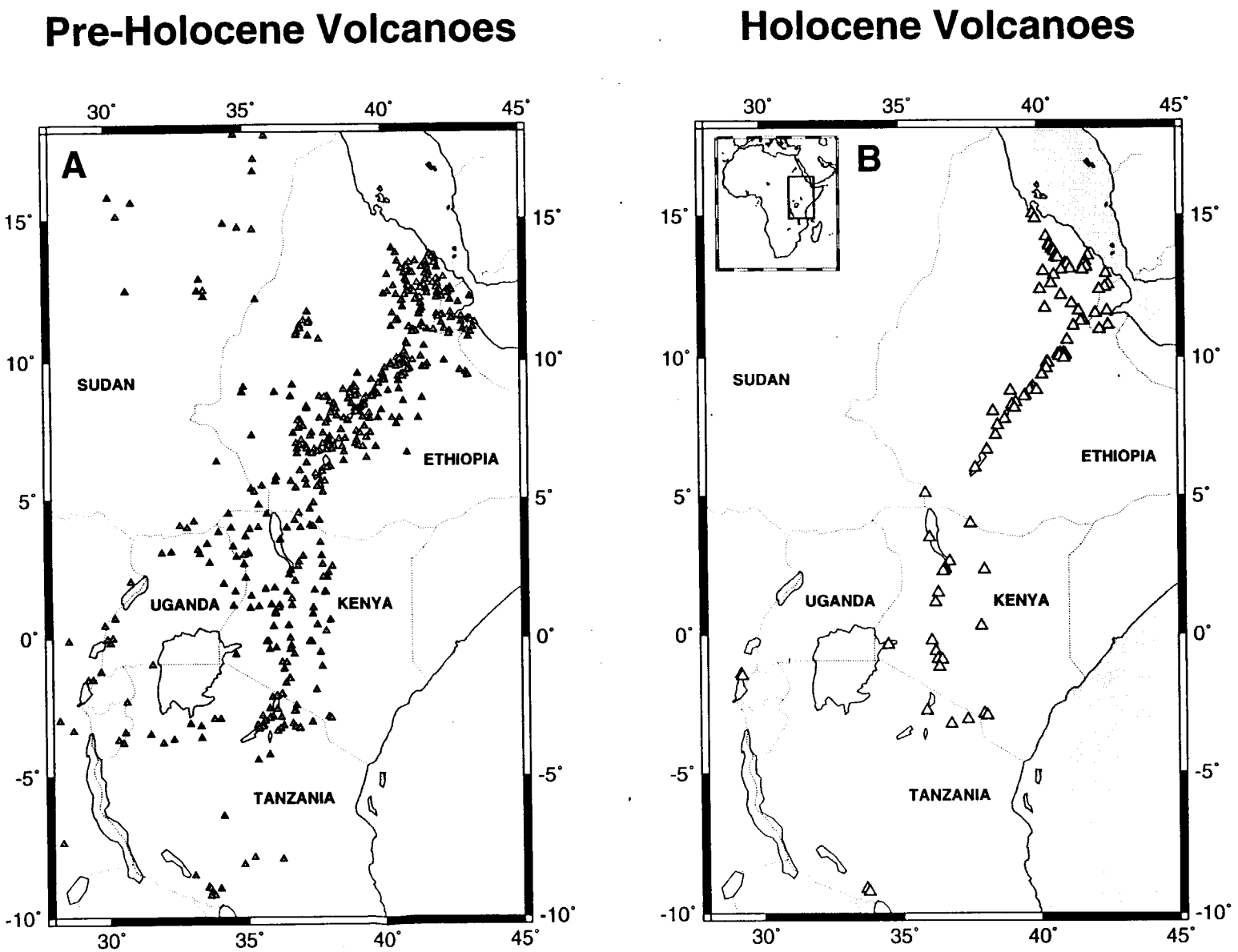

Fig. 1.11. Volcanoes of east Africa, from Nusbaum et al (1994); A. Pre-Holocene volcanoes; B. Holocene volcanoes.

1.11A while Holocene are given in figure 1.11B. The volcano locations are taken from Nusbaum *et al* (1994).

The locations of most of the volcanoes given by Nusbaum *et al* (1994) were found from satellite imagery. The coverage of the imagery used is shown in figure 1.12 and is either Landsat MSS or TM. As it is virtually impossible to distinguish Holocene from pre-Holocene activity from satellite imagery the Holocene data from Simkin *et al*, (1981); McClelland *et al*, (1989); Geothermal Reconnaissance Study, (1987) and various Seismic Event Network Bulletins were used. Further data were obtained from detailed maps; data sheets of The International Association of Volcanology (Richard & Neumann Van Padang, 1957); and U.S. Defense Mapping Agency (DMA) databases. Accuracy in location from the satellite scenes is to within 0.04° (about 4 km), (Nusbaum *et al*, 1994). Some volcanoes have remained intermittently active for millions of years and thus some classified as Holocene are also included in the pre-Holocene listing. However, the majority (96%) of pre-Holocene volcanoes have shown no activity within the last 10 000 years.

A number of volcanoes, within the region, have been active within the last decade: these being; Nyamuragira and Nyiragongo (Zaire); Ol'Doinyo Lengai (north Tanzania) and Erte'Ale (Ethiopia). Two of these lie in the western branch, one in the eastern branch and the other in Afar.

The cause of volcanoes off the rift axis, in Kenya, has been the source of much debate. They were observed by Suess (1891) and their cause has been considered by many authors since (e.g. Girdler *et al*, 1969; Bosworth, 1987; Morley, 1988b; Ellis & King, 1991). The pre-Holocene volcano locations (figure 1.11B) show a spread of volcanic centres away from the Kenya rift axis which appear to align to the west and east of the rift at a distance of about 100 - 150 km. The western off-axis line is only extant west of Lake Turkana to about 1°N; while the eastern line is virtually continuous from the Ethiopian rift south to Kilimanjaro; though Dawson (1992) argues that Kilimanjaro is not strictly 'off-axis' as it lies at the intersection of the Pangani graben with the southern end of the Kenya rift. In the Holocene only one volcano lies to the west of the Kenya rift and this lies near the Kavirondo side-branch. A series of off-axis volcanoes are still observed to the east. Lithospheric thinning has been proposed as one source for the off-axis volcanoes (e.g. Brown & Girdler, 1980) while Bosworth (1987) suggested a series of detachment faults which induced thinning and volcanism at their apexes. The idea of detachment fault-induced volcanism breaks down when the smaller cones are considered and when the Miocene age of Mount Elgon is taken into account (Morley, 1988b). The

Imagery for Volcano Location

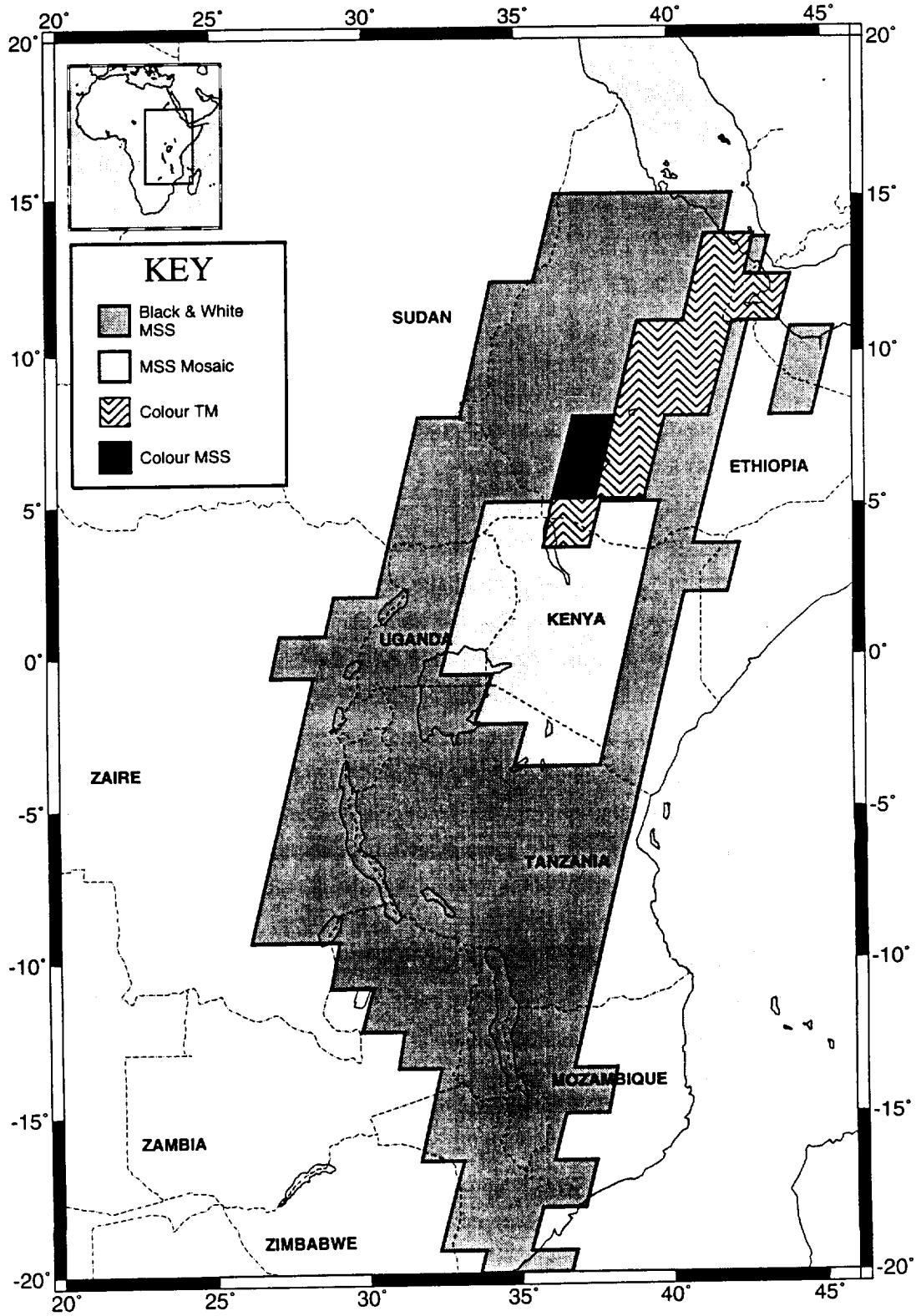

Fig. 1.12. Imagery used for locating volcanoes, from Nusbaum et al (1994).

presence of off-axis volcanism could be related to older structures away from the rift axis which have acted as a conduit for magma to the surface (Smith & Mosley, 1993) however the reason for magma being concentrated away from the rift has not been solved. In Ethiopia the pre-Holocene centres exist in a broad swath which, in the Holocene, has become focused along the rift axis. While there existed no distinct off-axis lines of volcanism in Ethiopia the evidence points to a focusing towards the rift. This focusing to the axis has been pointed out by many authors (e.g. Girdler *et al*, 1969; Baker *et al*, 1972) and the continued presence of off-axis volcanism in Kenya may be due to the fact that the Kenya rift is as yet less magmatically mature than the rift in Ethiopia. Other authors (e.g. Swain *et al*, 1994) have argued for the presence of an extensive magma pond off the rift axis which provides the magma source for the off-axis volcanism.

A study of the distribution of Holocene and pre-Holocene volcanoes, figure 1.11, reveals that of 99 Holocene volcanoes 4 (4%) lie in the western branch while about 30 out of the 516 (6%) pre-Holocene volcanoes are within or close to the western branch.

The commencement of volcanism was in the Eocene-Oligocene in Ethiopia and early Miocene in Kenya. Baker *et al* (1972) divided the eastern branch into the Kenya and Ethiopia sections and further divided the succession into the fissure or multicentre eruptions and central volcanoes. In Kenya the fissure eruptions, since the Miocene, have been characterised by basalts, phonolites, ignimbrites, rhyolites, trachytes and mugearites: the central volcanoes have produced; nephelinites, phonolites, carbonatites, basalts, trachytes, and ignimbrites. In Ethiopia the situation is less complex with the fissure eruptions giving mainly basalts with some trachytes and mugearites. The central volcanoes in Ethiopia are again largely producers of basalt with trachybasalts, basanites, melanephelinites, phonolites, trachytes, pantelleritic ignimbrites and obsidian lavas.

The Miocene, pre-rift, flood basalts and Quaternary flood basalts away from the rift in Kenya are more alkaline than the more recent flood basalts on the rift floor (Baker *et al*, 1972). The Kenyan basalts are, on average, higher in CaO-MgO-FeO and lower in SiO_2 than those in Ethiopia and may be due to a deeper origin in Kenya. In general the petrochemistry of the Kenyan and Ethiopian igneous rocks show that they are significantly different, causing problems in the origins of the two parallel fractionation series. This was explained, by Baker *et al* (1972), as being derived from melting in parts of the mantle with different water contents; a difference in the amount of partial melting; or a combination of the two. Estimates for the eruptive volumes in the eastern branch

give 144 000 km^3 for Kenya (Williams, 1972) and 345 000 km^3 in Ethiopia (Mohr, 1992).

Ol'Doinyo Lengai, in northern Tanzania, is unique in its active carbonatite eruptions, though carbonatite lavas have been present, in the past, elsewhere in the eastern branch. Despite the fact that the volcano's recent eruptions have been of alkaline carbonatite much of the volcano is made up of silicate igneous rocks (Dawson *et al*, 1994). In the eruption of June 1993 the carbonatite lavas and ash contained some silicate spheroids and the lava was far more viscous than previously observed. This led Dawson *et al* (1994) to conclude that silicate and carbonatite magmas coexist at the volcano.

The volcanic centres in the western branch are distinct regions of volcanism separated by regions where there is no evidence of volcanic activity. The volcanic provinces are, from north to south: Toro-Ankole (north Ruwenzori), Virunga (north Kivu), South Kivu and Rungwe. However, regions of hydrothermal activity and traces of volcanic rocks on Lake Tanganyika have led Coussement *et al* (1994) to add two extra regions to this list: Pemba/Cape Banza and Kalemie-Mahali, both within the Lake Tanganyika trough.

Quaternary volcanism in Toro-Ankole and Virunga are characterised by potassic or hyperpotassic lavas while in South Kivu theoleiitic or alkaline lavas predominate (Pasteels *et al*, 1989).

1.5.3 Kimberlites

It has been suggested that kimberlites are related to continental rifting (e.g. Mitchell & Garson, 1981). This premise is based on the linking of carbonatites and rifting and kimberlites with carbonatites. However, Mitchell (1986) argues that in the majority of cases true kimberlites do not occur within rifts, including the East African Rift System. Dawson (1970) and Mitchell (1986) suggest that the majority of kimberlites in East Africa lie in inter-rift regions.

Figure 1.13 shows the location of kimberlites, from the UNESCO (1968) tectonic map, and the location of rift faults. Dawson (1980) suggests that some kimberlites mapped in East Africa may not be true kimberlites. The main region of kimberlites, in the locality of the East African Rift System, is in Tanzania, between the western and eastern branches. While there may be some links between the branches in this region the rifts are not fully developed and thus the kimberlites must pre-date the full rift development. The two

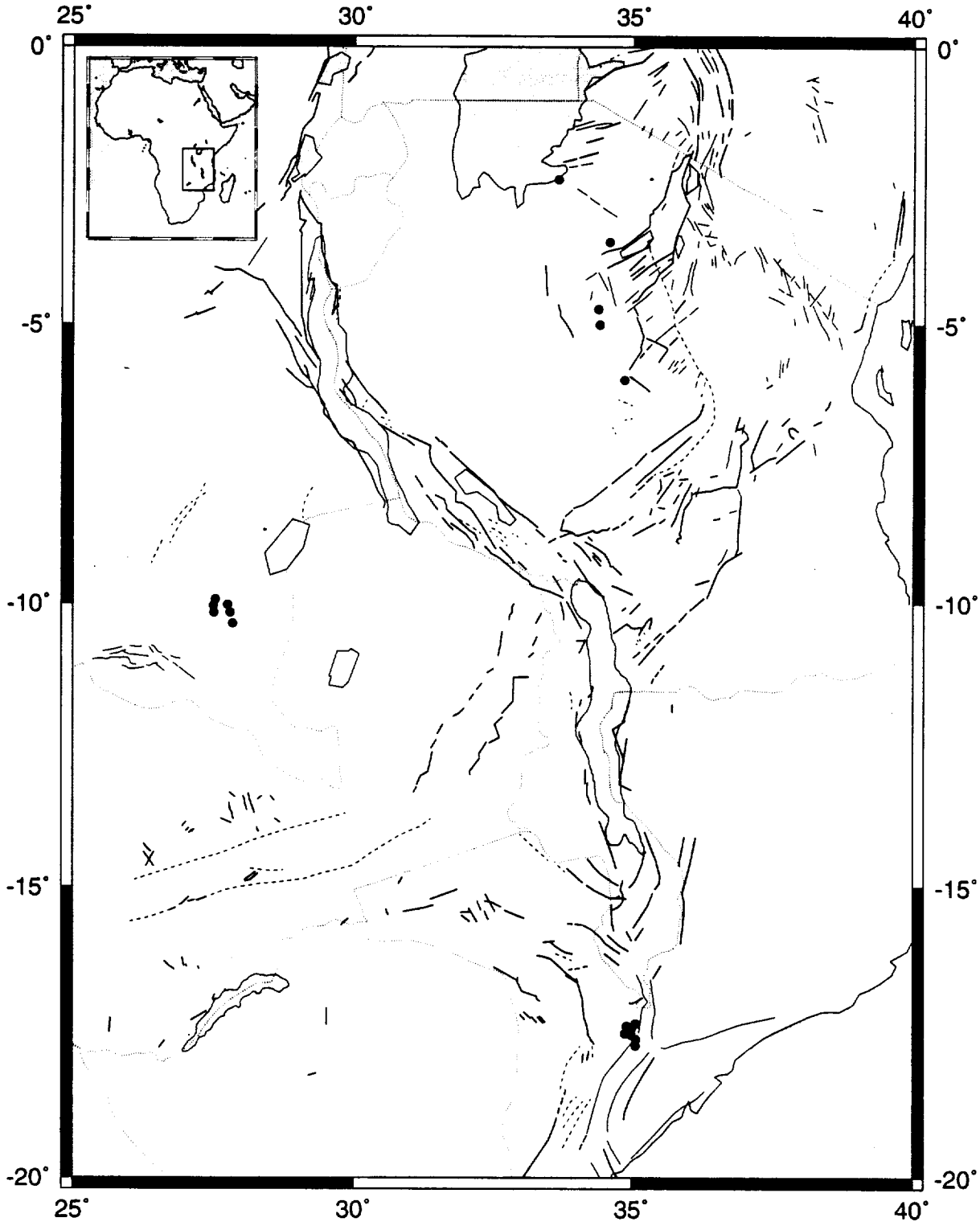

Fig 1.13. Kimberlites (circles) and faults of East Africa, from the UNESCO Tectonic map of Africa (1968).

other areas of kimberlites are southwest of Lake Mweru, in a region considered to be a possible southwesterly extension of the East African Rift System, and south of Lake Malawi. The area south of Lake Malawi lies at the junction of the Zambesi, Urema and Shire grabens. The small number of kimberlites in East Africa makes it impossible to draw firm conclusions about their links to rifting.

1.5.4 Economic Importance of the East African Rift System

Economic minerals in the Rift System include Soda and Diatomite. Soda exists along the southern end of the Kenya rift in Lake Magadi, where the mineral has been extracted since 1914 (Pulfrey, 1969) and Lake Natron. Diatomite is also found in some of the rift valley lakes (Pulfrey, 1969).

The East African Rift System is remarkably devoid of metalliferous mineralisation (Dunham, pers. comm.). Copper is mined in Uganda but this is not related to the Rift System. Gold and silver have been mined in the Kavirondo region of Kenya and some copper has been located around the Elgeyo escarpment (Pulfrey, 1969).

The rift is economically useful for geothermal power. Geothermal energy is exploited within the Kenya rift and there is good potential for increasing output at various sites throughout the northern part of the eastern branch. Additionally isolated pockets along the western branch may be exploitable.

Oil and gas have been sought within parts of the rift system, such as the Rukwa and Luangwa rifts, but no reservoirs of economic importance have been located. While older rifts have the potential for oil and gas, rifts which are young and currently tectonically active seem to contain much less. Lake Kivu contains a potentially exploitable supply of gas, its source is uncertain but may be due to local volcanic activity (Fukata, 1984). Coal, of pre-rift age, has been mined along parts of the southwestern rifts and Zambesi valley, the rift exposing it by large-scale faulting.

1.6 Mesozoic Rifting

Rifting has not been confined to that associated with the current East African Rift System but has continued throughout the geological history of the build up of the continent. Many of the oldest phases have undoubtedly been overprinted by orogenesis

and more recent rifting episodes, however, features from failed rifts in the region are still traceable (e.g. Rosendahl, 1987).

The Anza rift, figure 1.14, crossed northern and eastern Kenya during the Jurassic (Reeves *et al*, 1987; Bosworth, 1992). This rift linked with the more extensive central African rift (e.g. Browne & Fairhead, 1983) which extended throughout much of southern Sudan and on to Libya. The scale of rifting is comparable to the East African Rift System of the present time. The Anza rift is now largely covered by Cretaceous to Quaternary sediments but its location, using geophysical techniques, has led Reeves *et al* (1987) to suggest that it is a failed arm of a triple junction at the current coast of Kenya. They further suggest that Madagascar was located in the south-eastern sector of the triple junction.

The development of the central African rift is thought to have taken about 100 Ma (Bosworth, 1992) compared to the upper limit of about 30 Ma for the East African Rift System (Baker & Wohlenberg, 1971). Three phases of rifting have been recognised in southern Sudan, each associated with thermal subsidence or isostatic uplift (Schull, 1988). Bosworth (1992) suggested that each of these three phases was comparable, in duration, to that in some failed rift zones such as the Gulf of Suez.

The Kenya sector of the East African Rift System cuts the Anza rift in northern Kenya. The intersection angle is about 45° yet there is no evidence of reactivation in the Anza rift and seemingly no directional control of the present rift valley. Thus rifting here does not follow pre-existing structures (cf. McConnell, 1972).

1.7 Palaeozoic Rifting

In the localities of Lakes Tanganyika, Malawi and Kariba there are zones of rifting which were initiated in the Karoo (Permian), figure 1.15. Sections of these rifts have been reactivated or reoccupied during the current rifting cycle (Rosendahl, 1987), areas such as the Rukwa rift zone and parts of the Malawi and Tanganyika rift zones. The term reoccupation is used here to denote the fact that in these regions the current rifting has crossed older rifting but there is little evidence for actual reactivation of the pre-existing structure in all but the Rukwa rift.

The Karoo rifting was largely oriented in a SW-NE direction and included regions such as the Luangwa and Kariba valleys as well as a number of old rifts to the north and east

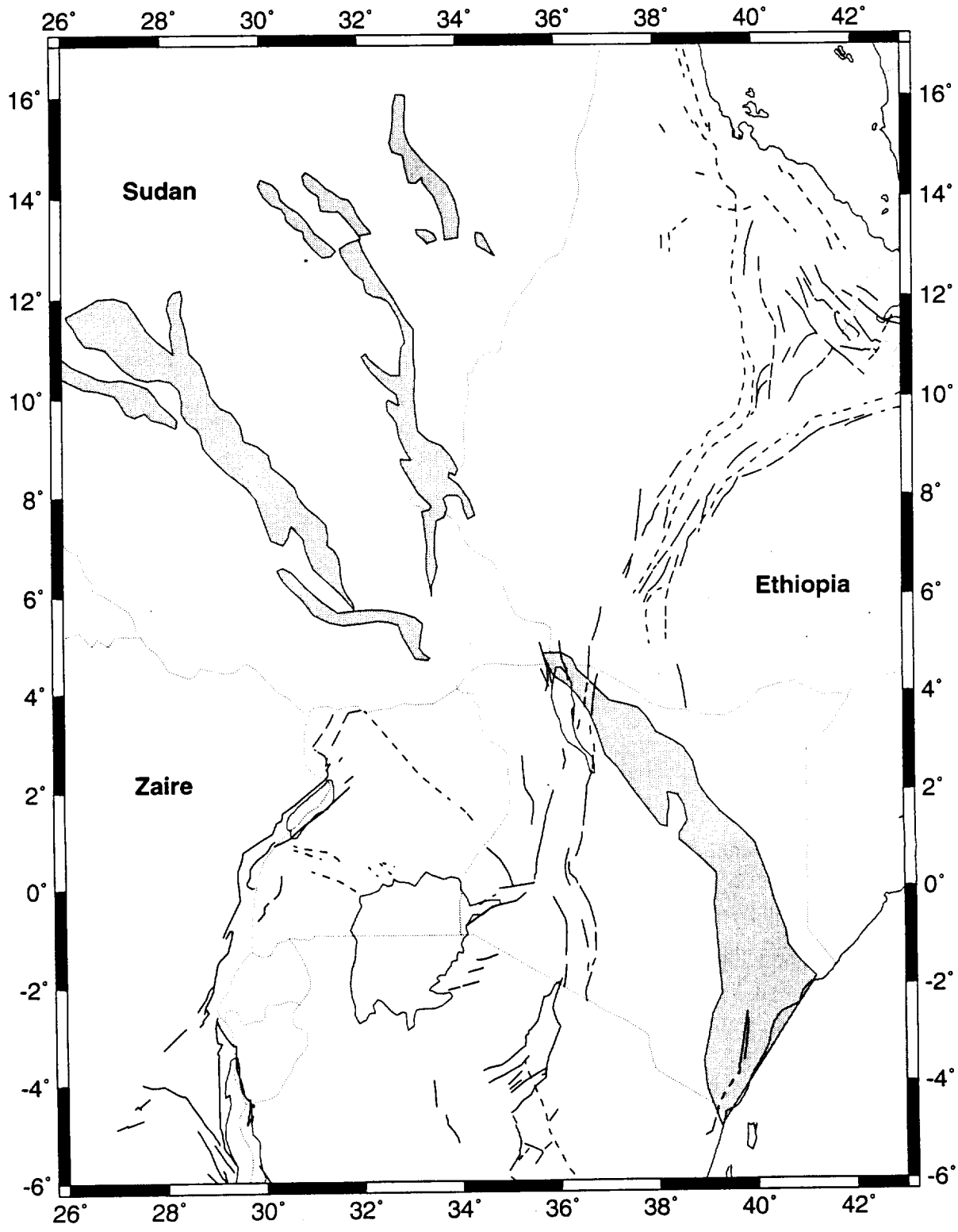

Fig. 1.14. The NW - SE Anza rift system (shaded), including south Sudan and Nile rifts, from Bosworth (1992).

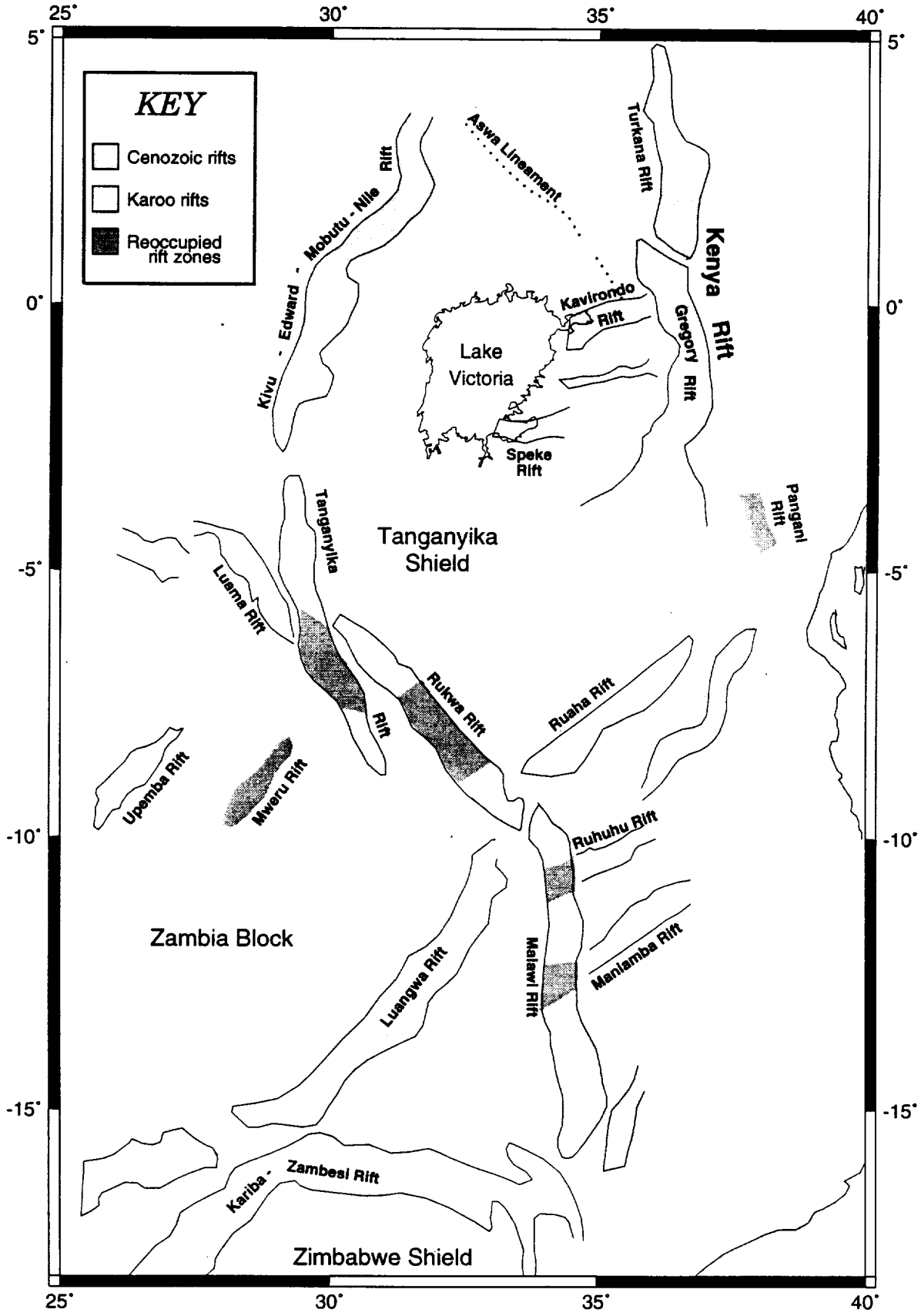

Fig. 1.15. Sections of the East African Rift System and Karoo rifts, from Rosendahl (1987).

of Lake Malawi. A second NW-SE orientation is observed for the Luama rift zone which lies to the west of Lake Tanganyika and in line with the Rukwa rift. The Zambesi Valley is also thought to have been rifted in the Karoo. There is some argument as to whether these Karoo rifts are still active or might be reactivated as a conduit for propagation of the East African Rift southwards. Rosendahl (1987), Figure 1.15, firmly separates the Cenozoic and pre-Tertiary (Karoo) rifting while McConnell (1972) groups them all together, claiming that Cenozoic reactivation has occurred within these pre-Karoo rifts. Karoo rifting in the Lake Rukwa area has been reactivated in the Cenozoic and the presence of seismicity along the south-west trending Karoo rifts such as the Luangwa Valley suggest that they are experiencing some form of reactivation.

1.8 Precambrian (Cratonic) Framework of Africa

There have been seven major orogenic cycles affecting the African continent which can be identified from existing geological remnants (Clifford, 1970), these are summarised in table 2.1.

	Dates. Ma	Orogeny name
1	3000	
2	2700 ± 200	Shamavian
3	1850 ± 250	Eburnian (Ubendian) & Huabian
4	1100 ± 200	Kibaran
5	600 ± 200	Damaran & Katagan (Pan African)
6	400 - 200	Acadian & Hercynian
7	200 - 0	Alpine

Table 2.1. The orogenic events effecting the African continent.

Only the Acadian/Hercynian and Alpine cycles have not affected the region surrounding the East African Rift System. The regions that have been unaffected since about 2500 Ma are considered to be the nuclei around which the cratons have grown.

1.8.1 African Nuclei

Only three of the cratonic nuclei in Africa, figure 1.16, border the East African Rift System; these being:

Africa: Oldest Nuclei

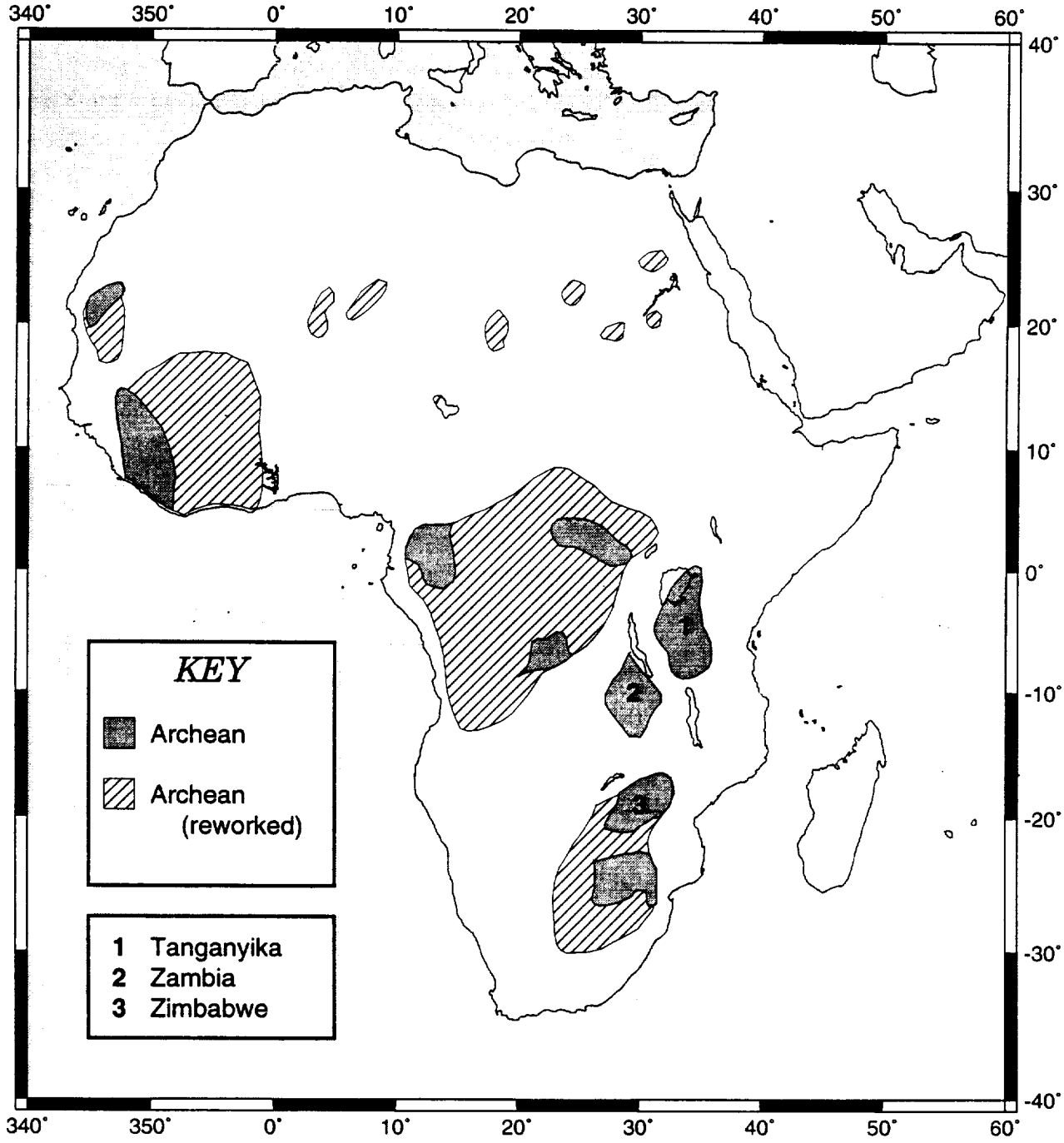

Fig. 1.16. Regions of the African continent which have remained stable since the Archean (3400 Ma), from Hargraves (pers. comm.).

(1) The Tanganyika nucleus.
(2) The Zambia nucleus
(3) The Zimbabwe (Rhodesia) nucleus.

1. THE TANGANYIKA NUCLEUS

The Tanganyika (Dodoma-Nyanza) nucleus makes up most of the Victoria Block and is, virtually surrounded by the western and eastern branches of the rift system. The northern portion of the nucleus is characterised by acid and basic volcanic rocks and quartzites overlain by medium to fine grained sediments (Clifford, 1970). Radiometric dating indicates an age of at least 2300 Ma though probably much older (Cahen & Snelling, 1966). Further south the nucleus rocks are probably at least 2550 Ma and some are almost certainly older than 2900 Ma (Clifford 1970).

2. THE ZAMBIA NUCLEUS

McConnell (1972) refers to the Zimbabwe and Tanganyika nuclei as the Rhodesian shield and Tanganyika shield respectively. The term 'shield' is used to denote a "craton of early Precambrian rocks outcropping as a broad topographic dome flanked by younger tabular cover of fold belts" (McConnell, 1972). However, McConnell refers to the Zambia nucleus as the 'Zambia block'. The 'block' differs from a 'shield' in having "syneclises of Proterozoic or Phanerozoic rocks", i.e. the Zambia nucleus differs from the other two in having some post-Precambrian rocks, in sag basins, but acts in the same way as other cratonic regions.

3. THE ZIMBABWE NUCLEUS

The Zimbabwe nucleus borders on the southern end of the Malawi rift to its east and on the Zambesi valley and Lake Kariba area to its north and north-west. Radioactive dating (K-Ar, Rb-Sr, and U-Th-Pb) give ages of 3300 Ma (Vail & Dodson, 1969) with ages of up to 2700 Ma being determined by Nicolaysen (1962). The Great Dyke cuts across the region for about 480 km in a NNE direction and has been dated at 2500 - 2800 Ma (Alsopp, 1965).

1.8.2 Cratonic Evolution

The African cratons and nuclei shown in figures 1.16, 1.17, and 1.18 are their present day locations within the continent. The building Africa has involved the accretion of old continental plates by plate tectonic processes, thus these cratons would not have been at the locations shown at the times indicated but may have been separated by considerable distances. Linear belts between cratons were formed as part of this collision and accretion process.

The Eburnian orogenic events (1600 to 2100 Ma) affected a number of linear belts in East Africa, figure 1.17. The Ubendian belt, between the Zambia and Dodoma-Nyanza nuclei, is characterised by crystalline rocks and has a lower age limit of 1800 Ma (Clifford, 1970). The Ubendian belt extends for over 500 km from northern Malawi into Zaire, on the western side of Lake Tanganyika, and has almost certainly dominated later tectonics in northern Malawi (McConnell, 1972). The corresponding belt between the Transvaal and Zimbabwe nuclei, the Limpopo belt, also suffered orogenesis during this cycle. In Uganda the Burganda-Toro was another such region and has, like the Ubendides, been dated at 1800 ± 100 Ma, as a lower limit, (Cahen & Snelling, 1966). Other regions affected by the Eburnian include much of Angola and the southern Zaire (Congo) basin and much of north-west Africa.

Since the end of the Eburnian, four regions of the continent have been stable, figure 1.17. Three of these zones border the East African Rift System; in the case of the Tanzania craton this is now traversed, by the Tanganyika - Rukwa - Malawi shear zone, along the line of the Ubendian Belt.

The Kibarides, between the Tanzania and Angola cratons, was affected by the Kibaran Orogeny of 1100 ± 200 Ma with intruded granite in the 850 - 1100 Ma age range, figure 1.18. The Kibaran belt extends from the Upemba Lakes region in a NNE direction to Uganda and lies unconformably on the Buganda-Toro (Clifford, 1970). The Irumides of eastern Zambia are also of Kibaran age (Cahen & Snelling, 1966), where they follow the general trend of the Luangwa valley.

Following the Kibaran the Kibarides have been incorporated into the block forming the Congo Craton. This cratonic region extends form the west coast of Angola to eastern Tanzania and from the Central African Republic south to southern Angola. The post-Kibaran craton in Southern Africa extends to cover most of South Africa and Zimbabwe as well as southern Namibia and Botswana, figure 1.18.

Africa: Nuclei at 1600 Ma

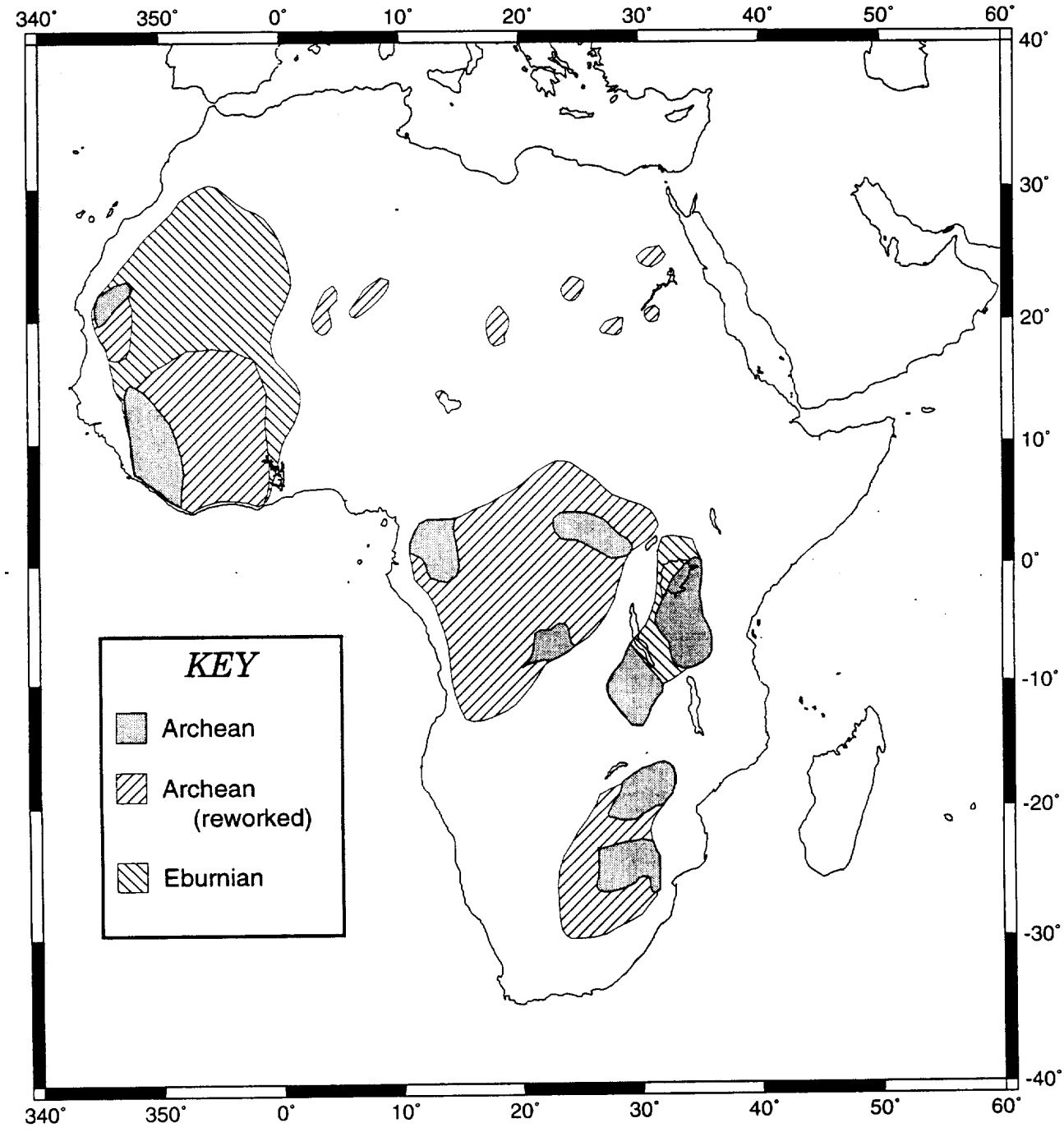

Fig. 1.17. Regions of the African continent which have remained stable since the Eburnian (1600 - 2100Ma), from Hargraves (pers comm).

Africa: Nuclei at 850 Ma

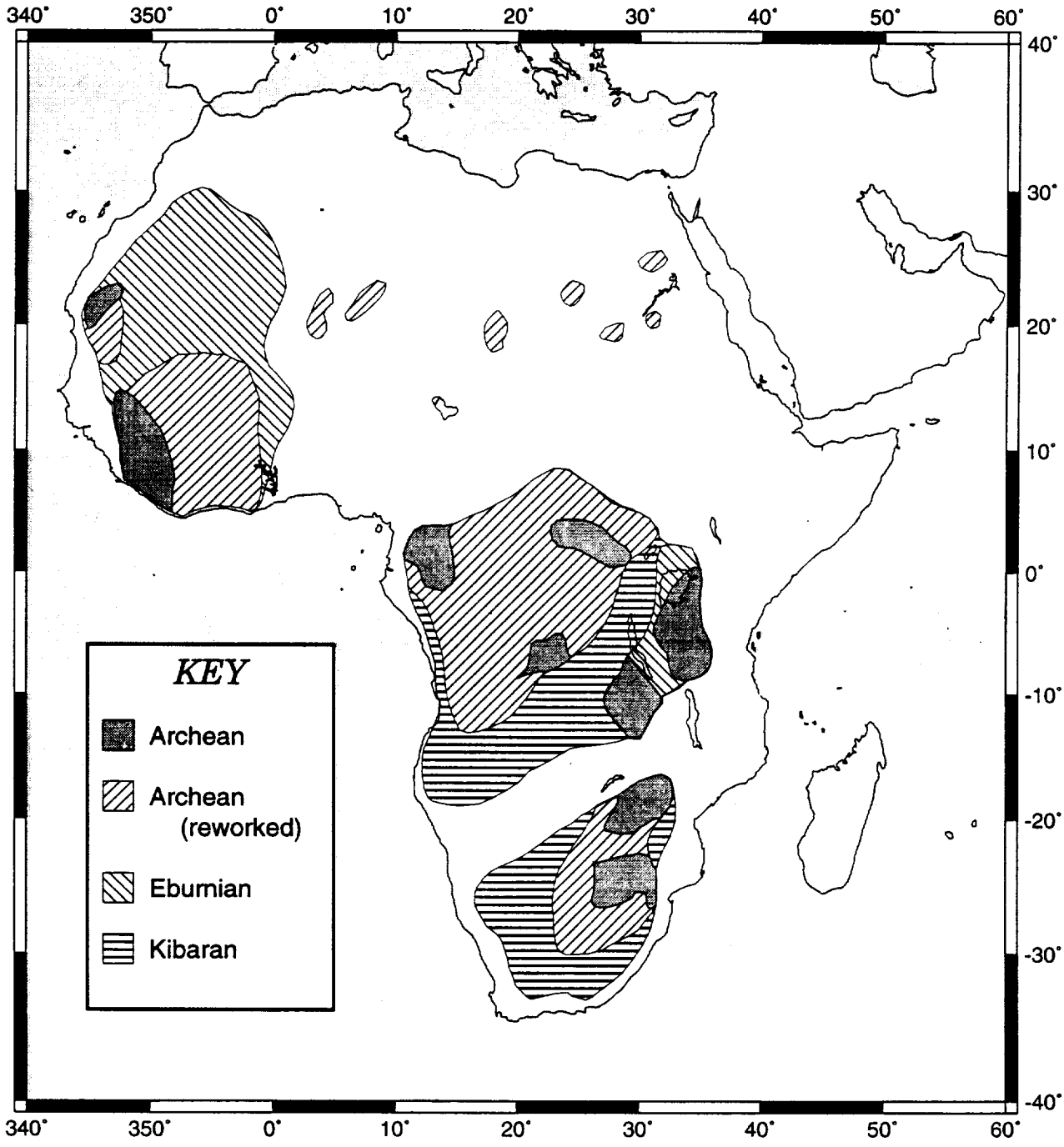

Fig. 1.18. Regions of the African continent which have remained stable since the Kibaran (850 - 1100 Ma), from Hargraves (pers. comm.).

The Damaran and Katagan, or Pan African, Orogeny had widespread affects over much of the remainder of Africa. In many areas bordering the cratons there are zones of deformed Precambrian sediments while elsewhere the 'Pan African' is shown as regions of rejuvenated basement.

The Mozambique belt is roughly equivalent to the Katagan, being dated at between 900 and 450 Ma (Cahen & Snelling, 1966). The Mozambique belt skirts the Zimbabwe craton and extends northwards through Mozambique, eastern Tanzania, Kenya and into Ethiopia (McConnell, 1972). It is of particular importance due to the fact that it parallels Lake Malawi and the majority of the eastern branch of the East African Rift System.

The most recent orogenic cycles, since 400 Ma, have not affected East Africa. The Acadian and Hercynian is traceable in the Anti-Atlas and west coast of North-west Africa as well as in the Cape Fold Belt on the southern tip of the continent. The Atlas Mountains are the only manifestation of the Alpine Orogeny.

1.9 Influence of Earlier Structures on Cenozoic Rifting

The influence of older structures on the location of Cenozoic rifting has been the basis of much discussion; McConnell (1972) pointed out that the rift followed the more recent mobile belts in preference to the older cratonic regions, figure 1.19 bears out this observation. The Cenozoic rifting skirts the old Archaean cratons with few rifting features seen within the nuclei. The Kenya rift follows the eastern edge of the Tanganyika craton while the western branch, from the Aswa lineament to southern Lake Tanganyika, follows the Kibaran belt along the western edge of the Tanganyika craton. The Rukwa rift follows the Ubendian belt between the Tanganyika craton and Zambia block. Other faulting indicated on the UNESCO tectonic map (1968), figure 1.19, skirts the eastern and southern edges of the Zambia block while other faulting is seen to the northern and eastern edges of the Zimbabwe craton.

McConnell (1972) considered that much of the eastern branch was intimately associated with the Mozambique belt and its track through Kenya was due to pre-existing structure within the Mozambique mobile belt. Baker *et al* (1972) argued that the idea of 'resurgent tectonics' was flawed and that while some Precambrian structures have been followed in Kenya this is the exception rather than the rule. The Kenya and Ethiopia rifts meet the Anza rift in northern Kenya: there is no evidence of reactivation in the direction

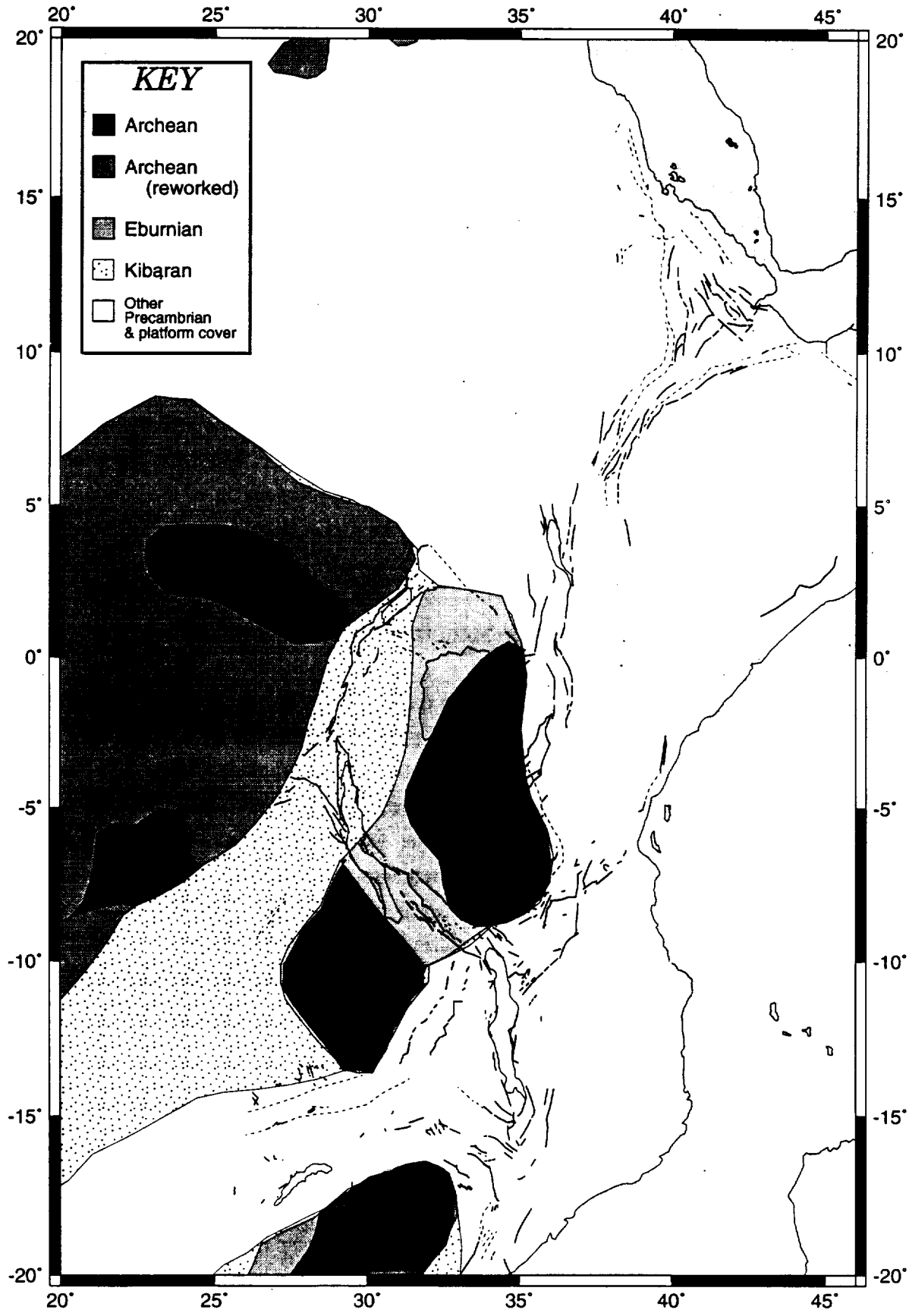

Fig. 1.19. Cratonic framework of East Africa, from Hargraves (pers comm).

of the Anza rift but the offset in the eastern branch may be related to the older rift structure in the region.

Figure 1.15 (Rosendahl, 1987) indicates that the Rukwa rift and sections of the Tanganyika and Malawi rifts have been reoccupied in the Cenozoic. Only the Rukwa rift shows signs of reactivation of older structures, in particular the Lupa fault (Rosendahl, 1987). While the Tanganyika rift crosses the Luama rift and the Malawi rift crosses both the Ruhuhu and Maniamba troughs there is little evidence for reactivation or structural control exterted by the older rifts (Rosendahl, 1987).

1.10 Causes of Rifting

Despite the fact that rifting has been studied for over 100 years the comprehension of the processes that govern it are still unclear. While the theory of plate tectonics has generally been accepted the details are still uncertain and this is particularly true in the case of continental rifting.

The hypotheses of rifting can be split into 'local' and 'remote' causes. In simple terms, one mechanism by which rifting occurs is intimately associated with a local effect while the other hypothesis accounts for rifting as a result of more distant phenomena. With local causes the location of rifting is an inevitable consequence of the cause while in the remote model the location of rifting is not ordained by its cause. Thus one might expect rifting caused remotely to follow pre-existing fabric, lines of weakness, while in the local model rifting would be more likely to follow its own course.

Local causes of rifting are usually seen to be a response to regional uplift, arching or doming, or isostatic readjustment. The concepts behind this general model are the older of the two, being supported by Gregory (1896, 1921). While the local theories have been conveniently grouped together they are diverse: the causes of doming provide one such problem. Doming could be considered to be the result of compression of the plate or to be the result of asthenosphere upwelling or diapirism. Gass (1975) considered the East African Rift System to be the result of two domes (Ethiopia and Kenya) which have resulted in the complete rift system as seen today.

The remote models are generally more recent (e.g. Baker *et al*, 1972). These models require that subsidence occurs first and that doming occurs due to isostatic adjustment.

The initial subsidence is due to stretching and thinning of the lithosphere due to regional plate stresses.

One addition to the argument was presented by Brown & Girdler (1980). This considered lithospheric thinning and seismicity to attempt to suggest whether rifting followed thinning or *vice versa*. The evidence for lithospheric thinning was partly based on gravity measurements over the region. The presence of distinct zones of seismic activity outside the region of lithospheric thinning lead to the conclusion that rifting precedes thinning. While this is true there is also thinning in regions where there is no seismicity and no evidence of major rifting such as across Angola, thus the situation would appear to be more complex.

Neither local nor remote models contain clear-cut arguments and it is frequently accepted that different models may be relevant to different rifts (e.g. Baker & Morgan, 1981).

It has been argued that Africa presently provides a stationary reference frame in the consideration of continental drift (e.g. Burke & Wilson, 1972) yet the continent is surrounded to the west, south and east with oceanic spreading centres. Pavoni (1989, 1992) suggested a simple convection hypothesis for the Earth using a bicellular model. In this model two nodal, but diffuse, plumes are considered to be upwelling; one below Africa and the other under the Pacific Ocean. The diffuse nature of the upwelling would give rise to differential and increasing rates of drag away from the central node. This model is then able to explain ridge movement away from Africa as well as the paring off of Madagascar and the rifting in East Africa.

Local seismic tomography has been used to investigate the Kenya rift (Slack & Davis, 1994). The results of modelling the lithosphere below the Kenya rift indicate a 12% increase in P-wave velocities below the rift itself and a 6% positive anomaly over a wider zone, extending to about 165 km. The models tend to point towards the existence of a plume below the rift, consistent with a local model for rifting but not totally inconsistent with the remote causes. The hot plume would account for the 12% anomaly while the interface zone between plume and lithosphere would account for the broader, 6%, high.

In conclusion, the two models of rifting (local and remote) can both be successfully applied to the East African situation. Recent developments, in particular seismic tomography, however, would hint more strongly towards a local plume below the rift zone as the cause of rifting in the area (e.g. Slack & Davis, 1994). Unfortunately the

local and remote causes hypotheses are not clear cut and it could be argued that a remote process initiated what is now a locally driven rift. Overall, the evidence would seem to point towards a locally driven rifting process in East Africa but it is not possible to discount any role played, either now or in the past, by more remote processes.

CHAPTER 2

Satellite Imagery and Data Processing

2.1 Advanced Very High Resolution Radiometer

2.1.1 The sensor

Advanced Very High Resolution Radiometer (AVHRR) data are acquired on the National Oceanographic and Atmospheric Administration (NOAA) series of satellites. The satellites are in near-polar, sun synchronous orbit at a nominal altitude of 833 km. The fact that they are sun synchronous means that they pass over the same point twice daily (once in ascending and once in the descending orbit segment) at the same local time from day to day. For NOAA-9 the equatorial crossover times are approximately 0100 and 1300. The AVHRR sensor is a cross track, or line scanning system, with a mirror sweep of ±55.4°, corresponding to a view swath of about 2900 km.

The AVHRR sensor acquires 5 bands of data ranging from the visible to the thermal infra-red part of the spectrum. The scene is transmitted as 10 bit data with thermal band calibration information imbedded within it. Figure 2.1. shows the spectral response for each of the 5 wave-bands on the NOAA-9 satellite. The wave-bands for the AVHRR sensor are listed in table 2.1.

Band	Wavelength (μm)	Description
1	0.58 - 0.68	Red Visible
2	0.725 - 1.10	Near Infra-Red
3	3.55 - 3.93	"
4	10.30 - 11.30	Thermal Infra-Red
5	11.50 - 12.50	"

Table 2.1. Wave-bands of the AVHRR sensor, from Kidwell, 1986

Normal operation obtains data in the global area coverage (GAC) mode of approximately 4 km resolution, at nadir. Local area coverage (LAC) mode acquires data at 1.1 km resolution at nadir with a sampling interval of about 780 m. The 2900 km swath width means that towards the image edges the resolution is significantly reduced. 2048 pixels make up each scan line.

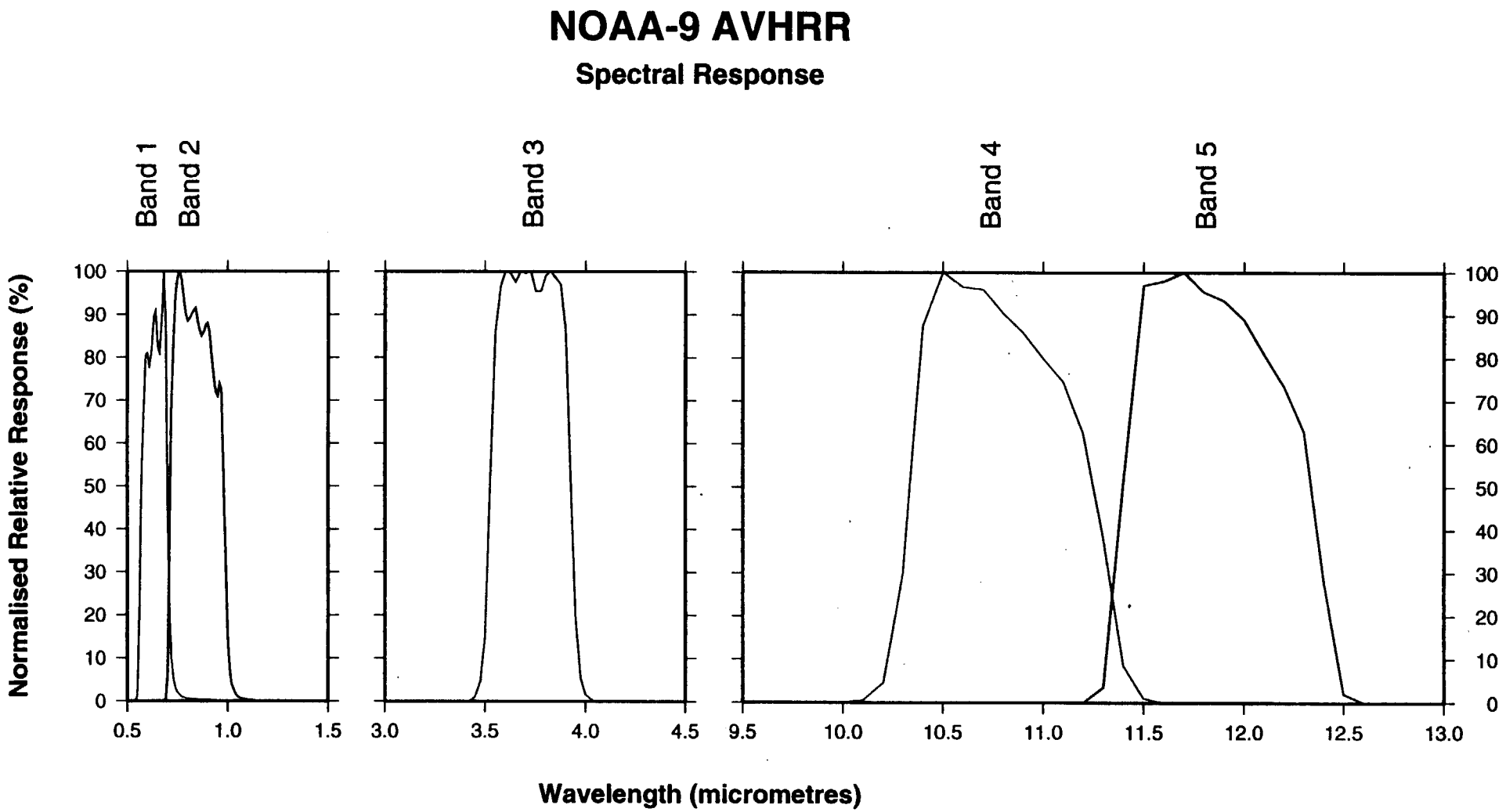

Fig. 2.1. Spectral response for the AVHRR sensor on the NOAA-9 satellite, (red, band 1, through to thermal infra-red, band 5), from Kidwell (1989).

Within sight of an Earth receiving station data are downloaded as they are acquired, however, out of range of such a station only 10 minutes of LAC data can be stored on the satellite. For this reason the sensor is usually run on the GAC mode to enable better areal coverage, for the meteorological design role of the satellite.

Calibration with a stable black body and space is carried out for the infra-red channels while no in-flight calibration is performed on the visible bands (Kidwell, 1986). Bands 1 and 2 use a silicon detector, band 3 indium antimonide and bands 4 and 5 mercury cadmium telluride.

Band 3 is frequently rather noisy and tends to be of limited use for ground surface studies. Also, bands 4 and 5 are very similar in their response to surface conditions with a slight offset being almost all that normally separates them.

Before an AVHRR data-set is usable for interpretation there are a number of processing steps that need to be carried out. This processing removes distortion; converts the original 'pixel - line' format into latitude - longitude; and enhances the image to make full use of the available colour output. A flow diagram of the processing carried out on an AVHRR image is given in figure 2.2.

2.1.2 Image Distortion Corrections

Due to the method of acquisition the distortions of the images are particularly pronounced near the scene edges. Later steps of rectification are simplified if this distortion is removed first. Legackis & Pritchard (1976) derived an algorithm to carry out this correction, (Appendix E). The correction is given by:

$$\tan\left(\frac{I\omega}{S}\right) = \frac{[\sin(\frac{DN}{R})]}{Y}$$

Where:

$$Y = \left[\frac{a+R}{R} - \cos\left(\frac{DN}{R}\right)\right]$$

And:

	a	Satellite altitude
	D	Distance between samples on image after correction
	I	Original sample number from nadir
	N	New sample number, (N = 0,1,2, etc.)
	S	Sampling rate of radiometer

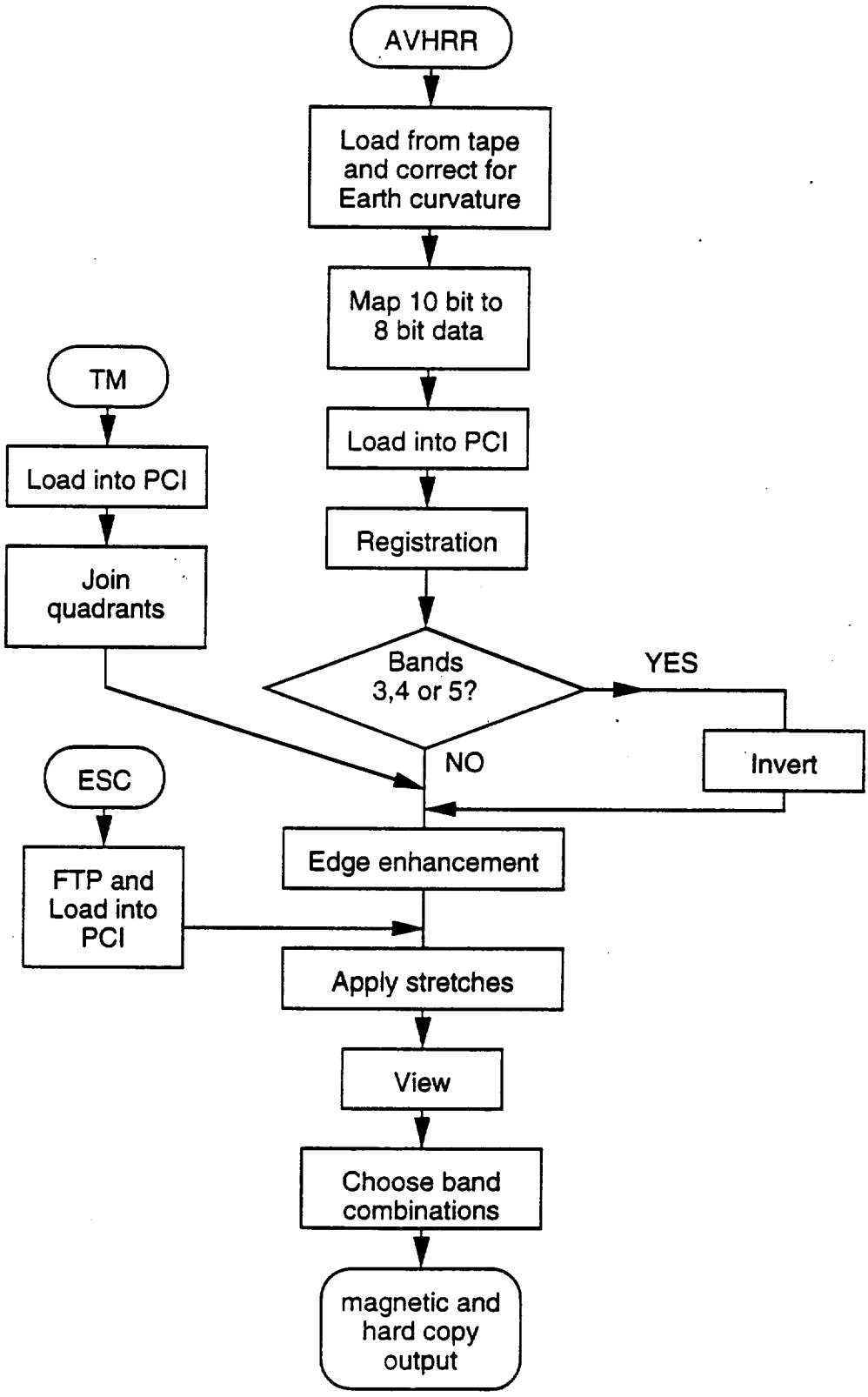

Fig. 2.2. Flow diagram of the processing sequence for AVHRR and other remote sensing data used.

R Earth's radius

ω Radiometer scan rate (rpm)

The software used to read the data from the 9 track tapes, i.e. *LACIN* in LAS (see appendix C), incorporated this correction. Any distortion errors that occurred during this correction were eliminated in later rectification. Other corrections to account for Earth rotation and satellite attitude errors were also discussed by Legackis & Pritchard (1976) but these were not applied as rectification by standard techniques could be used to provide more consistent and accurate resultant scenes. The accuracy achieved by using the algorithms is sensitive to slight errors in constants and requires information about the satellite which was not fully available. The partially corrected images are only slightly distorted from the 'real' situation, they are inclined at about N14°W and are slightly skewed, due to the orbital path of the platform and Earth rotation effects.

AVHRR imagery is acquired in 10 bit format but the full range is rarely used and a reduction to 8 bit format is desirable for later stages. The data transformation was carried out using *MAP* in LAS. The image data were then transferred to the image processing package PCI. Further details of the processing packages and main commands used in processing are given in Appendix C..

2.1.3 Image Rectification

Rectification of the images was carried out manually, i.e. latitude and longitude positions of certain points were found with an atlas and these were then located on the image as Ground Control Points (GCPs). For consistency the Times Atlas (1956) was used throughout to estimate latitudes and longitudes. For overlapping images the same GCPs were used wherever possible so as to reduce discontinuities between scenes.

Image registration can be carried out using 1st to 5th order polynomial fitting techniques in PCI. First order will simply rotate, stretch and scale the scene but will not account for a contorted image. Higher order transformations are non-linear and are able to contort the image in more elaborate ways to create as good a fit as possible.

For a first order transformation the polynomial used would take the form of:

$$x_0 = a_0 + a_1 x_i + a_2 y_i$$
$$y_0 = b_0 + b_1 x_i + b_2 y_i$$

Where:

x_i and y_i are input co-ordinates,

x_o and y_o are the output (rectified) co-ordinates,

a_i and b_i are the transformation coefficients, computed from the GCPs.

Extending this for a transformation of order 3 would give:

$$x_0 = .A + Bx + Cy + (Dx^2 + Exy + Fy^2) + (Gx^3 + Hx^2y + Jxy^2 + Ky^3)$$

similarly for y_O.

Where: A, B, C, D, E, F, G, H, J, K are transformation coefficients,

Where all combinations of x and y are used such that: $i + j \leq 3$.

The higher the order of transformation the more ground control points (GCPs) are required, as they are needed to calculate the coefficients in the above polynomials. Table 2.2 gives the minimum number of GCPs required for different orders of rectification.

ORDER	MINIMUM no. GCPs
1	3
2	6
3	10
4	15
5	21

Table 2.2. Minimum number of ground control points required for different order rectification in PCI.

It is usually advisable to have at least twice the minimum number of GCPs for a reasonable registration attempt. Wherever possible, GCPs are evenly spread over the full scene.

The distortion of the AVHRR scenes did not necessitate a transformation of more than order 3. At least 20 GCPs were used on each scene. The GCPs were chosen to give as good a spread as possible though were concentrated in the regions of interest.

The relatively low resolution of AVHRR imagery means that GCPs are not always easy to find. Road intersections, buildings and most rivers cannot be seen on the scenes

meaning that GCPs are generally restricted to lake and sea shorelines as well as distinctive features on a few of the larger rivers. The problem with using lake shoreline features in Africa is that many lakes change shape periodically, either seasonally or over longer periods. This lake level variation is generally more pronounced for the shallower lakes of the eastern branch of the East African Rift System and in Afar. Care was taken to make sure that the shape and size of the lakes on the maps and imagery matched before GCPs were positioned. This criterion meant that it was not possible to locate points around Lake Rukwa as the shape on the imagery is completely different from that seen on any maps.

GCPs were positioned on the imagery using the *GCIT* routine in PCI. The images were registered using *REG* with order set at 3. Once registered, the images were checked to make sure that the registration was correct; occasionally errors had occurred during input of the GCPs and these became evident after registration. Extraction of the required section of the full scene was also carried out with *REG*. The registration process required the original data to be resampled into a new grid; for this a cubic convolution was used.

Cubic convolution is the most accurate way of resampling data into a new grid. Simpler resampling techniques are the nearest neighbour and bilinear methods but these tend to suffer from a stepped appearance and data smoothing respectively. Cubic convolution is computationally intensive but this is not a particularly big problem with the AVHRR subscenes. The technique uses the 16 closest values to the resampling point (c.f. 1 for nearest neighbour and 4 for bilinear), with pixels further away having less weight than the closer ones.

Errors

Cross checking the GCP locations back from the corrected image to their map latitudes and longitudes allows the errors involved in the procedure to be quantified. The error in locations did not exceed 0.05° (about 5 km) and were typically less than this (0.01° to 0.03°, about 1 to 3 km). The larger errors were extant nearer the edges of the scenes with the most accurate reproductions being the case in the centre where the majority of the features of interest were located.

Taking into consideration the errors inherent in locating the original GCPs and possible mapping errors the inaccuracy in location of features on the AVHRR imagery to their true ground position is of the order of ± 2 km, or about 3 pixels. Higher accuracy may

have been achievable with highly accurate and up to date maps of the area but these are generally lacking. It is also difficult to obtain an accurate pixel positioning for features on AVHRR and thus it is unlikely that much improvement on the ± 2 km error would be attainable with current resources.

2.1.4 Infra Red Inversion

The AVHRR sensor is designed for weather studies and as a result of this the infra-red bands (3, 4 and 5) are inverted as this causes clouds to look white. While good for weather studies this does not aid geological interpretations as cold areas appear 'hot' and *vice-versa*. To counteract this, the three infra-red bands were inverted prior to further image enhancements.

Image inversion was carried out using a simple linear mapping as illustrated in Table 2.3. This inversion follows the equation:

$$N_o = 255 - N_i$$

Where: N_i = Input pixel value (0 - 255)
N_o = Output pixel value (255 - 0)

Original Value	New Value
0	255
1	254
2	253
:	:
127	128
128	127
:	:
255	0

Table 2.3. Examples of mapping for an image band inversion

2.2.5 Edge Enhancement

Edge enhancement is used to highlight edges on an image: strong linear features and sharp breaks in intensity will be picked out and their effects enhanced. In this study edge

enhancement was carried out to highlight linear tectonic features. This was done using the routine *FSHARP*, in PCI.

A 3 by 3 pixel filter was used which can be represented by the equation:

Output DN = [2 x original DN] - [neighbourhood average DN]

DN being the pixel values in the filter array. The Output DN is the new value for the centre pixel.

Edge enhancement can also be represented by a filtering matrix:

-1	-1	-1
-1	17	-1
-1	-1	-1

x 1/9 = DN

An example set of data would give:

67	70	80
66	69	77
62	65	68

→ **68**

2.1.6 Linear Stretching

The linear stretch is the simplest form of stretch that can be applied to image data. A stretch is applied so as to utilise the full range of available greyscale values (0-255 for 8 bit data). Almost all images acquired by satellite use only a small segment of the scale hence the need for stretching: this is illustrated in figure 2.3. Figure 2.3A shows a pre-stretched image, 2.3B the histograms for the original data and stretched data; and 2.3C shows resultant image (the figure is illustrative, only, and is not at full image resolution). The linear stretch illustrated here maps the original values in the range 40-120 to the new range, 0-255. Original data which falls below 40 are assigned 0 on the new scale; likewise data above 140 becomes 255.

The linear stretch can be carried out selectively. For example, the original data may stretch from 20 - 200 but values below 40 may be related to water bodies and values above 140 may be associated with clouds. Thus for geological and tectonic studies

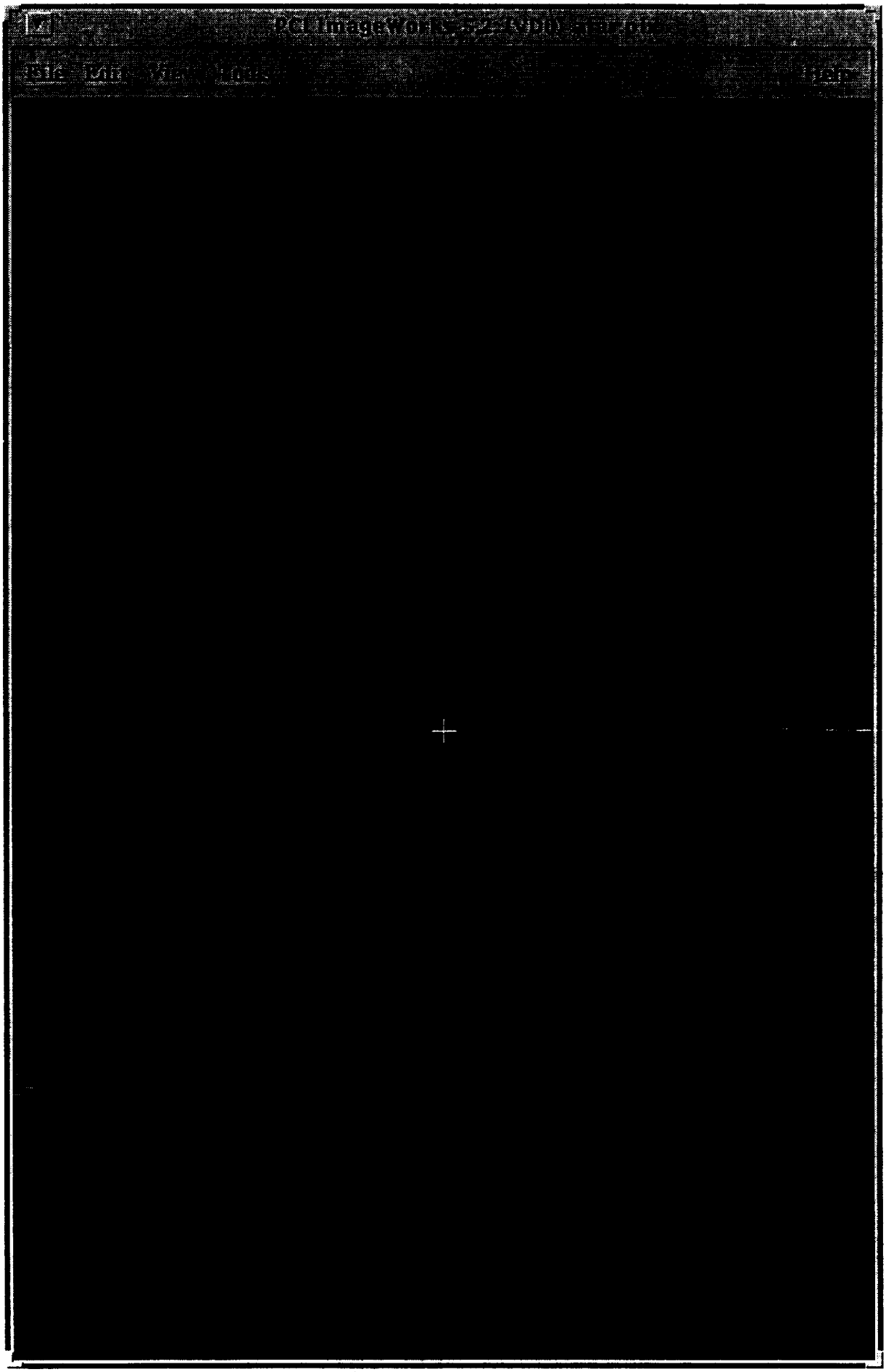

Fig. 2.3A. AVHRR B211 = RGB image of Afar prior to application of linear stretch.

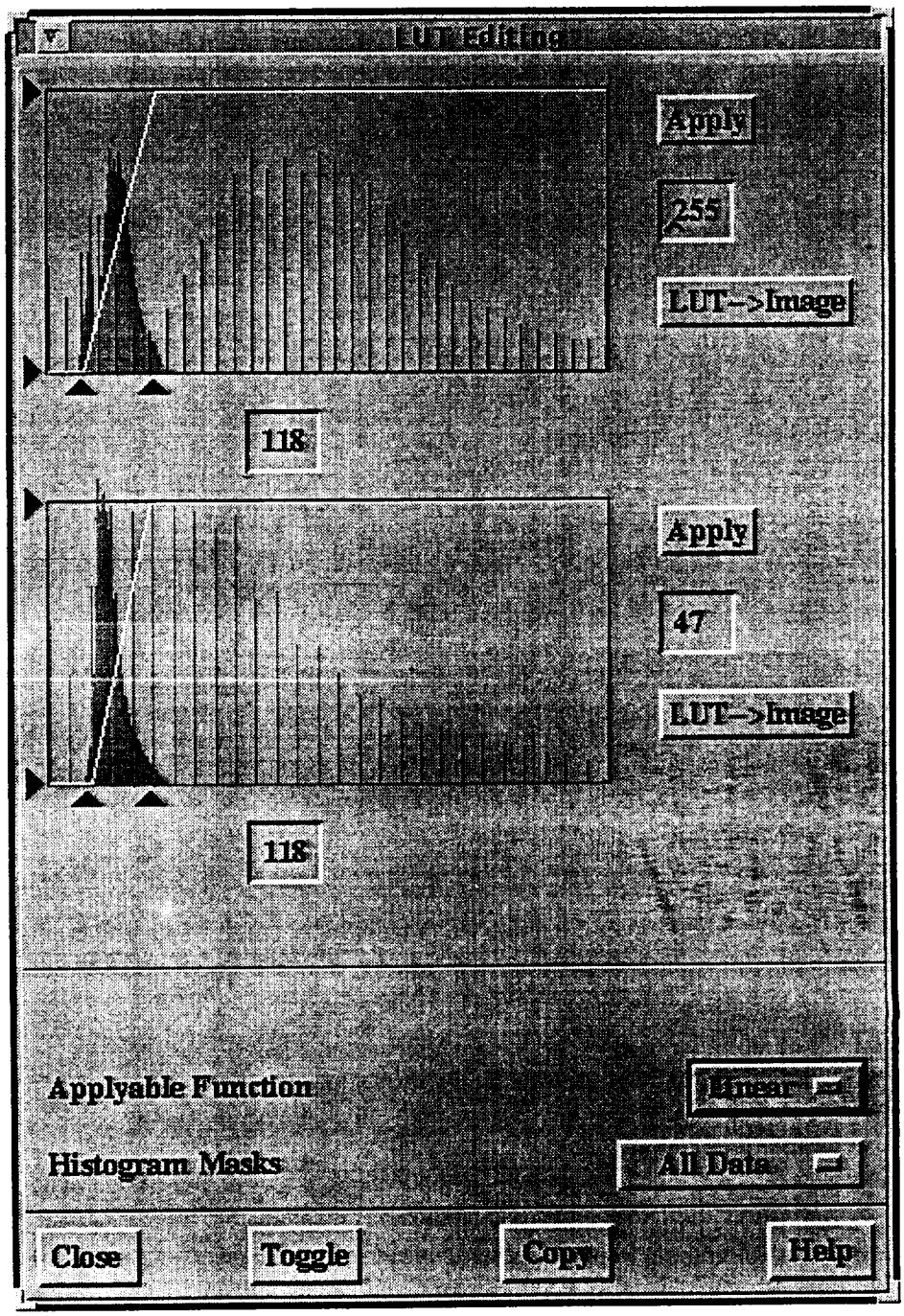

Fig. 2.3B. Stretches applied to bands 1 & 2 of the AVHRR scene of Afar (figure 2.3A). Upper histograms refer to band 1, lower ones to band 2. Grey-green shaded histograms refer to the original data. The white line indicates the linear stretch applied and the red and green line histograms are for the data with stretch applied. The image resulting from the application of the linear stretch is given in figure 2.3C.

Fig. 2.3C. AVHRR B211 = RGB image of Afar after application of linear stretch.

values in the ranges 20 - 40 and 140 - 200 are of little use and the stretch in the range 40 - 140 makes the most of the useful data. This will give nearly all water bodies the value 0 and clouds the saturation value, 255. Due to various effects such as atmospherics, local weather and temperature conditions, time of year, etc. the linear stretches are both band and image specific. That is to say that all bands and images have their own, unique, stretch applied to enable features to be shown to their best advantage. It is sometimes the case that a band on one scene and its counterpart on another will have the same stretch applied but this is unusual. A stretch will only be of use for part of the scene and the area that is of particular interest must be highlighted to its best advantage, at the detriment of other regions.

A stretch can be represented, numerically, using a 'look-up table'. In the case of PCI the 'look-up table' is created using *STR* and applied to the required image band using *LUT*. The look up table is essentially gives the output value for any input value in the 0 - 255 range. For example:

LUTREP Look-Up Table Segment Report EASI/PACE 14:45 20-Apr-93

4:d3.lut Type:170 [Look-Up Table] Last Update: 14:31 20-Apr-93
Contents: lut for day band 3

	0	1	2	3	4	5	6	7	8	9	10	11	12	13	14	15
0	0	0	0	0	0	0	0	0	0	0	0	0	0	0	0	0
16	0	0	0	0	0	0	0	0	0	0	0	0	0	0	0	0
32	0	0	0	0	0	0	0	0	0	0	0	0	0	0	0	0
48	0	0	0	0	0	0	0	0	0	0	0	0	0	0	0	0
64	0	0	0	0	0	0	0	0	0	0	0	0	0	0	0	0
80	0	0	0	0	0	0	0	0	0	0	0	0	0	0	0	0
96	0	0	0	0	0	3	7	10	14	17	20	24	27	31	34	37
112	41	44	48	51	54	58	61	65	68	71	75	78	82	85	88	92
128	95	99	102	105	109	112	116	119	122	126	129	133	136	139	143	146
144	150	153	156	160	163	167	170	173	177	180	184	187	190	194	197	201
160	204	207	211	214	218	221	224	228	231	235	238	241	245	248	252	255
176	255	255	255	255	255	255	255	255	255	255	255	255	255	255	255	255
192	255	255	255	255	255	255	255	255	255	255	255	255	255	255	255	255
208	255	255	255	255	255	255	255	255	255	255	255	255	255	255	255	255
224	255	255	255	255	255	255	255	255	255	255	255	255	255	255	255	255
240	255	255	255	255	255	255	255	255	255	255	255	255	255	255	255	255

This 'look-up table', taken directly from PCI, represents a linear stretch in the range of 100 to 175, such that numbers below 101 are mapped onto the output value 0 and those above 174 are assigned the output value 255.

2.1.7 Band Combinations

Usually three of the sensor bands are chosen for viewing at any one time. This is achieved by assigning each of the three to one of the primary colours; red, green or blue, to produce a colour composite image. True colour scenes can be achieved where, as in the case of Landsat TM etc., three of the bands correspond to the detection of red, green and blue visible light. In the case of AVHRR this is not possible as only red is detected in the visible part of the spectrum.

If three out of the five AVHRR bands are chosen there are 10 possible permutations of bands as listed below:

1 2 3	1 2 4	1 2 5	1 3 4	1 3 5	1 4 5
2 3 4	2 3 5	2 4 5			
3 4 5					

However, it is possible to repeat certain bands which will yield monochrome and bicolour images. For example:

1 1 1	2 2 2	3 3 3	4 4 4	5 5 5
1 1 2	1 1 3	1 1 4	1 1 5	
2 2 1 etc....				

It is also possible to vary which bands are represented by red, green and blue, i.e.:

1 1 2 $\Rightarrow$ R G B	1 2 1 $\Rightarrow$ R G B	2 1 1 $\Rightarrow$ R G B

This may be desirable to make water bodies blue rather than green or red, for example.

Therefore, with five bands there is a total of 125 possible combinations. It is also possible to assign ratios of bands to one of the colours, giving more possibilities. It is obviously not practical to look at each of these to judge which resultant image to produce, and choices based on other arguments are made.

Band choices can be made using a number of criteria, such as; final image requirements and band quality. The noise in AVHRR band 3 and the similarity of bands 4 and 5 mean that bands 3 and 4 can be set aside for use only when necessary, such as the production of day/night images. At night only bands 3, 4 and 5 are acquired and so to get the most

from the ratioing technique ratios are made of all three available bands. Normally, for day images, only bands 1, 2 and 5 need to be considered, reducing the combinations drastically.

With the number of bands cut to three, there are still 27 possible variations meaning that other factors must be brought into play. One obvious combination would simply include bands 1, 2 and 5 as an image containing all three should contain the most information. For this combination band 5 being thermal infra red, would logically be assigned to red. Band 2 is near infra-red which often highlights vegetation well, thus green would be a reasonable colour for this. Hence the chosen combination is: 5 2 1 ⇒ R G B.

Honey (1982), Honey *et al* (1984) and Tapley (1988) used AVHRR imagery to study the geology and tectonics of parts of Australia. They concluded that bands 2 and 1 were the best for mapping of lineaments. Honey's (1982) chosen combination includes the ratio of bands 2 and 1 such that: [2/1] [2] [1] ⇒ R G B. The simpler combination of 2 1 1 ⇒ RGB provides equally good images for lineament mapping. Most of the AVHRR image mosaics used in the National Geographic Atlas (1989) used the 2 1 1 ⇒ R G B combination and this was chosen here.

In summary the chosen AVHRR combinations were:

2 1 1 ⇒ R G B
5 2 1 ⇒ R G B

2.1.8 Day-night ratioing

The day-night ratioing technique using the thermal infra-red bands on the AVHRR sensor can be used to give some idea of the different thermal properties of rocks through relative thermal inertia. Faults and zones of faulting will frequently contain brecciated country rock with a higher water content. Thermal inertia will be altered by the presence of water and other fluids in the fault and thus will be highlighted on the ratio image.

The technique of using a ratio of day to night AVHRR imagery was used by Andre & Blodget (1984) to study the Nadj fault system in Arabia. A small subset of an AVHRR scene was used for this purpose and an image of [D3/N3] [D4/N4] [D5/N5] ⇒ R G B was produced. This technique was never followed up due to the difficulties in producing the ratioed image (Blodget, pers. comm.). The distortions of the AVHRR images have been mentioned in sections 2.1.1 and 2.1.2 and these problems are compounded with the

use of day and night images of the same region, which have different orbital path orientations for the two scenes. It is also difficult to find corresponding day and night pairs for which LAC data were acquired and which are cloud free. For these reasons, only one region (25°E - 36°E, 5°S to 20°S) is considered using this technique.

A day and night image pair from August 8th 1988 was obtained and used to produce the ratio image. Rectification was carried out on both day and night scenes using as many common ground control points as possible. The problems of different orbital path directions and different cloud coverage meant that this was not always possible. Adequate rectification was found to be particularly difficult towards the scene extremities and thus the matching of the day and night images is not entirely satisfactory towards the edges. Despite the problems it was decided that in order to be consistent with the requirements of the daytime coverage the same area would be used for the ratio image. The ratios were carried out on unprocessed data, prior to infra-red inversion, and thus the band ratios appear to give the inverse of what would be expected.

2.1.9 Hard Copy Output and Coverage

The production of hard copy images was carried out at the NASA GSFC. A 'colorfire' negative was produced of the images which, like the image processing package, assigns one band to each of red, green and blue. The resultant negative is then printed in the same way as any other photographic negative.

Figure 2.4 shows the coverage of AVHRR used in this study; the images are given in plates 1 to 6 (see p126). Plate 1 centres on the Afar region, plate 2 on the Ethiopia rift and plate 3 covers the Kenya rift. The western branch is covered by plate 4, the Mobutu rift; plate 5, the Tanganyika rift and plate 6, the Malawi rift and southwestern rifts. Plates 1A to 6A show the B211 band combination while plates 1B to 6B give the B521 image. Plates 6C and 6D are of the day/night combination imagery.

2.2 Landsat Thematic Mapper and Multi-Spectral Scanner

2.2.1 Landsat sensors

The first Landsat satellite, then called ERTS-1, was launched in 1972 with the intention of acting as the first remote sensing platform that could provide continuous, high

Location of Satellite Imagery

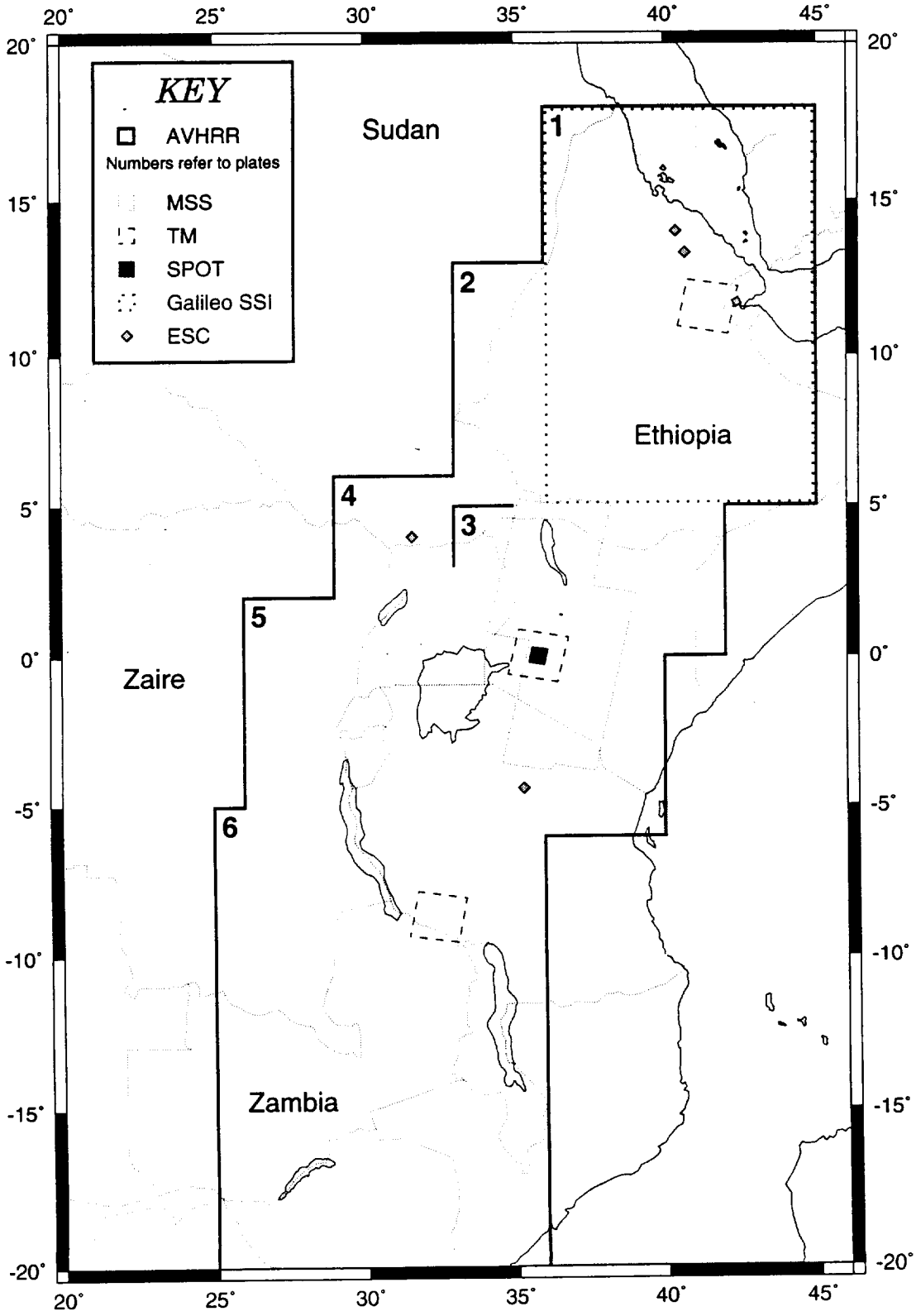

Fig. 2.4. Location and coverage of satellite imagery. Numbers refer to AVHRR plates

resolution data for civilian uses. The resolution of the first Multi-spectral scanner system was about 80 m and its potential was soon recognised in many diverse fields. Mohr (1974) used images from this sensor to map lineaments in the East African Rift System. The MSS sensor had 4 data channels, as listed in table 2.4.

The Thematic Mapper (TM) instrument was first flown on Landsat-4. This instrument has 7 bands, as listed in table 2.4, which have a ground resolution of 30 m; except for band 6, thermal IR., which has a resolution of 120m.

Band	Wavelength	(μm)
	MSS Sensor	TM sensor
1	0.5 - 0.6	0.45 - 0.52
2	0.6 - 0.7	0.52 - 0.60
3	0.7 - 0.8	0.63 - 0.69
4	0.8 - 1.1	0.76 - 0.90
5	-	1.55 - 1.75
6	-	10.4 - 12.5
7	-	2.08 - 2.35

Table 2.4. Channels on the Landsat MSS and TM sensors

2.2.2 Landsat TM data processing

The processing for Landsat TM imagery is also shown in the flow chart, figure 2.2. Rectification was not carried out as the distortions in a TM scene are minor and it is easier to reference the resultant interpretation rather that the initial image. Rectification of the original image also requires too much computer processing time and capacity to make it worthwhile.

Landsat TM imagery contains 7 bands of data. Limitations on computer storage space meant that the choice of bands had to be made prior to down-loading the data. The availability of 7 bands gives a large number of possible combinations from which to choose, a problem considered by Crippen (1989). Band 6 has a resolution of 120m and can thus be disregarded as the aim of using TM is to compare its 30m resolution against the 1.1 km resolution of AVHRR. One quadrant of data was considered at first, allowing the full suite of bands to be considered. Crippen (1989) ranked various combinations for different regions. B 2 4 7 $\Rightarrow$ R G B was eventually chosen as standard, a combination

consistently above average in Crippen's rankings. Once the band choice was made the other three quadrants were loaded.

The scene has first to be reassembled from the four quadrants of data provided. Reassembly consists of inserting each quadrant into its correct location in a blank, full scene size, image file in PCI. The useless edge data, which occur in the first and last few pixels for each data line, can also be cut out during this step. Once assembled the scene can be processed and enhanced.

Edge enhancement and linear stretches for the utilised bands were carried out in exactly the same manner as for the AVHRR data, sections 2.1.5 and 2.1.6 respectively. Hard copy output was also carried out in the same way as AVHRR, section 2.1.9.

2.2.3 Landsat Coverage

One Landsat TM scene covering part of the Kenya rift at the equator has been processed and the band combination B 7 4 2 $\Rightarrow$ R G B was used. In addition, two Landsat TM scenes covering part of the Afar region were provided by Dr David Harding of NASA GSFC. These scenes have been edge enhanced and a linear stretch has been carried out. The band combination chosen for the hard copy output was: B 7 4 3 $\Rightarrow$ R G B, (Harding, pers. comm.). One of these scenes was used in its entirety, part of the other for comparison with an Electronic Still Camera (ESC) image, figure 2.4. One black and white, band 4, Landsat TM scene was used to study part of the Rukwa rift.

The Landsat MSS mosaic of Kenya, figure 2.4, was produced by the United States Geological Survey (USGS). The scenes had been registered with latitude and longitude given on the hard copy. No details of the band combination used was given nor was any information of processing. Due to the fact that vegetation-covered areas are particularly prominent as red areas on the image it is likely that band 4 was assigned as red.

2.3 Electronic Still Camera

2.3.1 The Instrument

Hand-held camera photographs are routinely collected during missions of the Space Shuttle. For the most part the images are taken using a standard camera and film through

the shuttle observation windows. On some more recent missions an Electronic Still Camera (ESC) has been used which provides digital images.

The Electronic Still Camera is mounted on a Nikon F4, single lens reflex camera body, with the interchangeable lenses and filters that any other F4 is able to use; instead of film the image is recorded electronically on a 1024 by 1024 electronic array. The images can either be sent directly to the ground or stored for down-loading later. The files produced by the camera are 1024 pixels by 1024 lines in size and the data are 8 bit (giving 256 grey shades). The images are black and white and are acquired in the 400 to 800 nm range. This range is reduced from the 400 to 1100 nm range that the instrument can achieve by the protective coatings on the windows of the Shuttle (Israel, 1992). Five images are considered, see figure 2.4.

2.3.2 Processing of ESC data

Very little processing was carried out on the ESC images, which were obtained by 'ftp' from NASA, Johnson Space Center. These images are single band only. Rectification was not carried out and edge enhancement was found to be detrimental. The images have a component of noise, which though unnoticeable on the original image is enhanced as a 'data edge'. Therefore, while geological edges ware marginally improved, the overall scene quality was degraded. Linear stretches were applied to the data as for AVHRR, section 2.1.6.

2.4 Satellite Probatoire pour l'Observation de la Terre

2.4.1 The Sensor

Satellite Probatoire pour l'Observation de la Terre (SPOT) imagery has a resolution of 20m in its multispectral mode and 10m in its panchromatic mode of operation. Acquisition is by means of a 'pushbroom' system, this system obtains a full swath of data instantaneously using a linear array of sensors. The advantages of this system over others are that there are no moving parts, making the sensor more durable and simple to construct, and that the detector is able to view an area for a longer duration thus reducing the signal to noise ratio. The main disadvantage is that the detectable wavelengths are reduced due to the construction of the sensor cells. The wavebands of the SPOT sensor are given in table 2.5.

Band	Wavelength (μm)	Resolution (m)
1	0.50 - 0.59	20
2	0.61 - 0.68	20
3	0.79 - 0.89	20
Pan	0.51 - 0.73	10

Table 2.5. Channels on the SPOT sensor.

2.4.2 SPOT Scene of Kenya

One SPOT scene has been used. The coverage of this is of a small section of the Kenya rift, figure 2.4, an area covered by AVHRR, and Landsat TM and MSS also. The scene was acquired in the multispectral mode of operation of the SPOT sensor. The band assignments are the standard B 3 2 1 = R G B.

2.5 Galileo

The Galileo spacecraft was designed for a mission to Jupiter, however, *en route* the platform took images of the Earth, the moon, and other bodies that were encountered. The views of the Earth were of prime importance for assessing the imaging instruments and in particular the use of narrow band infra-red filters used in the Solid State Imaging (SSI) system (Geissler *et al*, 1995), see table 2.6. Bands 1, 2, 3, 4 and 7 are considered in this study, of which SSI band 3 overlapped with AVHRR band 1 and SSI band 7 with AVHRR band 2.

Band no.	Filter designation	Centre wavelength (μm)	Full width at half max. (μm)
1	VIO	0.404	0.045
2	GRN	0.559	0.065
3	RED	0.671	0.060
4	.73	0.734	0.010
5	.76	0.756	0.019
6	.89	0.887	0.016
7	1 μm	0.986	0.050

Table 2.6. Band Filters on the Galileo SSI system, from Belton *et al*, (1992)

The resolution of this imagery is not fixed as the data were acquired as the platform retreated from the Earth (Geissler *et al*, 1995). In the Afar region the resolution is of the order of 4 km and is therefore useful for comparison with the AVHRR as an example of the use of lower resolution data (compared to the higher resolution of MSS, TM, ESC and SPOT).

2.5.1 Processing of Galileo SSI imagery

The majority of the Galileo SSI imagery over East Africa was heavily cloud covered, but the Afar region of Ethiopia, Djibouti and Eritrea were relatively clear. The processing techniques required for producing a Galileo SSI image of Afar were very similar to those used for AVHRR processing. The low resolution of the data caused problems in registering the scene as there were very few clearly defined points visible for which accurate latitude and longitude could be determined; enough points could, however, be found for a reasonable level of registration. Linear stretches were required for the SSI bands. The scene coverage is shown in figure 2.4.

2.6 Image Interpretation

The interpretation of the satellite imagery is essentially confined to the mapping of lineaments. The term 'lineament' is here considered to be any geological, tectonic or morphological feature which is linear or sub-linear, and follows the definitions set down by O'Leary *et al* (1976).

A lineament is a mappable, simple or composite linear feature of a surface, whose parts are aligned in a rectilinear or slightly curvilinear relationship and which differs distinctly from the patterns of adjacent features and presumably reflects a subsurface phenomenon.

In this definition almost all features which are linear or sub-linear are considered, though care has to be taken not to include roads, cultivation or other man-made structures. The problems with man-made linear features are only really of concern for higher resolution imagery such as Landsat scenes as few such features are large enough to be shown on AVHRR imagery.

Lineaments are frequently related to faulting, either individual faults or fault zones. Lineaments result when erosion works selectively on the fault or where a major offset, vertical or horizontal, has occurred. A lineament may also be due to lithological contacts or geomorphological features (Mohr, 1974). It is often difficult to assign a cause for a lineament and such features may be due to underlying structure or may turn out to be spurious. Shackleton (1967), considering aerial photography, suggests that "dislocations of trivial importance can give rise to conspicuous lineaments, while major strike faults or slides, especially if pre-metamorphic, might be invisible." Mohr (1974), using ERTS (Landsat) imagery, considers this to be an over-pessimistic viewpoint but concedes that it is difficult to assign the importance of a feature simply from its expression on imagery.

It is desirable to carry out field checks of mapped lineaments leading to more precise details of faulting and other geological features. Often it is not practical to carry out field studies over a small area, such as a Landsat scene. This study involves the entire East African Rift System and a field study is impractical.

Interpretation consisted of manual mapping on hard-copy imagery; resultant lineaments were then digitised from these interpretations. There are a number of advantages of manual over computational techniques. A computer sees an image as a set of numerical cells and will consider a road or field edge in the same way as a fault. The simplest form of edge detection, on an image, will therefore highlight all edges regardless of their cause. Manual interpretation is largely able to get round this problem but will inevitably miss some features and may include others that are at best tenuous. The manual mapping procedure also introduces errors in the location of the lineament as the resultant interpretation then has to be digitised.

The procedure for mapping lineaments from AVHRR imagery involved tracing all the lineaments seen on one, systematic, look over the image. This was then repeated a second time to pick up lineaments missed first time. Further sweeps were not carried out as more and more tenuous lineaments tend to be picked up on subsequent mapping. In the case of other, higher resolution, imagery it was necessary to carry out the mapping in periods of not more than half an hour. No overall time limit was set to interpret a scene and as with the AVHRR two sweeps were carried out.

Recognition of faults on Landsat and ESC imagery is not usually a problem, however, the positioning of the fault can be difficult. Figure 2.5 shows the situation for a normal fault, most common in East Africa. Figure 2.5A shows a fault scarp in shadow; in this case the lineament seen at position a/a' will be the most distinct while b/b' will be in

Sun Angle

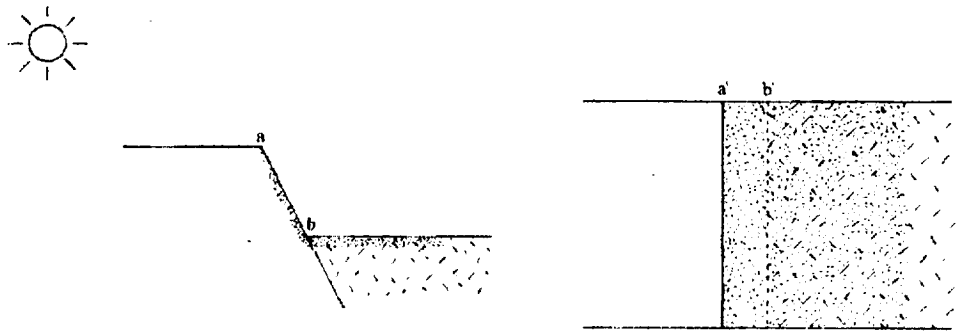

A. Fault scarp in shadow

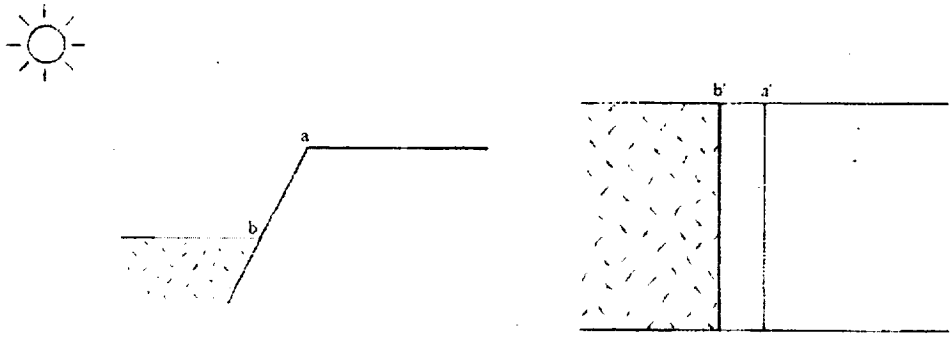

B. Fault scarp illuminated

Fig. 2.5. The affect of sun angle on the mapping of a normal fault from an image. a/a' represents the top of a fault scarp while b/b' represents the bottom line. A. The scarp in shadow: a/a' will be most distinct while b/b' is hidden in shadow. B. The scarp illuminated: both a/a' and b/b' will be seen but b/b' may be more distinct due to the different rock types across the lineament.

shadow. Figure 2.5B shows the same situation but with the scarp illuminated; both a/a' and b/b' will be seen but b/b' may be more distinct as the boundary of different rock types. To be consistent during image interpretation the scarp top (positions a/a') has been mapped wherever possible.

2.7 Rose Diagrams

Determining the mean directional trends of lineaments is useful for assessing the regional stress. The rose diagrams presented here were produced using 'psrose' in the GMT software (Wessel & Smith, 1993). The input required by 'psrose' is in the form of a list of length and azimuth data for the lineaments. 'psrose' also calculates means, modes and totals.

Calculating the length and azimuth of lineaments can pose problems due to the fact that not all lineaments are straight; thus, it is not possible to take the end points of a line for the purpose of calculation. The situation is, however, eased by the fact that in digitising lines from a map or image it is necessary to approximate curves by short straight line segments. It is then possible to calculate the length and azimuth of each of these line segments.

In Cartesian co-ordinates a line from (x_1, y_1) to (x_2, y_2) has a length (l):

$$l = \sqrt{(x_2 - x_1)^2 + (y_2 - y_1)^2}$$

In latitude, longitude co-ordinates the length depends on the latitude of the line. An approximation can be made for short lines such that the latitude of the central point of the line is used in calculation. Assuming that each degree of longitude is 111.3 km at the equator and each degree of latitude is 110.6 km (Snyder, 1982) the length (l) of the line will be approximately:

$$l \approx \sqrt{\left[(x_2 - x_1) \times 111.3 \cos\left((y_1 + y_2)/2\right)\right]^2 + \left[(y_2 - y_1) \times 110.6\right]^2}$$

The azimuth (θ) is given by:

$$\theta = \tan^{-1}\left[\frac{(x_2 - x_1)}{(y_2 - y_1)}\right]$$

Rose Diagrams

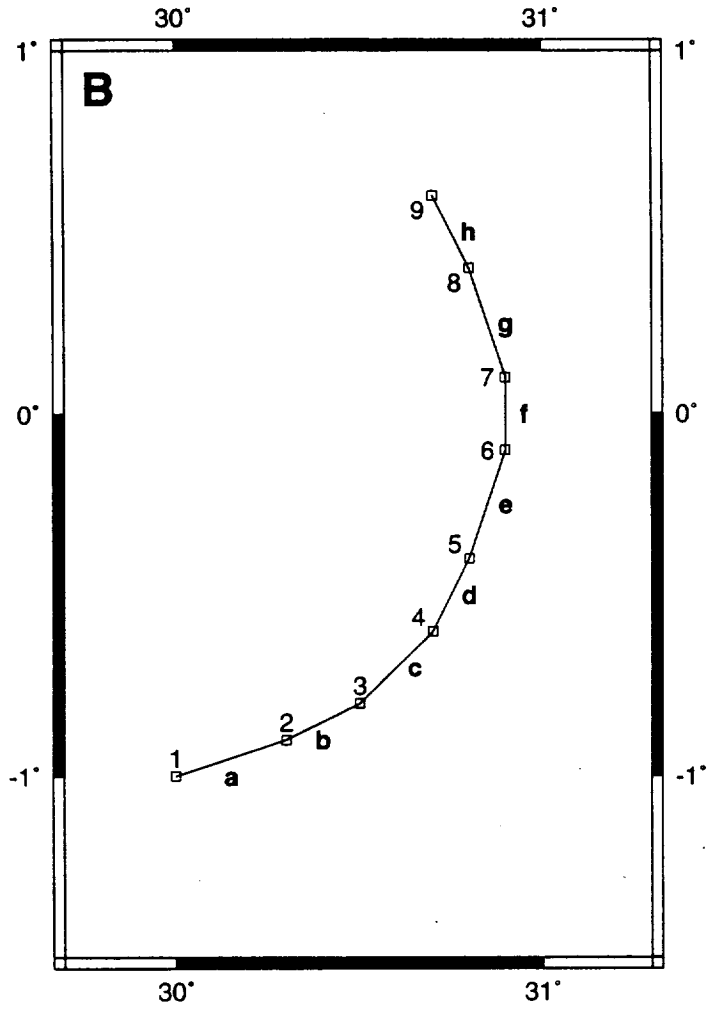

C

Line Segments

pt.	Long.	Lat.
1	30.0	-1.0
2	30.3	-0.9
3	30.5	-0.8
4	30.7	-0.6
5	30.8	-0.4
6	30.9	-0.1
7	30.9	0.1
8	30.8	0.4
9	30.7	0.6

Rose Output

Seg.	Lth	Az.
a	35.081	71.6
b	24.796	63.4
c	31.324	45.0
d	24.731	26.6
e	34.959	18.4
f	22.100	0.0
g	34.959	-18.4
h	24.731	-26.6

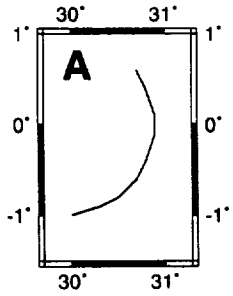

D Rose Diagram

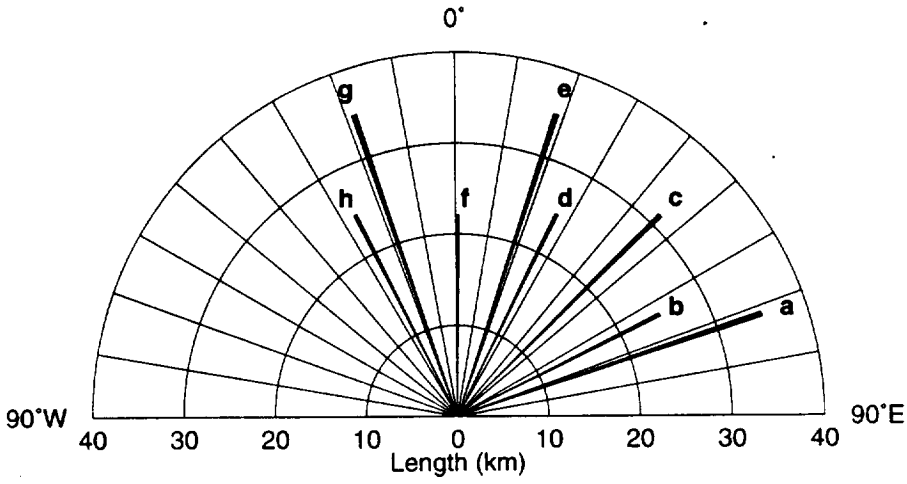

Fig. 2.6. Rose diagrams. Determination of length and azimuth values for line segments. A. Digitised line on scale of viewing. B. Enlarged version of A showing individual straight line segments. C. Table of line nodes and length/azimuth determinations for line sections. D. Resultant rose diagram.

The FORTRAN code to carry out these calculations is given in appendix D. A sample lineament and results is given in figure 2.6. Figure 2.6A shows an example line on the normal scale of viewing. 2.6B is the same line enlarged such that the separate line segments that make up the digitised line are seen. The rose diagram which results from this line is given in figure 2.6D. On this scale and with one line, the resultant rose does not show a smooth distribution of directions which would result from a line made up of many smaller segments. Averaged out over a large number of lineaments the rose diagram can give a reasonable approximation of the directional trends.

CHAPTER 3

Afar

The Afar region lies at the junction of the Red Sea, Gulf of Aden and Ethiopian section of the East African Rift System; figure 3.1, plates 1A & 1B. Much of the area is close to, or below, current sea level. It is bounded to the west by the Ethiopian Plateau and to the south by the Somalia Plateau. Between Afar and the Red Sea lies the Danakil Horst. The Aysha Horst separates southern Afar from the main part of the Djibouti and Somali coast. Between the Danakil and Aysha Horsts the Gulf of Tadjoura extends from the Gulf of Aden spreading centre. Afar is highly faulted and riddled with volcanic cones and recent lava flows.

3.1 Geological Background

The Precambrian basement to the west and south of Afar was affected by the Pan-African orogeny but foliation from this time seems to have little effect on Cenozoic rifting (Mohr, 1971). During the Mesozoic much of Ethiopia was covered by a marine transgression producing layers of Mesozoic sediments which lie unconformably on the basement. Downwarping and minor basalt volcanism occurred contemporaneously (Mohr, 1971). Uplift of the neighbouring plateaux followed the regression of the Mesozoic sea and occurred in several phases, as shown in table 3.1.

Phase	Time	Location
1	Cretaceous	Western Ethiopian plateau
2	**Upper Eocene - Lower Oligocene**	**Northern Somalia, Yemen, Eritrea**
3	Oligocene - Miocene boundary	Southern Ethiopian plateau, E Somalia
4	**Mid Miocene**	**Eritrea, N. Somalia, S. Yemen**
5	**Pliocene**	**Ethiopian Plateau**
6	Pliocene - Lower Pleistocene	Eritrea, Somalia plateau
7	**Mid Pleistocene (two)**	**Ethiopian and Somalia plateau**
8	Pleistocene - Holocene	Danakil and Aysha horsts

Table 3.1. Phases of uplift in the Arabo-Ethiopian swell. Bold type refers to largest phases. (From Mohr, 1971.)

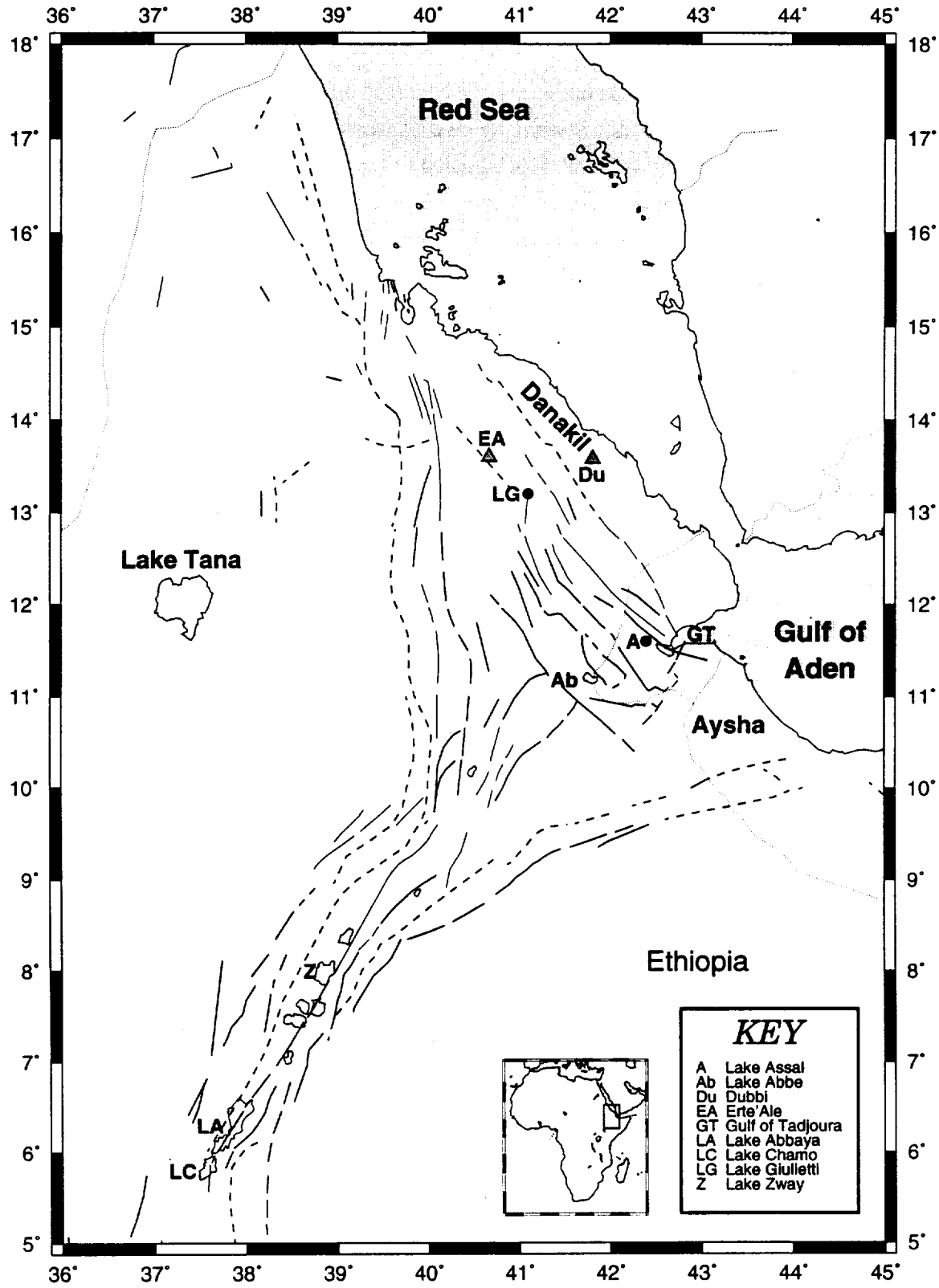

Fig. 3.1. The Afar region; location of geographical names used in the text.

The oldest lavas which are exposed in Afar are flood basalts of pre-Pliocene age. These may be equivalent to the 'trap series' of Ethiopia (Mohr, 1971) and are possibly up to 6000m in thickness. Volcanic activity has continued in Afar with fairly extensive, Holocene, flood basalts in the north of Afar. The floor of the Afar triangle is dominated by belts of mid-Pleistocene faults which rarely have a throw of more than 100m (Baker *et al*, 1972).

A 6 km wide marginal graben marks the western boundary between Afar and the Ethiopian plateau (Mohr, 1971). The western margin of Afar is faulted with ENE-WSW and ESE-WNW faults which can occasionally be traced across the area to Danakil. The boundary with the highly deformed Danakil Horst exhibits fresh faulting and fissure basalts.

The Wonji Fault Belt of the Ethiopian rift continues across Afar in an almost N-S direction to the north of Lake Abbe. According to Mohr (1971) this Belt then crosses Danakil to the Red Sea Coast at 14°N. Mohr (1971) also speculated that the Wonji Fault Belt marked the boundary between the Nubian and Arabian Plates, and that the change of direction at Lake Abbe was due to the meeting with the Gulf of Aden spreading centre. Thus, Lake Abbe would lie at the triple junction. However Gibson & Tazieff (1970) find no evidence for a continuation of this belt much beyond the northern end of the Ethiopian rift.

Extreme crustal thinning has occurred in Afar with seismic refraction profiles revealing a Moho depth of about 15km (Berckhemer *et al*, 1975) under the spreading axis. This axis is marked by the axial volcanic ranges, the Erte'Ale range and the Dubbi line (Mohr & Wood, 1976). Makris & Ginzburg (1987) proposed a two layer crust for Afar which were identical in nature to the adjacent plateau regions but stretched and thinned. However, Mohr (1989) proposed an upper layer of granitic-syenitic sheets separated by dyke screens. Below this a gabbroic layer is suggested which would be syn-rift and would be thickened by continuing intrusion. This model would give a 25 km thick crust on the margins of Afar thinning to about 15 km at the spreading axis. In other words, the two models suggest thinned continental crust (Makris & Ginzburg, 1987) or new igneous, or pseudo-oceanic, (Mohr, 1989).

3.2 AVHRR

One AVHRR scene of the Afar region has been studied using two band combinations; B 2 1 1 ⇒ R G B and B 5 2 1 ⇒ R G B, plates 1A and 1B respectively. The AVHRR scene used for the study of Afar, plate 1, is essentially cloud free, only a small region of cloud exists at the extreme southwest of the scene. The image was acquired on 2nd February 1987. In order to obtain a cloud free image the resolution towards the west of the image has had to be sacrificed as the Afar triangle lay towards the left edge of the AVHRR swath. This does not pose a problem as the Ethiopian rift, where the resolution is worst, is covered by another scene, plate 2.

Plates 1A and 1B clearly show the Afar triangle at the junction of the Red Sea, Gulf of Aden and Ethiopia rift. The bounding scarps are highlighted as a change from the higher, vegetated land around to the hot low-lying Afar triangle. The trends of the Red Sea and Gulf of Aden coasts follows on along the western and southern edges of Afar, respectively and shows how the region is part of these features. The Ethiopian rift branches out of the southwestern corner of Afar and is characterised by a line of small lakes.

The boundary graben along the western scarp is clearly shown on the imagery as following the entire scarp from about 14.7°N to 9.2°N. The three sub-elliptical basalt regions in the north of Afar, between Danakil and the western scarp are particularly visible on plate 1A where they appear black. The whole of Afar appears red in plate 1B indicating that the region has a particularly high thermal infra-red signature. Many volcanic cones are seen as darker spots on the scene. The fact that the volcanoes are darker indicates that they are cooler than the surrounding areas, almost certainly as a result of their height above the plains.

One other noteworthy feature visible on the AVHRR imagery is the clear linear trend in a SSE direction from the southern scarp slope of Afar, from about 42.5°E, 9.5°N. This lineament is part of the, Precambrian, Marde fracture zone which cuts across the horn of Africa and follows a similar trend to both the Aswa shear zone and Nadj Fault (Kazmin *et al*, 1978). The AVHRR scenes indicate and alignment of the Marde Lineament with the continuation of the western scarp of Afar to the north of the region.

Lineaments mapped from AVHRR B211 and B521, plate 1, are compared with UNESCO (1968) faults in figure 3.2. In this area the faulting in the UNESCO map is, for the most, part a over-simplification of the situation in the region. The scarps are clearly

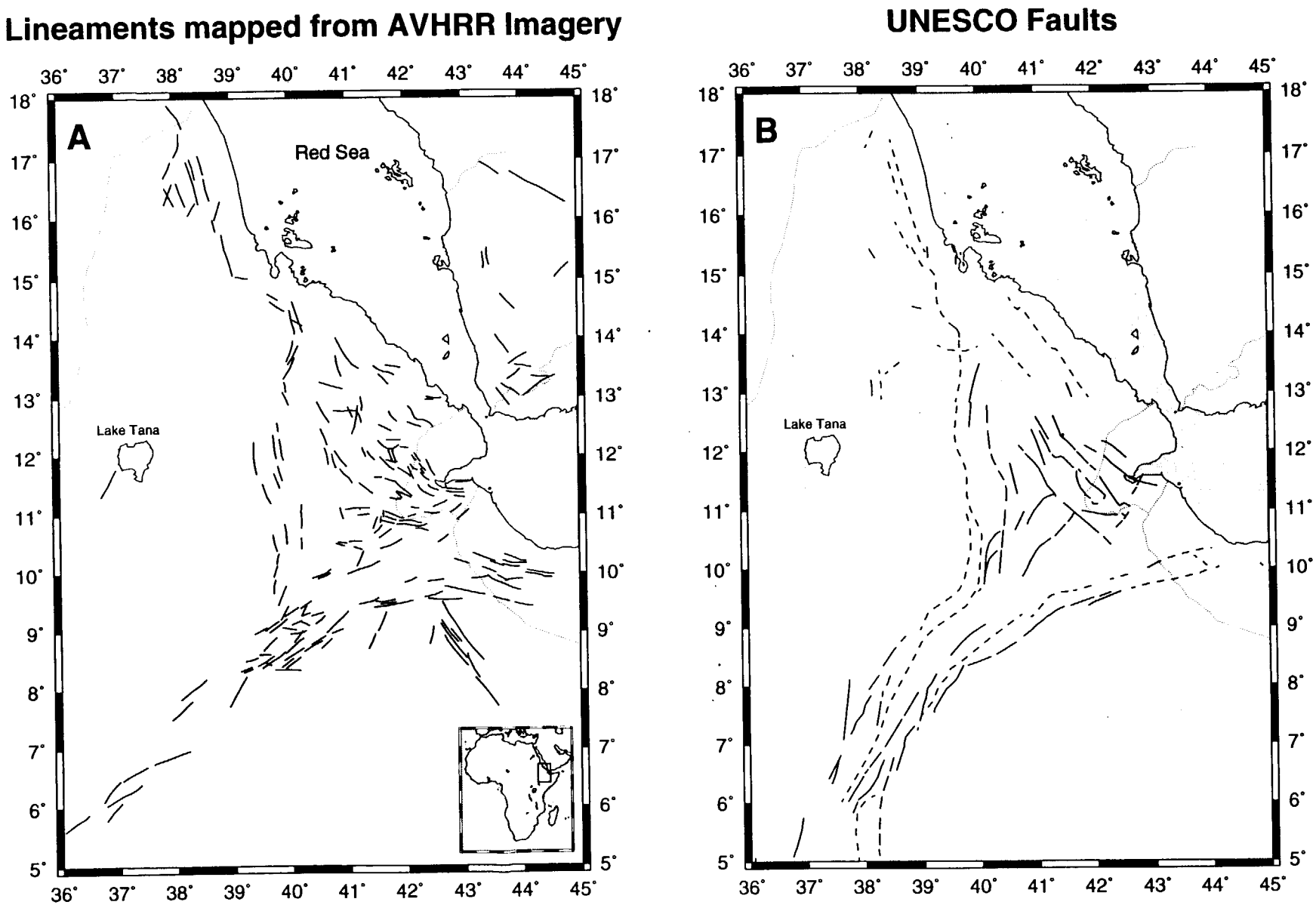

Fig. 3.2A. Lineaments and faults of the Afar region. A. Lineaments mapped from AVHRR (B521 = RGB) imagery: B. Faults, from UNESCO (1968).

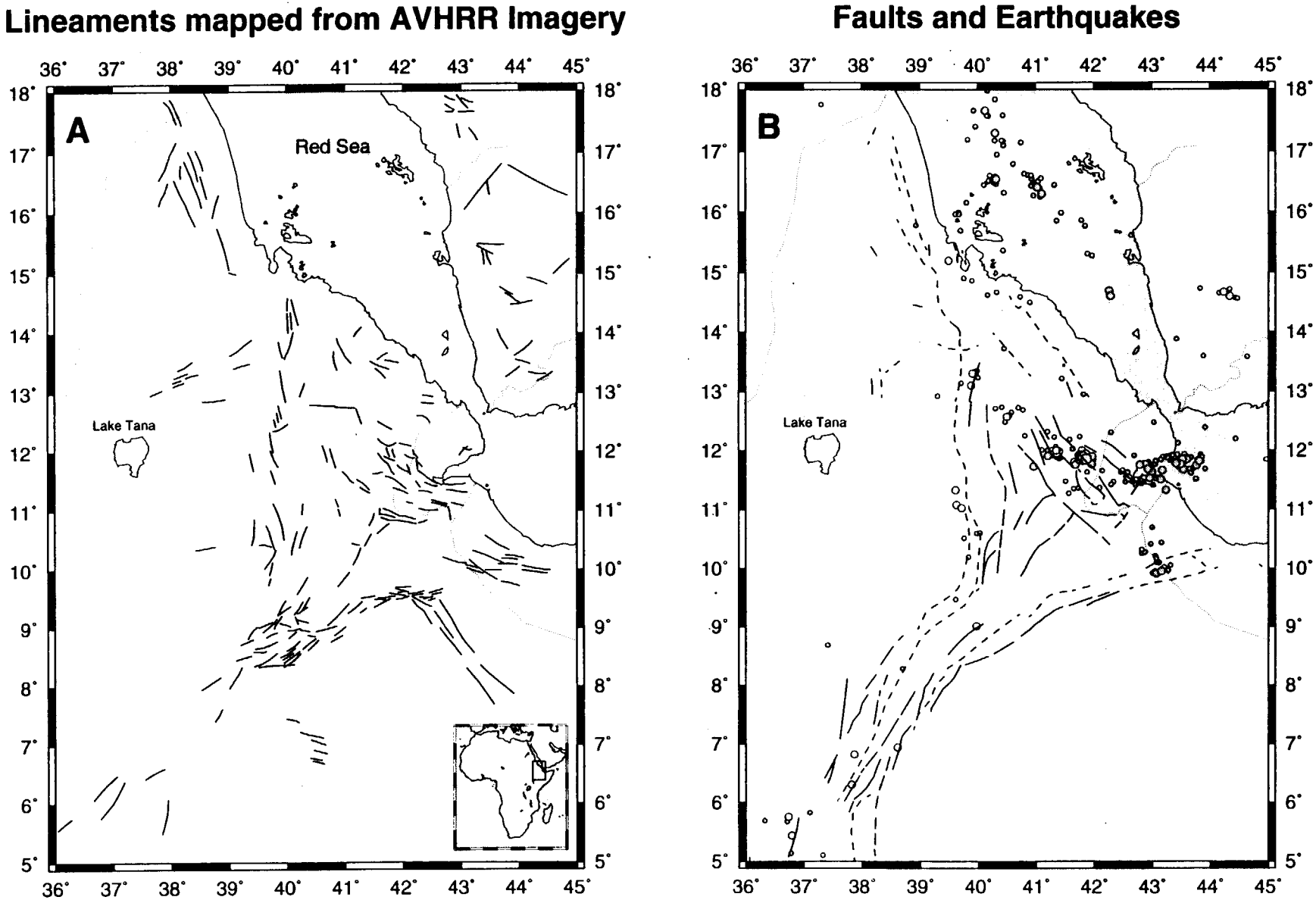

Fig. 3.2B. Lineaments and faults of the Afar region. A. Lineaments mapped from AVHRR (B521 = RGB) imagery: B. ISC earthquake epicentres (1964 - 1991).

defined on the UNESCO map but actual mappable lineaments are relatively scarce on the AVHRR, though the break between the low lying Afar plain and the highlands is clear, if hard to map. Relatively few lineaments and UNESCO faults are extant to the immediate downthrow side to the bounding scarps before the intense faulting of the Afar plain is reached.

Faulting within the Afar region is strikingly different between the UNESCO map and AVHRR. The distinct break between SW - NE trending faults, forming the NE extension of the Ethiopia rift, and the predominantly NW - SE faults of Afar as seen on the UNESCO map is not borne out by the satellite imagery (even more clearly visible on the TM scene considered below). If a trend can be picked out on the AVHRR it is for E-W structure in the Gulf of Tadjoura area veering to a NNW - SSE lineation in the northern part of Afar. The B521 scene differs from B211 in showing generally fewer lineaments. Though fewer lineaments are shown the similarity between the B521 and UNESCO map is closer where the Ethiopian trend meets the Afar faulting. Figure 3.2B also includes the earthquake epicentres of Afar. The location of epicentres bear out the lineament trends seen using AVHRR rather than those on the UNESCO map.

3.3 Topography

A 'beta' version of topography data "Terrain-30", which has a resolution of 30" has been acquired from the USGS. A few problems which existed with an earlier version, such as noise and a non-fixed coastline level, have been rectified. The data are combined with AVHRR imagery in figure 3.3 and are considered on their own, figure 3.4. The 30" resolution of these data makes it comparable to the resolution of AVHRR imagery.

Figure 3.3 shows two oblique views of the Afar region using AVHRR B211 imagery draped over the topography. This gives a valuable extra view on the Afar region. Figure 3.3A shows the Afar triangle viewed from the south. The southern and western elevated shoulders clearly mark the change from the low-lying Afar region to the highlands. The Ethiopia rift is seen clearly on both the southern view and view from the northeast, figure 3.3B as it enters the southwestern corner of the triangle. The slightly higher and more rugged Danakil horst is seen along the northeast coast of Afar. The scarps marking the boundary of the Red Sea are also clearly seen in figure 3.3A. The graben along the western scarp of Afar is very clear on both figures 3.3A & B. In addition to this figure 3.3B also shows evidence of a similar, if less well defined, feature along part of the southern scarp.

Fig. 3.3A. The Afar and Ethiopia rift region viewed from the south. Terrain-30 topography overlain by AVHRR (B211 = RGB) imagery.

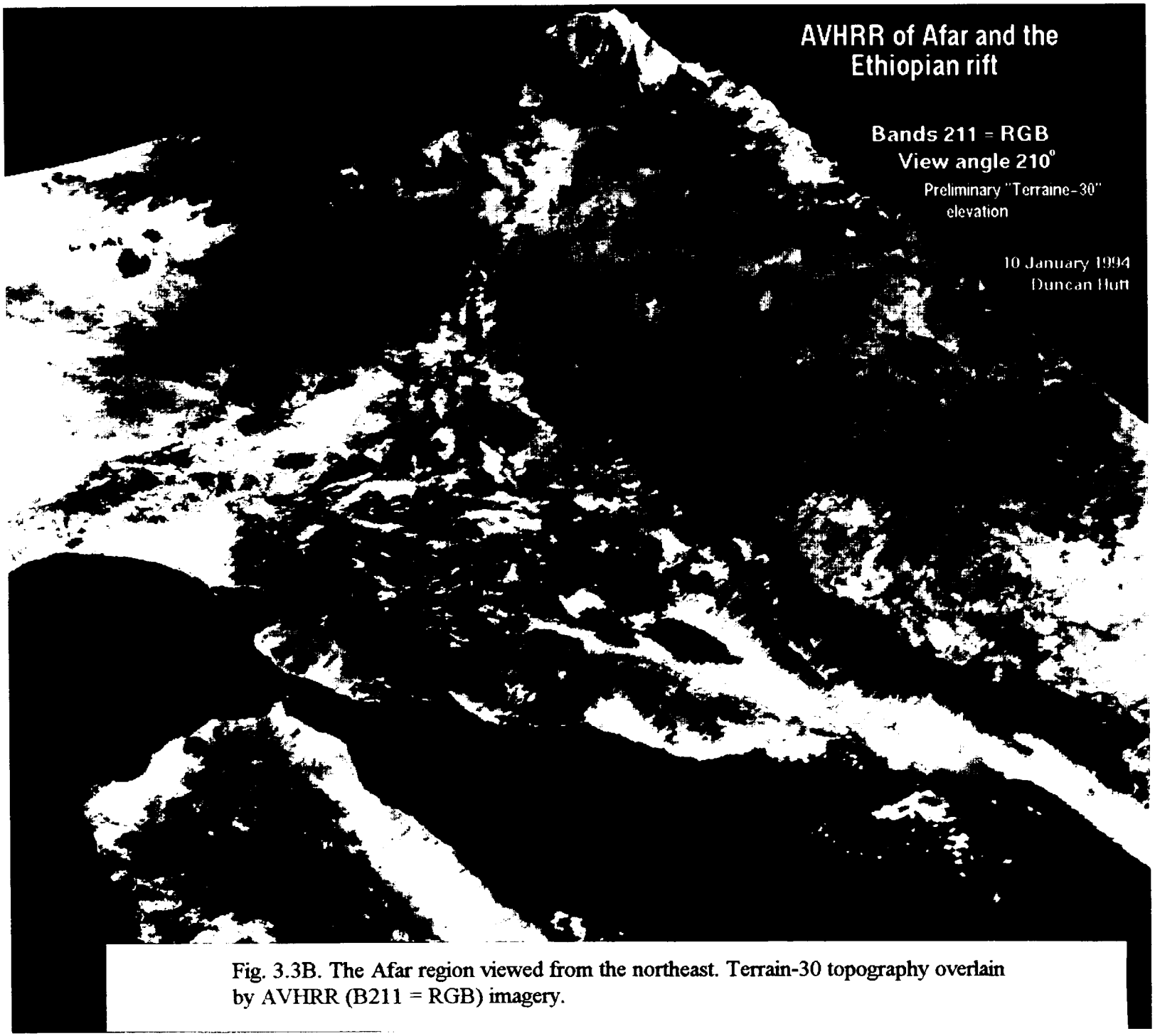

Fig. 3.3B. The Afar region viewed from the northeast. Terrain-30 topography overlain by AVHRR (B211 = RGB) imagery.

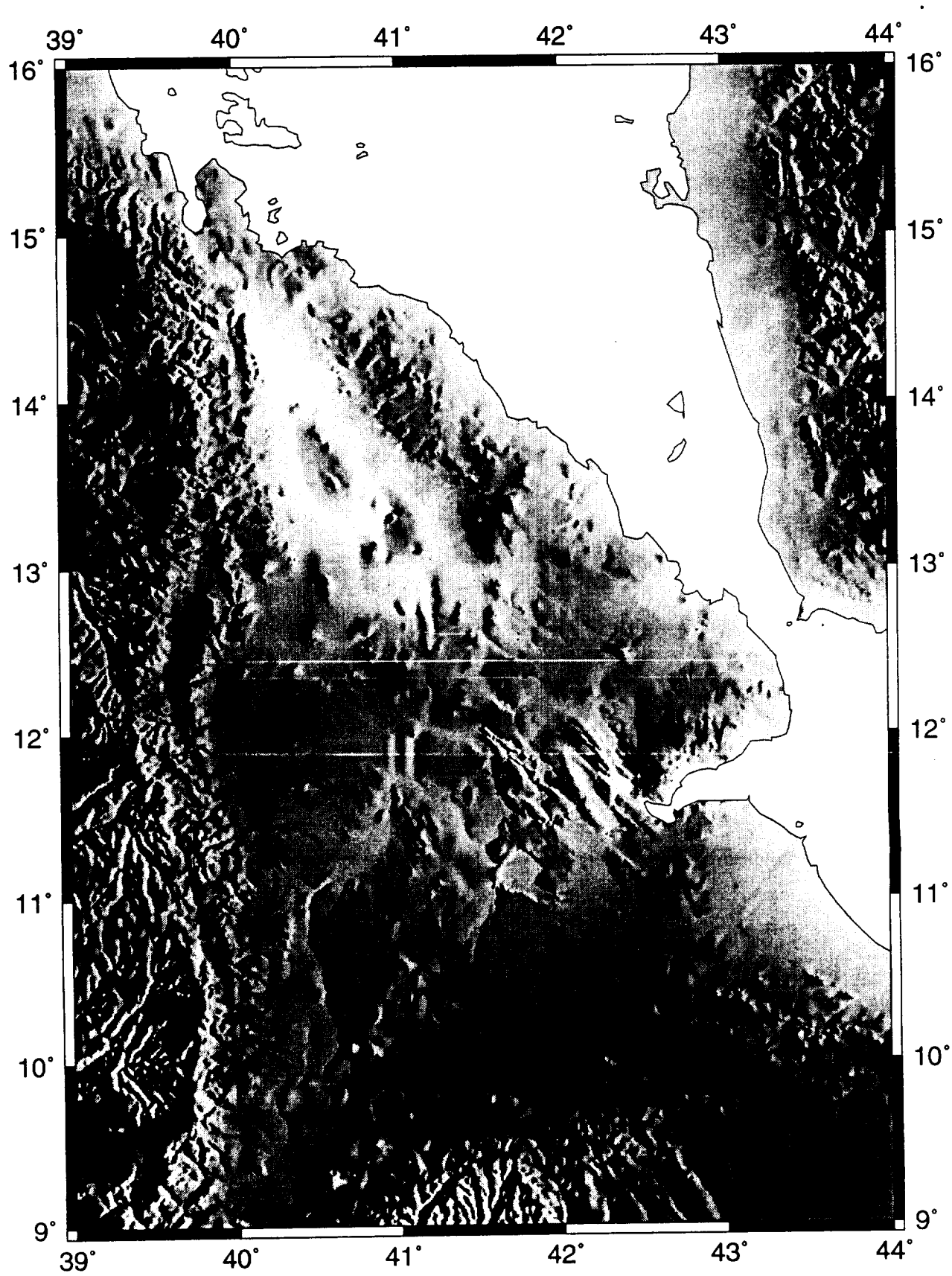

Fig. 3.4. Topography of the Afar region, illuminated from the east. Terrain-30 data.

Figure 3.4 shows the topography of the Afar triangle and neighbouring highlands. The Danakil horst in the northeast of Afar, and the Aysha horst to the south of the Gulf of Tadjoura are visible as higher, more rugged, terrain. The Erte'Ale range appears as a slightly raised sub-elliptical feature, at about 40.6°E, 13.6°N, surrounded by the Danakil depression. Other volcanic peaks are clearly visible over the entire triangle and a region of NW - SE trending structure is well defined in the Lake Assal/Lake Abbe area to the west of the Gulf of Tadjoura.

3.4 Seismicity and Volcanism

The seismicity in Afar for the period 1964 - 1991, figure 3.5, is largely confined to the Gulf of Tadjoura, the region between Danakil and the western scarp and the Aysha region in the south. A line of ISC determined epicentres follows a line from the Lake Assal region, arcing northwesterly towards the Erte'Ale range. A swarm of earthquakes occurred on the western bounding scarp of Afar on and around 1st June 1961 and were studied and relocated using the Joint Epicentre Determination (JED) technique by Fairhead & Girdler (1970): the magnitude of these events reached $m_b = 6.4$.

There are a number of fault plane solutions available for the Afar region, the majority of which come from Kabede (1989) or Kabede & Kulhänek (1991). These show predominantly strike slip mechanisms, either left-lateral in approximately a NNW orientation or right-lateral in an ESE direction, see figure 1.6.

Volcanoes of Holocene and pre-Holocene age are spread over the whole of the Afar region, within the region bordered by the scarp edges and not present on the northern section of the Danakil Horst. Despite the scatter the Erte'Ale range and Dubbi line are clearly visible running from the north-west end of Afar in a SSW direction. The trend of volcanoes following the line of the Ethiopian rift is clearly seen leading south-westerly from the south-west corner of Afar.

3.5 Galileo SSI

The Galileo SSI imagery provides a good example of low resolution, though narrow waveband definition, imagery. Figure 3.6 shows five of the seven bands of data for the Afar region. Unfortunately cloud has obliterated the southeastern sector of the triangle

Seismicity and Volcanism of the Afar Region

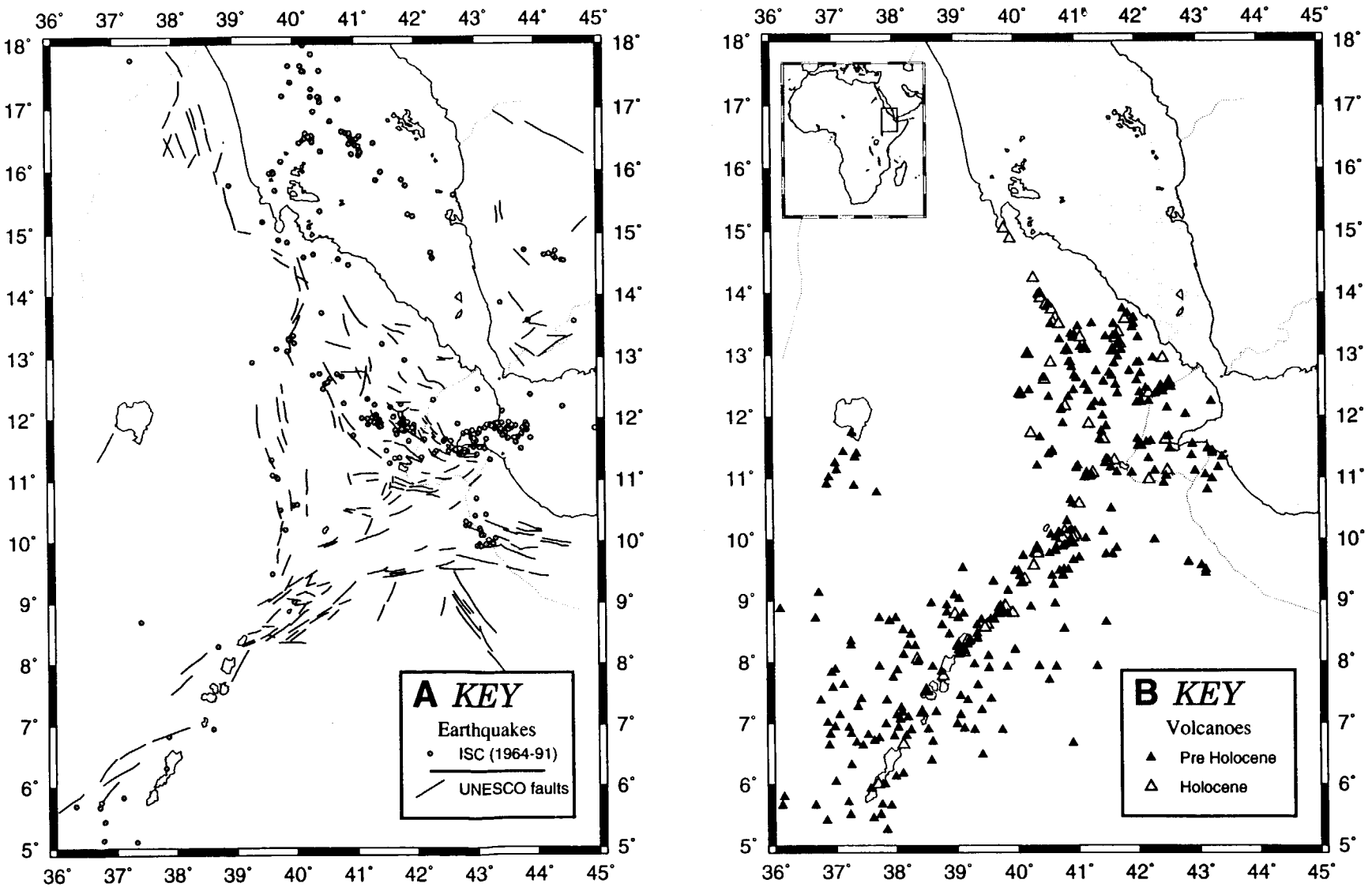

Fig. 3.5. The Afar region, earthquakes, volcanoes and faults. A. Earthquakes from ISC (1964-1991), lineaments from AVHRR (B211); B. volcanoes from Nusbaum et al (1994).

Fig. 3.6. Galileo SSI imagery of Afar; bands 1, 2, 3, 4 & 7. The western scarp of Afar is at the centre of the image. Lake Tana lies at the centre left with the Ethiopia rift lakes in the lower left corner.

but much of Afar is still clearly visible. The western scarp edge is particularly prominent on bands 1 and 2 and barely visible on bands 4 and 7. The three sub-elliptical regions of basalt in the Danakil depression (northern Afar) are visible on all bands though are least distinct on band 1. Beyond observing the bounding scarps and the large basalt areas very little structure is visible.

Figure 3.7 compares AVHRR band 1 with Galileo SSI band 3 (figure 3.7A) and AVHRR 2 with Galileo 7 (figure 3.7B). In this diagram the AVHRR is not at full resolution. These comparisons allow more features to be picked out on the Galileo imagery, such as the lineament associated with the Marde fracture zone running SSE from the southern scarp. However, most of these extra features are only obvious with the hindsight of studying the AVHRR images.

3.6 Northern Afar (ESC)

The ESC has a similar resolution to the TM considered below but the spatial coverage and positional control suffers from the hand-held acquisition technique. Three scenes cover small (c. 30 x 30 km) regions of Afar, two in the north of the area around the Erte'Ale range and one of Lake Assal. The Lake Assal scene is dealt with below (section 3.8).

Scene 04002, figure 3.8, covers a region in the northern part of Ethiopia near the border with Eritrea; the centre is at about 14.0°N, 40.4°E. Lakes Karum and Bakili lie to the right of centre and lower right of the scene, respectively. Gada Ale, volcano, is situated at the centre of the image. The area lies at the northern end of the Erte'Ale volcanic range within the Danakil depression and shows a number of lava flows (dark grey), regions of lacustrine evaporites (white) and the occasional small volcanic cone. The broad spectral response of the camera makes the differentiation of lakes and lava problematic.

The second scene (ESC04004) from northern Ethiopia, figure 3.9, is centred at about 40.7°E, 13.3°N. The cone to the right of centre lies approximately 8km west of the shore of Lake Giulietti (Afrera Bad), which is just off the image. The distinctive lava flow to the NE of the cone originates from Havli Gubbi which lies about 24 km north of the cone.

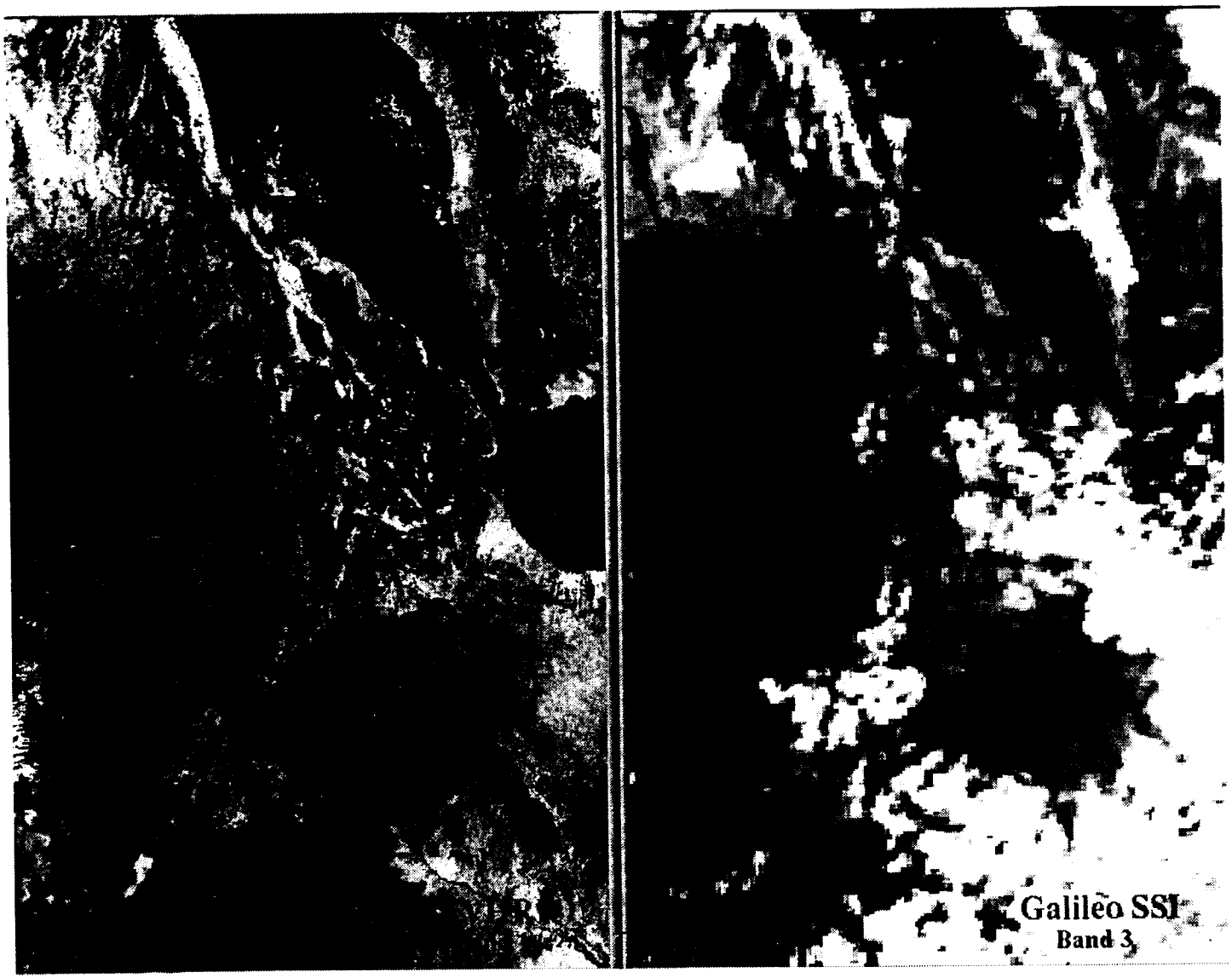

Fig. 3.7A. Comparison of AVHRR and Galileo SSI inagery of the Afar region. AVHRR band 1 and Galileo SSI band 3.

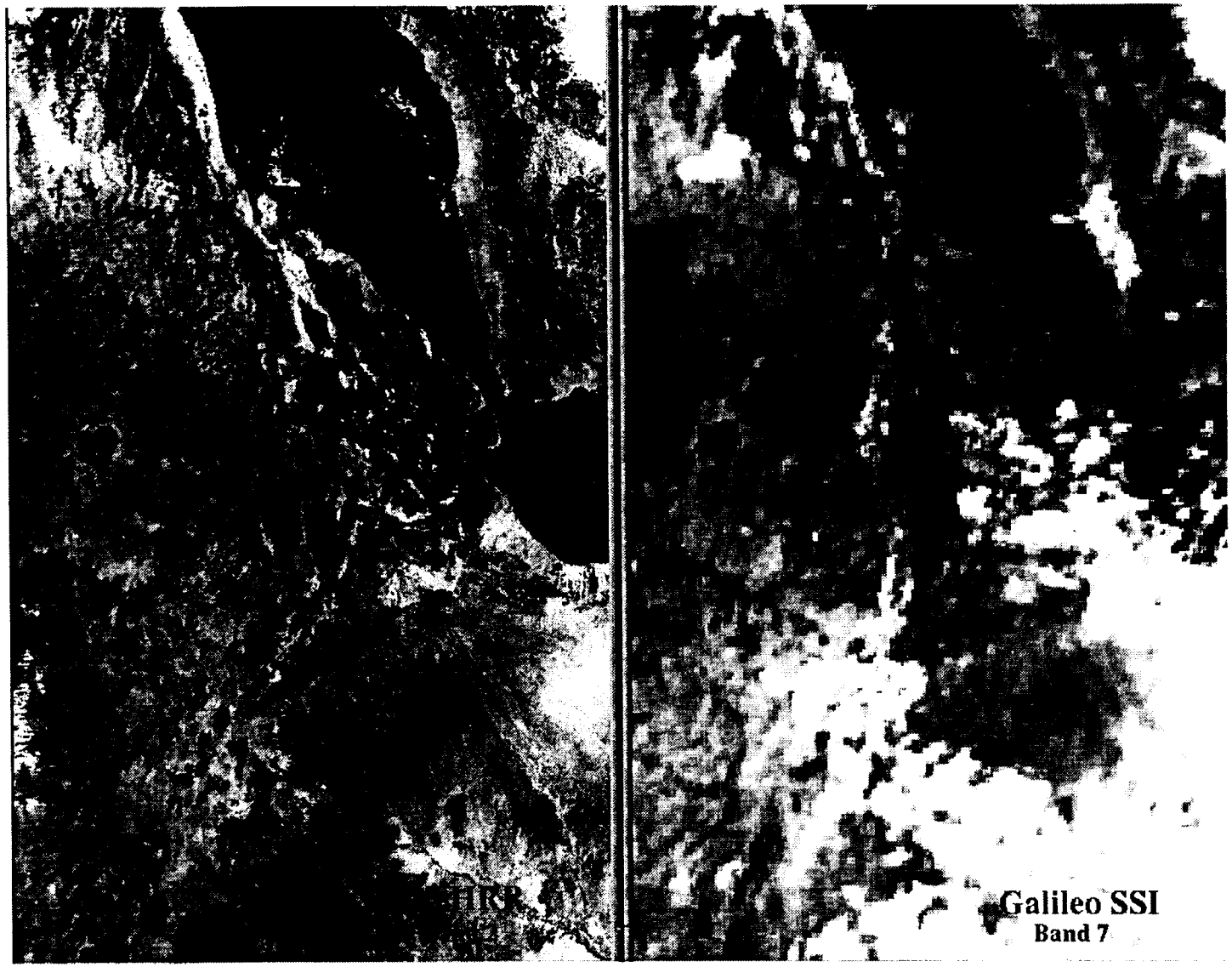

Fig. 3.7B. Comparison of AVHRR and Galileo SSI inagery of the Afar region. AVHRR band 2 and Galileo SSI band 7.

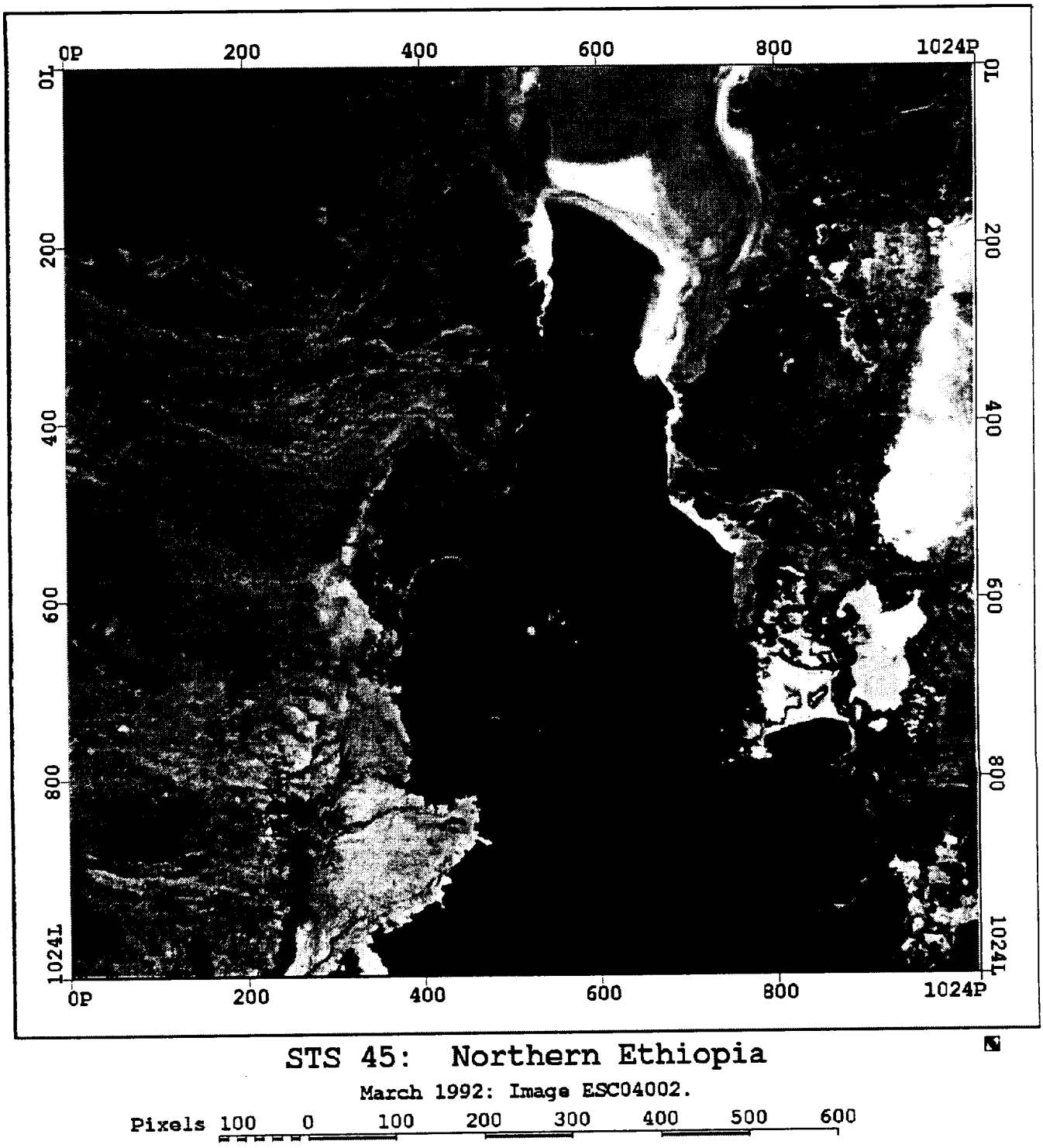

Fig. 3.8. Electronic Still Camera image of Northern Afar. Gada Ale lies at the centre of the scene.

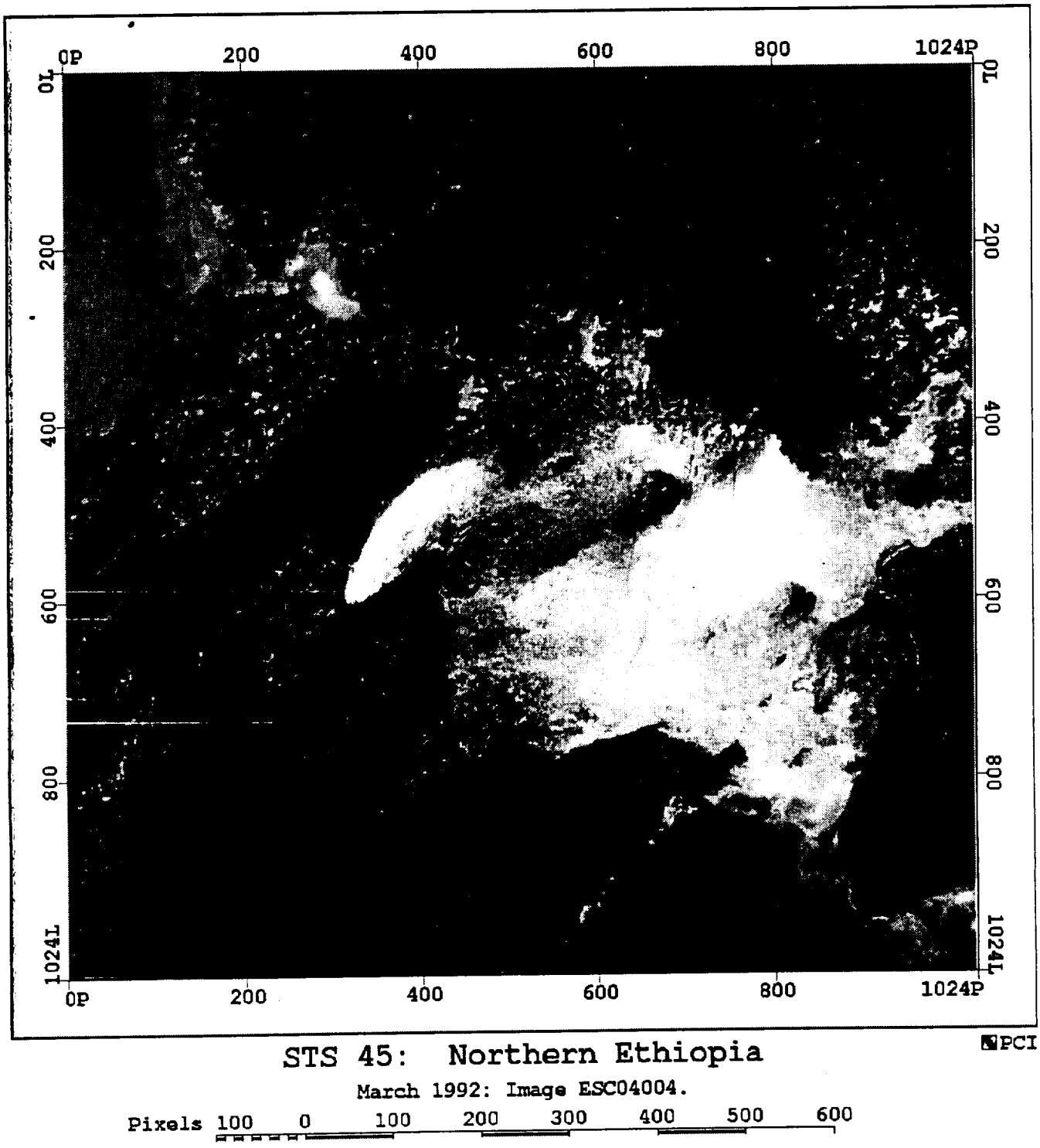

Fig. 3.9. Electronic Still Camera image Northern Afar. Lake Giulietti (Afrera Bad) is located just of the right side of the scene.

3.7 Central Afar (TM)

In stark contrast to the AVHRR and, particularly, the Galileo SSI imagery the Landsat TM scenes of Afar show a huge number of faults and other structural features. Two regions have been studied using TM, one complete TM scene in central Afar and a section around Lake Assal: the Lake Assal region is dealt with fully in section 3.8.

Figure 3.10 is the TM scene of central Afar: path 169; row 56. Figure 3.11 shows the interpreted lineaments, many of which can be termed faults as the resolution (30m) is good enough to pick specific faults as opposed to fault zones. Overlaid on these faults are the lineaments mapped from AVHRR (B211). For the most part the AVHRR lineaments match well with the general trends of faulting though it has frequently picked out boundaries of faulted terrain against the evaporite deposit regions where it does not match the local fault direction, e.g. at 41°15'E, 11°30'N. Two notable exceptions to the correlation between TM and AVHRR exist at 41°15'E, 11°0'N and 41°10'E, 11°8'N.

Most of the regions where rocks are exposed are seen to be densely covered by faulting. Exposure of rocks occurs throughout the scene with little vegetation to obscure it. Evaporite deposits and small lakes obscure some of the area and a few volcanic cones also exist over the scene. The small but distinct graben, seen on both TM and AVHRR, at about 41.7°E, 12.3°N, is the Gawa Graben. Its distinctness on AVHRR is partially to do with its evaporite fill.

Simple inspection of the TM mapped trends shows three distinct directional regimes, N - S in the SW corner; E - W in the SE corner and NW - SE over most of the rest of the region. The rose diagram on figure 3.11 shows the directional trends of lineaments on the TM scene and highlights the observation that there is a predominantly NW - SE orientation over the scene.

3.8 Lake Assal (TM & ESC)

The ESC scene, ESC04005, is shown in figure 3.12A. Lake Assal is situated in the centre of the image with a region of evaporite (gypsum and halite) deposits to its northern and western sides: the surface level of the lake is presently at 155 m below sea level. This region forms the on land extension of the Gulf of Aden spreading axis and links this with the volcanic axis in Afar. The rift region to the south of Lake Assal opened at a rate of about 40 cm over the period of 1979 to 1989 (Ruegg *et al*, 1990) and

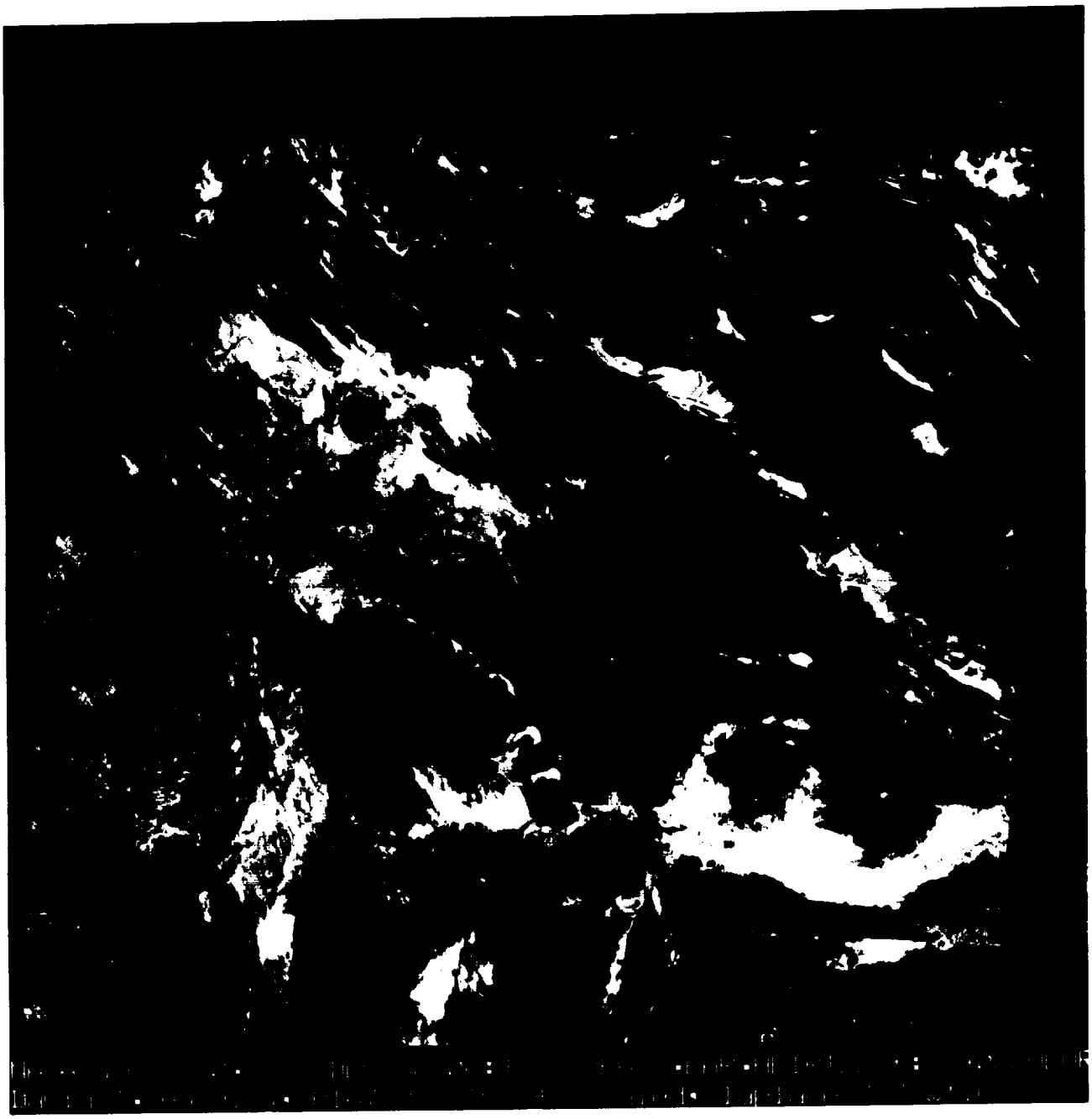

Fig. 3.10. Landsat TM scene of central Afar; B743 = RGB. From Harding (pers. comm.)

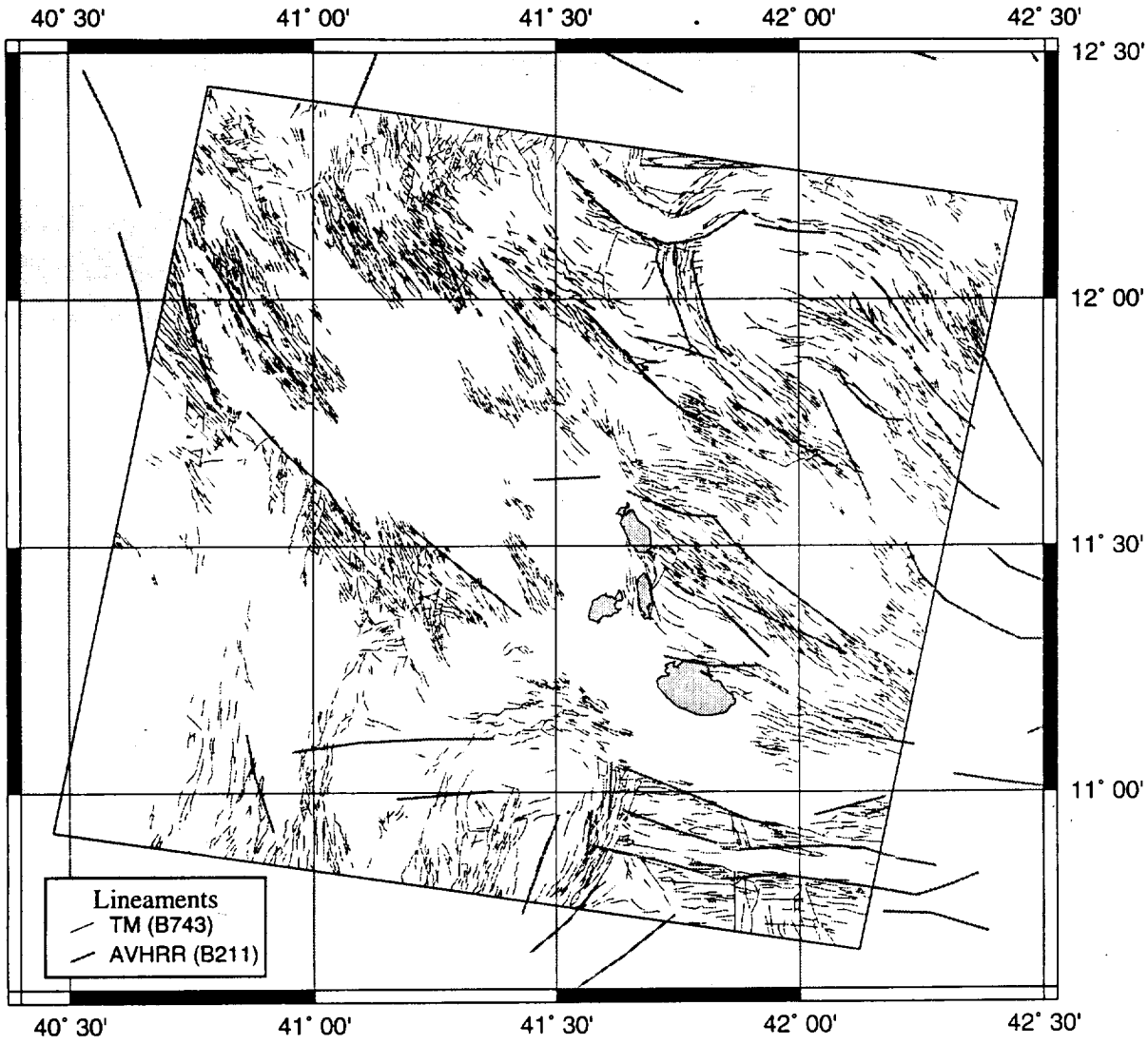

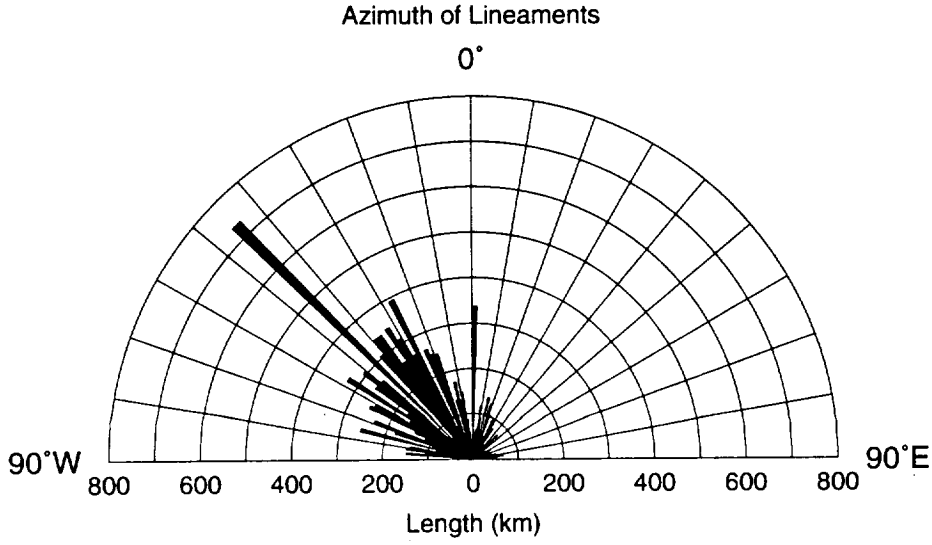

Fig. 3.11. Lineaments of Central Afar mapped from Landsat TM Imagery compared with lineaments mapped from AVHRR (B211) imagery.

is probably the closest thing to a mid ocean ridge on land. To the north of Lake Assal the axial coherency breaks down and a large number of faults in the Afar stratoid series are clearly seen trending southeast to northwest. Figure 3.12B is a Landsat TM subsection covering the same region as the ESC scene.

Figure 3.13 compares the faults and lineaments mapped using the ESC scene and Landsat TM and faults mapped by the CEGD (1974). The overall trending of faults is similar on all the three comparison views though the exact locations are not always consistent. The TM scene highlighted fewer lineaments that the ESC.

The region of basalt at the southern end of Lake Assal is not distinguishable from the water on the TM scene but can be picked out, albeit with difficulty, on the ESC scene. A few minor lineaments cross this basalt in a NW-SE direction. These are seen on the ESC scene and borne out by the CEGD map, they are not visible on the TM scene. Only two ISC listed epicentres lie in this small region around Lake Assal, figure 5.13B, both lie near the southeastern end of the lake on or within about 1 km of faults or lineaments mapped by the CEGD, and determined from ESC and TM interpretations.

The illumination direction on the ESC scene is approximately from the southwest. Illumination on images can cause a problem in mapping faults, see section 2.6. However, the illumination of the ESC scene is in an almost ideal direction as it is perpendicular to the main fault trends, so highlighting the scarp slopes of the faults. the illumination has enabled the lineaments to be classified as faults, where an obvious downthrow is seen, and other less certain lineaments.

It is not possible to compare the lineaments of the Lake Assal region mapped from ESC and TM with AVHRR as the region is too small to make matching possible.

Lake Assal, Djibouti

Electronic Still Camera Image
(STS 45: Scene 04005)

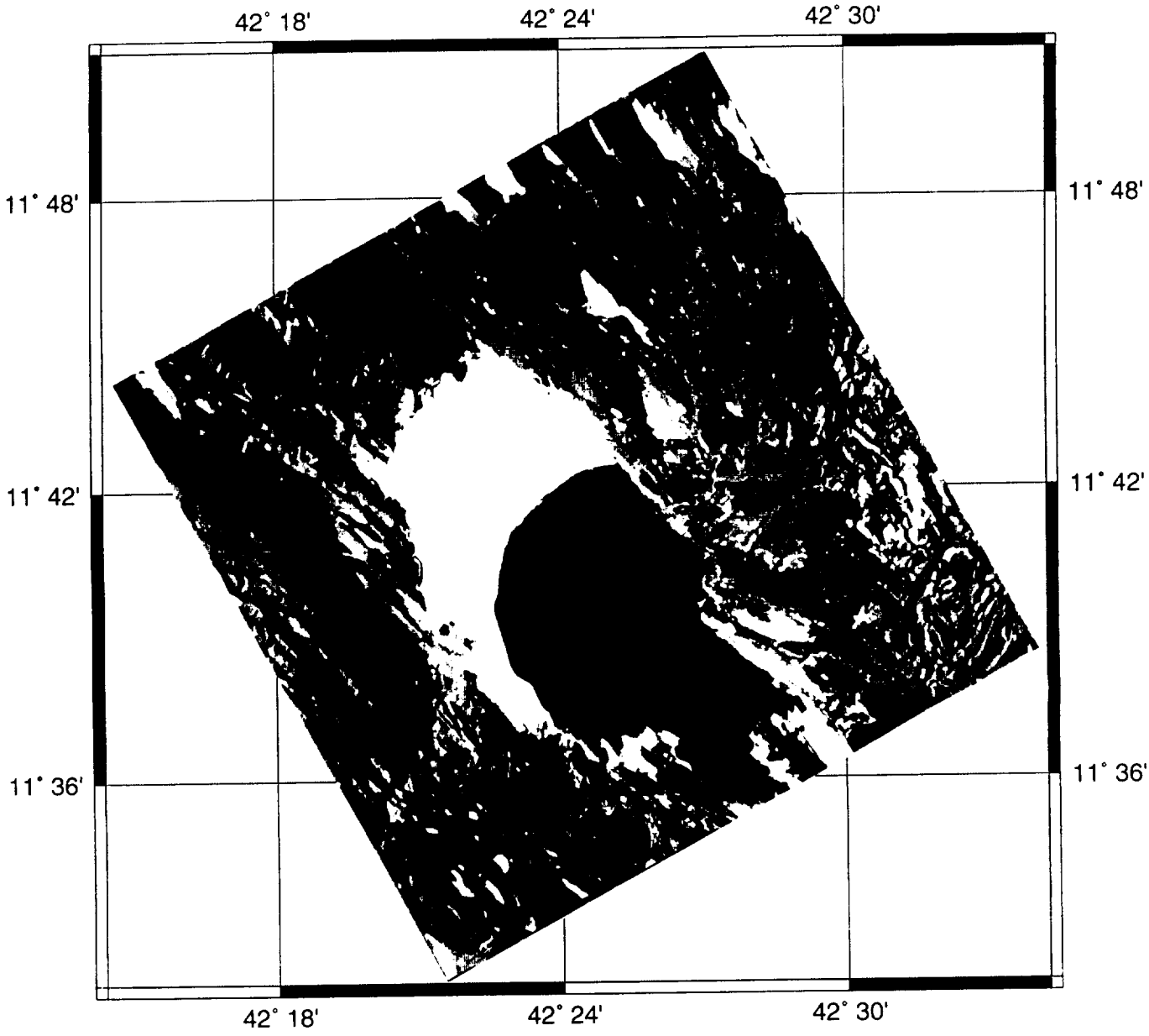

Fig. 3.12A. Electronic Still Camera image of Lake Assal.

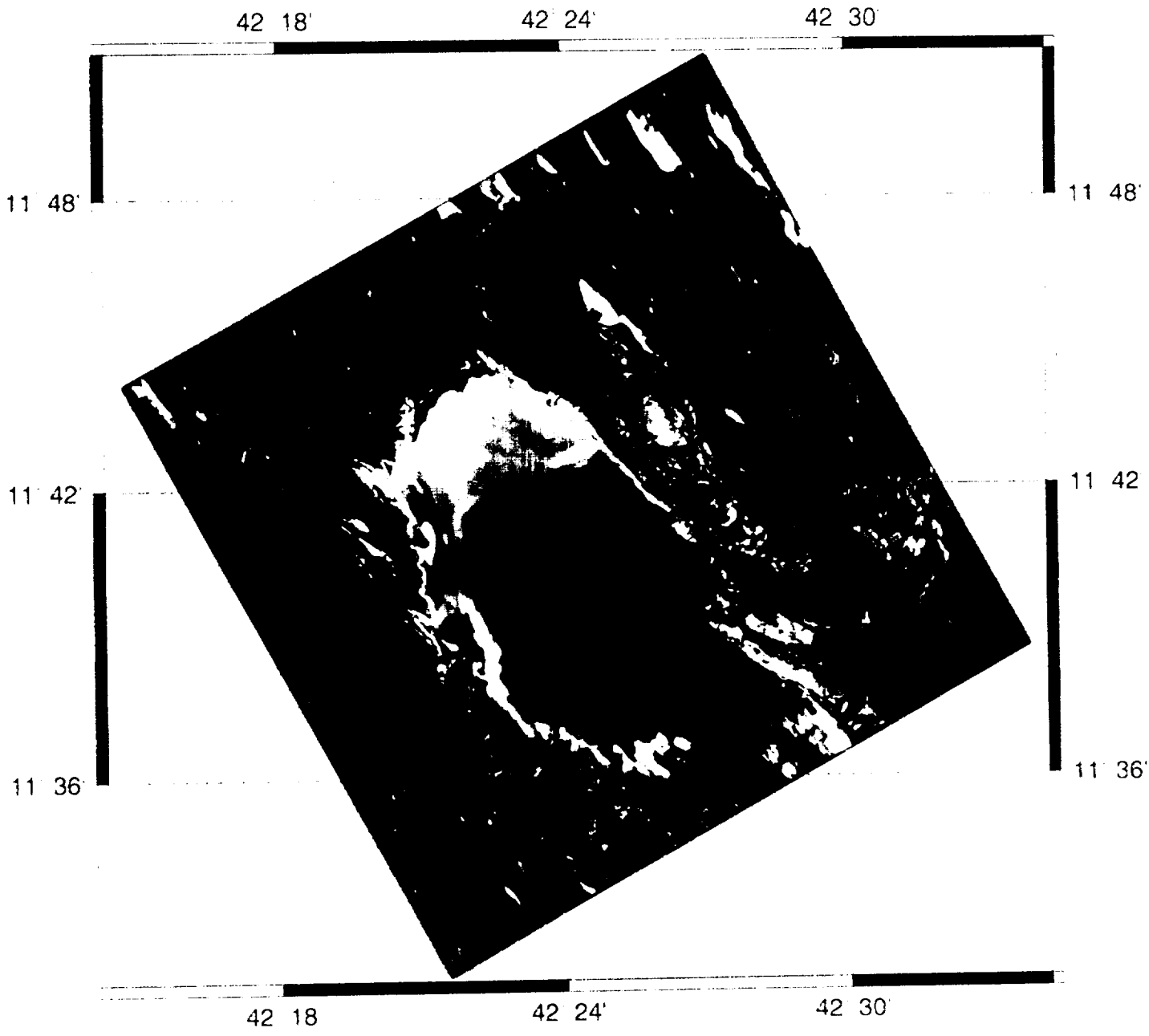

Fig. 3.12B. Subsection of Landsat TM scene covering Lake Assal. B743 = RGB.

Lineaments and Faults around Lake Assal

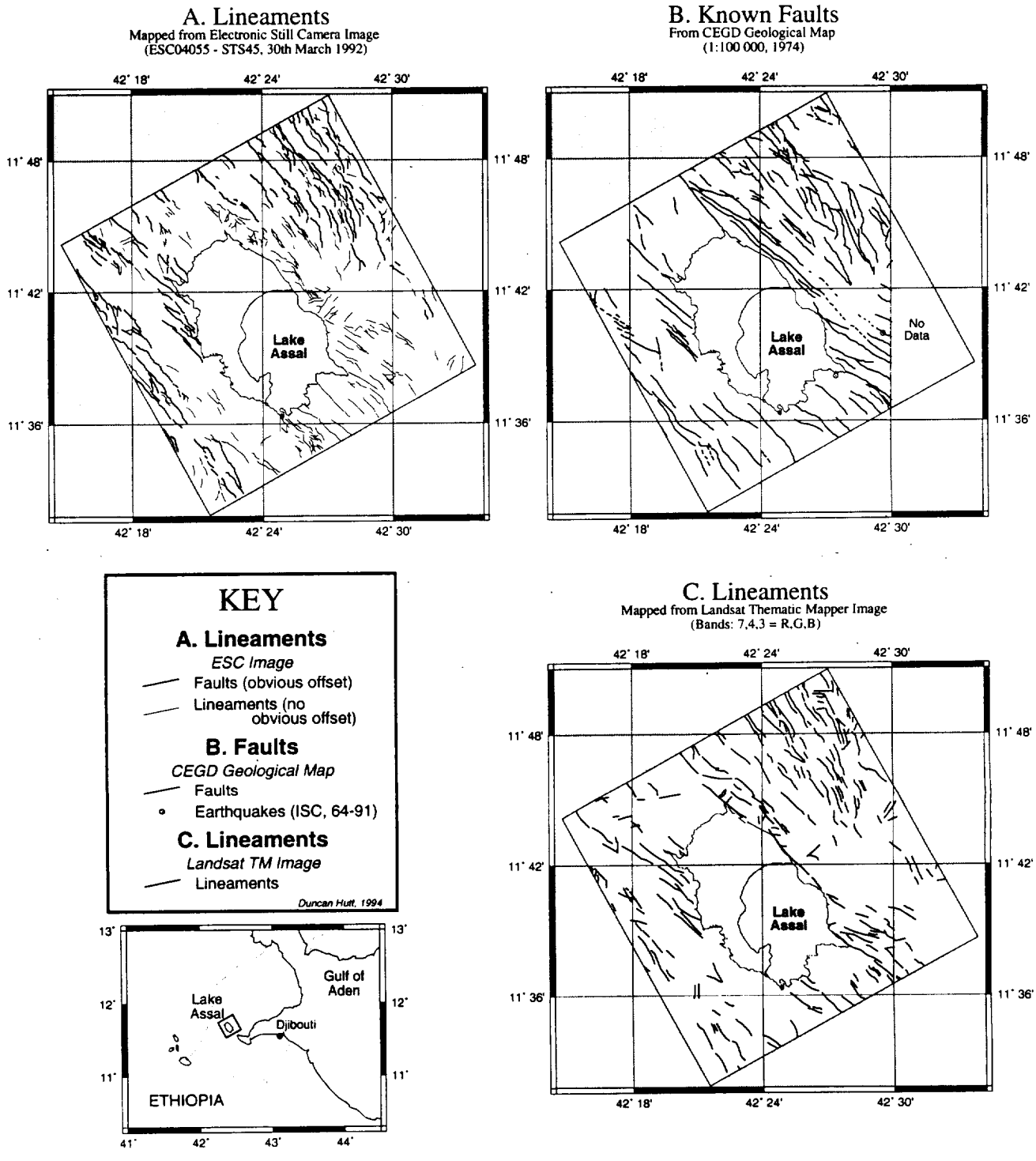

Fig 3.13. Lineaments and Faults in the Lake Assal region. Mapped from ESC and TM Imagery.

CHAPTER 4

The Ethiopia Rift

The Ethiopian section of the East African Rift links Afar with the Kenya rift zone, though the link in the Lakes Abaya, Stefanie and Turkana region is poorly defined. A line of small lakes marks the rift floor. The rift is bounded to the northwest and southeast by the Ethiopian and Somalia Plateaux respectively. Plates 2A and 2B show the AVHRR scene centred on the Ethiopian Rift while figure 4.1 highlights the main geographical features used in the text.

4.1 Background Geology

Upper Palaeozoic sandstones and shales, equivalent to the Karoo, are found in limited locations in central Ethiopia; these are unconformably overlain by Mesozoic marine sediments (Baker *et al*, 1972). As much as 2000m of sediments in central Ethiopia suggest that a subsiding trough lay along what is now the Ethiopian rift, in the Jurassic (Mohr, 1962).

Plateau uplift in Ethiopia, Cenozoic flood-basalt volcanism and rift development are thought to be associated with a mantle hot-spot beneath the Ethiopian plateau (e.g. Burke & Wilson, 1972). The Ethiopia dome has undergone three major phases of uplift. These uplift episodes occurred in the upper Eocene, lower-middle Miocene and in the Pleistocene. Further down-warping of the rift trough accompanied the mid-Tertiary uplift phase (Baker *et al*, 1972). The largest uplift phase has been the most recent; it was associated with major faulting and graben formation in the Ethiopia rift valley (Baker *et al*, 1972).

At the southern end of the Ethiopia rift lies the Amaro Horst (to the east of Lake Chamo) and this causes a bifurcation of the rift into the Chamo and Galana Grabens (Ebinger *et al*, 1993). The Amaro Horst is made up of Precambrian gneisses and Tertiary volcanics; it rises to a height to 2000 m above the flanking grabens and its eastern side is step-faulted, showing evidence of repeated uplifts (Baker *et al*, 1972). The Chamo Graben contains an axial swarm of faults which extends along the entire rift valley. Mohr (1960) termed this axial band of faulting the Wonji Fault Belt.

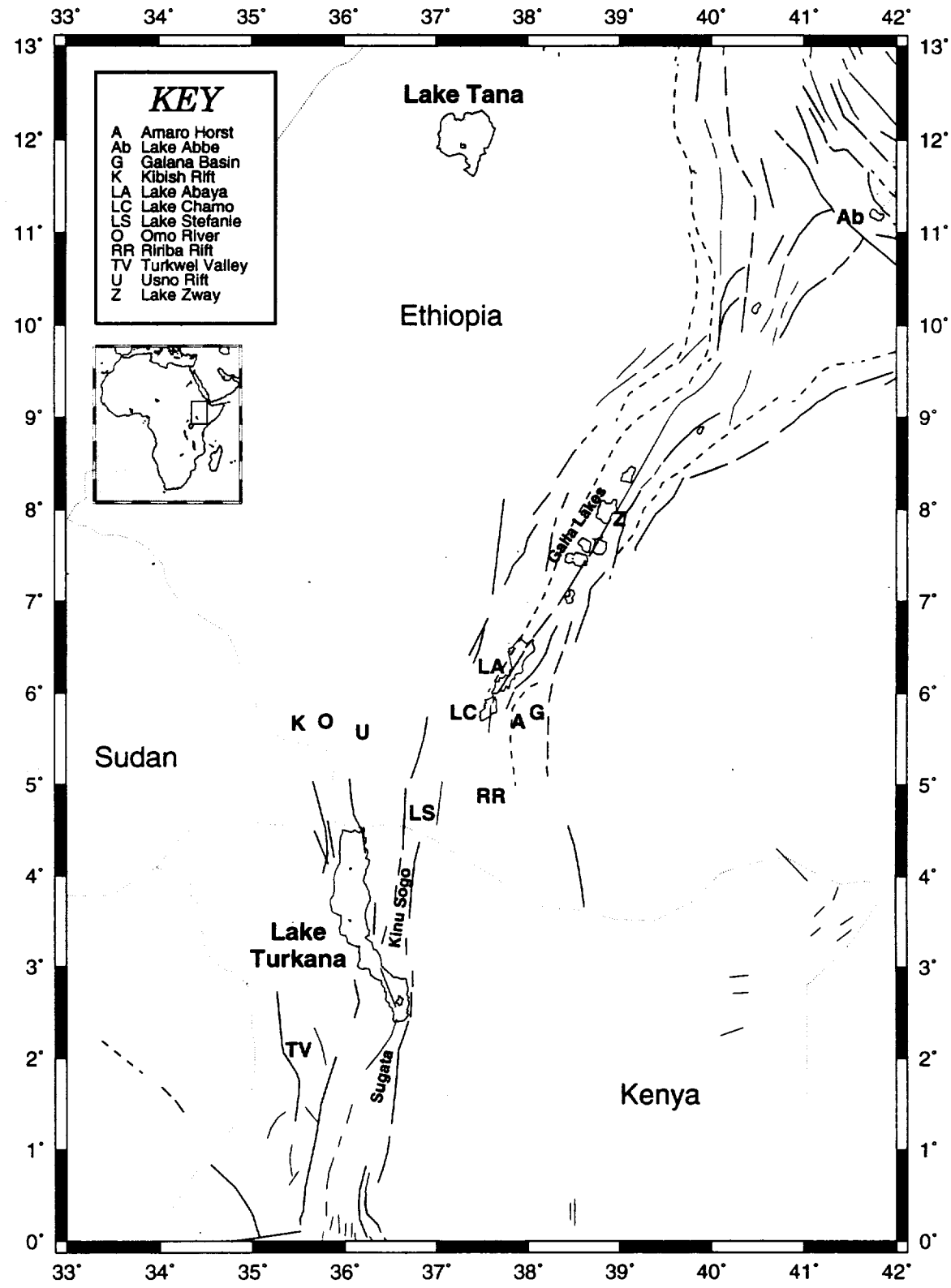

Fig. 4.1. The Ethiopia rift region; location of geographical names used in the text.

The Chamo and Galana Grabens merge to the north of the Amaro Horst in the Lake Abaya region where the rift is about 60 km wide (Baker *et al*, 1972). The rift valley continues NNE with a number of small lakes along its centre. The eastern escarpment of the rift is characterised by a broad zone of rejuvenated faults in the south while in the Lake Awasa region a single escarpment of late Pleistocene faulting is present, with evidence of late Miocene-Pliocene down-warping of the Somalia plateau (Baker *et al*, 1972). East of the Galla Lakes the eastern escarpment is up-warped from the Katar depression of the Somalia Plateau and is characterised by SSW - NNE trending faults of late Pleistocene age (Baker *et al*, 1972). Much of the western flank is obscured by a series of small volcanic cones. West of Lake Abaya the western flank trends northwards to cause a widening of the rift to about 80 km at 8°N, at which point the faults curve back to the normal, NNE, trend of the rift (Baker *et al*, 1972).

The Wonji Fault Belt is a 5 - 12 km wide band of faulting which lies axially along the rift valley (Mohr & Wood, 1976). The faults are associated with the most recent phase of rifting and are generally short and normal with occasional tensional fissures (Gouin & Mohr, 1967). The Wonji Fault Belt is made op of 12 *en echelon* segments which are NNE trending, these segments are 60 ± 12 km long with mean offsets of 21 ± 8 km; the separating segments are 8 ± 2 km long (Mohr & Wood, 1976). While the Wonji belt is generally axial, north of the Galla Lakes it lies next to the eastern rift flank leaving the majority of the rift floor without any major faulting (Baker *et al*, 1972).

Geological evidence suggests that the Ethiopia rift has opened by 2 km in 0.9 Ma, a rate of about 2 mm/yr, (Mohr *et al*, 1980). This value gives 35% total extension ($\beta = 1.35$) of which all but 2% has occurred within the Wonji Fault Belt (Mohr, 1973). In central Ethiopia a rate of 0.6 mm/yr for the 13 Ma of development is recognised (Mohr, 1987). Plate tectonic considerations have suggested rates of 4.3 mm/yr (McKenzie *et al*, 1970) and 2.7 mm/yr (LePichon & Francheteau, 1978). Mohr (1987) accounts for the differences between geologically determined rates and those found from plate tectonics as being due to the existence of low-angle decollements, with low-angle reverse, simple shear in the lithosphere.

Studies using teleseismicity have indicated that the crustal thickness of the plateau is 30 - 35 km at a distance of 500 km west of the rift and 40 - 45 km thick along the rift flanks (Searle & Gouin, 1971). Gravity studies along the rift are consistent with the presence of tapering asthenoliths as close to 3 km below the rift floor (Mohr, 1987). Searle & Gouin (1972) determined that these asthenoliths are 70 km wide at the base of the crust at 7.8° N, 55 km at 7.4°N and 40 km at 7.1°N and are discontinuous.

Rifting in southern Ethiopia is more complex than that of a single rift valley as seen further north. This region marks the junction between the Kenya rift and the Ethiopia rift. At 5.5°N the whole rift system is 300 km wide and is made up of a number of discrete rift valleys. West to east these are the Kibish, Omo, Usmo, Stefanie and Ririba rifts. The Omo and Usmo rifts are the northerly extension of the Turkana rift, the Stefanie rift is a continuation of the main Kenya rift trend and the Ririba rift is connected to the main Ethiopia rift (Moore & Davidson, 1978).

4.2 AVHRR

Two band combinations of the AVHRR data are considered; B211 ⇒ RGB and B521 ⇒ RGB, plates 2A and 2b respectively. The image is largely free of cloud except in the southwest corner where cloud is lying over the Turkwell and Uganda escarpments. A few, small, regions of cloud are also present on some of the highland areas but very little interferes with the view of the rift itself. The resolution of the image worsens towards the northeast, in Afar. The Afar region is, however, covered adequately by plates 1A and 1B and thus no attempt was made to use this image to map lineaments in Afar. The scene was acquired on 30th December 1986.

Plate 2A (B211) highlights the vegetation in red, while plate 2B (B521) shows it as green; the arid desert and semi-desert regions are highlighted in red on plate 2B. Much of the highland regions are characterised by vegetated regions and are the areas where most of the cloud cover is situated. While there are relatively few mappable lineaments along the Ethiopia rift, its course is clearly visible, with a line of small rift floor lakes along its centre.

The rift funnels out of the southwestern corner of Afar and trends in a southwesterly direction through Ethiopia. At about 8.5°N the rift appears to be offset by about 50 km to the west, south of which it resumes the same directional trend as it had to the north. South of Lake Abaya the rift becomes less clearly defined and bifurcates. One branch continues on the same directional trend towards Lake Stefanie while an eastern graben trends almost north-south from Lake Abaya.

A NW - SE trend across Lake Turkana is clearly seen on the B521 imagery as a break between the vegetated highland regions. Structure trending in a southeasterly direction from the southern end of Lake Turkana is also seen, and matches the Jurassic, Anza rift

direction and location. The cross over of the Cenozoic rifting in East Africa and the Jurassic, Anza rift appears to be characterised by a diffuse zone of rifting, the opening of the largest of the eastern branch lakes and an almost rhombic lowland region between 1.5°N and 5°N.

The lineaments mapped using AVHRR imagery are shown in figure 4.2 where they are compared to mapped faults (UNESCO, 1968). Lineaments in Afar have not been mapped from these AVHRR scenes, plates 2A and 2B, as they are already mapped using the scenes in plates 1A and 1B.

Figure 4.2A shows the lineaments mapped using B211 AVHRR imagery. Lineaments along the rift valley associated with the Wonji Fault Belt have been mapped. In Afar the western and southern scarps were clearly visible but in the Ethiopia rift they are not so clearly defined. The rift limits are fairly well controlled in the Galla Lakes region but further south this is not the case. The western edge of the Amaro Horst has been mapped but neither the eastern side or the Galana Graben have been picked out. Part of the Stefanie rift is seen as is the Kinu-Sogo extension of the Kenya rift.

The lineaments mapped from AVHRR B521 are shown in figure 4.2B. The lineaments mapped using B521 are comparable to those mapped using B211 though less structure is mapped along the valley floor. The B521 imagery has, however, picked out the Amaro Horst and the Galana Graben to its east. A NNW-SSE structure has been picked out on the Ethiopia border at about 38°E, this corresponds to a N-S fault on the UNESCO map.

In general the lineaments mapped from AVHRR imagery do not compare well with the faults shown on the UNESCO (1968) map, however these faults do not show features such as the Amaro Horst and seem to indicate an idealised rift structure rather than a true representation.

4.3 Topography

Figure 4.3 shows the topography of the Ethiopia rift. Few features along the rift floor are of a large enough scale to be seen using this topographic data, though some volcanic cones are visible. The valley scarps are well defined along the eastern flank while the western scarp is less distinct. The broadening of the valley from 7°N to 8°N and the subsequent narrowing towards Afar are also clear. The Amaro horst and the Chamo and Galana grabens to its west and east respectively are also seen at about 6°N. South of

Lineaments mapped from AVHRR Imagery

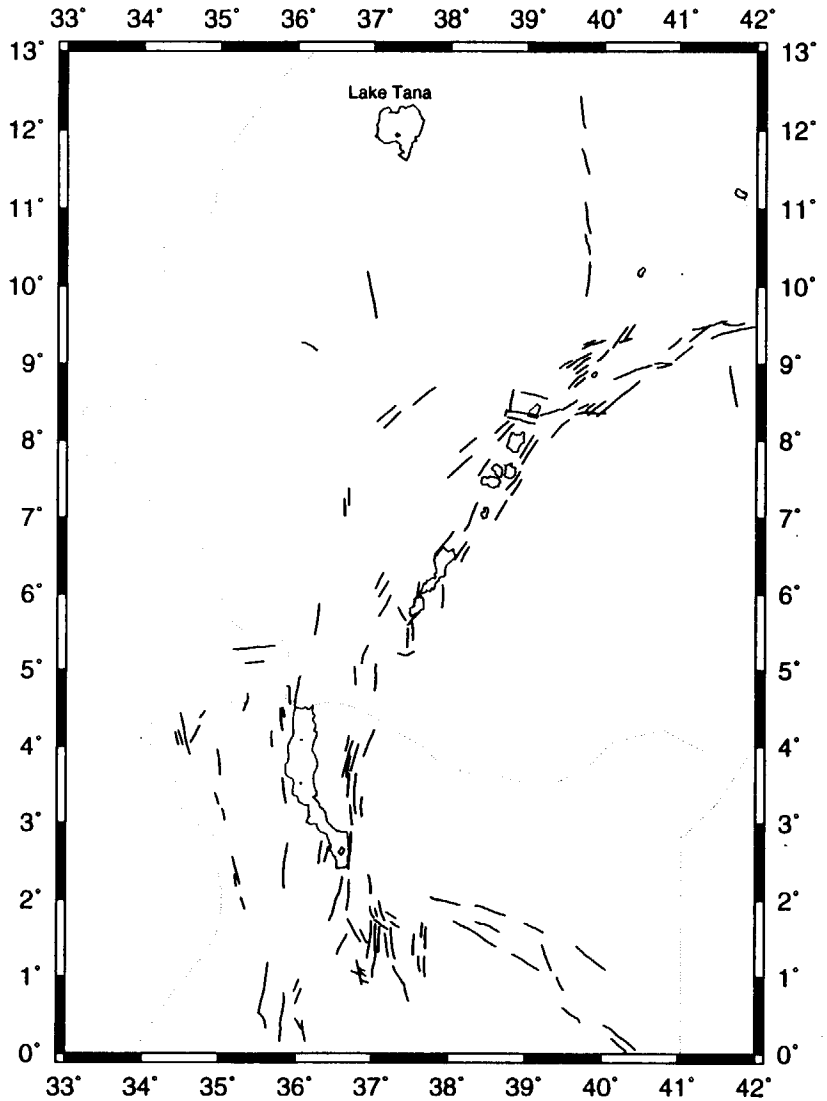

Faults of the Ethiopia Rift Region

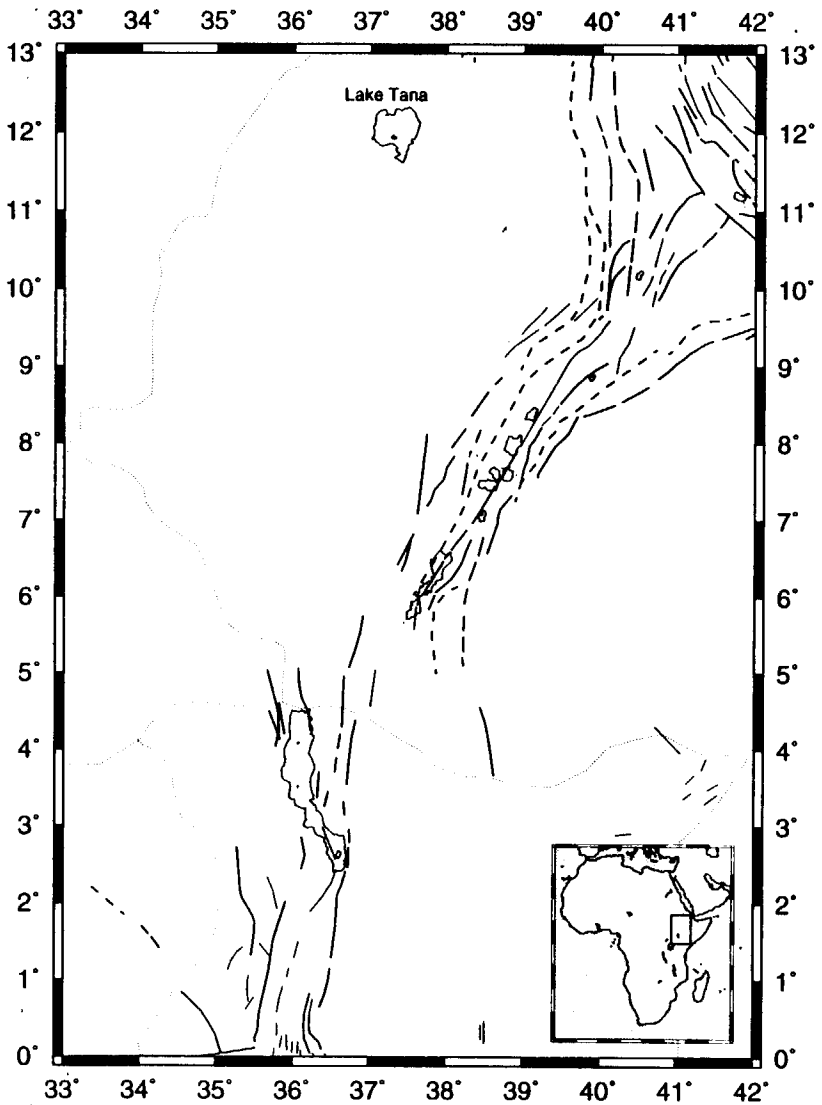

Fig. 4.2A. Lineaments and faults of the Ethiopia Rift region. A. Lineaments mapped from AVHRR (B211 = RGB) imagery: B. Faults from UNESCO (1968).

Lineaments mapped from AVHRR Imagery

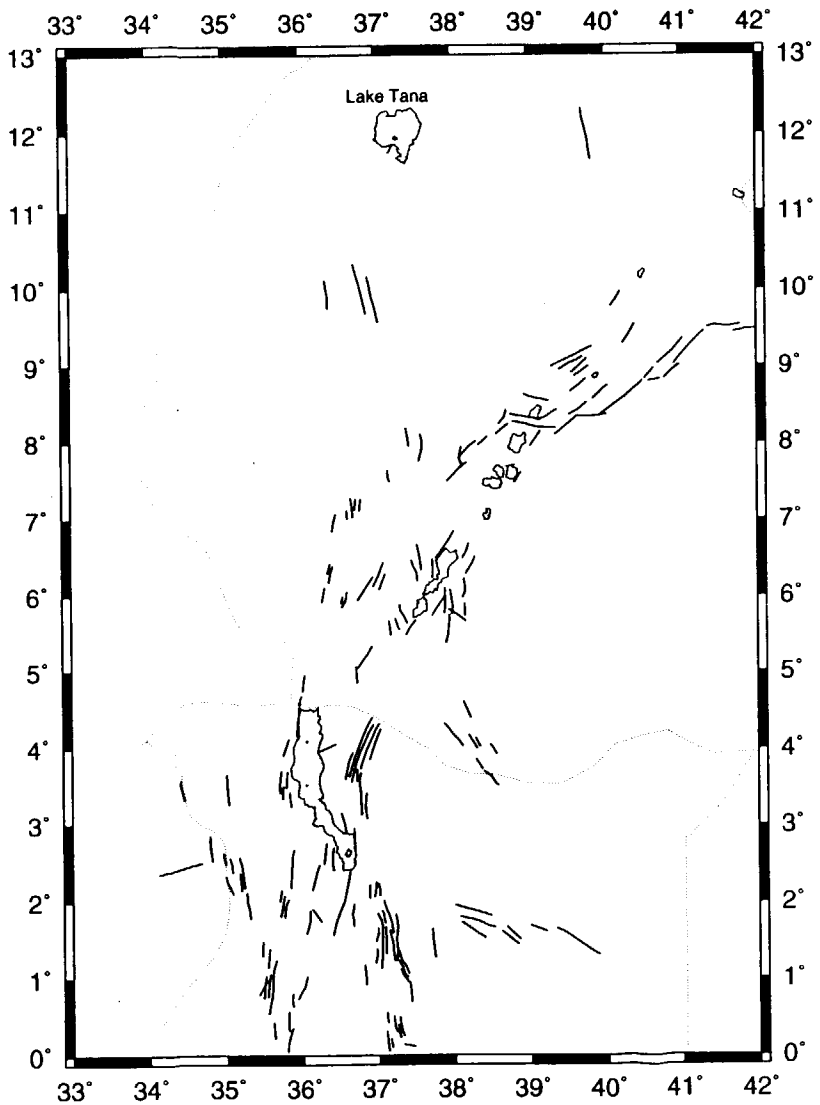

Faults of the Ethiopia Rift Region

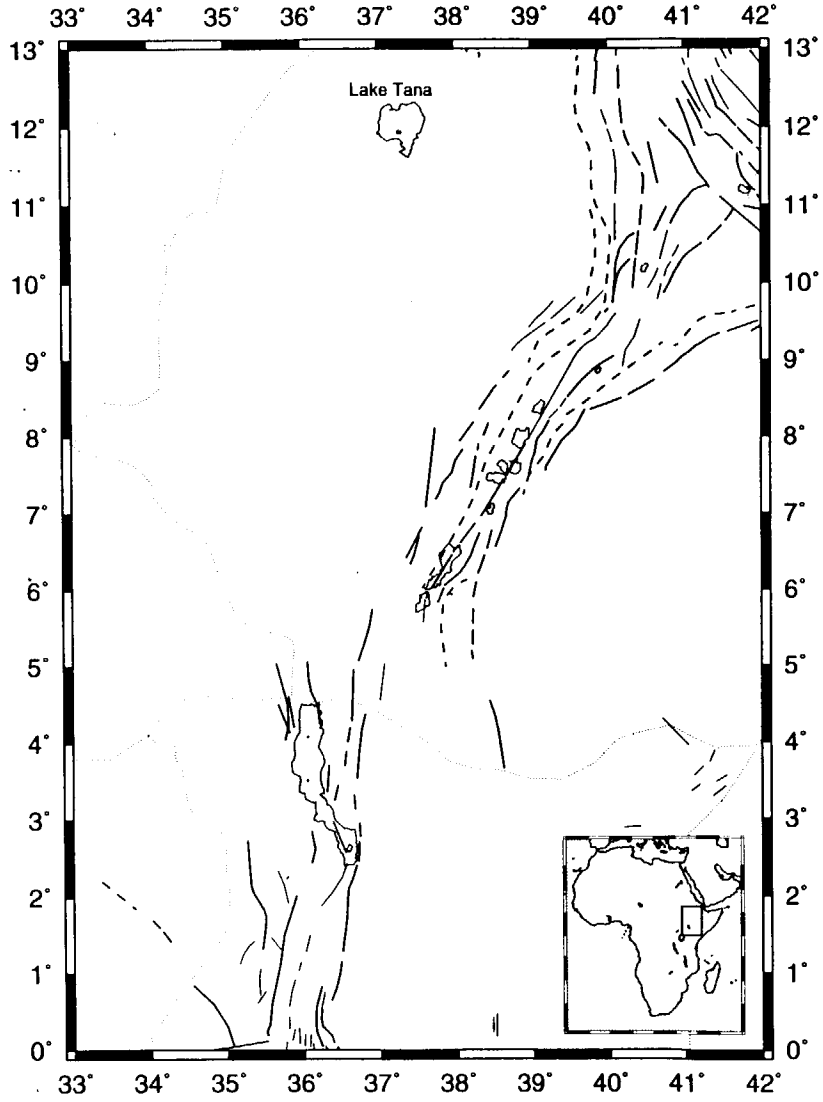

Fig. 4.2B. Lineaments and faults of the Ethiopia Rift region. A. Lineaments mapped from AVHRR (B521 = RGB) imagery: B. Faults from UNESCO (1968).

Topography of the Ethiopia Rift

Terrain-30 Topography Data

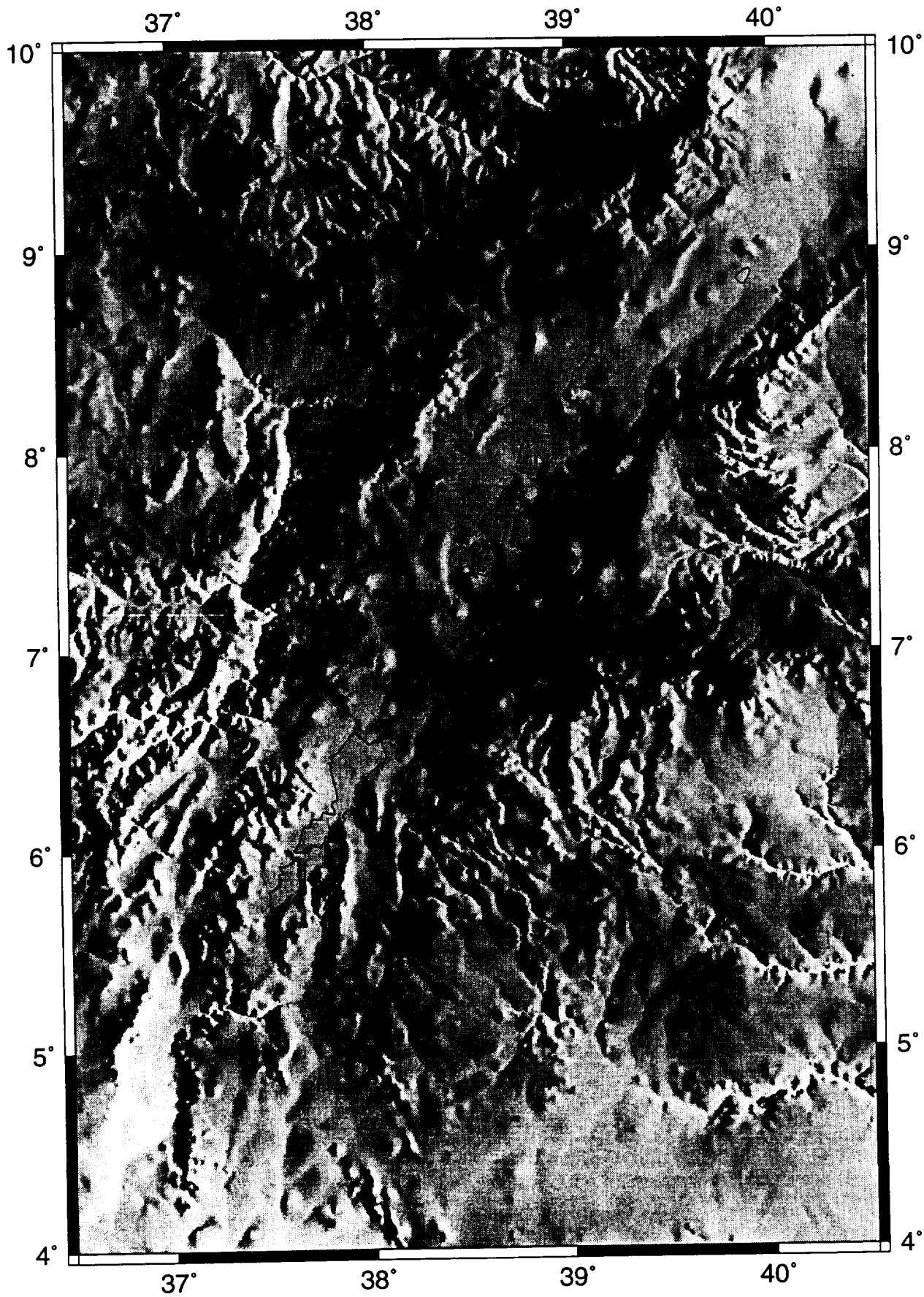

Fig. 4.3. Topography of the Ethiopia rift, illuminated from the east.

Lake Chamo the rift dies out and this is highlighted by the topography. The Lake Stefanie rift (around 5°S, 36.8°E) is also visible. The offset at about 8.5°N is also visible on the topography of the area though not so clear as seen using AVHRR.

AVHRR imagery draped over topography was considered for the Afar region, figure 3.3, and this also includes much of the Ethiopia rift valley. The oblique views of the rift, figures 3.3 A & B, clearly shows the highest point of the rift between Lake Zway and the Awash River (an elevation of 1700 m (Baker *et al*, 1972)). On these views it is also clear that the rift is at its broadest at 8°N. The Amaro horst and northern end of the Stefanie rift can be seen at the top of figure 3.3B.

4.4 Seismicity and Volcanism

The teleseismicity and volcanism of the Ethiopia rift are shown in figure 4.4. Very few earthquakes have occurred within the rift in the period of 1964 to 1991 with only 6 being recorded by the ISC between 6°N and 10°N. Four of these rift events have had a magnitude of $m_b \geq 5.0$. A magnitude $m_b = 5.0$ event occurred at about 7°N on 20th January 1995 (NEIS, preliminary determination). The focal plane mechanisms (Dzeiwonski *et al*, 1983 etc) have all shown normal faulting which have generally indicated extension perpendicular to the rift, figure 1.6. Nine events have been recorded in the zone linking the Ethiopia and Kenya rifts.

Volcanoes are widespread in and around the Ethiopia rift. The majority of Holocene centres lie axially along the rift valley and are generally confined to the Wonji Fault Belt (Mohr & Wood, 1978). Mohr & Wood (1978) determined that the mean spacing of volcanoes which have been active in the Pliocene and/or Holocene is 43 ± 13 km. Eight of these volcanoes have calderas. The pre-Holocene volcanoes mapped by Nusbaum *et al* (1994) are much more broadly spread than the Holocene centres and extend across a zone of about 500 km perpendicular to the rift.

Seismicity and Volcanism of the Ethiopia Rift Region

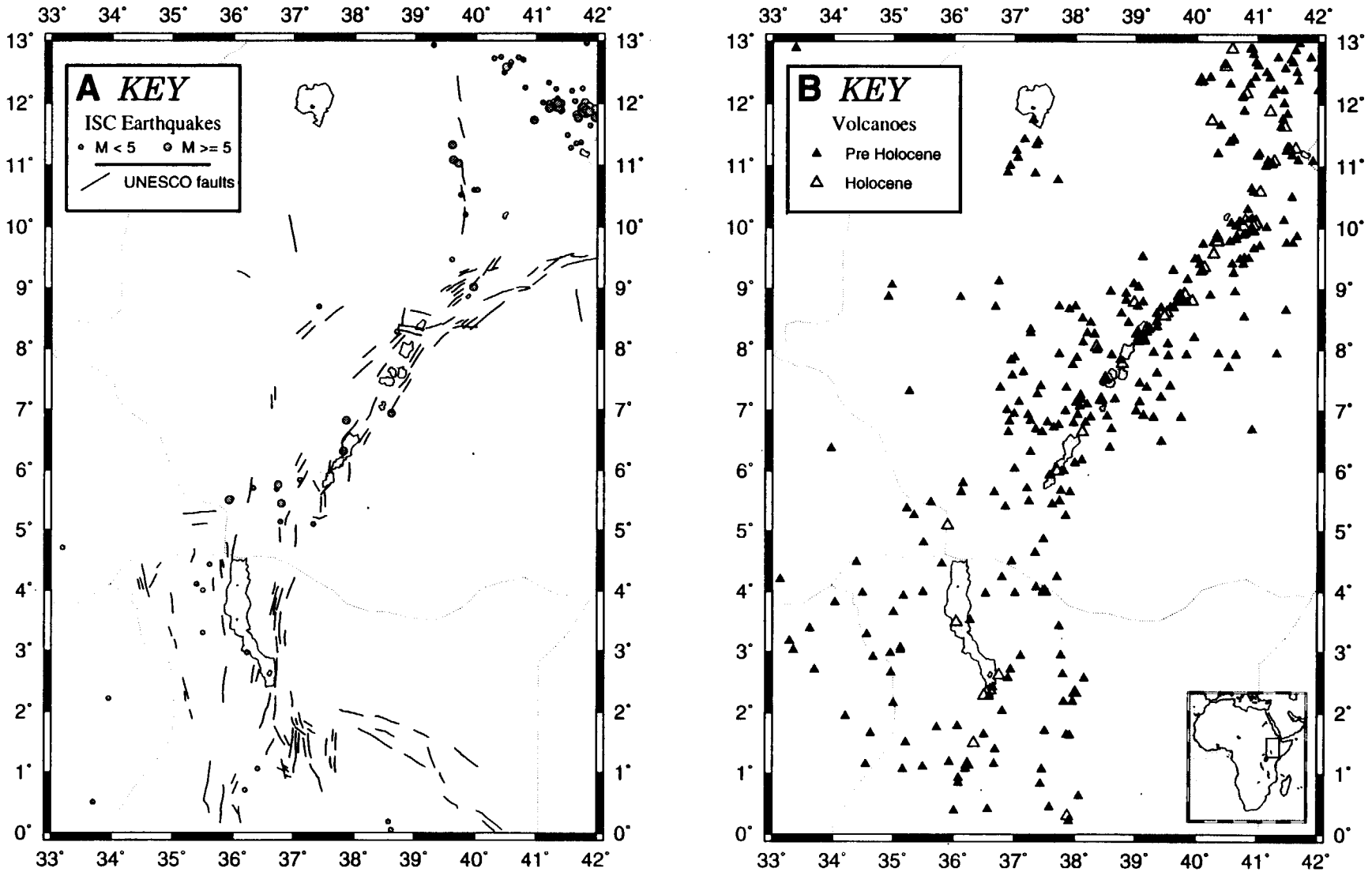

Fig. 4.4. The Ethiopia rift region, earthquakes, volcanoes and faults. A. Earthquakes from ISC (1964-1991), lineaments from AVHRR (B211); B. volcanoes from Nusbaum et al (1994).

CHAPTER 5

The Kenya Rift

The Kenya rift extends from Lake Turkana south to northern Tanzania. Plates 3A and 3B show the AVHRR scene centred on the Kenya rift; the location of the main geographical features mentioned in the text is given in figure 5.1. Between the south end of Lake Turkana to about 3°S the rift trends approximately north-south between about 35.5° and 37°E. South of 3°S the rift splays outwards to form a series of grabens, half-grabens and horsts somewhat similar to basin and range features. In the north the rift widens towards Lake Turkana with the Turkwell and Uganda escarpments trending northwest from about 1°N. The trend of the Kenya rift continues northwards from the southern end of Lake Turkana along the Kinu-Sogo rift while the Lake itself is also rift-bounded with minor rifts continuing to the north of Lake Turkana. The Kavirondo (Nyanza) rift is an east-west rift running from Lake Victoria to the Kenya rift valley at the equator.

5.1 Geological Background

The rift in Kenya cross cuts the Kenya dome, an elliptical area of uplift approximately 1000 km across and with a maximum uplift of about 1700m in the region of 36°E, 0°N, (Baker & Wohlenberg, 1971). The oldest rift structures are mid Tertiary with the first extensive rift faults dated as early Pliocene (Baker & Wohlenberg, 1971). There have been a number of episodes of faulting which have continued into the Recent and the rift has also been characterised by major periods of flood basalt extrusion (Baker *et al*, 1972). Within Kenya, the rift is essentially a graben structure though the side of greatest throw alternates in a series of half graben like zones (Bosworth, 1985; Rosendahl, 1987). In Northern Tanzania and the Lake Turkana regions the classic rift valley morphology breaks down into a series of splayed faults which are generally down-thrown to the east (Baker & Wohlenberg 1971; Dawson 1992).

The geological history of the Kenya rift is essentially an interrelated sequence of domal uplift, faulting and flood basalt flows. Though a few of the faults in the region may have been associated with a Jurassic rift system cutting across northern Kenya (Reeves *et al*, 1987) and reactivated since, the majority of rift faults are mid Tertiary or younger. McConnell (1972) suggested that the rift followed pre-existing structures in the

The Kenya Rift

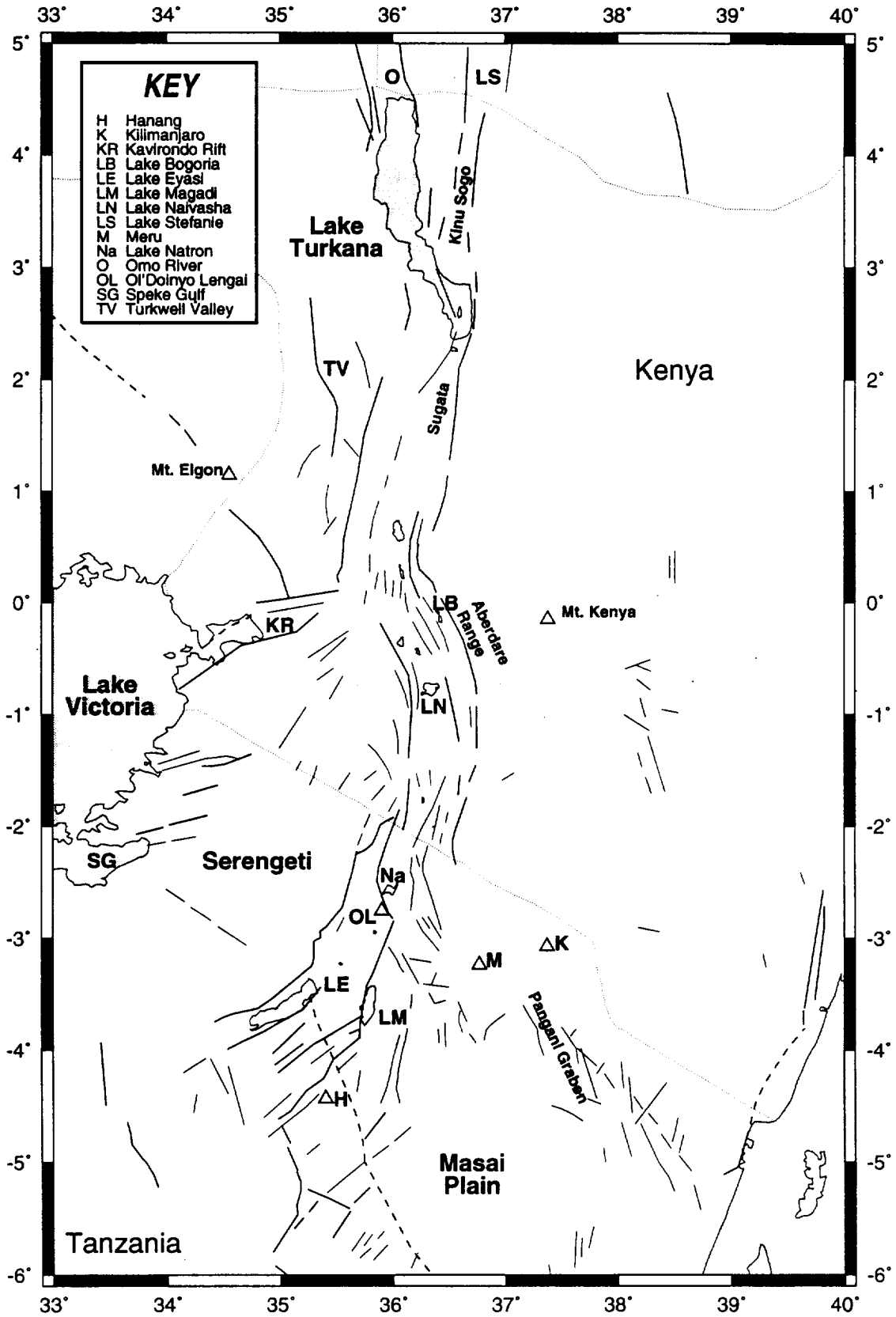

Fig. 5.1. The Kenya rift. Location of geographical features used in the text.

Mozambique belt though Baker *et al* (1972) suggest that the number of faults following former trends is not greater than would be expected.

The oldest recognisable basalts in the Kenya rift region are in the Allia Bay area of Lake Turkana which have been dated to 35.2 ± 1.8 Ma (Hackman *et al*, 1990). Further basaltic flooding occurred through the Oligocene. In the early Miocene monoclinal upwarping occurred on the Kenya/Uganda border region which caused downflexing in the Turkana region and the initiation of faulting. The Turkwell fault was initiated at this time and is the oldest recognisable fault relating to the Kenya rift: Miocene volcanics partly filled the newly forming Turkana depression (Baker *et al*, 1972).

Domal uplift of about 300m maximum occurred on the Kenya dome in the mid to late Miocene and deformation and uplift in northern Tanzania created a depression in the Lake Natron area which was fault or 'warp' bounded and bifurcated around the Masai block to the south (Dawson, 1992). Major shield volcano eruptions within this depression immediately followed; the oldest lavas are not exposed, however dates of up to 8.1 Ma have been obtained (Bagdasaryan *et al*, 1973).

At the culmination of the Miocene uplift phase extensive faulting formed a meridianal trough faulted on the west side. This was followed by minor phonolite and trachyte flows, in the newly formed central trough, and later by extensive basalt eruptions along the entire length of the trough and the formation of the Aberdare Range (Baker & Wohlenberg, 1971).

While minor faulting continued in northern Tanzania the late Pliocene in Kenya was characterised by massive eruptions of trachytic ignimbrites, in the Naivasha region, which filled the rift and overflowed its flanks (Baker *et al*, 1972). This was followed by the major phase of uplift which lifted the marginal plateaux by up to 1400 m (Baker & Wohlenberg, 1971). At this time the first of several graben phases began which created the outline of the present Kenya rift, which was followed by trachyte volcanisn that flooded most of the graben floor (Baker *et al*, 1971).

Local rejuvenations of the Kenyan graben continued into the mid Pleistocene, also at about this time the graben floor was shattered by swarms of minor faults (Baker *et al*, 1972). In northern Tanzania, however, a major faulting phase began which gave rise to the present line of the rift valley (Dawson, 1992). A major fault, down-thrown to the east, formed to the western side of the present day Lakes Natron and Manyara and is dated to between 1.2 and 0.9 Ma (McIntyre *et al*, 1974). The eastern margin of what is

essentially a half graben in this region is formed by a number of small faults and downwarps.

The most recent phases of activity in the Kenya rift have been associated with volcanism. In northern Tanzania high explosive volcanism occurred into the late Pleistocene characterised by pyroclastic deposits and tuff cones (Dawson, 1992). Meanwhile, in Kenya trachytic, basalt-trachytic and phonolite caldera volcanoes built up axially along the floor of the inner graben while basaltic, multi-centre chains and fields formed to the east of the rift (Baker & Wohlenberg, 1971).

The Kavirondo rift branches from the Kenya rift at the equator, at the centre of the Kenya uplift (Baker *et al*, 1972). The rift trends west and then southwest near Lake Victoria. It is about 20 km wide and made up of two grabens separated by a region with monoclinal downflexing rather than faulting (Shackleton, 1951). The rift probably formed in the early Pliocene and contains no Quaternary faulting or volcanism (Baker *et al*, 1972).

5.2 AVHRR

The Kenya rift is covered with AVHRR imagery, from 1st March 1987, with two band combinations being used in the studies; B211 $\Rightarrow$ RGB, and B521 $\Rightarrow$ RGB, plates 3A and 3B respectively. This image is largely cloud free with only minor cloud cover along the rift valley. Many of the higher peaks have cloud caps but these are mainly confined to the peaks themselves. The Serengeti and Masai plains to the south and southwest of the scene are characterised by scattered cloud cover.

The two AVHRR scenes, plates 3A and 3B, clearly highlight the vegetation cover in the southwest of Kenya and in much of Tanzania. The volcanic peaks of Kilimanjaro and Meru are seen to be isolated within less vegetated lowlands and both have a cloud cap. Mounts Elgon and Kenya are also clearly seen from the cloud associated with them.

The Kenya rift, and to a lesser extent the Kavirondo rift, are seen as bands passing between the more vegetated highland flanks. The line of small rift valley lakes also highlights the course of the rift valley. North of about 1°N the narrow, well-defined, valley is no longer traceable as it splays out into the Turkana region. A line of vegetated peaks, trending north-northwest from 1°N, 36°E marks the boundary escarpments of the Turkwell depression. To the east of Lake Turkana a slightly arcing structure

(aproximately trending N-S) is a manifestation of the Kinu-Sogo rift with the Lake Stefanie Rift barely visible to the north. Also in the northern part of the scene, the trend of the Anza Rift is seen following a northwesterly direction form about 1°N, 40°E.

The clearly defined rift is seen as far south as about 3°S. At this point the rifting associated with Lakes Manyara and Eyasi continue south and southwesterly respectively. To the southwest of Lake Eyasi two areas of wet, marshy, land are seen to arc the southwesterly trend of the Eyasi rift to a more southerly direction at 34°E. South of Kilimanjaro the Pangani graben is clear. The Speke rift, at the sourtheast corner of Lake Victoria, is not seen on either AVHRR scene.

Figure 5.2 shows the AVHRR mapped lineaments compared to the mapped faults of the Kenya rift region (UNESCO, 1968). Both B211 and B521 show the Kinu-Sogo rift to the east of Lake Turkana and both indicate some northward continuation of the Turkana trough. The eastern scarp of the Sugata trough is also clear on both scenes but only B521 shows any linear features to the west of that trough. The B211 image shows very little of the rift between 0.5°N and 1.5°N, particularly on the eastern flank. The B521 delimits this section of the rift reasonably well and has also indicated the presence of the Turkwell escarpment better than the B211 scene. The B521 image delimits the Kavirondo rift better than B211 although the main rift valley from the equator to about 3 °S is more clearly defined on the B211 image.

Some of the valley floor faulting shows on both B211 and B521 imagery between Lakes Naivasha and Natron. Both AVHRR band combinations show a SW - NE band where no lineaments are observed, trending NE from Lake Eyasi. This hiatus is not seen on the UNESCO map but is shown by Baker *et al* (1972, figure 11) as a band with distinctly less faults than the surrounding areas. The Eyasi fault scarp is seen on both scenes but the faulting around Lake Manyara is unclear.

The Pangani rift trending SSE from Kilimanjaro shows on both AVHRR scenes but is clearer on B211. Likewise lineaments trending SE from the south end of Lake Turkana, associated with the failed Anza rift, are also picked out more clearly on B211. SSE lineaments paralleling the Pangani graben and running to the east of Kilimanjaro are observed on both AVHRR scenes. These match the local direction of ductile shear in the Mozambique belt as presented by Mosley (1993, figure 1).

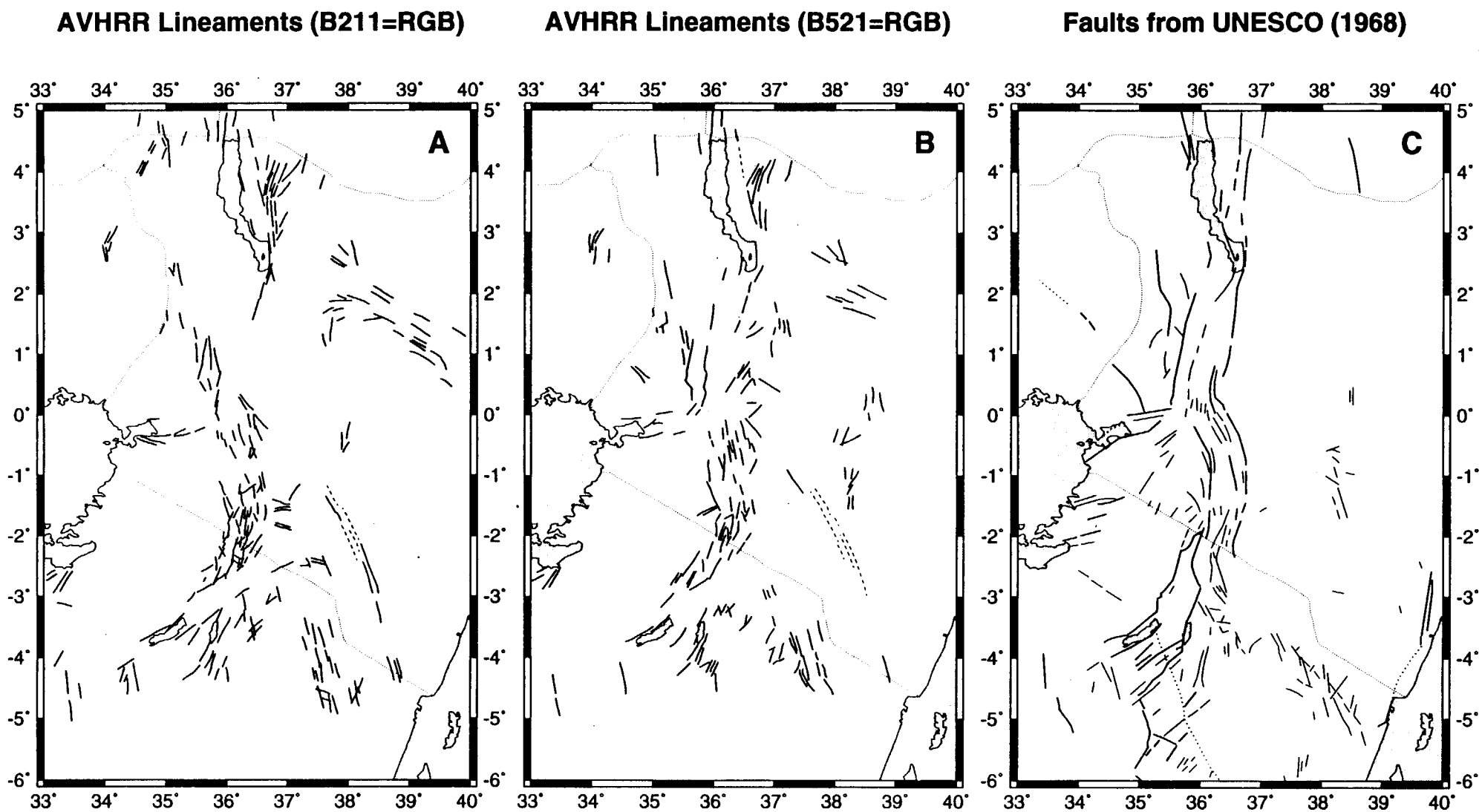

Fig 5.2. Faults and Lineaments of the Kenya Rift. A. AVHRR mapped lineaments, B211 = RGB; C. AVHRR mapped lineaments, B521 = RGB; C. Faults from UNESCO (1968).

5.3 Topography

The topography north of the equator is shown in figure 5.3A while the main rift, south of the equator, is given in figure 5.3B. An overlap with the Ethiopian rift topography, figure 4.3, occurs in the Lake Stefanie rift region and some features relating to the Kinu-Sogo rift which joins this to the Kenya rift can be seen at around 3.9°N, 36.7°E.

Lake Turkana lies at the eastern edge of a relatively featureless triangle which marks the northern termination of the Kenya rift graben. This depression ranges from altitudes of 300 to 1000 m compared to elevations up to 3500 m on the Turkwell escarpment, which marks the south-western edge of the depression (Baker *et al*, 1972). The Omo and Usmo rifts which extend northwards from Lake Turkana are unrecognisable as rift valleys on the topography.

South of the Lake, the Turkana depression narrows to a minimum at about 1°N. Immediately south of Lake Turkana lies the Sugata Valley, the eastern scarp of which is clearly seen. At about 1°N the classical graben topography of the Kenya rift becomes visible. The eastern scarp is not well defined but there is a distinct change from the relatively flat valley floor to more rugged terrain. To the west there are two scarps, the innermost at 35.8°E and the outermost, the Elgeyo escarpment, at 35.5°E. Mount Elgon is clearly seen at 34.5°E, 1.1°N. The floor of the rift valley between 1.5°N and 0.5°N is seen as a flat valley punctuated by a number of small volcanic cones, mostly near the east side.

South of the equator, figure 5.3B, the rift valley is clearly seen from its junction with the almost indistinguishable Kavirondo rift at the equator. At this point, the rift valley is trending SSE towards Lake Naivasha where the valley veers southwards again. A double scarp marks the eastern boundary of this section with the Aberdare range to the east. A more distinct single scarp marks the western boundary with the Mau range. As the rift trends south the limits of the valley become less distinct until at 2.5°S, Lake Natron, the graben morphology breaks down. At 3.5°S the scarps marking the western edges of the Eyasi and Manyara half grabens are visible the latter of which is traceable as far south as 4.5°S. At 4.4°S, 35.4°E a small volcanic cone, Hanang, can be seen just to the south of the scarp.

An almost W-E trending line of volcanoes marks the change in rift morphology at around 3.2°S, this line terminates at Kilimanjaro at about 37.2°E, 3°S. To the south of Kilimanjaro the Pangani rift trends SSE; the eastern scarp, with the Pare Mountains, is

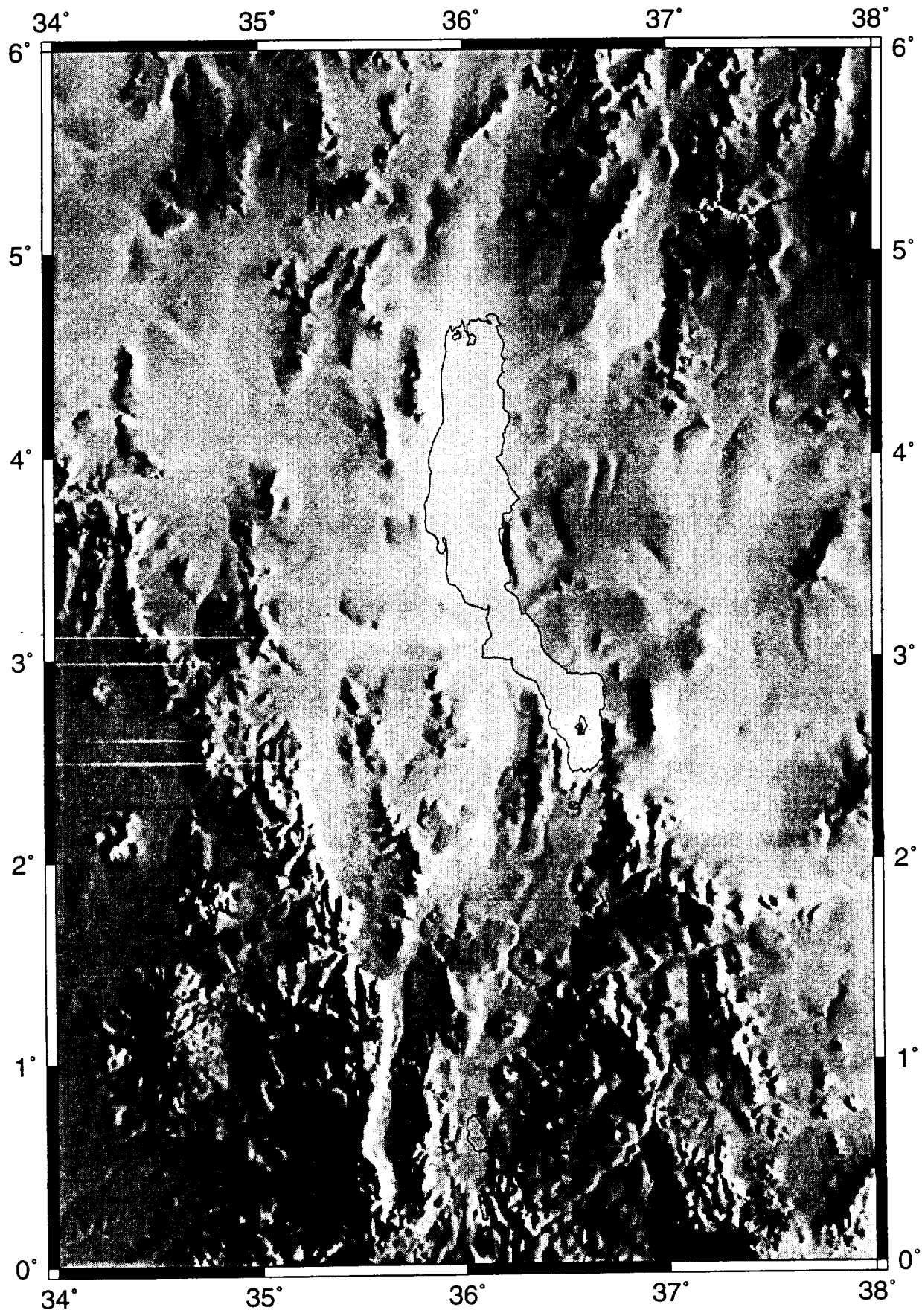

Fig. 5.3A. Topography of the Kenya rift north of the equator, illuminated from the east.

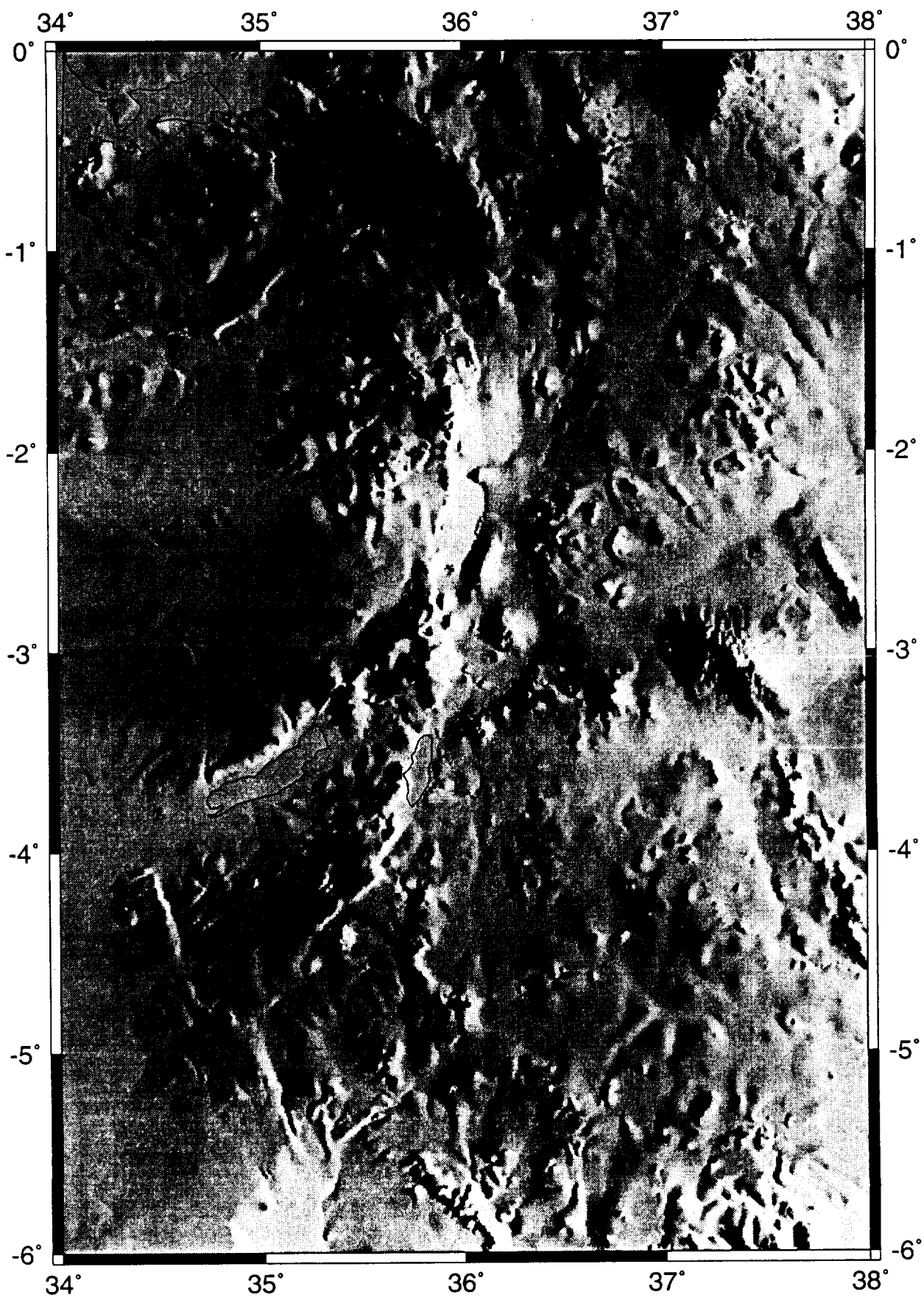

Fig. 5.3B. Topography of the Kenya rift south of the equator; illuminated from the east.

clearly defined on the topography. Between the Manyara rift and Pangani rift is the Masai plain. South and west of Hanang the terrain is cut by a series of lineaments which parallel both the Eyasi and Manyara escarpments in a SW-NE trend. In addition some perpendicular linear features are also seen.

5.4 Seismicity and Volcanism

Figure 5.4 shows that, for the period of 1964 through to 1991, there were fewer than 10 ISC determined epicentres for the region north of 3°S. Data from earlier this century and evidence from microseismic studies indicates that the rift does have seismic activity. In 1929 a large, M_S = 6.9 (Ambraseys, 1991b), event occurred at Subukia. Studies of microseismicity, using local seismometer networks, have shown that the rift is far from aseismic (e.g. Tongue *et al*, 1992). Tongue *et al* (1992) showed that there were three main regions of microseismic activity: southern Lake Turkana and the Sugata valley, The Kavirondo rift; and the Kenya rift around Lake Bogoria. Additionally some scattered activity also occurred on the eastern rift flank. There are some ISC listed earthquakes in the Kavirondo rift. An interesting change in seismicity occurs at about 3°S; to the south seismicity becomes more widespread. At 3°S there is a W - E line of epicentres, figure 5.4, which matches a line of volcanoes.

The northern Tanzania portion of the rift is also active on a microseismic scale, Rykounov *et al* (1972) observed about 30 events per day in the M_L = 0.5 - 3.5 range. Less events were observed in the Kilimanjaro and Meru areas than in the Eyasi and Manyara rifts, with a small swarm being observed at the southern end of Lake Manyara. All the depths were in the 35 - 45 km range.

Volcanoes are frequently present in the Kenya rift north of 3°S but south of this point the volcanoes die out, figure 5.4. The Kenya rift valley contains a line of volcanic centres, those such as Menengai are now seen as large calderas following explosive eruptions along the rift. Ol'Doinyo Lengai, in northern Tanzania (at about the point where teleseismicity is observed to start), is the only volcano with active eruptions in the Kenya rift (e.g. Dawson *et al*, 1994), however, many others still have hot springs associated with them and some have erupted in historic times.

The Kenya Rift

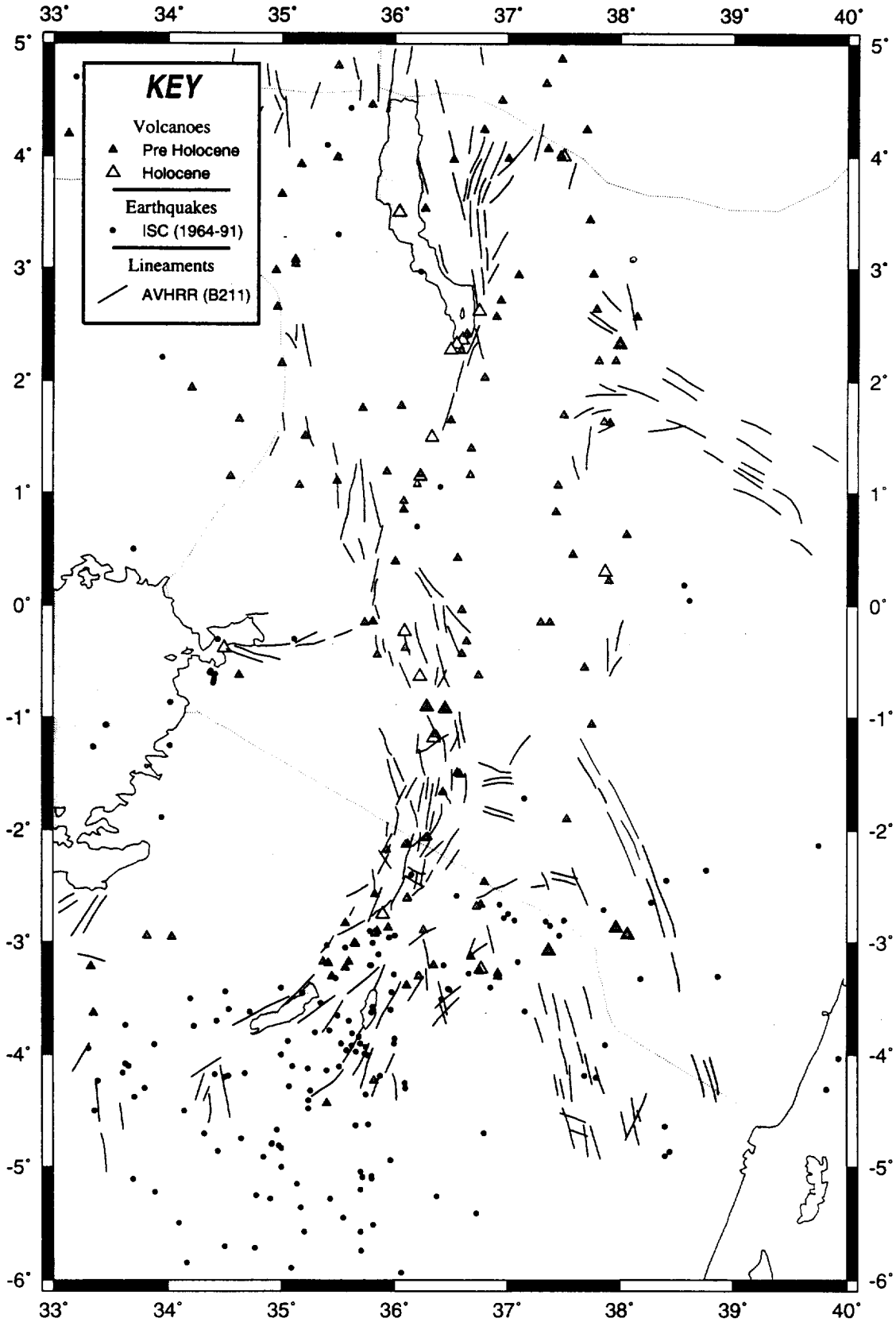

Fig. 5.4. Earthquakes, Volcanoes and Faults of the Kenya rift. Earthquakes from the ISC (1964 - 1991); Volcanoes from Nusbaum et al (1994); lineaments from AVHRR (B211).

5.4. MSS Mosaic

Lineaments from a mosaic of thirteen MSS scenes of the Kenya rift, figure 5.5, have been mapped and are shown in figure 5.6. Most of the rift valley is well defined with the line of the rift clearly shown through Kenya.

East of Lake Turkana the Kinu-Sogo rift trends south to the southern end of the Lake from where the Sugata Valley continues the rift line. At the southern point of Lake Turkana another band of lineaments diverges SSE from the SSW trending rift valley. This band dies out at Mount Kenya and is possibly related to shear zones in the Mozambique belt (e.g. Mosley, 1993). West of Lake Turkana the Turkana depression bounded to the west by the Uganda and Turkwell escarpments is seen narrowing to the main rift valley at about 0.5°N.

Rift valley fault swarms are present from about 1°N to the equator where a hiatus occurs at the junction with the Kavirondo rift. Valley floor fault swarms are seen again south of Lake Naivasha at about 1.2°S and extend as far as the Tanzania border. Where the simple rift valley morphology changes to basin and range structures, in northern Tanzania, the coherency seen on the MSS scenes is lost and only a few faults are recognisable. A number of lineaments have been mapped on the western flank of the valley between about 0.5°S and 1.5°S: some of these lineaments may be faults but others are almost certainly due to drainage patterns on the high land to the west.

A rose diagram for the directions of MSS mapped lineaments, figure 5.6, shows a very strong N-S trend with three directional peaks, 0°, 8° and 352°. These reflect the changes in rift direction from just west of north to just east of north, near the equator. The mean azimuth is N3.3°E, averaged over 17 300 km of lineaments.

Figure 5.7 compares the MSS lineaments with those mapped from AVHRR (B211). The Kinu-Sogo rift and eastern scarp of the Sugata valley show good correlation but otherwise the two data-sets show poor correlation north of the equator. To the south of the equator the correlation in the rift valley is good and the break in faulting observed at about 3°S, running NE from Lake Eyasi, is seen on both maps.

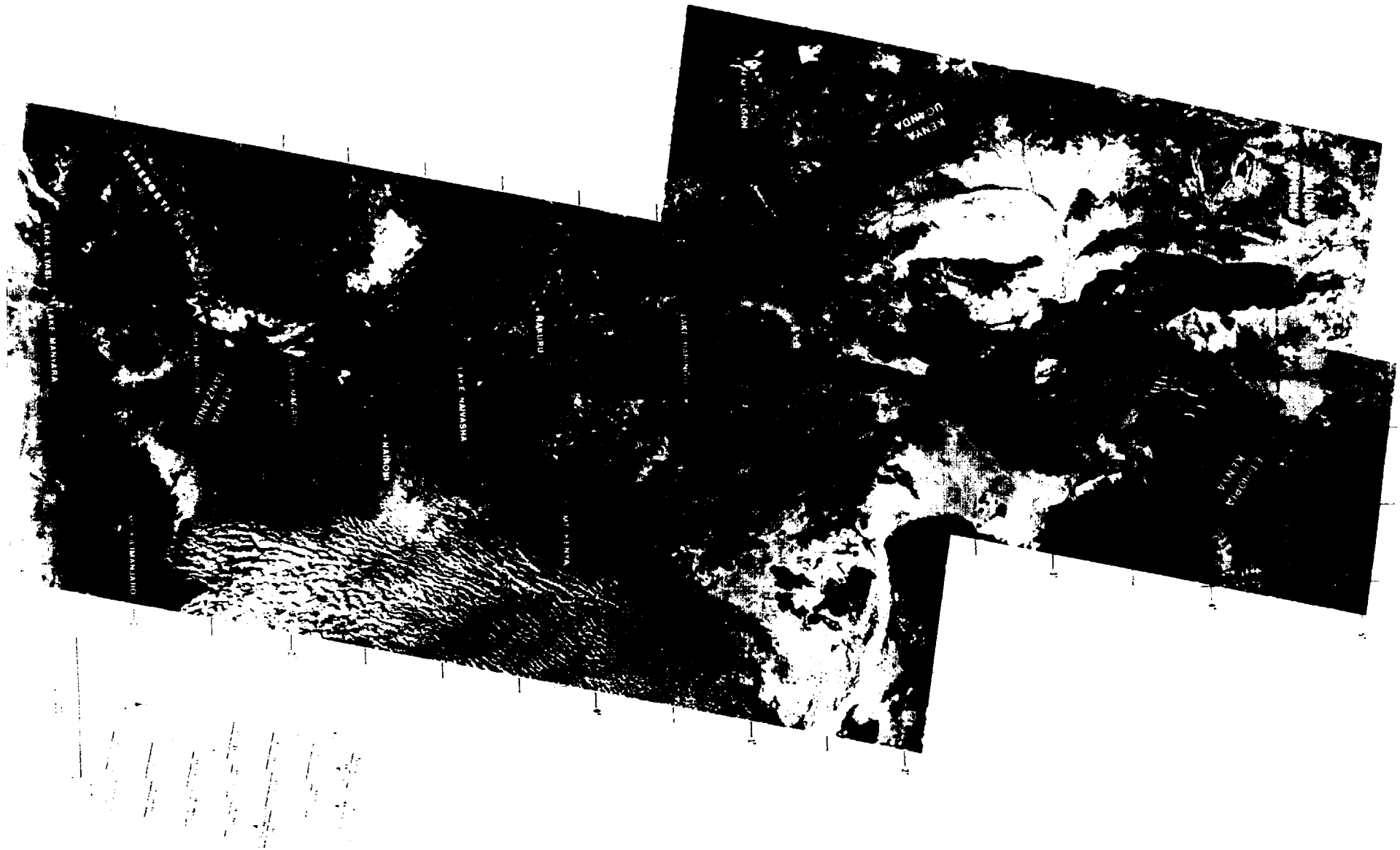

Fig. 5.5. Landsat MSS mosaic of the Kenya rift. Mosaic of 13 scenes from 24th and 25th January 1976 and 18th January 1978. From U. S. Geological Survey.

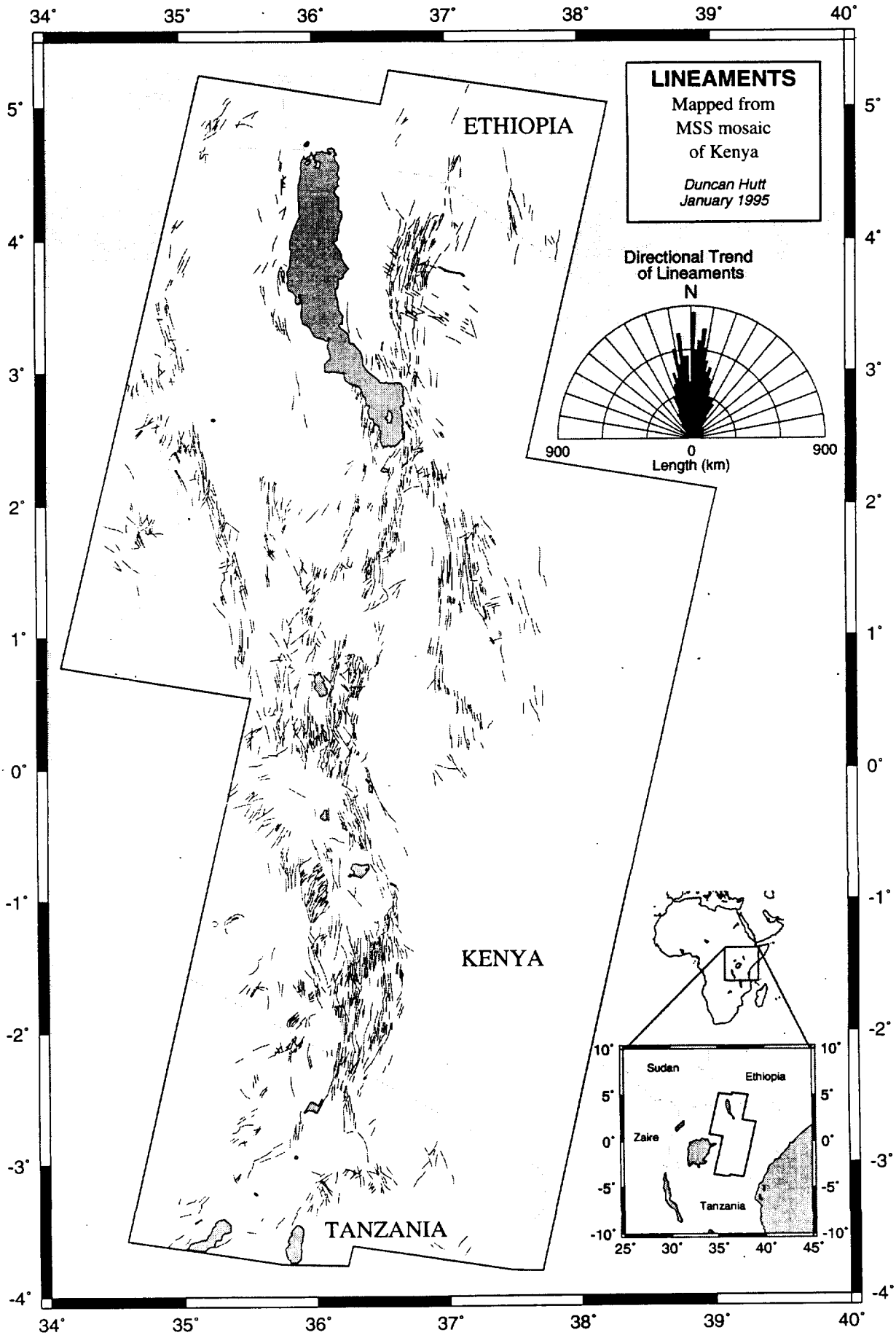

Fig. 5.6. Lineaments of the Kenya rift mapped from the USGS mosaic of 13 MSS scenes.

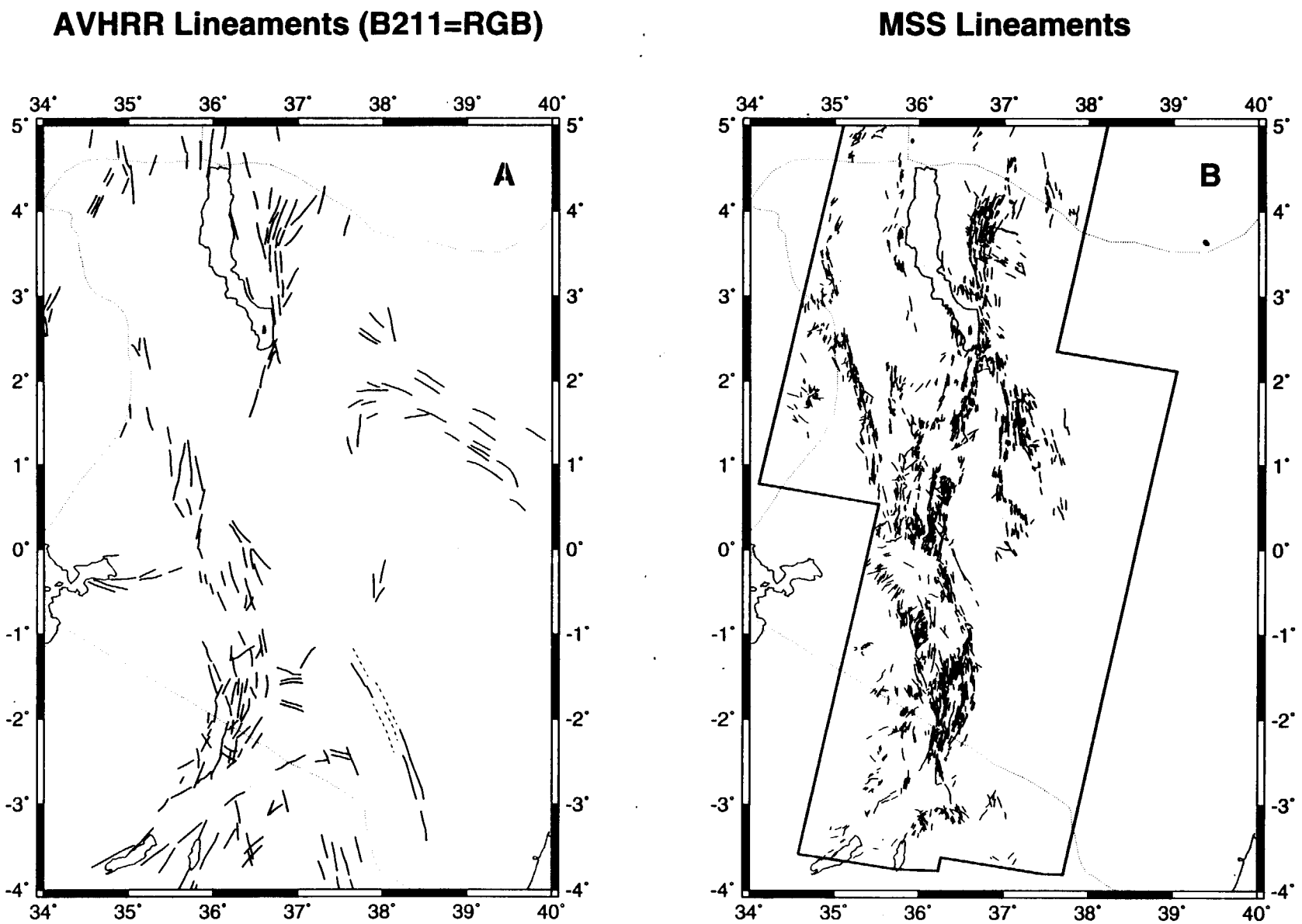

Fig 5.7. Lineaments of the Kenya Rift. A. AVHRR mapped lineaments, B211 = RGB; B. MSS mapped lineaments.

5.5 The Central Kenya Rift (TM and SPOT)

The Landsat TM scene, figure 5.8, straddles the equator and covers the section of the rift between Lake Baringo and Lake Naivasha. This region is the point at which the rift veers slightly eastwards and also marks the junction with the Kavirondo rift. Figure 5.9 shows the lineaments mapped from the TM scene with those mapped from AVHRR overlaid.

The TM lineaments show grid faulting of the valley floor but the heavily dissected boundary scarps do not show up well on the imagery. The valley floor faults are small scale and recent and hence well preserved. The older scarps are much larger and may have overall throws of 1000m or more; these older, larger faults, or series of step faults, have been eroded and cut through. The erosion makes it difficult to map these scarps on high resolution imagery. In contrast the 1.1km resolution AVHRR delimits both the Kenya and Kavirondo rifts as large scale topographic features. Some close matching of AVHRR and TM lineaments is seen at the southern edge of the TM scene particularly at the boundary of the Aberdare Range to the northeast of Lake Naivasha. Directional trends of lineaments west of Lake Baringo are also similar to the AVHRR mapped features but the AVHRR lineaments appear to be offset by about 5 km to the east of TM lineaments. The rose diagram, figure 5.9, of the lineaments mapped from the TM image shows the same strong N-S directional trend as the MSS.

The SPOT scene lies to the southwest of Lake Bogoria (Hannington) and is shown in figure 5.10. Much of the scene is characterised by agricultural areas, on the lower ground, and partially forested regions at higher altitudes. The northeastern quadrant shows dense faulting of the rift floor. Figure 5.11 shows the mapped lineaments. The fault trends are once again predominantly N-S.

Figure 5.12 compares the interpretation of the SPOT image with that from other imagery of the same area. In general the SPOT and TM lineaments show a good correlation in terms of density and orientation; however the MSS mapped lineaments highlight the relative low resolution of this data-set compared to TM and SPOT. Certain faults have been highlighted on all three data-sets, in particular the line of faulting directly south of Lake Bogoria. In this case the AVHRR lineaments do not match those seen on other imagery. As to be expected the AVHRR does not show the relatively small network of valley floor faults around Lake Baringo but sees the change from valley floor to more hilly terrain. This change is observed on the SPOT image but no specific lineaments are mappable.

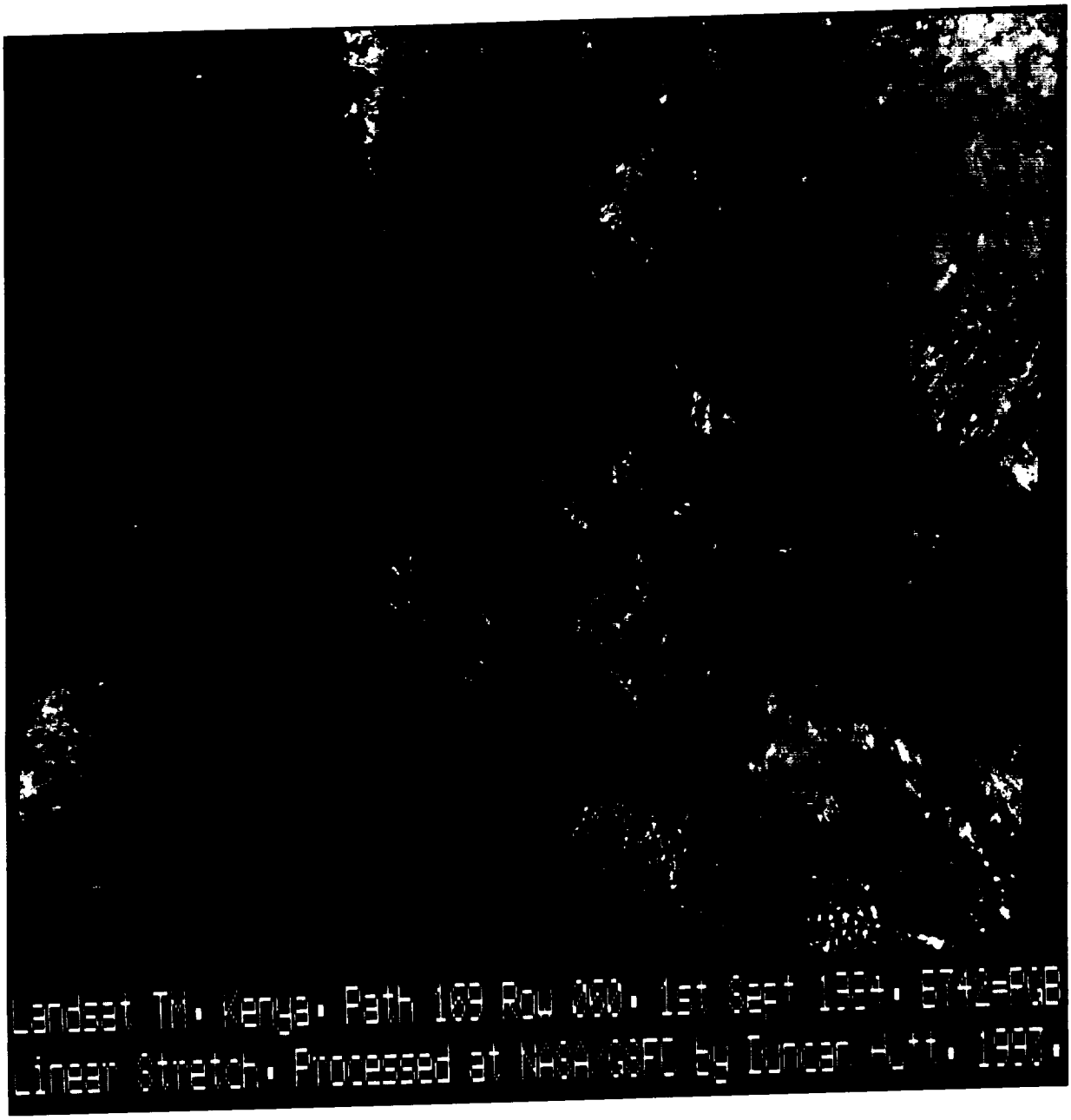

Fig. 5.8. Landsat TM scene of part of the central Kenya rift; B742 = RGB.

Lineaments in Central Kenya

Mapped from Landsat Thematic Mapper Image

(Bands: 7,4,3 = R,G,B. Path: 167, Row:52)

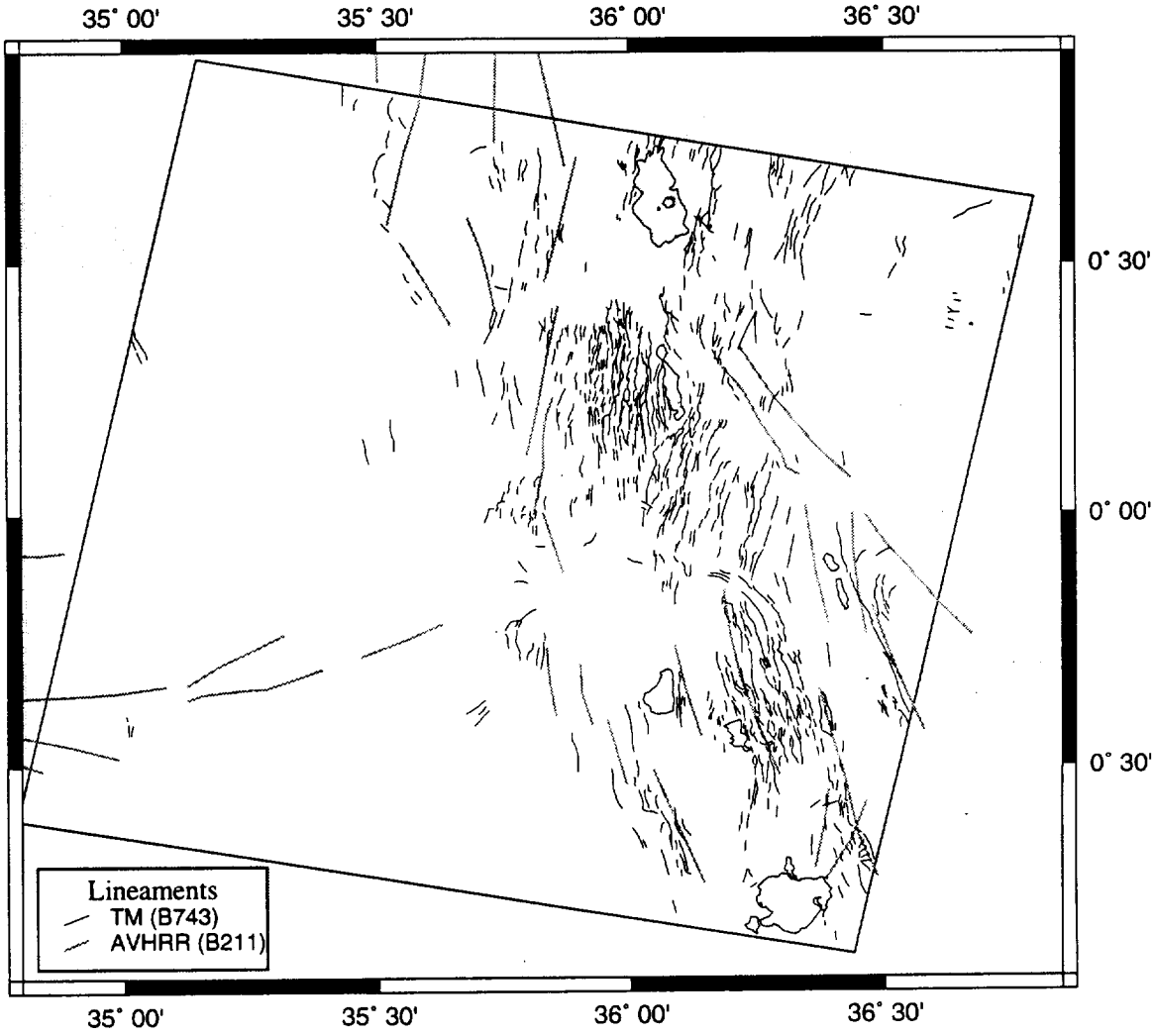

Directional Trends of Lineaments mapped from Landsat TM

Azimuth of Lineaments

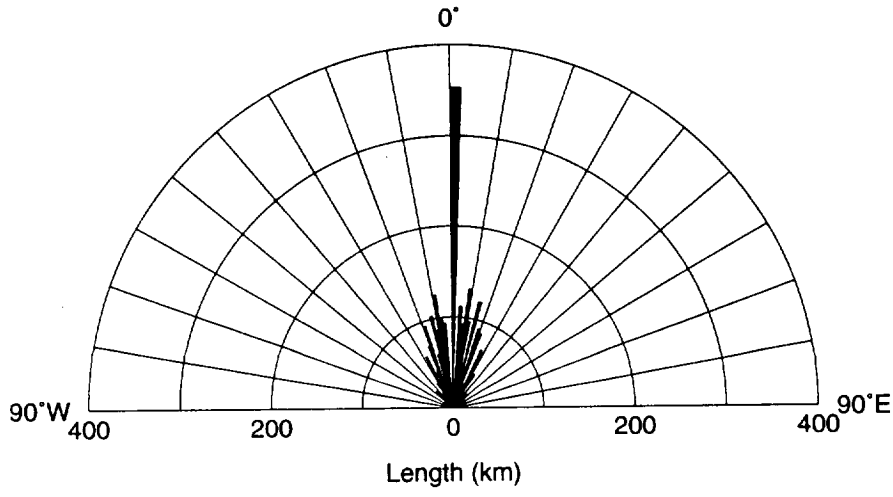

Fig. 5.9. Lineaments of a region of the Kenya rift mapped from Landsat TM Imagery.

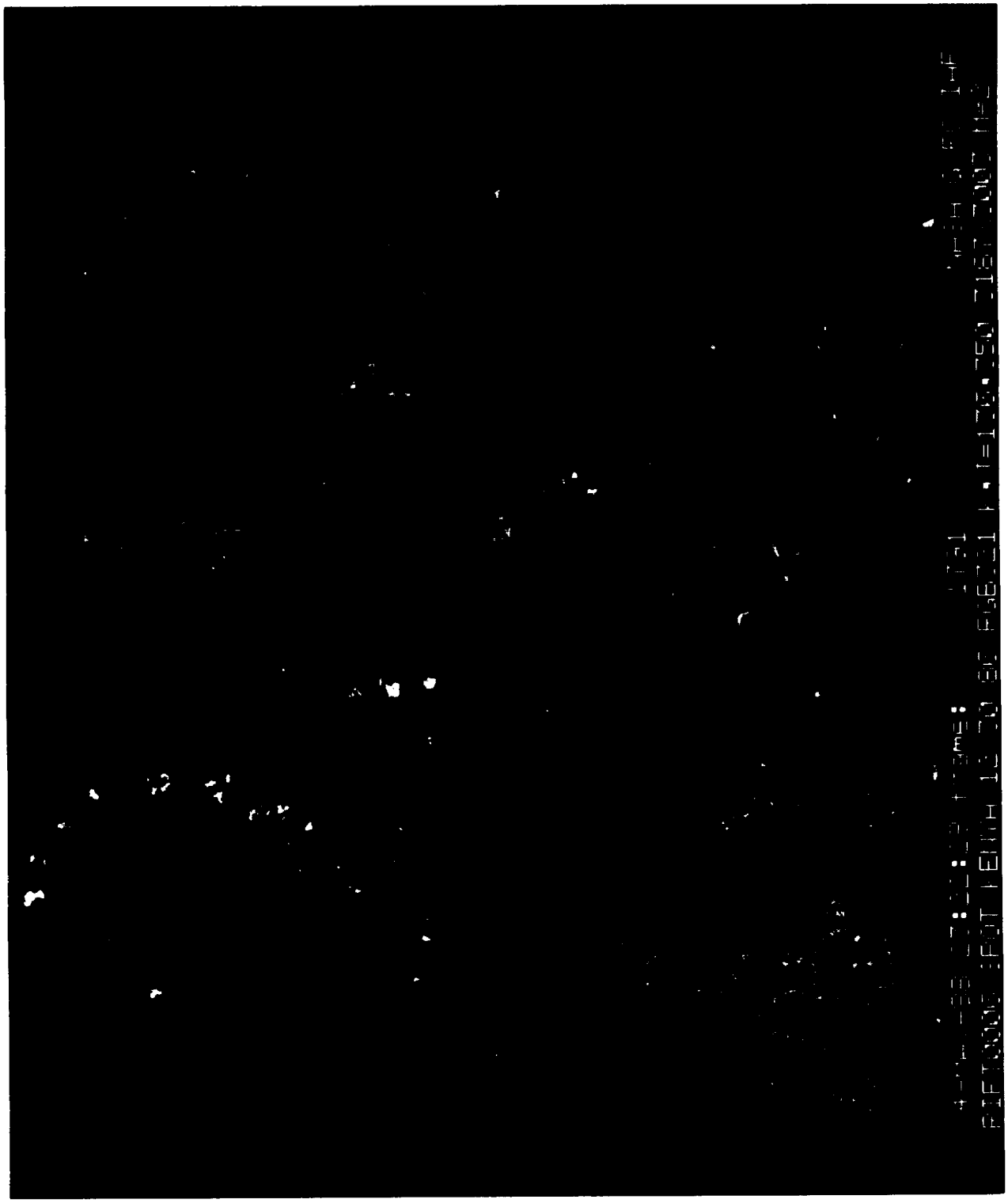

Fig. 5.10. SPOT scene of part of the central Kenya rift; B321 = RGB.

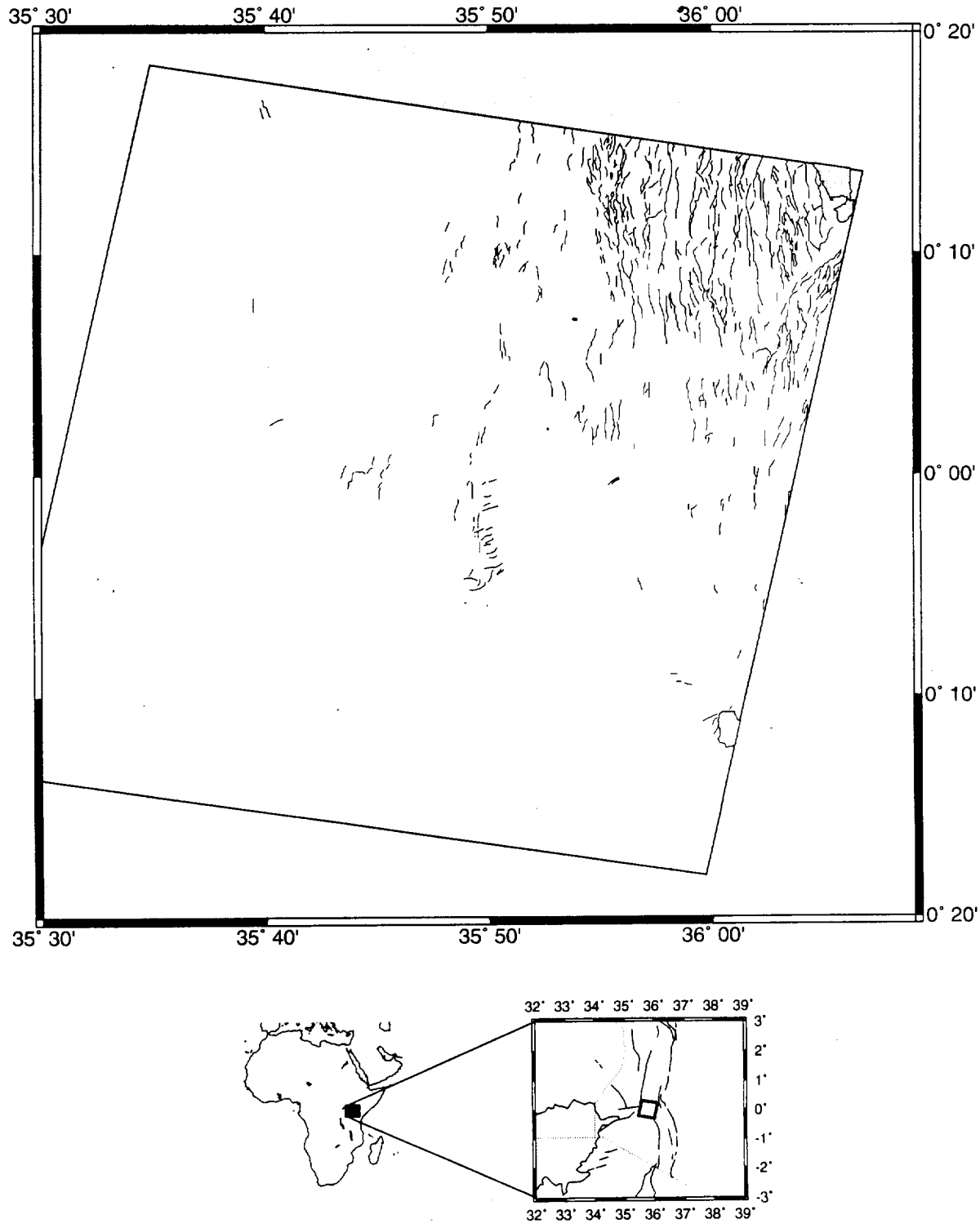

Fig. 5.11. Lineaments of part of the Kenya rift mapped from SPOT Imagery.

Lineaments of Central Kenya

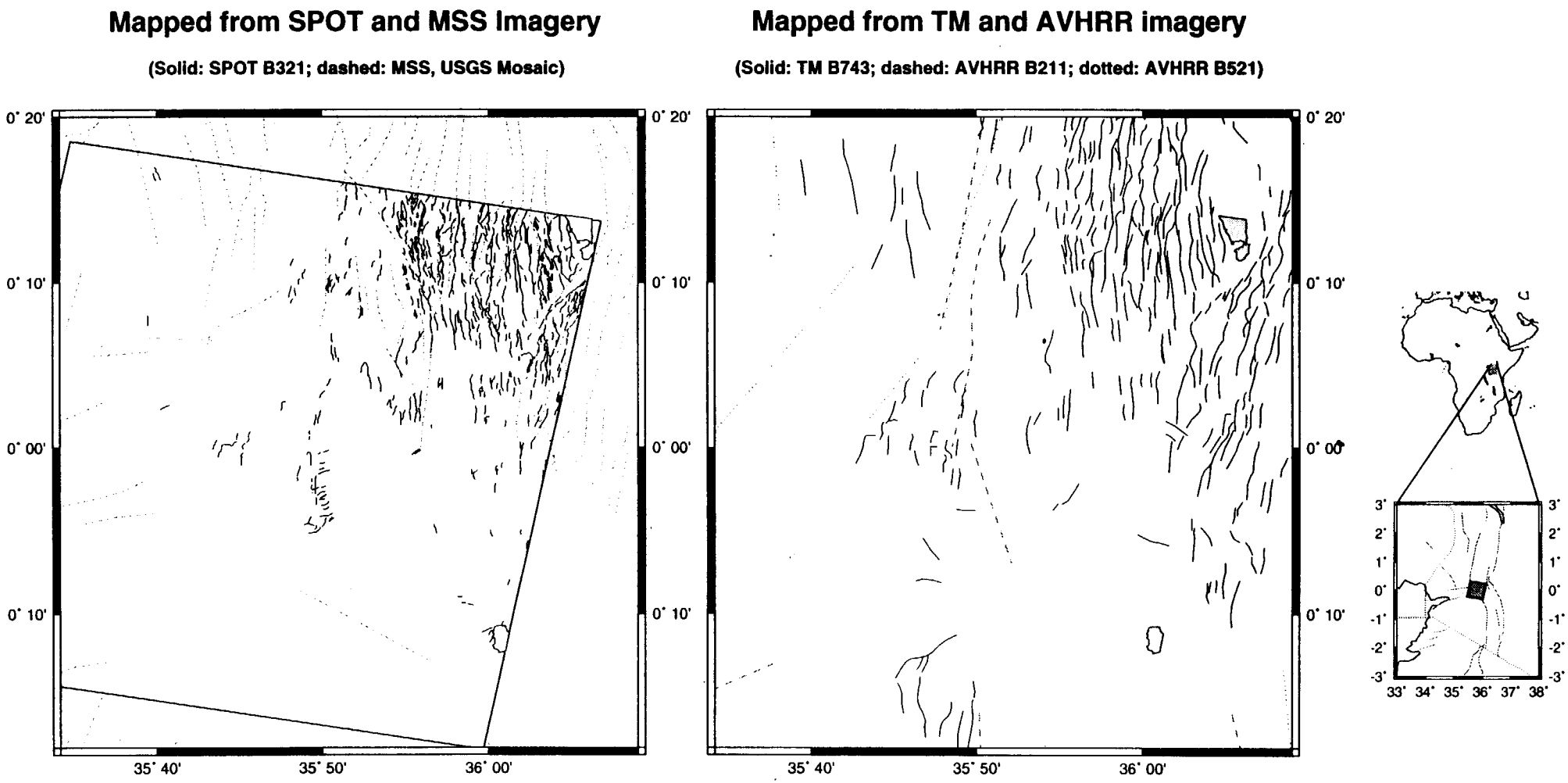

Fig. 5.12. Lineaments of part of the Central Kenya rift valley mapped using various types of imagery

5.6 Northern Tanzania

The change in rift morphology as well as seismic and volcanic activity observed in northern Tanzania deserves further consideration. Figure 5.13 summarises the available information; seismicity, volcanism and lineaments. The presence of a WSW - ENE chain of volcanoes which crosses the rift and marks the boundary of rift morphology was observed by Fairhead (1980). This observation and gravity studies led Fairhead to suggest that it represented an early stages of a transform fault which is 'leaky'.

Figure 5.13 would seem, in part, to confirm the presence of a transform type structure at the southern termination of the main rift valley, at about 3°S. However, the northernmost anomalous area lies about 0.5° north of the line chosen by Fairhead (1980). A line of pre-Holocene volcanoes stretch ENE from Lake Eyasi and coincide with a line of earthquake epicentres. This line also coincides with a hiatus in lineaments as observed from AVHRR imagery. The eastward termination of this belt, between 36.5°E and 36.8° E, matches the commencement of a second ENE trending band about 0.5° further south. This second band includes the volcanoes of Meru and Kilimanjaro and is also associated with a band of earthquake epicentres. Focal plane mechanisms indicate that the majority of faulting events are normal, however one event, 7th May 1964, does show a predominantly strike slip mechanism. The evidence presented in figure 5.13 would support the existence of a transform structure marking the boundary between classical rift graben morphology to the north and a basin and range type structure to the south. The data also suggest that this transform structure trends ENE and is offset '*en echelon*' to the south.

5.6.1 Lake Balangida (ESC)

Figure 5.14 shows image ESC03013, the lake at the centre is Lake Balangida and the mountain at the lower centre of the image is Hanang which rises to a height of 3417 metres. The centre of the scene is at about 35.3°E, 4.4°S and the scene is oriented at about 330° to north.

The image shows a distinct scarp slope forming a half-graben like feature, which is now partially filled by the small Lake. The fault line is part of a major east facing escarpment which runs approximately N-S from Lake Natron to Lake Balangida (Dawson, 1992); the fault is dated at between 1.2 and 0.9 Ma (MacIntyre *et al*, 1974). A smaller parallel lineament is also visible above the cultivated region in the upper centre of the image.

The Rift in Northern Tanzania

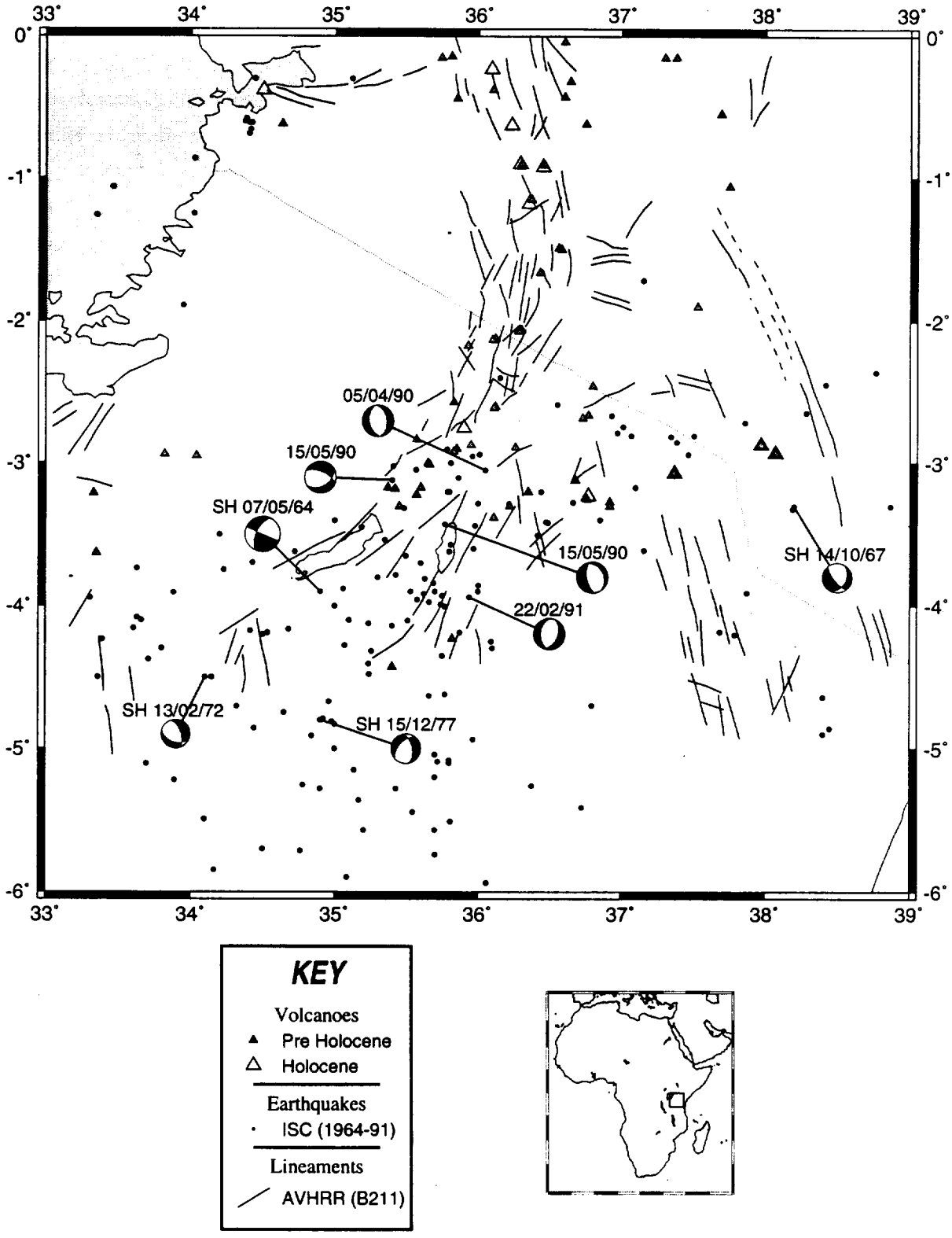

Fig. 5.13. Earthquakes, Volcanoes and Lineaments of Northern Tanzania. Earthquakes from the ISC (1964 - 1991); Volcanoes from Nusbaum et al (1994); lineaments from AVHRR (B211). Fault Plane Solutions from Shudofski (1985) [SH] and Dzeiwonski (Various).

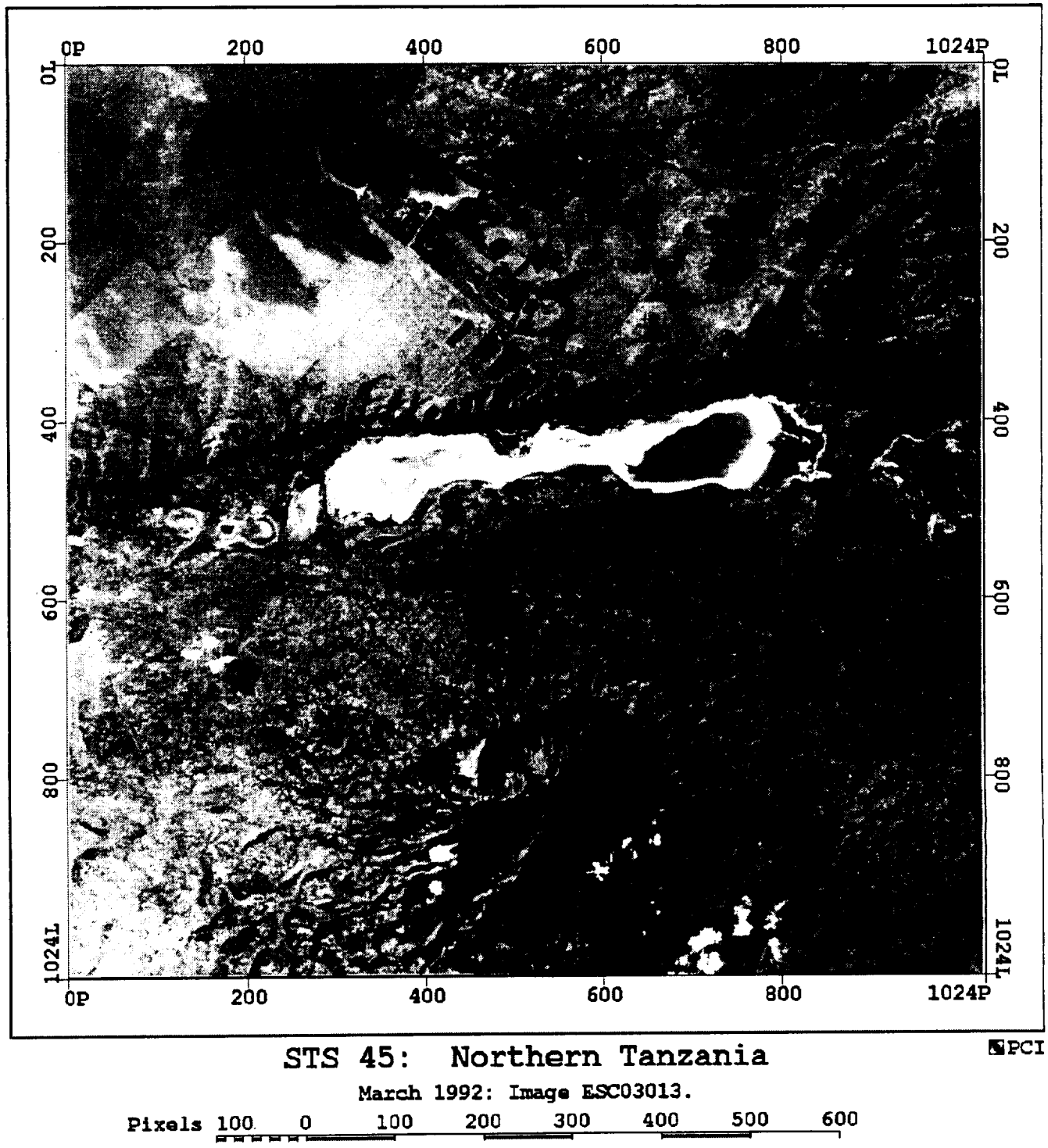

Fig. 5.14. Electronic Still Camera image of Lake Balangida and Hanang (Northern Tanzania).

Hanang is a relatively steep volcanic cone dated at 0.9 - 1.5 Ma (Bagdasaryan *et al*, 1973) and is dominated by pyroclastic materials.

CHAPTER 6

The Kivu - Mobutu Rift

The divisions of the western branch of the East African Rift System are less clear cut that those of the eastern branch. The Kivu - Mobutu rift lies north of the Tanganyika rift zone (chapter 7) and includes Lakes Kivu, Edward, and Mobutu (Albert); with an extension northwards along the Nile valley. Its trend is generally SSW - NNE until at its northern end it doglegs west. The generally accepted northern termination of the Western Branch, is against the Aswa Lineament in the locality of Nimule (Southern Sudan). There is some evidence, however, to suggest a northerly extension (Girdler & McConnell, 1994). Figure 6.1 shows the main geographical features used in the text.

6.1 Geological Background

The section of the western branch of the East African Rift System between Lakes Mobutu and Kivu is probably the least studied of the entire rift system in East Africa. This section of the rift extends south from the Aswa lineament along the Nile valley and through Lake Mobutu. Between Lakes Mobutu and Edward lies the Ruwenzori block and nearby Toro-Ankole volcanic region. The Virunga volcanic province lies between Lakes Edward and Kivu. South of Lake Kivu is the south Kivu volcanics, at this point the rift direction changes from a NNE - SSW direction to a NNW - SSE orientation.

The western branch of the rift system largely follows Proterozoic mobile belts around the Archean cratons (e.g. McConnell, 1972, Delvaux, 1992). The timing of the onset of rifting along any part of the western branch is not certain but most sedimentary fill in Lake Tanganyika is probably Miocene or younger (Rosendahl *et al*, 1992) though there is some suggestion that Karoo sediments are found at the southern end of the Lake (Delvaux, 1992). The earliest date assigned for the volcanism in the Kivu area is 10 Ma (Pasteels *et al*, 1989) and Ebinger (1989a) has correlated this with the onset of faulting and basin formation in Lake Kivu. The oldest dated sediments in Lake Mobutu are about 8 Ma and may be contemporaneous with the initiating of rifting (Ebinger, 1989b).

The western branch of the rift system is a narrow valley, about 50 - 70 km wide. The rift valley is segmented into a series of alternating half-graben extensional basins (e.g. Ebinger *et al*, 1984; Ebinger, 1989b). The Cenozoic border faulting is discontinuous

The Lake Mobutu Region

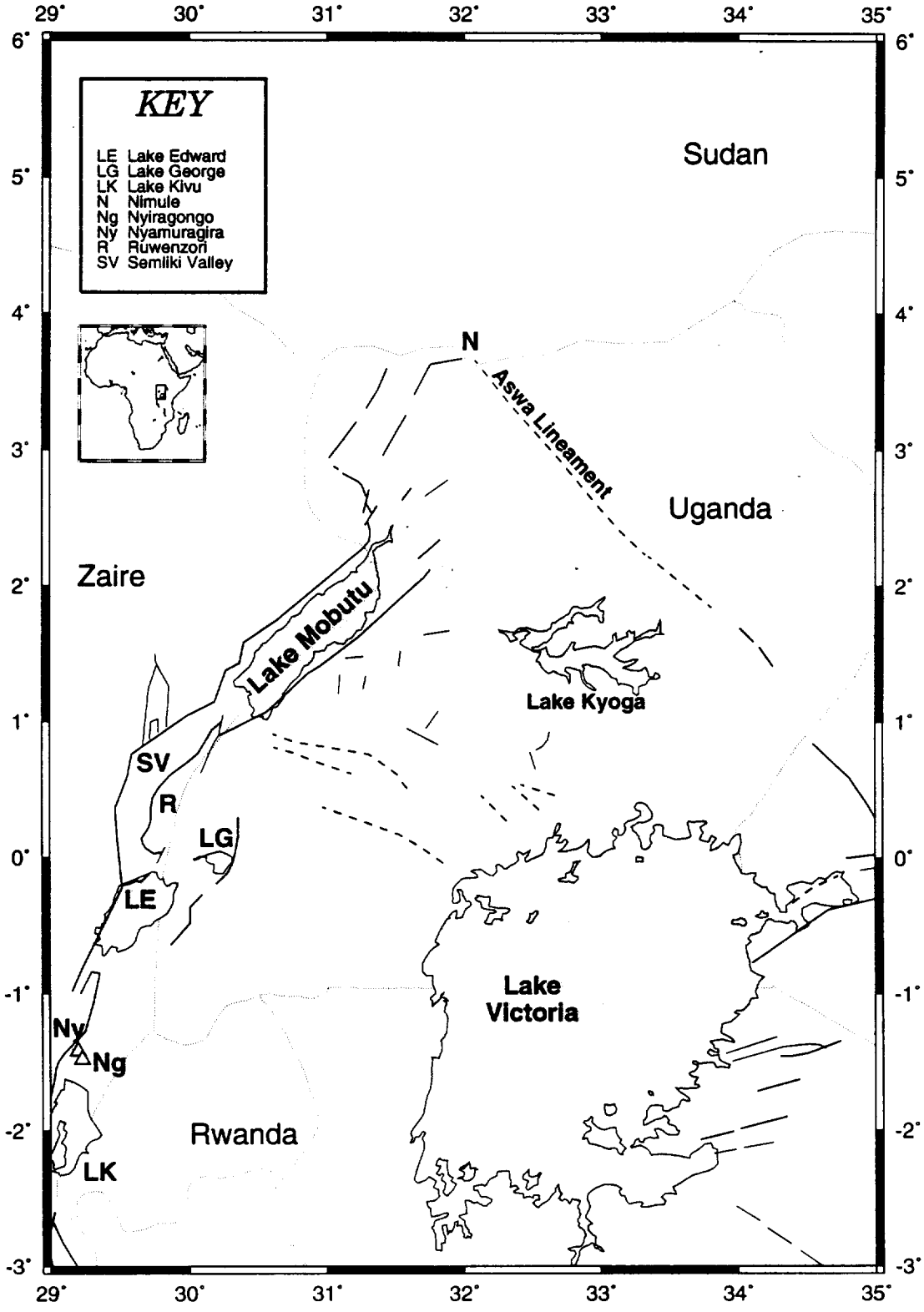

Fig 6.1. The Lake Mobutu region (northern part of the western branch)

along the length of the rift. The rift flanks are characterised by 150 - 200 km wide zones of uplift which rise to 1 km above the level of the East African plateau and about 4 km above sea level (Ebinger, 1989a).

The feature which dominates the section of the rift between Lakes Edward and Mobutu is the Ruwenzori Block. This Block all but cuts the rift into two distinct sections and constricts the rift valley to about 15 km wide at 0.5°N, compared to a width of about 50 km across Lake Mobutu. The block is about 120 km long, 50 km wide and rises to an elevation in excess of 5000 m, over 4 km above the lake surface of Lake Mobutu. Ruwenzori is the highest non-volcanic mountain in Africa (Holmes, 1944). The block is made up of Precambrian gneiss and schist and is fault bounded to the west and upwarped on its eastern flank (McConnell, 1972). McConnell also notes the presence of restricted volcanism but without appreciable extrusions. The block also forms a minor bifurcation of the rift with the Semliki rift joining the Edward and Mobutu rifts around the west of Ruwenzori and the Lake George rift forming a spur to the east of the block. Recent uplift at the northern end of Ruwenzori is observed where alluvium deposits from the Semliki valley occur on raised terraces (Holmes, 1944).

Lake Kivu lies at the knee point of the western branch and is dominated by volcanics to its north and south. The Virunga province to the north end of the Lake dammed the Lake to the north in Holocene times forcing the current southward drainage along the Ruzizi River (Hecky & Degens, 1973). Lake Kivu itself is made up of a western and eastern grabens separated by the Idjwi Island horst. The older, eastern basin has highly altered theoleiitic volcanism of 10 - 6 Ma overlying metamorphic basement: the western basin has alkali basalts of 8.0 - 4.1 Ma over metamorphic basement (Ebinger, 1989a). Both basins show evidence of recent faulting with rifting in the northern part of the western basin forming in the last 3 Ma (Ebinger, 1989a).

6.2 AVHRR

Two AVHRR band combinations, from 9th January 1989, are considered, B211 $\Rightarrow$ RGB and B521 $\Rightarrow$ RGB, plates 4A and 4B respectively. Attempts to locate a cloud free scene of the area between Lakes Mobutu and Tanganyika proved fruitless (Derickey, pers. comm.). Most of the rift south of Ruwenzori is covered by cloud and all rift features are lost south of Lake Edward. Much of the land east of 32.5°E is also obscured by cloud but the Lake Mobutu and Nile valleys are clear. As a result of the cloud cover parts of this section of the rift are also considered in chapter 7.

Plate 4A shows the B211 view of the area. The red domination in the south and west of the image is due to vegetation cover while the more arid regions to the north and east appear more blue. Vegetation following the Nile River is seen from Lake Mobutu to the Aswa Lineament and again at the top of the scene. Cloud cover dominates much of the scene. Plate 4B is the B521 image with green characterising vegetated regions and red the hotter, drier areas. The course of the Nile is clearer on this scene than on the B211 view and the offset caused by the Aswa Lineament is clearly visible. The southeastern scarp of Lake Mobutu is more clearly seen on the B521 scene than on the B211 image due mainly to the colour contrast between the two areas. The Semliki Valley linking Lakes Edward and Mobutu is seen on both images as a darker belt skirting to the west of Ruwenzori, and partially covered by cloud associated with the Ruwenzori massif.

Figure 6.2 shows the lineaments mapped from the AVHRR scenes, compared with the mapped faults of the area (UNESCO, 1968). The Aswa lineament is the clearest feature seen on the AVHRR imagery where it trends northwest from The Sudan/Uganda border. The lineament is not seen on AVHRR southeast of this point and conversely the UNESCO map has only indicated the Uganda section. The scarp edges of the Nile valley between the Sudan border and Lake Mobutu are not clearly seen on either AVHRR band combination. Lake Mobutu essentially marks the scarps of the rift along its NW and SE shores, however, the southeastern scarp has been picked out on AVHRR as a slightly more complex structure than that shown on the UNESCO map. This more complex scarp is borne out, to a degree, on the topography. Part of the northwestern scarp is also seen on AVHRR and is seen slightly better on the B521 imagery. Some lineaments associated with the northern end of Ruwenzori are observed and match the trend seen on the UNESCO map as do some lineaments around Lake Edward. Other parts of the rift are obscured by cloud.

6.3 Topography

The topography of the rift between the Aswa lineament and southern Lake Mobutu is given in figure 6.3. Unlike the Kenya rift few sections of the western branch contain volcanic flows and thus the rift maintains its classical graben or alternating half-graben morphology.

Figure 6.3 shows the section of the western branch north of the equator. The high block situated at about 0.5°N, 29.9°E is the Ruwenzori massif, an uplifted Precambrian block

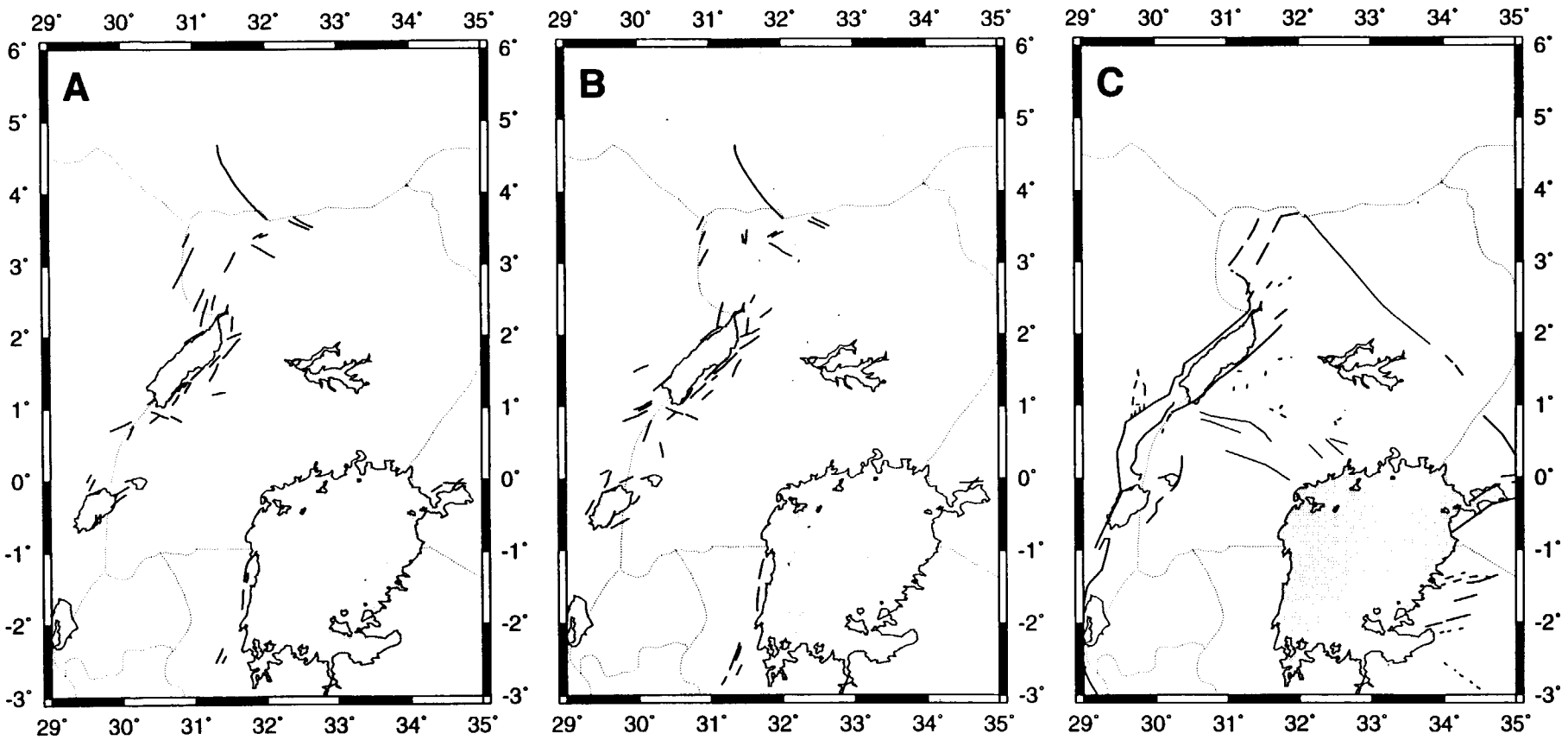

Fig. 6.2. Lineaments and faults of the Lake Mobutu region (northern part of the western branch). A. Lineaments mapped from AVHRR (B211); B. Lineaments mapped from AVHRR (B521); C. Faults from the UNESCO Tectonic Map of Africa (1968).

Topography of the Lake Mobutu Region

Terrain-30 Topography Data

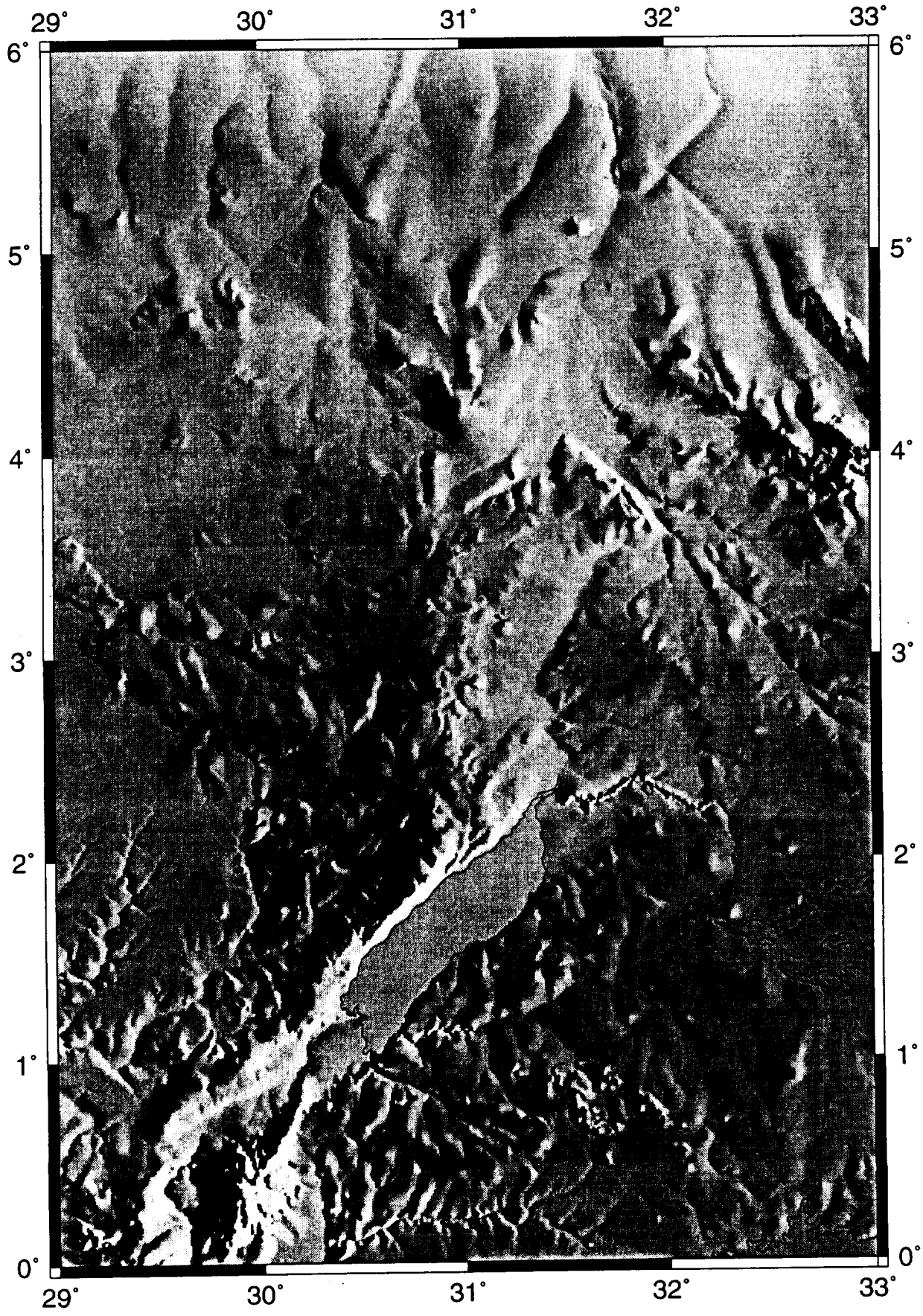

Fig. 6.3. Topography of the northern part of the western branch, Illuminated from the east.

which constricts the rift to a narrow valley to its west. Lake Mobutu marks the northwestern and southwestern scarps of the northernmost section of the western branch which exhibits symmetrical rift structure. The rift in the Lake Mobutu region is consistently about 50 km wide and dies out just to the northeast end of the Lake. The rift continues north along the valley of the Nile. The topography indicates that the Nile marks the eastern scarp of the rift in this region while no western scarp is observed. The eastern scarp is made up of a series of *en echelon* faults leading as far north as the Aswa Lineament. The Aswa Lineament is clearly traceable from the topography, it trends in a southeasterly direction from 4.1°N, 31.5°E. The section of the Lineament between 4.1° N, 31.5°E and Nimule at 3.7°N, 31.9°E is the most obvious where it is followed by the Nile. Southeast of Nimule the trend of the lineament is obvious and it appears to exhibit an *en echelon* nature or to be characterised by minor splays. North of the Aswa Lineament the course of the Nile can be traced but there is no obvious sign of rift structure.

6.4 Seismicity and Volcanism

The western branch of the rift system is characterised by widespread seismic activity. Figure 6.4A shows the teleseismicity of the Lake Mobutu area. Microseismicity in the area is also common (e.g. Rykounov *et al*, 1972; Zana *et al*, 1989). Volcanism is confined to a number of distinct provinces. A number of fault plane solutions, for the northern end of the rift, were given by Shudofsky (1985), see figure 1.6, and indicate predominantly normal faulting.

The teleseismicity in the northern part of the western branch, figure 6.4A, shows scattered epicentres along the rift and two distinct swarms. The northernmost of these swarms lies in southern Sudan, north of the Aswa Lineament and thus north of the region usually regarded as the rift. The majority of these events in the south of Sudan occurred in 1990-1992. Girdler & McConnell (1994) considered that the swarm along the Nile Valley was indicative of an extension, or propagation, of the western branch northwards along the Nile Valley. The magnitude of the main event (m_b = 7.2) was amongst the largest recorded in East Africa and suggests an active process rather than the resettling of older structure. The second region where there are many epicentres is between Lakes Mobutu and Edward. This swarm coincides with the Ruwenzori Block, studied by Rykounov *et al* (1972).

Earthquakes and Volcanoes of the Lake Mobutu Region

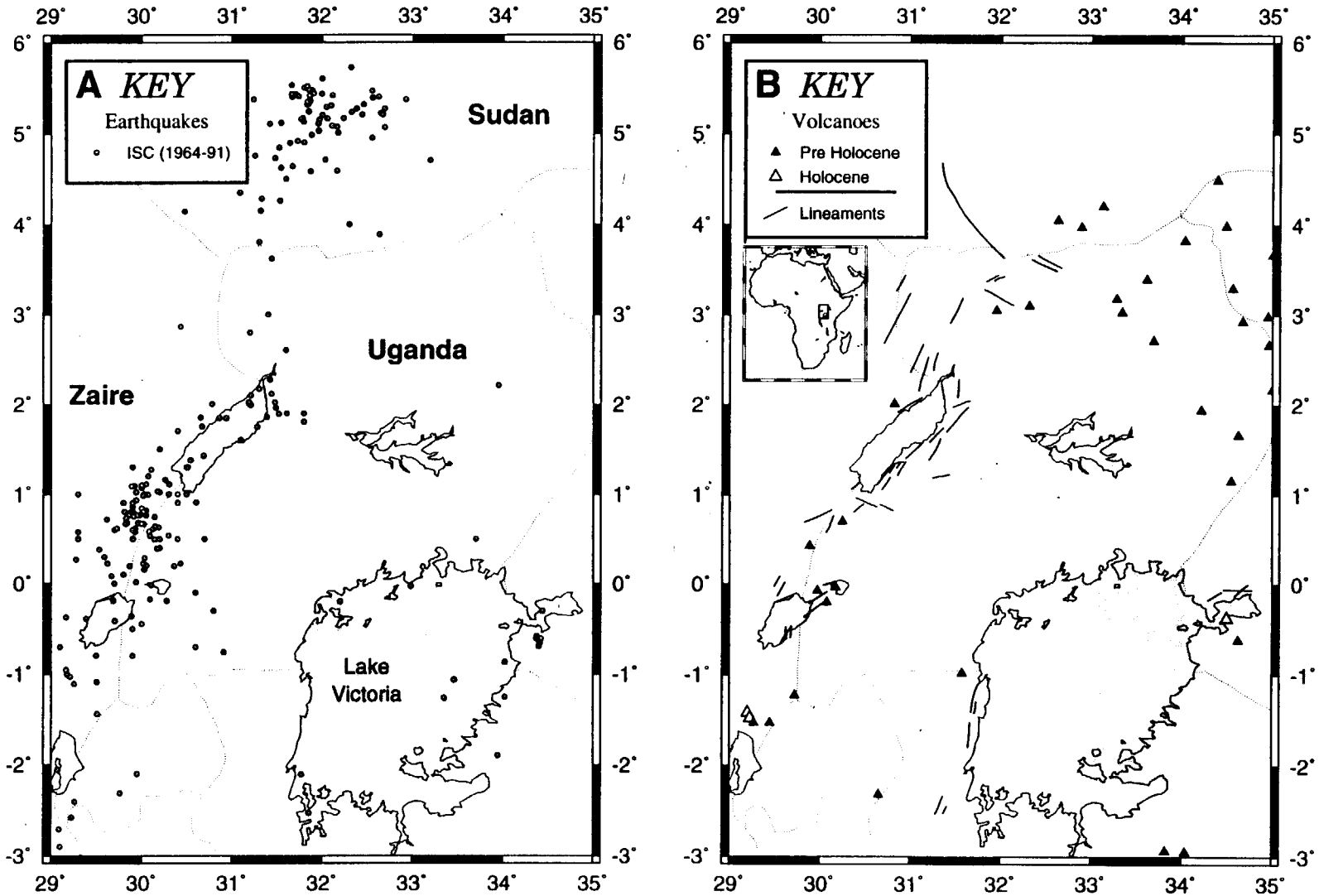

Fig. 6.4. Earthquakes and volcanoes of the Lake Mobutu region (northern part of the western branch). A. Earthquakes from the ISC (1964 - 1991); B. Volcanoes from Nusbaum et al (1994), lineaments mapped from AVHRR (B211).

The volcanism of the western branch, between Aswa and Lake Kivu is characterised by small but distinct volcanic provinces, figure 6.4B. The northernmost province of Toro Ankole lies around the Ruwenzori Block and has not shown activity within the Holocene. The largest province is around Lake Kivu; this province is often divided into two regions, north and south of the Lake. The Virunga volcanics to the north of Lake Kivu contains two active volcanoes, Nyiragongo and Nyamuragira. Ages of initiation of volcanism show a general younging from about 10 Ma in Virunga to 7 Ma in the Rungwe province (see chapter 7), Toro-Ankole, however, has only been active for a short period since about 1 Ma (Ebinger, 1989b).

6.5 The Aswa Lineament (ESC)

One ESC scene is available for part of the western branch and lies at the far northern end, on the Aswa Lineament, figure 6.5. Scene ESC03010 shows part of the White Nile to the south of Juba, Sudan. The Nile is flowing approximately northwesterly at this point and can be seen crossing the image. The scene's centre is at about 31.6°E, 4.0°N.

The continuous lines of high topography left of the Nile are associated with the Aswa Lineament. The Nile follows this Lineament from Nimule, 60 km to the SE of the image, to the point at the upper end of the scene, where it begins to veer towards a more northerly direction again. A number of faults cross cutting the Aswa Lineament are also visible. A continuous central belt of faulting is observed with divergent lineaments to the southwest side. This divergent trend dies out as it peels away from the main trend.

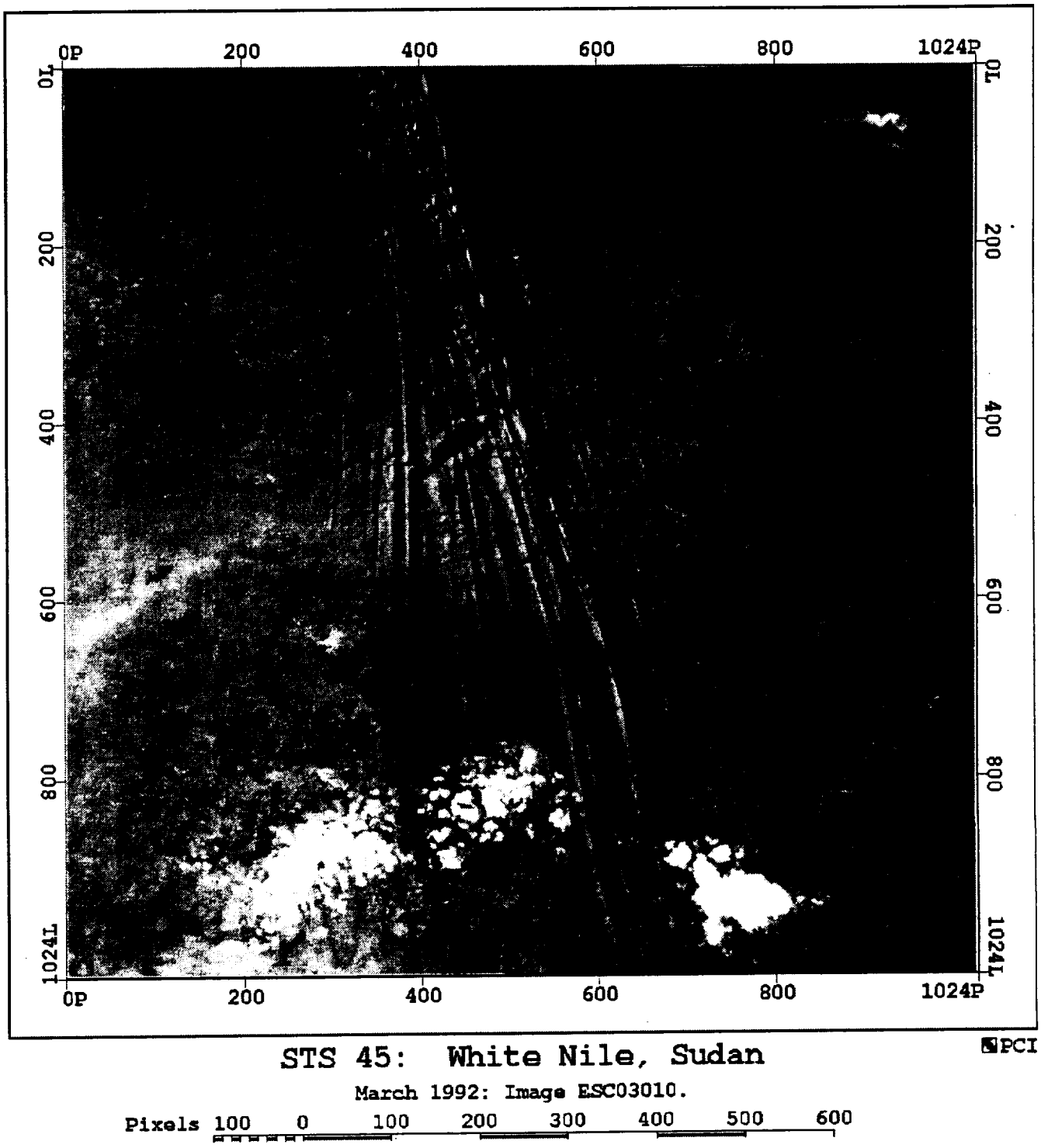

Fig. 6.5. Electronic Still Camera image of the White Nile and Aswa Lineament (Southern Sudan).

CHAPTER 7

The Tanganyika and Rukwa Rifts

7.1 The Tanganyika Rift

The Tanganyika rift zone includes the Lake itself and the Ruzizi Plain to the north. Extensive seismic profiles have been carried out on Lake Tanganyika (e.g. Rosendahl *et al*, 1986) and thus knowledge of the sub surface structure is probably more well known for this zone than any other in East Africa. Figure 7.1 gives the main geographical names used in the text.

7.1.1 Geological Background

The Lake Tanganyika trough has been the location of an extensive seismic project to determine the structure of the subsurface rifting (e.g. Rosendahl *et al*, 1986). Lake Tanganyika is about 550 km long, 60 km wide and up to 1500 m deep. The Lake surface is currently about 762 m above sea level and it has as much as 5000 m of sediments giving an amplitude of the rift from base of sediments to top of rift flanks in excess of 7.5 km. Rosendahl *et al* (1986) observe four sedimentary basins separated by ridges of crystalline basement rocks; two ridges have acted as near perfect barriers throughout the basins' history while the Moba ridge, separating the southernmost basins, is now buried with sediments. The northernmost basin, the Ruzizi basin, extends beyond the current extent of the Lake: this basin formed after 6 Ma but before about 2 Ma (Ebinger, 1989a). Most of the basins are half-graben structures with eight (Rosendahl *et al* 1986) or twelve (Rosendahl *et al* 1992) such half grabens, depending on the criteria used for defining them. Morley (1988a) interprets the seismic sections to include more full graben structures.

Morley (1988a) calculated extension across the central part of the Tanganyika trough to be about 4.5 km (10%) and 0.5 - 1 km at the Lake ends. The calculation of extension was based on the assumption that the direction of extension was E - W. Scott *et al* (1989) consider a WNW - ESE or NW - SE direction more likely. The calculation of extension by Morley (1988a) suggest that the rifting initiated at the centre of the Lake and worked north and south: Sander & Rosendahl (1989) favour a two centre initiation in the north-central and south-central parts of the Lake.

The Tanganyika Rift

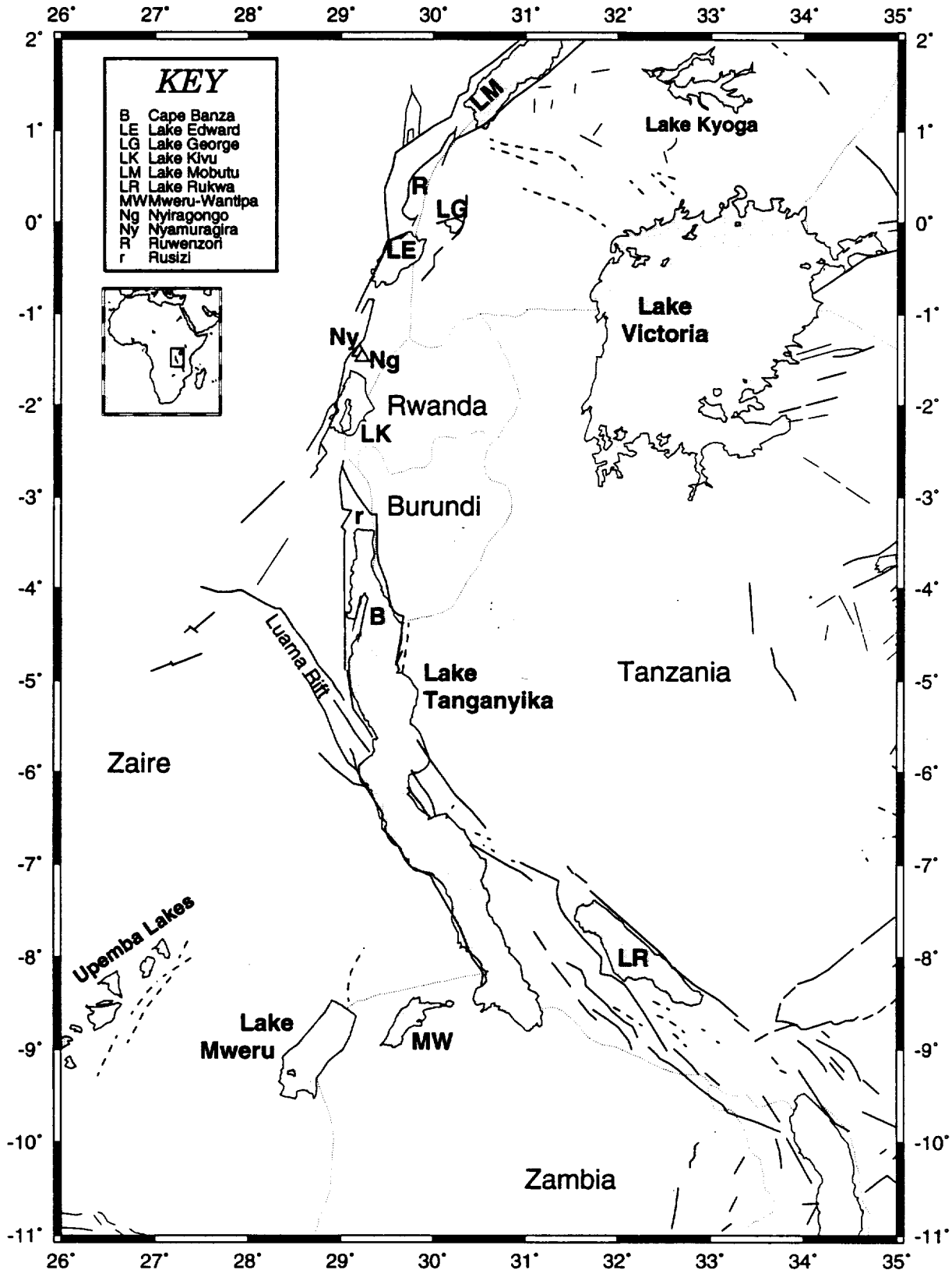

Fig. 7.1. The Tanganyika rift, geographical names used in the text.

At the central point of Lake Tanganyika the Tanganyika-Rukwa-Malawi zone meets the Tanganyika rift. This zone forms part of a Karoo age rift and is observed to cross Lake Tanganyika and continue in a NW direction on the western side of the Lake. The point at which this Karoo rift crosses the Lake is contiguous with the Kavala Island ridge across the Lake.

The Tanganyika rift dies out at about 9°S, just south of the Lake limit. At 8.5°S Cameron Bay forms a slight westerly inlet in the lake-shore on a line with Lake Mweru-Wantipa and Lake Mweru. Lake Mweru itself is clearly fault bounded and forms a small SW trending rift, parallel to The Upemba rift and Luangwa Valley (Rosendahl, 1987). In addition to the SW trending valleys the E - W Cameron Bay - Lake Mweru is also fault bounded: E - W faults mark the Sumbu structure between Cameron Bay and the western side of Lake Mweru-Wantipa at which point NE - SW faulting characterises the structures further west (Mondeguer *et al*, 1989).

7.1.2 AVHRR

Plate 5 shows the AVHRR B211 and B521 scenes of the Tanganyika and Rukwa rifts, acquired on 24th July 1989. Once again the Lake Kivu-Edward section of the rift is obscured by cloud and a line of cloud crosses Lake Tanganyika, however, the majority of the regions around Lakes Tanganyika, Rukwa, Mweru and the Upemba region are cloud free; the subcircular region of cloud at about 34°E, 9°S covers the Rungwe volcanic province. The B211 AVHRR scene (plate 5A) highlights the difficulty in processing a scene of this geographical coverage; the northeast of the image is bright while the southwest is dark. The Mobutu-Kivu section of the rift, and the surrounding areas, are well vegetated (shown as red) while the region to the southeast of Lake Victoria appears almost devoid of vegetation cover. The B521 image (plate 5B) highlights the southwestern corner of the image as having a high thermal infra-red signature. The structure and fabric of this southwestern corner is much more apparent on this scene than on the B211 combination.

Figure 7.2 shows the AVHRR mapped lineaments of the region. The most striking feature seen on B211 AVHRR is not the lineaments mapping much of the Tanganyika rift but a belt of lineaments arcing from the northeast of Lake Tanganyika to the western shores of Lake Victoria. This belt is observed also on B521 imagery but not so clearly. This is the Karangwe-Ankole belt of Kibaran age (McConnell, 1972); to its southeast is

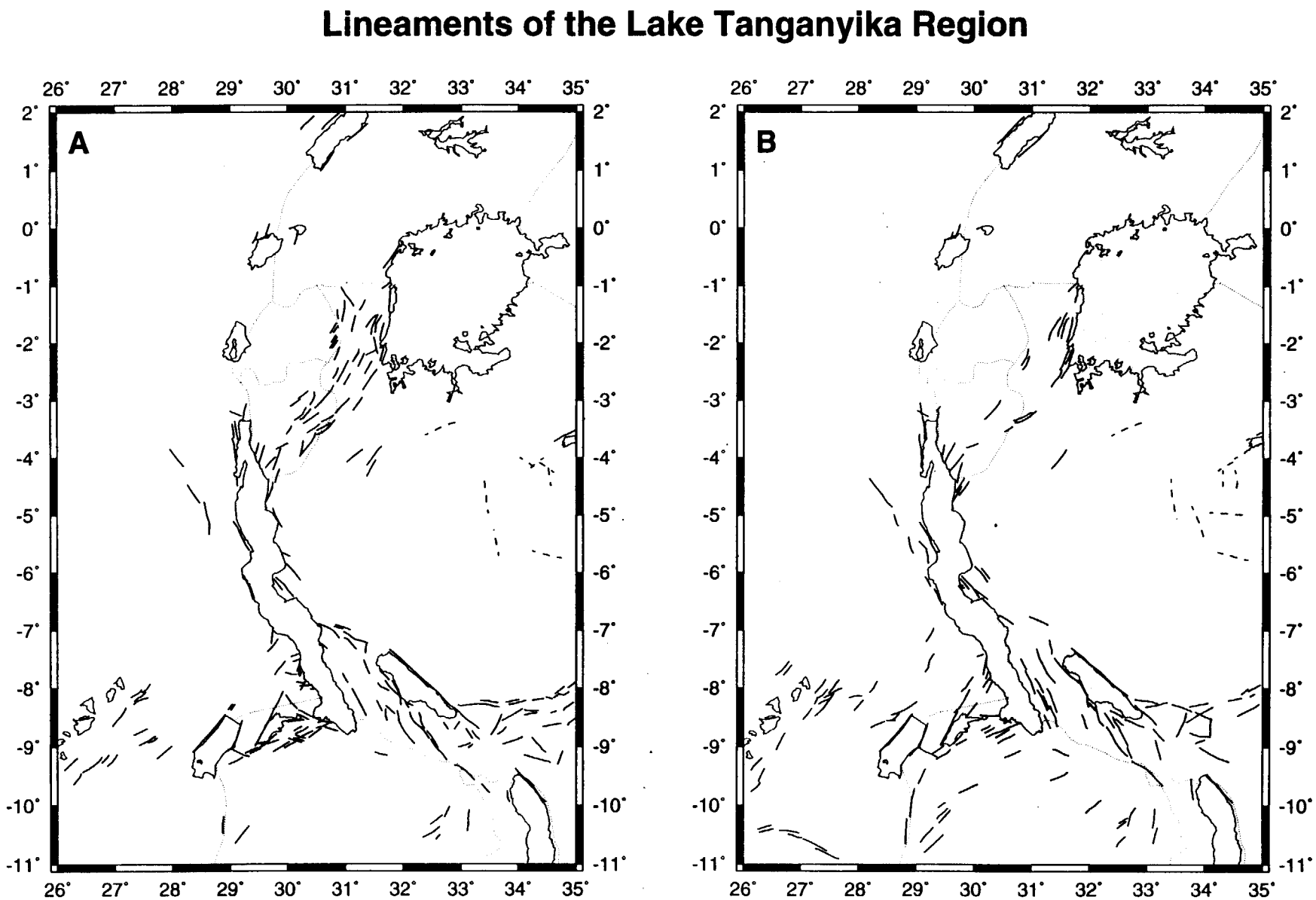

Fig. 7.2. Lineaments of the Lake Tanganyika region mapped from AVHRR imagery. A. AVHRR B211; B. AVHRR B521.

the Tanganyika shield. Lake Tanganyika, like Lake Mobutu, largely marks the scarps of its rift and thus it is not always easy to pick a lineament, as opposed to the lake shore, from AVHRR. A line of lineaments pares off from the western shore of Lake Tanganyika at about 5.5°S and is associated with the Luama rift, of Karoo age. This line trends northwesterly and is in continuation with the trend of the Rukwa rift. At the southern end of Lake Tanganyika the situation is complex. Both B211 and B521 indicate a highly faulted region around Lake Mweru-Wantipa with connections beyond to Lake Mweru. The lineament trends in this region are both NE - SW, western edge of Lakes Mweru and Mweru-Wantipa, and ENE - WSW, between Cameron Bay and Lake Mweru. B521 has indicated slightly fewer lineaments in the Lake Mweru-Wantipa region, although the trends are the same, but has also shown an arcing trend from the south end of Lake Mweru-Wantipa to about 10.7°S, 28.8°E. Additionally a few lineaments are also observed on the Bangweulu Block, part of the Zambia Nucleus. Lineaments are also observed to the southeast of the Upemba Lakes and following their trend. Few lineaments are observed on the Tanganyika Shield, to the east of Lake Tanganyika. This region contrasts with the Zambia Block (see chapter 8) in having little observable structure and fabric seen on the AVHRR imagery.

7.1.3 Topography

The section of the rift south of the equator as far as the centre of Lake Tanganyika is given in figure 7.3A while Lake Tanganyika is shown in figure 7.3B. Lake Edward appears to lie in a half-graben section of the rift with a distinct western scarp cutting the lake off from the Congo basin while the eastern side rises less sharply to the plateau. The rift between 1°S and about 4°S is characterised by graben type rift morphology. The boundary scarps are clearly defined taking the elevation from the rift floor to the flanking highlands. The rift shoulders are typically 50 - 100 km wide. On the western side of the rift the land drops sharply towards the Congo basin while the eastern flank drops less severely to the East African plateau. A change in morphology on the plateau itself is clearly seen as a line between about 2.5°S, 31.5°E and 4.3°S, 29.7°E. This marks the boundary between the Karangwe-Ankolean belt, to the northwest, and the Tanganyika Shield, to the south and southeast (McConnell, 1972).

The western edge of Lake Tanganyika, figure 7.3B, is also marked by very distinct scarps though these drop low enough to permit drainage out from the Lake at 5.9°S along the Lukuga River. South towards 5.5°S the western shoulder narrows, this northwest trending structure marked by the edge of the uplifted flanks is the Karoo,

Topography of the Lake Kivu Area

Terrain-30 Topography Data

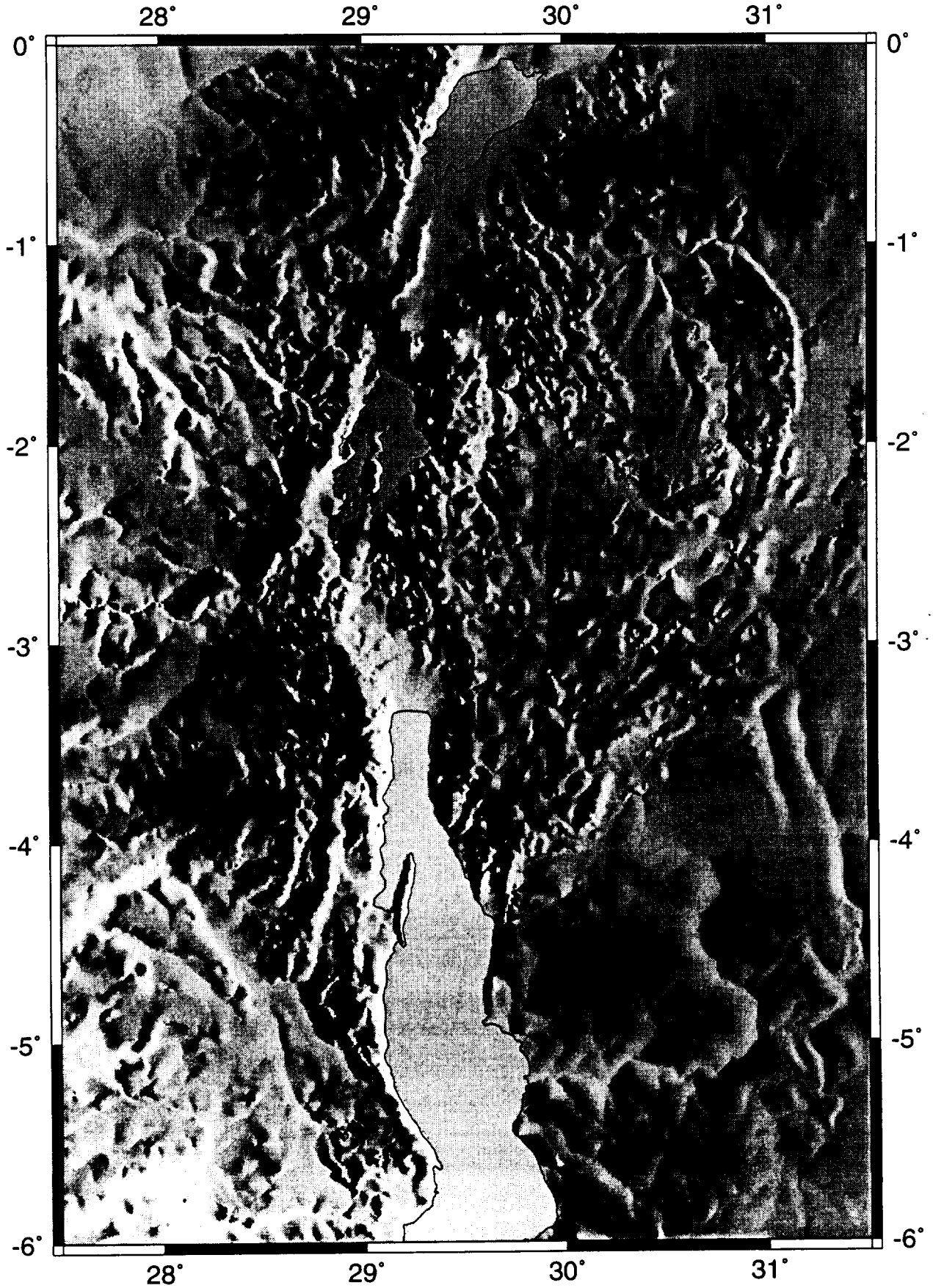

Fig 7.3A. Topography of the Lake Edward, Kivu, Tanganyika region. Illuminated from the east.

Topography of the Lake Tanganyika region

Terrain-30 Topography Data

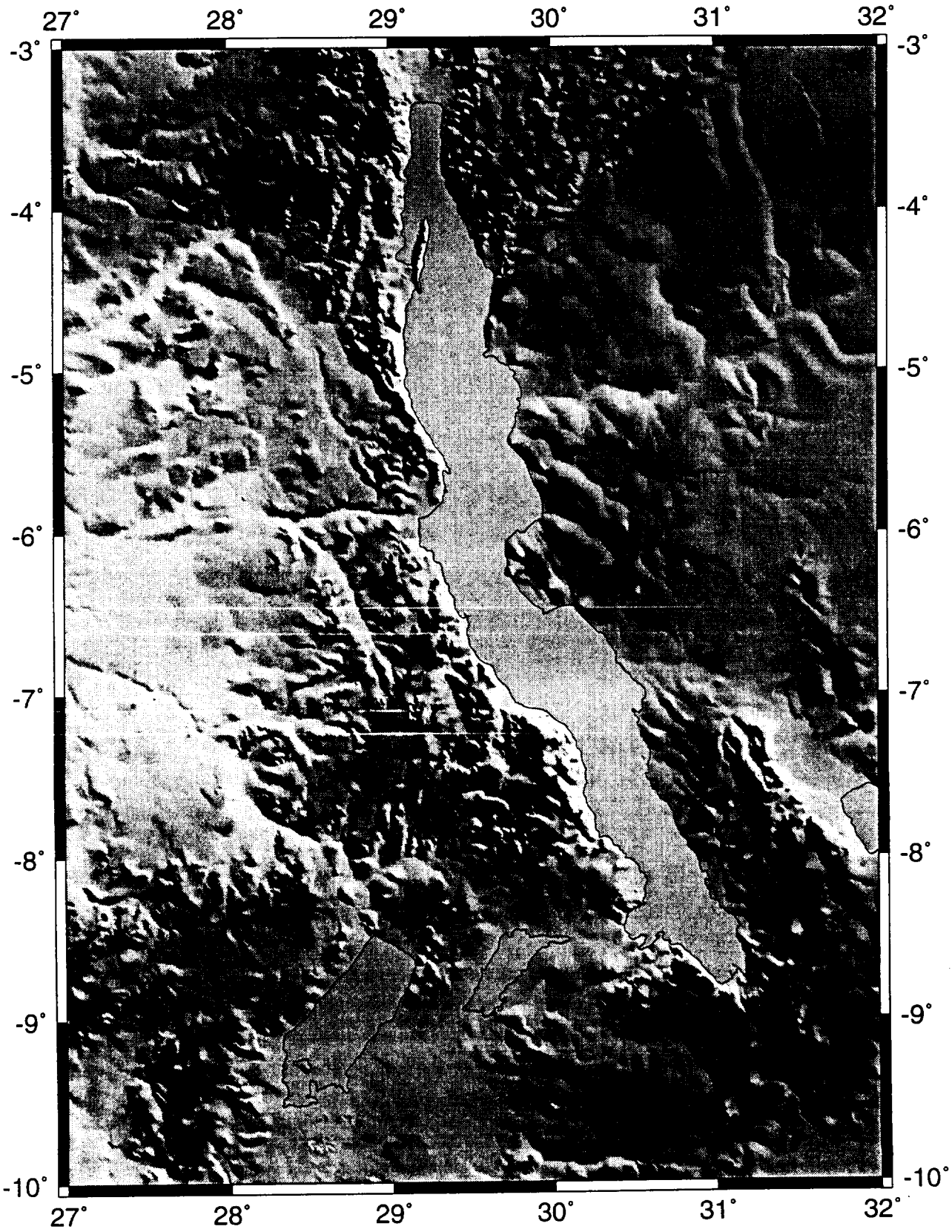

Fig. 7.3B. Topography of the Lake Tanganyika region, illuminated from the east.

Luama rift which is in continuation with the Rukwa rift. At the southern tip of Lake Tanganyika a southwestern scarp is seen which dies out just beyond the Lake end. At 8.7 °S this SW scarp gives way to a WSW trending lineament paralleling the shores of Cameron Bay and trending towards the southern end of Lake Mweru-Wantipa. The scarps bordering Lake Mweru are not clearly seen on the topography. The eastern side of Lake Tanganyika does not show the large scale scarps seen to the west of the Lake. SSE trending lineaments are seen to dominate much of the land immediately to the east of the Lake shore.

7.1.4 Seismicity and Volcanism

Figure 7.4A shows the teleseismicity of the Lake Tanganyika rift and the regions around it. In this section of the western branch, Lake Kivu and Lake Tanganyika, the epicentral locations are broadly scattered along the line of the rift but extend to about 200 km on either side. The broad scatter along this part of the rift may, in part, be due to the remoteness of this section of the rift and the lack of local recording stations. However, the activity seen on the western side of the rift was highlighted by Zana *et al* (1989). Zana *et al* studied the area around Lake Kivu; three zones of anomalously high seismicity were noticed, southern Lake Kivu; The Negweshe region, around 3.5°N, 28.2°E; and the Walikale zone, around 2.5°N, 28.5°E. The Ngweshe area is characterised by dislocated, Precambrian, highlands and the region of earthquakes matches the trend of the highland region (Zana *et al*, 1989). The Walikale zone lies outside the rift valley and extends in a WSW direction towards the Congo craton and is only one of a number of WSW and SW trends west of the rift valley. The southernmost of these trends, along the Upemba lakes and Lake Mweru, seen in the lower left corner of figure 7.4A may be related to SW trending, propagating rifts (section 8.2).

The volcanoes of the Tanganyika and Rukwa rifts are shown in figure 7.4B. The volcanic provinces shown along the western branch are the Toro-Ankole and Kivu to the north of Lake Tanganyika and the Rungwe province to the southeast of Lake Rukwa. Hydrothermal activity in Lake Tanganyika has led Coussement *et al* (1994) to add two further volcanic provinces in the Lake although these are almost certainly on a small scale and have given rise to little or no magmatic extrusions (Rosendahl *et al*, 1992).

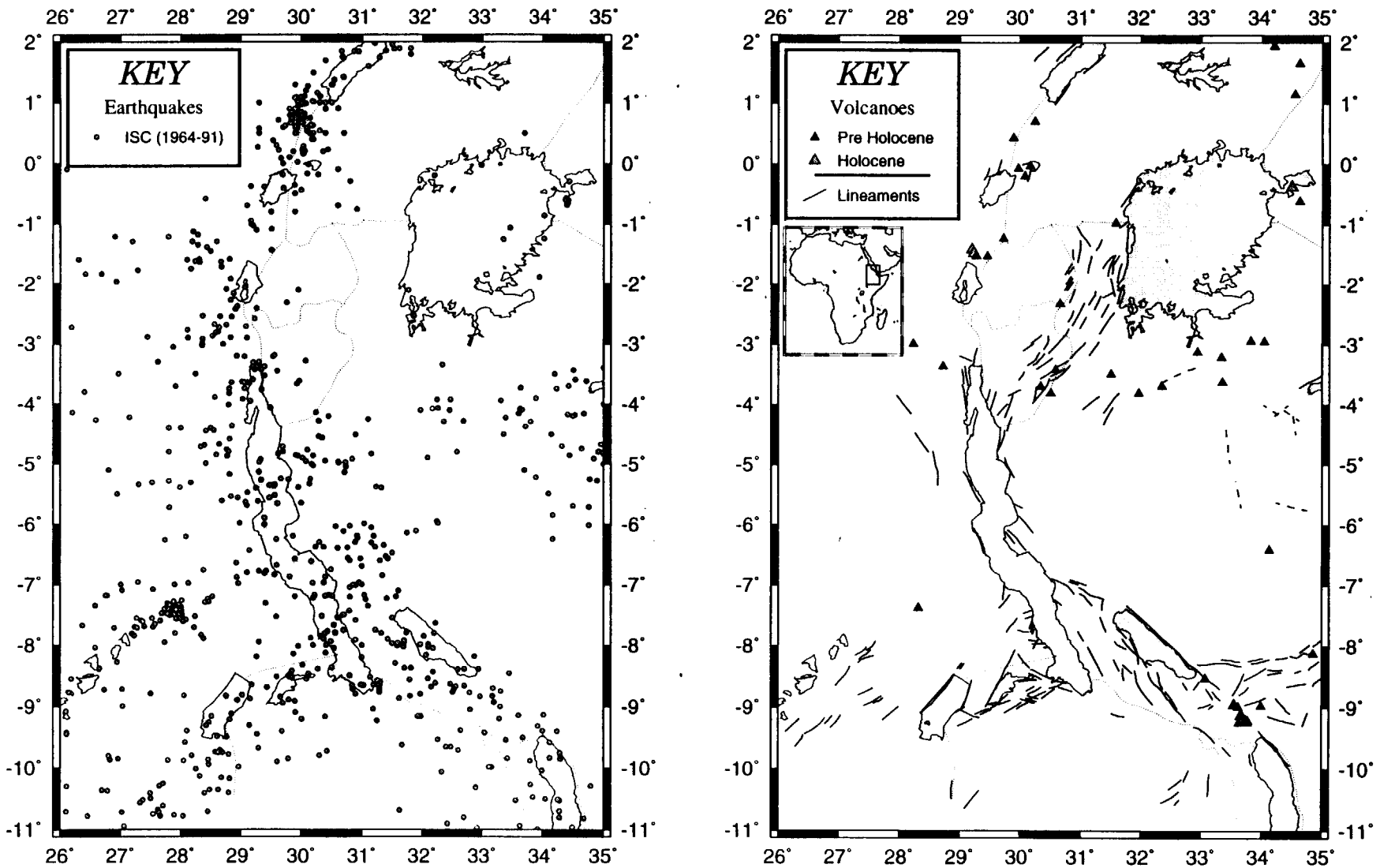

Fig. 7.4. Earthquakes and volcanoes of the Lake Tanganyika region. A. Earthquakes from the ISC (1964 - 1991); B. Volcanoes from Nusbaum et al (1994) and lineaments mapped from AVHRR (B211).

7.2 The Rukwa Rift

The Rukwa rift zone is an anomalous zone within the western branch of the East African Rift System. Its orientation is approximately NW-SE, compared to the almost N-S trend of most of the Tanganyika rift. It has been extensively studied, using seismic reflection, gravity and drilling, due to its potential for hydrocarbons. Surveys have been carried out for Petro-Canada, Amoco, Pecten and Petrofina (amongst others) under an agreement with the Tanzania Petroleum Development Corporation. Figure 7.5. shows the Rukwa Rift Zone with faults taken from Peirce & Lipkov (1988). Locations of the major features and geographical names are shown.

7.2.1 Geological Background

The Rukwa rift zone joins the Tanganyika and Malawi rift zones of the western branch of the East African Rift System. It is completely enclosed, with drainage from the rift flanks flowing into Lake Rukwa, which has an average depth of about 13m (c.f. Lakes Malawi and Tanganyika with depths of about 1 km). The north-western end of the trough joins to the Tanganyika rift zone through the low relief Karema depression (Morley *et al*, 1992). The southeastern end of the rift terminates against the Tertiary to Recent Rungwe volcanics (e.g. Tiercelin *et al*, 1988; Ebinger *et al*, 1989).

The present Rukwa rift valley follows the pre-existing Precambrian (Ubendian) fold belt which was also followed by the Karoo (Permian) age tectonic fabric (e.g. McConnell, 1972). Tertiary rifting began about 7 Ma ago in this previously rifted region. Dating of basalts from the Rungwe massif gives ages of 40-35 Ma (Tiercelin *et al*, 1988) which may correspond to an initial rifting stage in the region.

The Rukwa rift zone is essentially a 'down-to the-northeast' half graben with the Lupa (or Rukwa) fault, which lies along the northeastern shore of Lake Rukwa, forming the main boundary fault. (e.g. Peirce & Lipkov, 1988; Rosendahl *et al*, 1992). Morley *et al* (1992) considers that the Lupa fault was originally Karoo in age and was reactivated in the Tertiary. The southwestern flank is formed by the Ufipa fault (termed the Tunduma fault by Tiercelin *et al* (1988)) which bounds the Ufipa Plateau to the southwest. To the south of the current limit of Lake Rukwa the rift bifurcates around the Mbozi fault block, a basement horst. The western most of the two valleys is the Msangano Trough which dies out about 30 km beyond the junction. The eastern and major trough is the Songwe Trough which terminates against the Rungwe volcanics. It is this trough which appears,

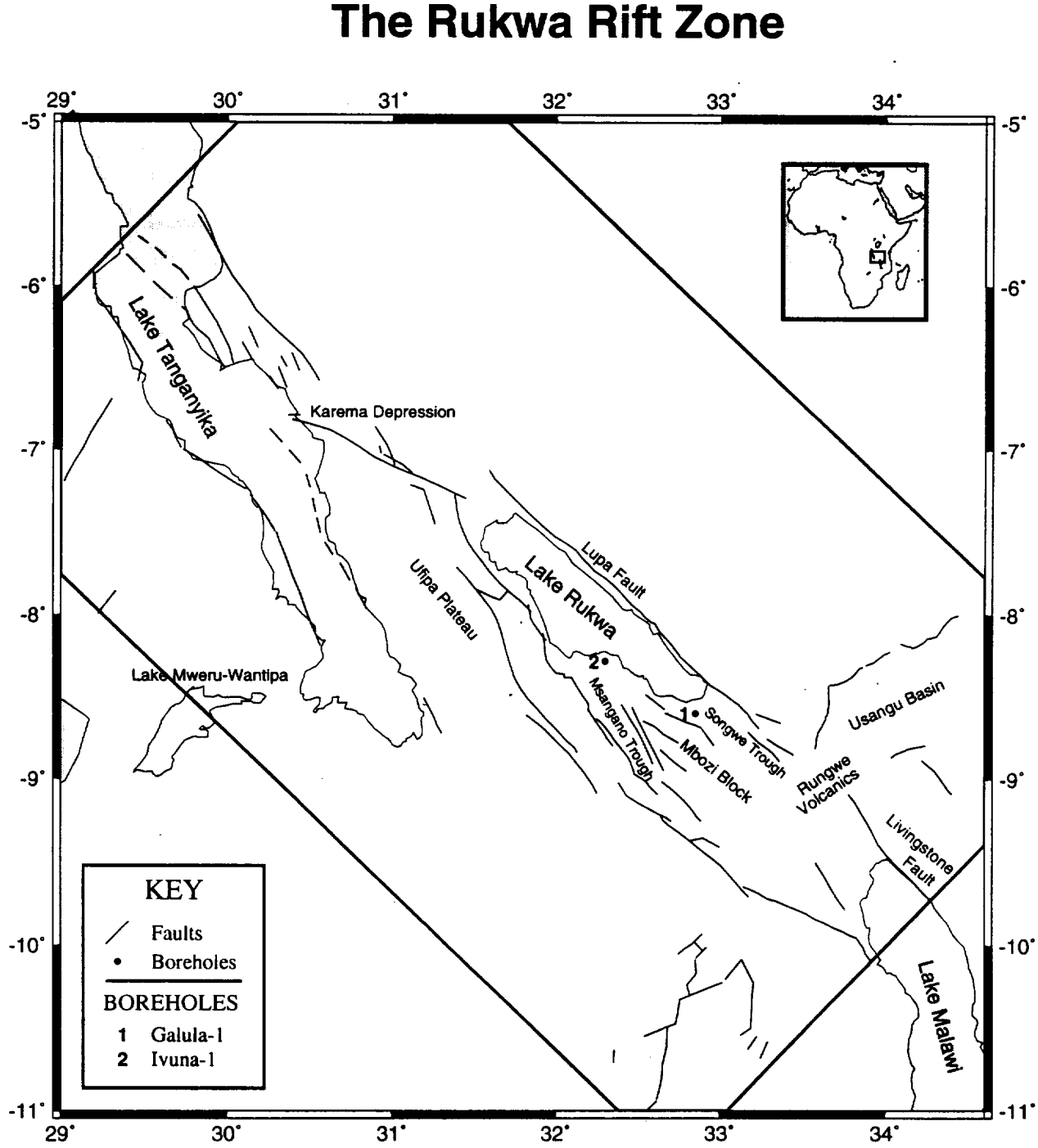

Figure 7.5 The Rukwa Rift Zone; faults taken from Peirce and Lipkov, 1988.

but for the Rungwe volcanics, to join through to the northern end of Lake Malawi; with the Lupa fault of Rukwa corresponding to the Livingstone fault of northern Lake Malawi.

Seismic refraction studies (Morley *et al*, 1992, Rosendahl *et al*, 1992) in the region confirm the half graben nature of the rift and indicate that minor faulting becomes more common on the flexural margin, opposite the Lupa fault. Some minor faulting is listric in cross section (Morley *et al*, 1992).

The Rukwa rift is oblique to other sections of the rift system and has been used to try to ascertain the direction of regional extension. Various opinions exist as to the regional extension direction, ranging from E-W (e.g. Morley 1988a; Strecker *et al*, 1990.) to NW-SE or NNW-SSE (e.g. Fairhead & Girdler, 1970; Chorowicz & Mukonki, 1980; Versfelt & Rosendahl, 1989; Kilembe & Rosendahl, 1992). All models require a certain amount of strike-slip motion in the region from almost entirely strike-slip for the NW-SE model to oblique extension for E-W. Tiercelin *et al* (1988) suggest a N140° extension direction although there is considerable uncertainty in this. A component of strike-slip is observed along the Lupa fault but there must also be a component of extension. The task of determining an extension direction is complicated by the existence of pre-existing structure in the area and possible changes in the stress direction with time. Morley (1992) considered the current evidence and was led to the conclusion that the direction of extension is most likely to be E-W. However, Kilembe & Rosendahl (1992) cite the predominance of features leading to a much greater component of strike-slip based on the size, width and sediment depth as well as seismic reflection evidence. The evidence led Kilembe & Rosendahl (1992) to suggest that the "direction of extension is well to the north of due west".

Three main sedimentary series make up the sedimentary column in the Rukwa rift, these being: The Karoo super-group, the Red Bed sequence and the Lake Bed formation.

a. The Karoo Super-group

There are a few small outcrops of Karoo sandstones, shales and coal along the south-western flank of the Rukwa rift. In all these locations the Karoo is in fault contact with Precambrian crystalline basement (Morley *et al*, 1992). In the Ivuna-1 well, to the immediate south-west of Lake Rukwa, 704 m of Permian Karoo sequences were found (Fig. 7.6) with no Triassic age occurrences (Westcott *et al*, 1991).

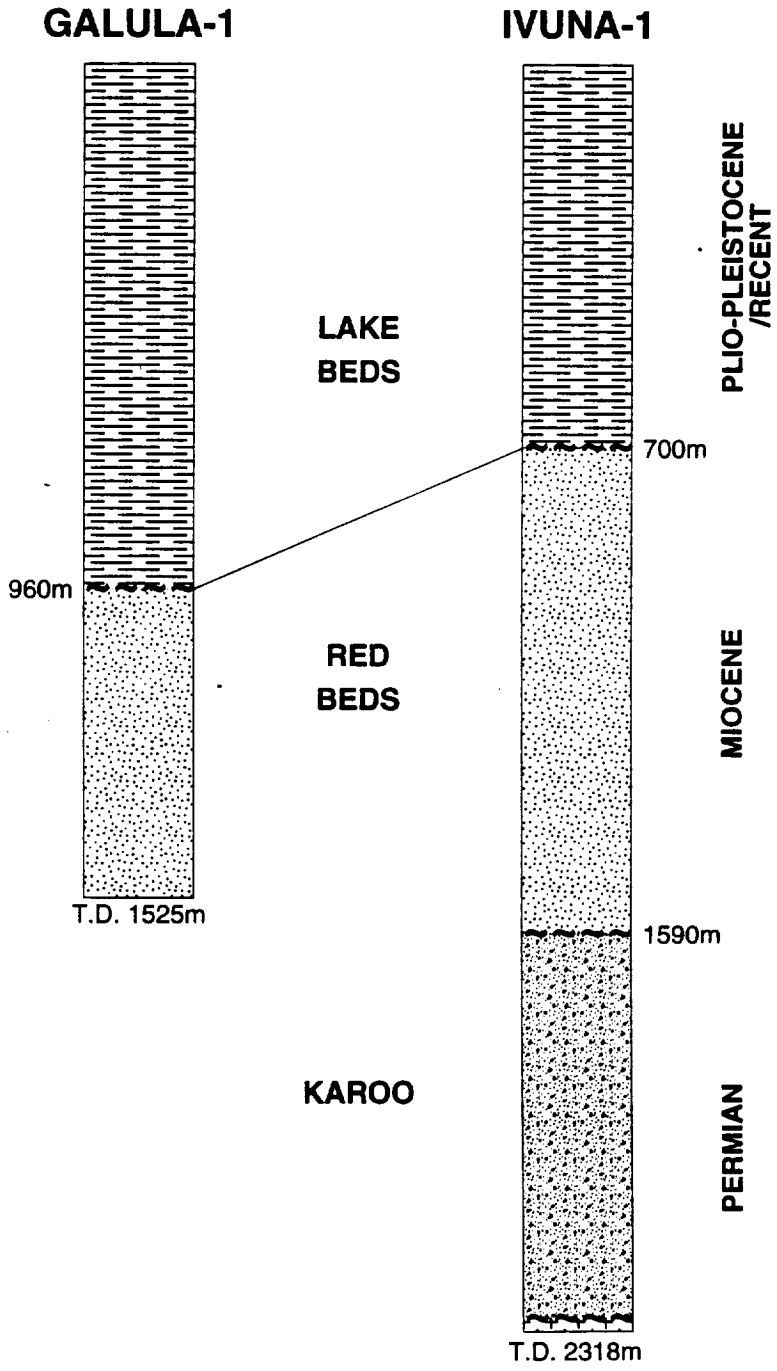

Fig. 7.6. Simplified Lithological logs for the Galula-1 and Ivuna-1 wells, the Rukwa rift zone After Westcott et al, 1991.

b. The Red Bed Formation

The Red Bed formation is predominantly composed of red sandstones of fluvial or alluvial origin (Dypvik *et al*, 1990). The Red Beds lie unconformably on the Karoo sediments which have dips averaging 15° on the rift margins (Morley *et al*, 1992). The age of these beds is uncertain, and has been assigned to the Cretaceous and Jurassic, palynological dating from the Ivuna-1 and Galula-1 wells (Fig 7.6) indicates an upper Miocene age (Westcott *et al*, 1991). The maximum thickness of the Red Bed formation and the underlying Karoo Super-group sediments is about 7 km (Rosendahl *et al*, 1992).

c. Lake Bed Formation

The Lake Bed sequence is made up of unconsolidated sediments of upper Miocene to Quaternary age. The sediments are fluvial-deltaic and lacustrine conglomerates, sands, silts and clays (Morley *et al*, 1992). The maximum thickness is about 5 km giving a total maximum thickness of sediments in the Rukwa rift of about 11-12 km (Rosendahl *et al*, 1992).

7.2.2 AVHRR

The two AVHRR band combinations used in mapping the lineaments of the Rukwa rift are given in Plates 5A and 5B, these being B211 $\Rightarrow$ RGB and B521 $\Rightarrow$ RGB respectively. The B521 image (plate 5B) shows the make up of the Rukwa rift very clearly. The two troughs separated by the Mbozi block are clearly seen to the southeast of the Lake; the westernmost (the Masangano trough) is seen trending and narrowing to the SSE. The Songwe Trough can be seen to the northeast of the Mbozi Block and trends towards the Rungwe volcanic province.

Figure 7.7 compares AVHRR lineaments with the faults used by Peirce & Lipkov (1988) and those on the UNESCO tectonic map of Africa (1968). Delineation of the Rukwa rift zone correlates well between the data sources. The Lupa fault is clearly defined on all data-sets, as are the boundary faulting to the southwest of the rift zone. The Mbozi block is indicated clearly by Peirce & Lipkov (1988) and is also clear on the B521 AVHRR though not on B211 AVHRR nor on the UNESCO map. Structures relating to the Usangu Basin are present on both AVHRR and fault maps, however the orientation is strikingly different. Both UNESCO and Peirce & Lipkov have the northern boundary of the basin trending SW - NE while both AVHRR interpretations indicate an almost due E

The Rukwa Rift Zone

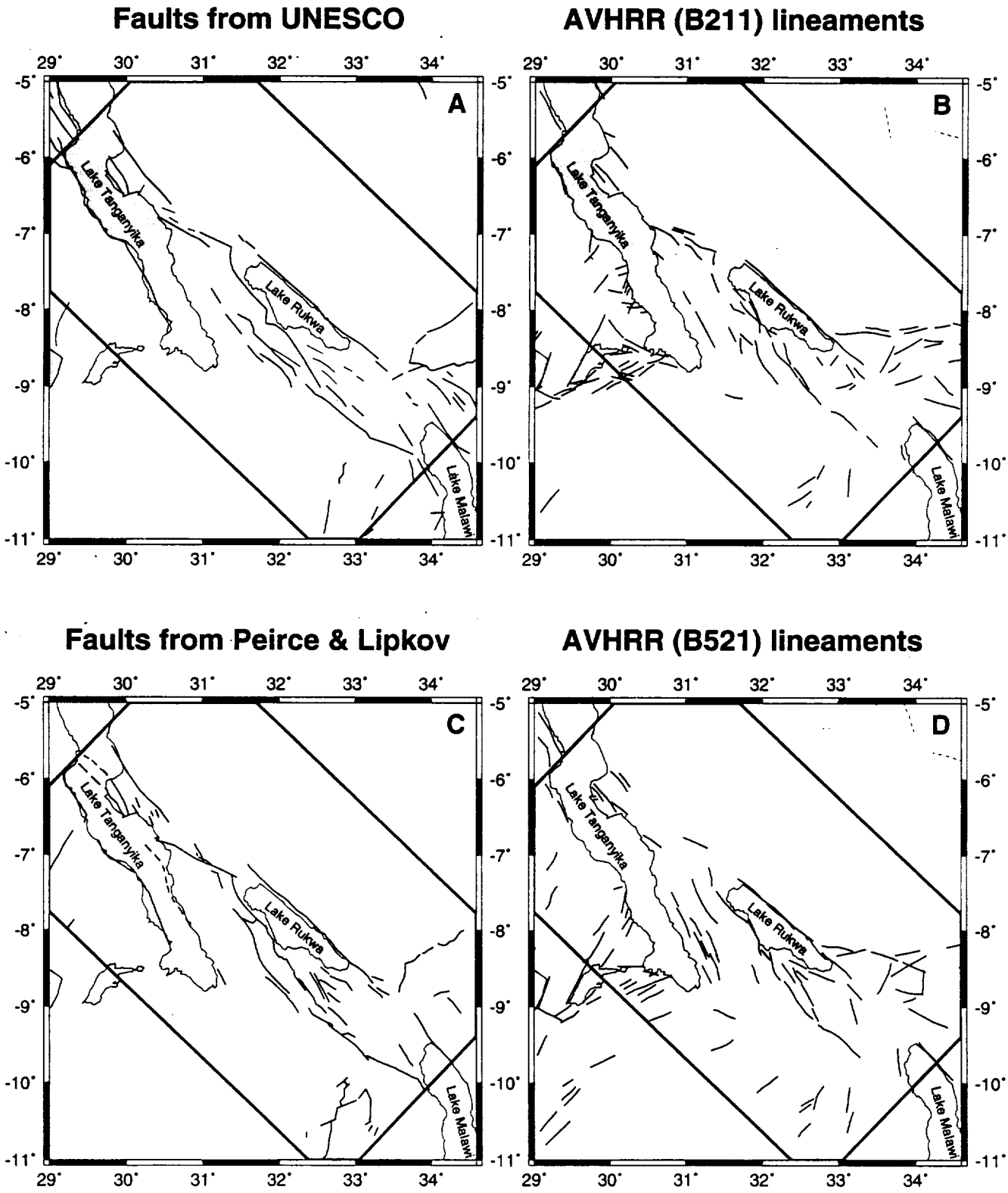

Figure 7.7 The Rukwa Rift Zone. A, Faults taken from UNESCO (1968) tectonic map of Africa. B. Lineaments mapped from AVHRR, bands 211 = RGB. C. Faults taken from Peirce and Lipkov (1988). D. Lineaments mapped from AVHRR, bands 521 = RGB.

- W edge. Differences between AVHRR and fault maps are particularly pronounced on the Ufipa Plateau where faults and AVHRR lineaments rarely coincide.

One region of considerable difference between both AVHRR data sets and other sources is the Lake Mweru-Wantipa region which is dealt with in chapter 8.

Figure 7.8 shows the directional trends of lineaments in the Rukwa rift zone. Only the area immediately surrounding Lake Rukwa and the rift extension as far as the Rungwe volcanics is considered. The confined region eliminates influences of trends from other, nearby, sections of the rift system. The azimuth of AVHRR mapped lineaments in this region is strongly oriented in NW - SE direction.

7.2.3 Topography

The topography of the Lake Rukwa region is given in figure 7.9. The lake edges are taken from AVHRR imagery of the area and are normally accurate to within a few kilometres, this is the case for the southern end of Lake Tanganyika and the northern tip of Lake Malawi however Lake Rukwa does not fit with the limits seen from topography. The level of this Lake is variable and even a small rise can flood much of the low lying southern and western edges. The differences between maps of the area and AVHRR, with particular reference to Lake Rukwa, was given in section 2.1.3. The topography of this area does not highlight as many rift features as is commonly seen in the eastern branch. The Lupa fault and its southeasterly extension as the Livingstone fault are clearly visible. The Songwe Trough and rugged terrain of the Rungwe volcanics are also discernible. However the Mbozi Block, Msangono Trough and much of the Ufipa scarp, except at its northern end, are not well defined.

7.2.4 Seismicity

The Rukwa rift exhibits seismicity, over the last 30 years, comparable to that of the rest of the western branch, figure 7.10. In 1910 an M_S = 7.4 event struck the region (Ambraseys, 1991a) which is the largest event recorded in this part of Africa. The epicentral position of this event is not certain due to the few recording stations at the time and was given as 8°S, 31°E by Gutenberg & Richter (1965). This position may be inaccurate by up to a degree and Ambraseys (1991) suggested 7°S, 30.5°E as a "marginally better" location. Its magnitude and location led Ambraseys (1991a) to

Directional Trends of Lineaments mapped from AVHRR
Rukwa Rift Zone

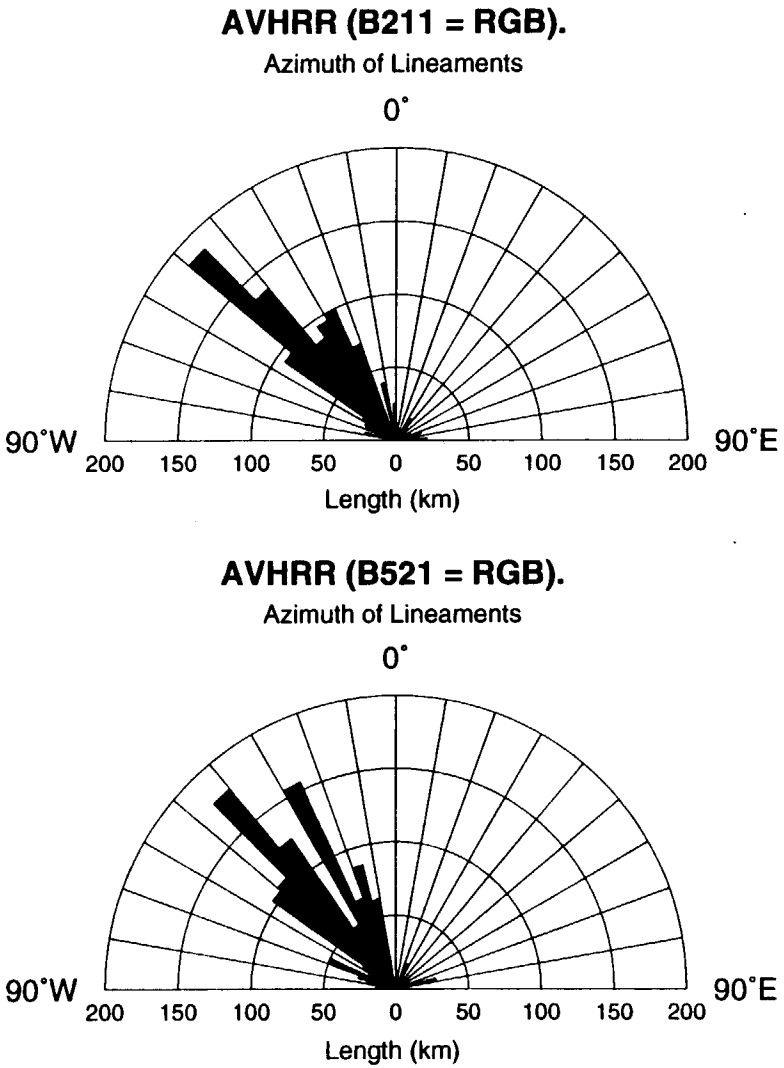

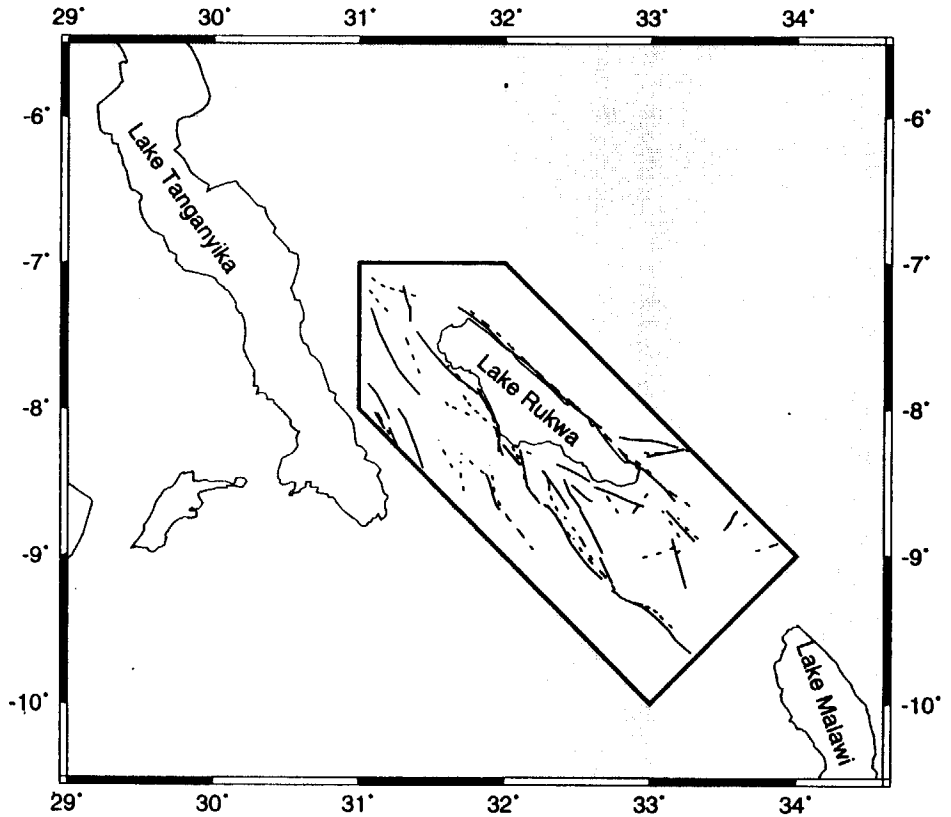

AVHRR Lineaments: B211=RGB (solid), B521=RGB (dashed)

Fig 7.8. Directional trends of lineaments, taken from AVHRR imagery, in the Rukwa rift zone.

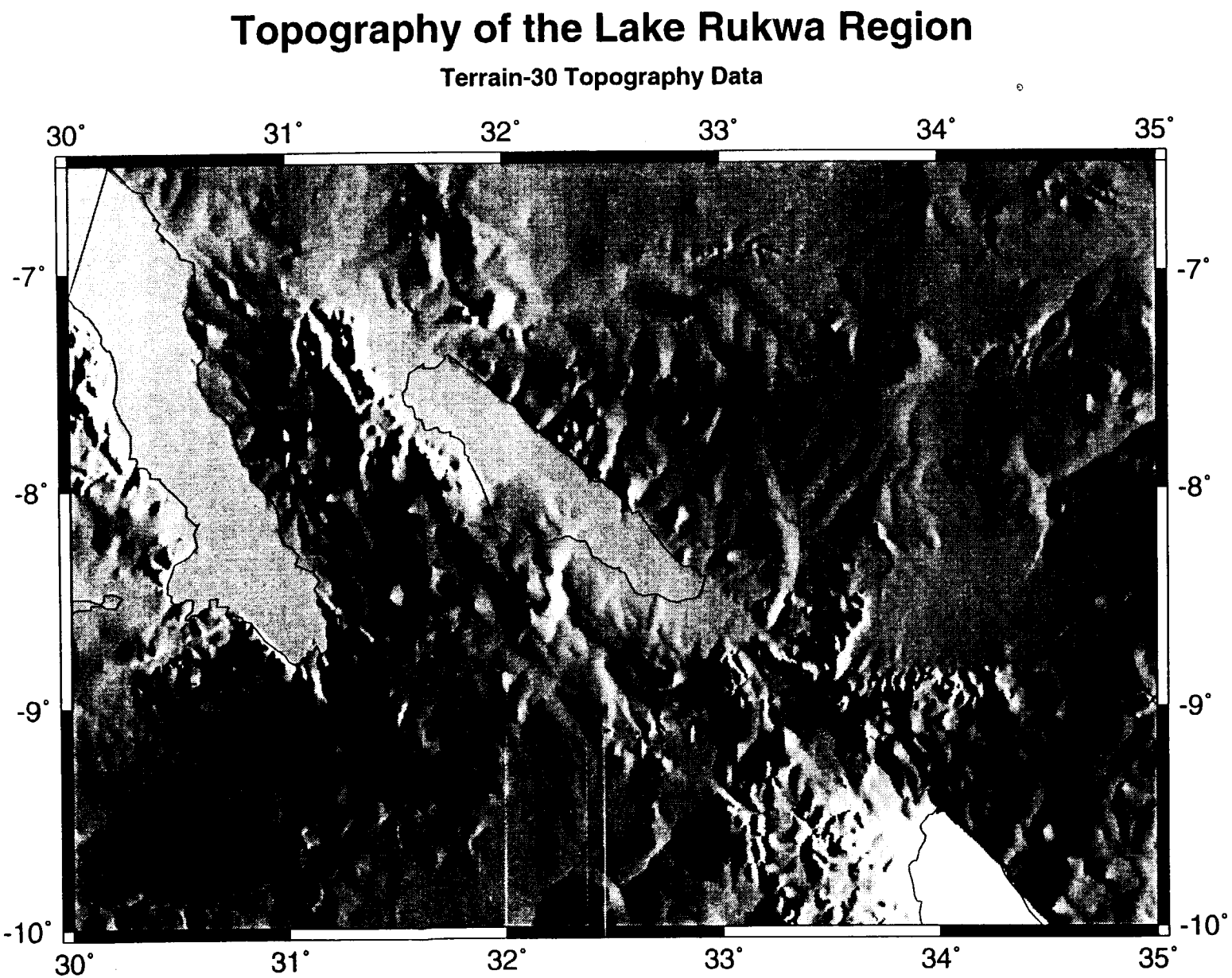

Fig. 7.9. Topography of the Lake Rukwa region, illuminated from the east.

Seismicity and Volcanism of the Rukwa Rift Zone

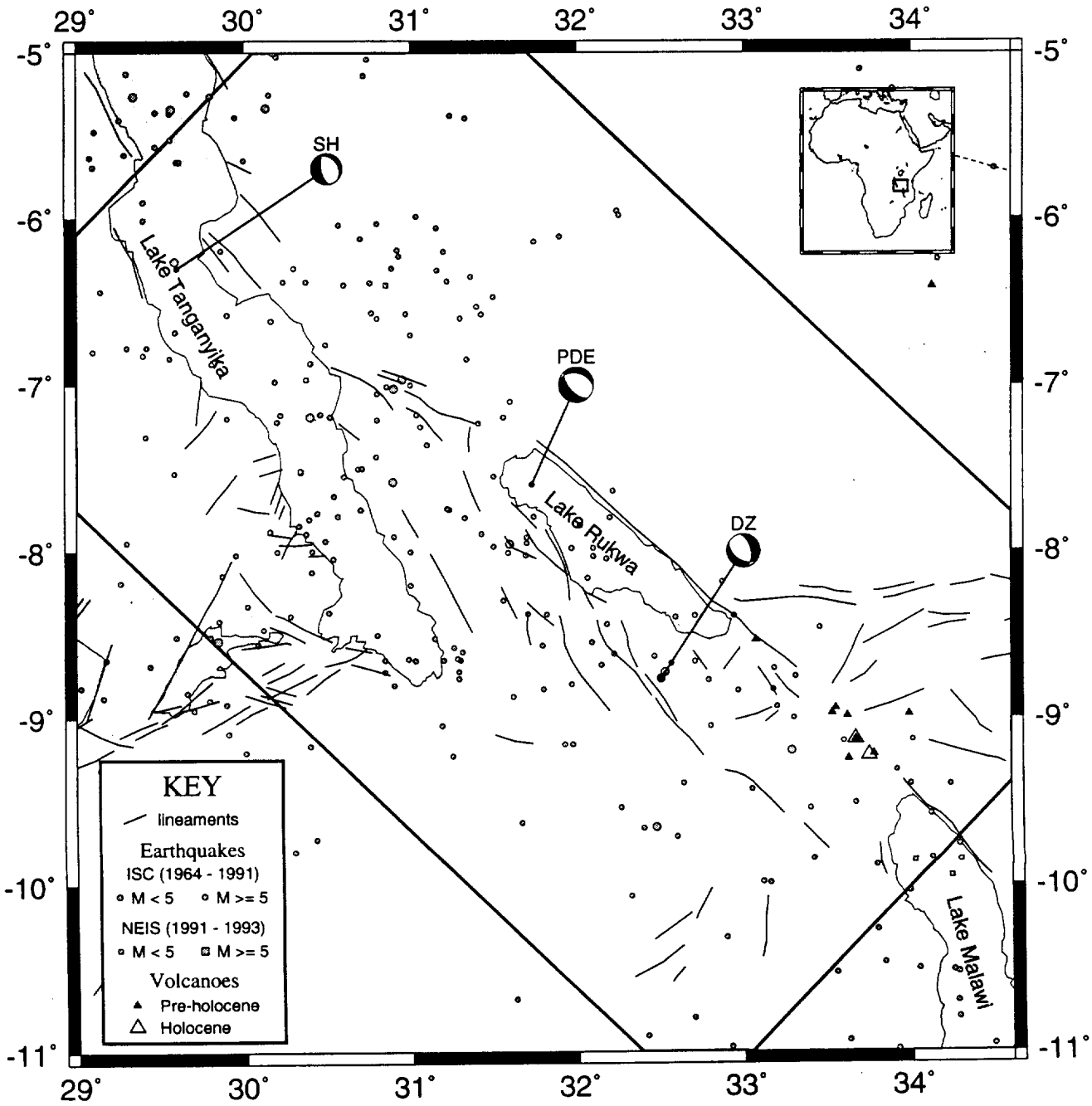

Figure 7.10 The Rukwa Rift Zone; earthquake epicentres (1964-1993) and lineaments mapped from AVHRR B521=RGB. Earthquake mechanisms from: DZ, Dziewonski et al (1985); SH, Shudofski (1985); PDE, Preliminary determination

suggest that there was probably a large strike slip component and was thus associated with strike slip faulting in the Rukwa rift zone.

Two fault plane mechanisms are available for the Rukwa rift, figure 7.10. One is situated on the Mbozi Block side of the Msangano Trough and shows an almost purely normal mechanism for this event, consistent with its location bounding the trough. The other mechanism also shows a normal faulting event and is located at the northern end of Lake Rukwa.

7.2.5 Southern Lake Rukwa (TM)

The band 4 Landsat TM scene of the southeastern part of Lake Rukwa is given in figure 7.11 while the lineaments mapped from it are given in figure 7.12. Once again the TM highlights a far greater number of lineaments than the AVHRR. However, many of the major faults and fault zones are seen clearly on the AVHRR imagery. The Lupa Fault is, if anything, more easily located on the AVHRR though the presence of the virtually linear lake shore may influence this. The Ufipa escarpment is shown as a narrow band of intense faulting on the TM scene which is simplified to a distinct lineament on AVHRR. Delimitation of the Mbozi block appears to be far more pronounced on the TM with those lineaments that are seen on the AVHRR extending further northwestwards than is shown by the TM.

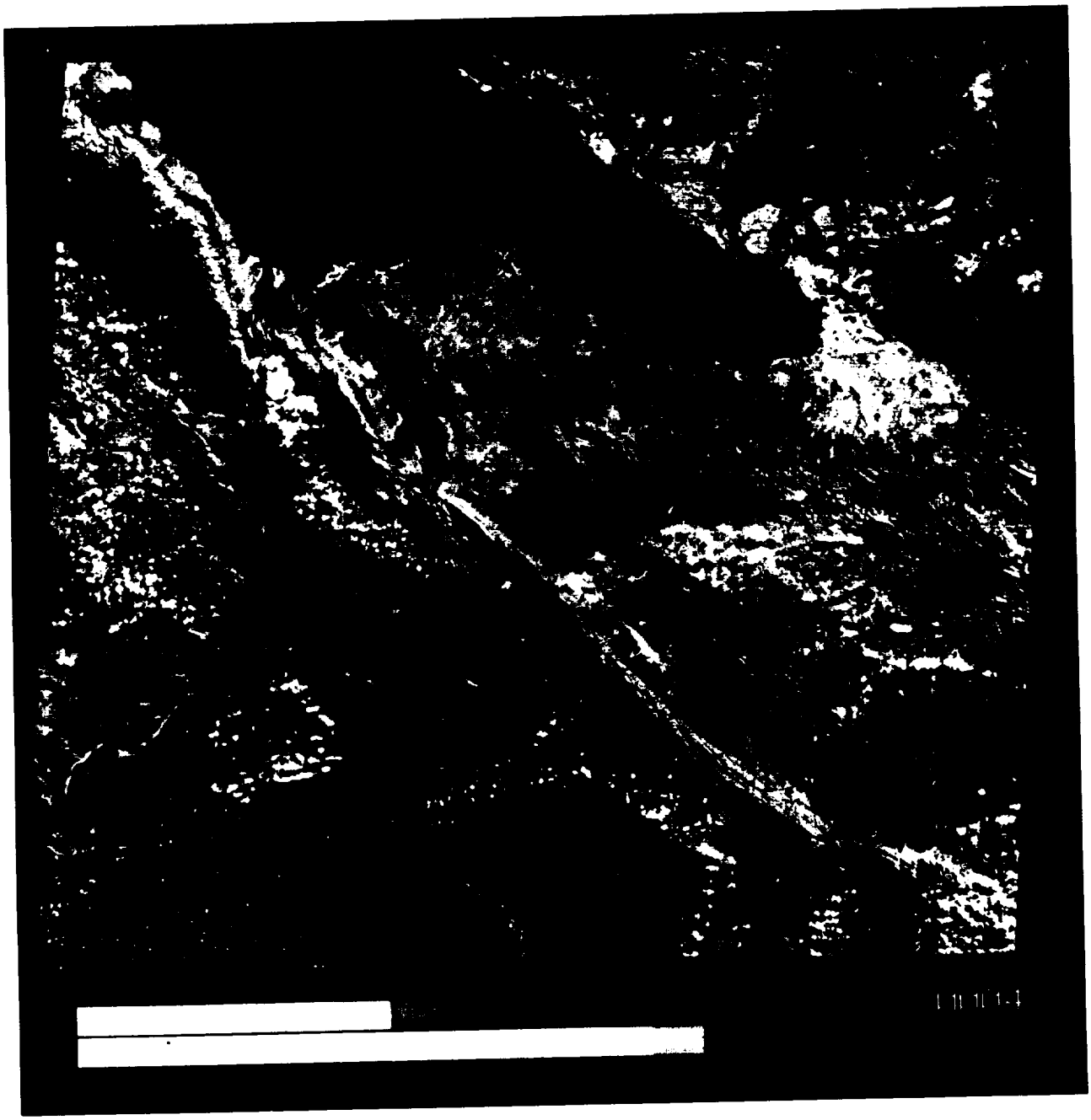

Fig. 7.11. Landsat TM scene of the southern part of Lake Rukwa; Band 4.

Lineaments of the Southern Lake Rukwa Region

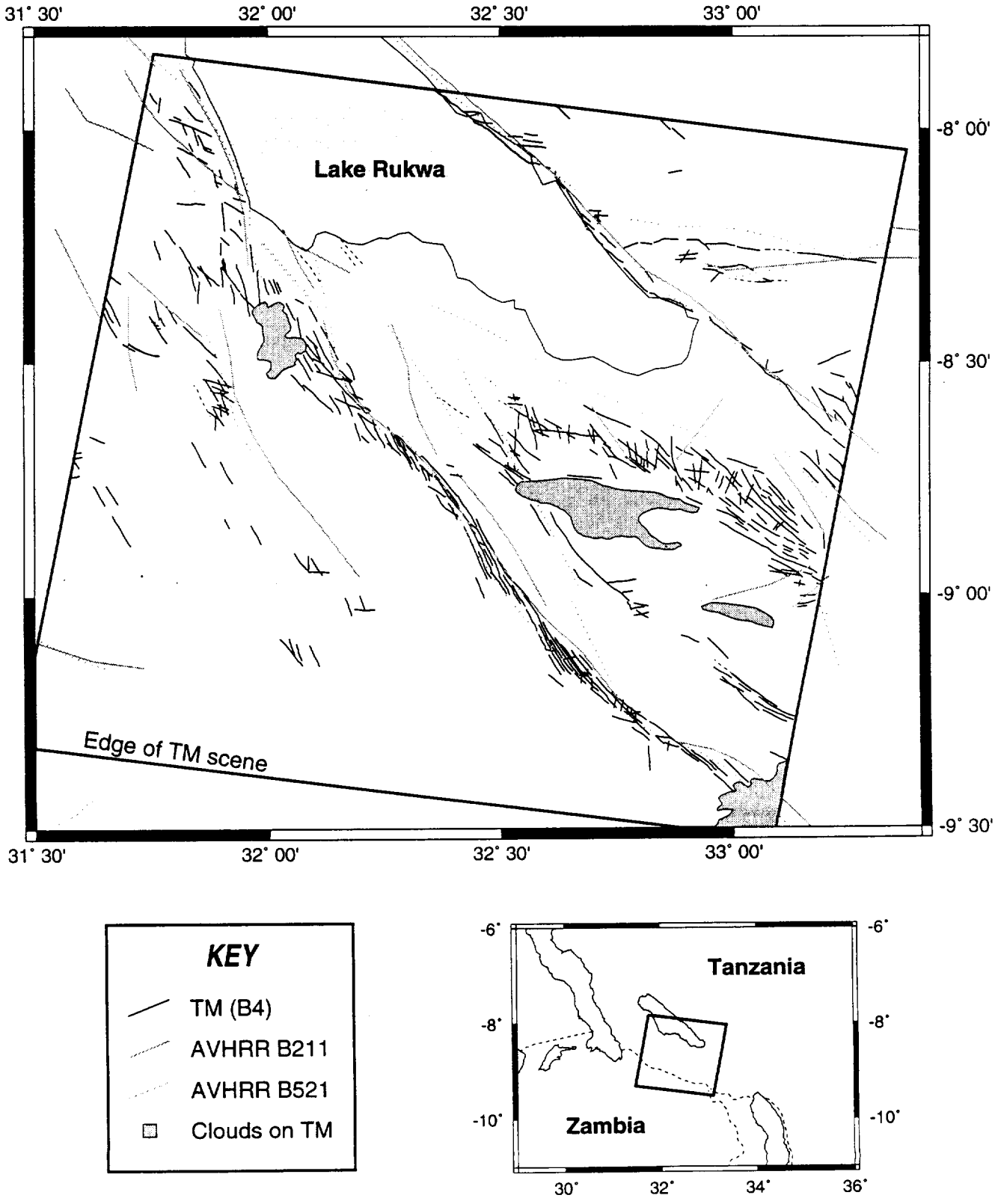

Fig. 7.12. Lineaments and faults of the southern Lake Rukwa region mapped from satelliite imagery.

CHAPTER 8

The Malawi and Southwestern Rifts

8.1 The Malawi Rift

Though linked to the western branch of the rift system through the Rukwa rift zone, the Malawi rift is aligned with the eastern branch. Tenuous links with the Eastern branch have been suggested along the Ruaha River valley which has experienced rifting in the Karoo (e.g. Rosendahl, 1987) and may have some contemporary activity along it. The Ruaha rift meets the western branch at the Rungwe volcanic province. The Malawi rift zone extends south from the current termination of Lake Malawi along the valley of the Shire River. The northern end of the zone is at the Rungwe volcanics where the oblique rifting of the Rukwa zone continues the western branch northwestwards. The location of geographical names, used in the text, are given in figure 8.1.

8.1.1 Geological Background

The Malawi rift is very similar to the Tanganyika rift in its morphology. Lake Malawi infills much of its rift and has dimensions similar to Lake Tanganyika, it is about 500 km long and up to 750 m deep. The rift itself extends for about another 200 km south of the Lake along the Shire River. Also like Lake Tanganyika, the Malawi rift is characterised by a series of alternating half graben basins separated by accommodation zones (Versfelt & Rosendahl, 1989). The criteria for defining a half graben unit are unclear (e.g. Ebinger *et al*, 1987); Specht & Rosendahl (1989) suggest seven half-grabens while Rosendahl (1992) indicates that Lake Malawi has nine (c.f. 12 for Lake Tanganyika).

The Livingstone Basin at the north end of the Lake is bounded by the Livingstone fault to its northeast. The Livingstone fault is cut off from, but is in line with the Lupa fault bordering the northeast side of the Rukwa rift. The half graben formed by the Livingstone fault has up to 4 km of sedimentary fill and the rift mountains rise a further 1.5 km above the Lake surface (Specht & Rosendahl, 1989). The rift mountains further south are less well developed.

At the southern end of Lake Malawi the rift bifurcates along the two south pointing spurs of the Lake. The border faults for these two half-grabens lie on opposite sides of

The Malawi and Southwestern Rifts

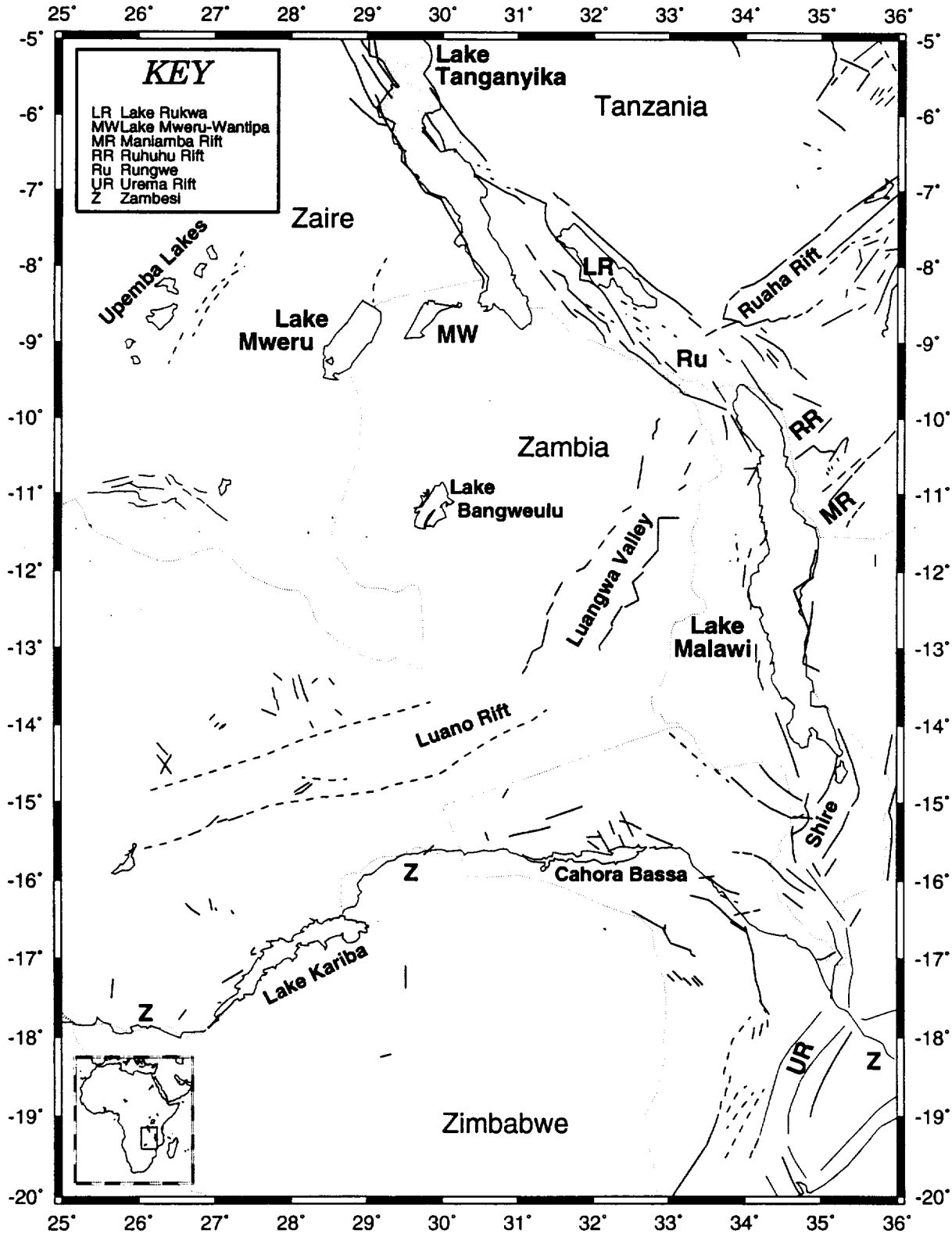

Fig. 8.1. The Malawi and southwestern rifts; location of geographic features used in the text.

the Lake and are situated about 10 km on shore. These basins appear to be recent and have less than 1 km of sedimentary fill (Specht & Rosendahl, 1989). The western limb is isolated at its southern end while the eastern limb links with the Shire valley.

Two Karoo age rift remnants abut on the eastern shores of Lake Malawi. The Ruhuhu Trough trends ENE from the shore at about 10.5°S and the Manimba Trough trends in the same direction from about 12.3°S (e.g. Rosendahl, 1987), see figure 1.14. Some pre-rift structure is also observed along the Henga Valley trending SSW from the western shore of Lake Malawi opposite the Ruhuhu trough (Versfelt & Rosendahl, 1989). The Luangwa Valley and Ruaha rifts meet the western branch of the rift system at the Rungwe volcanic province at the northern end of the Lake.

8.1.2 AVHRR

The Malawi rift and the area containing the suggested southwest trending rifts to the west of Malawi are covered by both day and night AVHRR imagery. Four band combinations of AVHRR imagery are considered, plates 6A, B, C & D. Day combinations B211 (plate 6A) and B521 (plate 6B) make the data comparable with other regions of the rift but two other combinations including night data are considered. The two other combinations are: B[d5/n5][d4/n4][d3/n3] $\Rightarrow$ [R][G][B] (plate 6C) and B[d5][n5]d5/n5] $\Rightarrow$ [R][G][B] (plate 6D), where d and n are day and night respectively.

The day scenes, plates 6A & B, are consistent with those for the rest of the rift system. The more red regions on the B211 image (plate 6A) and the green areas on the B521 image (plate 6B) are indicative of vegetation cover. The lower-lying river valleys are particularly dominant on the B521 image as being regions with a high thermal infra-red signature. Four distinct regions of marsh are seen on the B521 scene, these being; the Upemba Lakes, the south end of Lake Mweru, the area to the southeast of Lake Bangweulu and a valley to the north of Lake Kariba (at about 27°E, 15.7°S). All these regions are visible on the B211 image but are generally less distinct. Parts of the north and west of the day scenes are cloud covered.

The day/night combination scenes (plates 6C & D) provide an extra view on the area. The cloud cover on the night images was less extensive than the day image but different; thus combinations of the two will include cloud from both times. In the case of the ratio image (plate 6C) the day cloud is yellow while the night cloud is dark blue. Of the two combination images the band 5 combination scene (plate 6D) is the most striking. In this

the vegetation appears dark blue, the rift valleys and other low-lying areas are yellow-orange while the cratonic regions are generally red. The marsh regions are seen as cyan and are virtually indistinguishable from lakes and daytime cloud.

Figure 8.2 shows the lineaments mapped from the AVHRR images and figure 8.3 compares the B211 lineaments with the faults from UNESCO (1968). This section only deals with the Malawi rift, Lake Malawi and the Shire valley. The Rukwa and Tanganyika rifts are considered in chapter 7, while the southwestern rifts, including the Luangwa valley, are considered in section 8.2.

The AVHRR images which included night data show very few lineaments around Lake Malawi. The ratio image of day/night bands shows fewer lineaments than the band 5 combination scene (plate 6D); both pick out lineaments associated with the Livingstone fault at the north end of the Lake and hint at some of the scarps further south. The complex bi-directional faulting associated with the Livingstone fault is also mapped as neogene faulting by Chorowicz & Sorlien (1992). The band 5 scene suggests more border faulting, including opposite flexure faulting of the Livingstone half-graben and faulting associated with the southern end of the Lake. A lineament mapped on the western side of the Lake from about 13°S to 13.8°S matches the location of an inferred Neogene fault indicated by Chorowicz & Sorlien (1992). The band 5 combination scene also shows the western scarp of the Henga valley at about 34.0°E, 11.0°S. No scenes indicate rifting along the Shire valley.

The standard day scenes show a greater number of lineaments around Lake Malawi than the scenes including night data (this is in contrast to the rest of the coverage). Like the night combination scenes the Livingstone half-graben is clearly shown, and both B211 and B521 have indicated faulting on both sides. On the eastern side of the Lake there are signs of both the Ruhuhu and Maniamba Troughs where they meet Lake Malawi. The lineaments immediately to the north of the Maniamba trough match part of a 'master border fault' mapped by Versfelt & Rosendahl (1989). The western side of the Lake shows a more complex region of lineaments on the rift shoulders and there is some suggestion of a trend continuing along the line of the Maniamba Trough. Lineaments mapped on the western side of the Lake at about 12°S are similar to those shown by Chorowicz & Sorlien (1992). Correlation between B211 and B521 is reasonably good in this region although B521 appears to show more lineaments.

Figure 8.3 compares B211 (day) with UNESCO faults. There is little direct correlation between the two except in the case of the Livingstone half-graben. Both AVHRR and

AVHRR Lineaments and faults of the Southern rifts

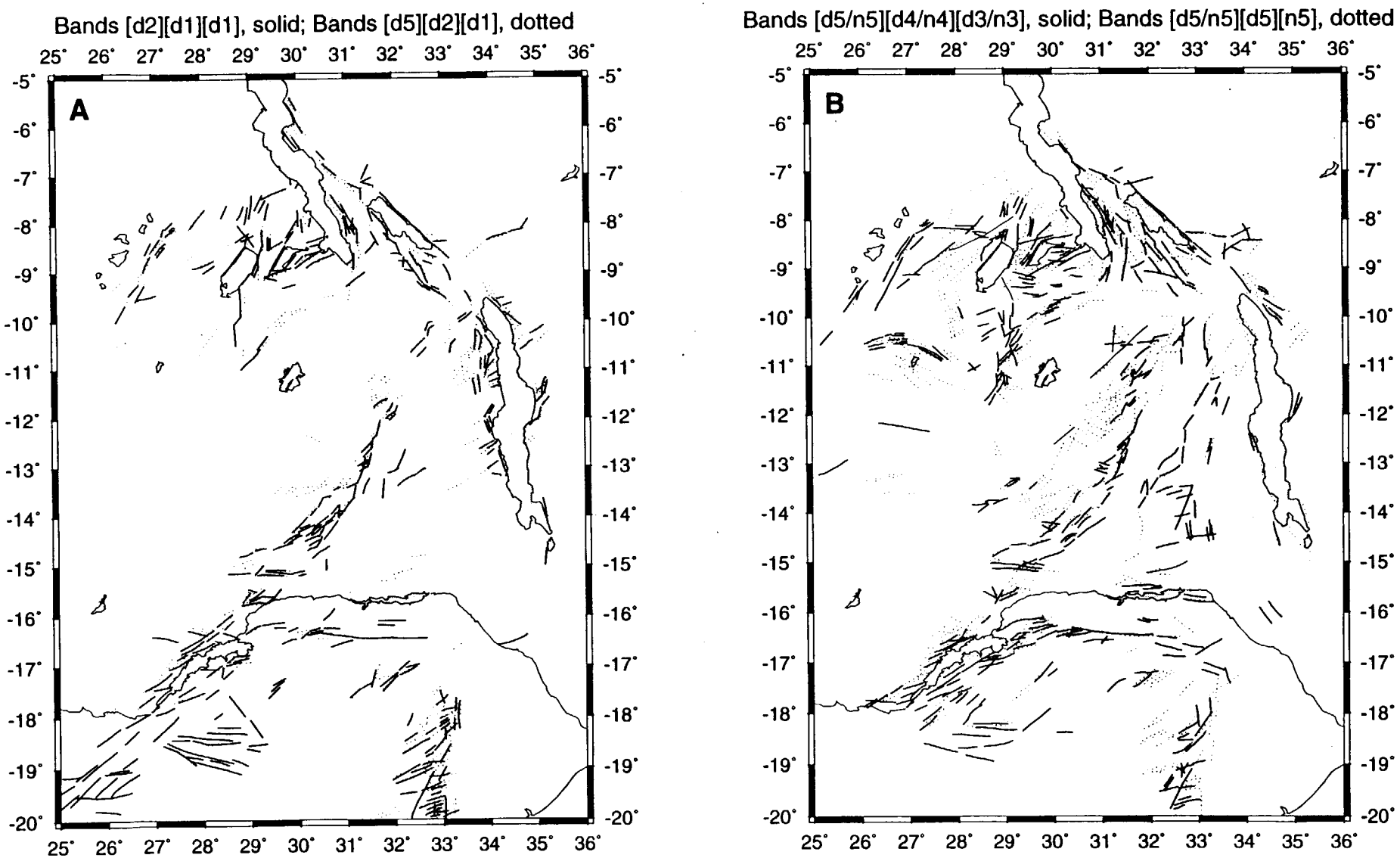

Fig. 8.2. Lineaments and Faults of the southern partof the east African rift system. A, Lineaments mapped from day AVHRR imagery; B, Lineaments mapped from day/night ratio and combination imagery.

Lineaments and faults of the Southern rift

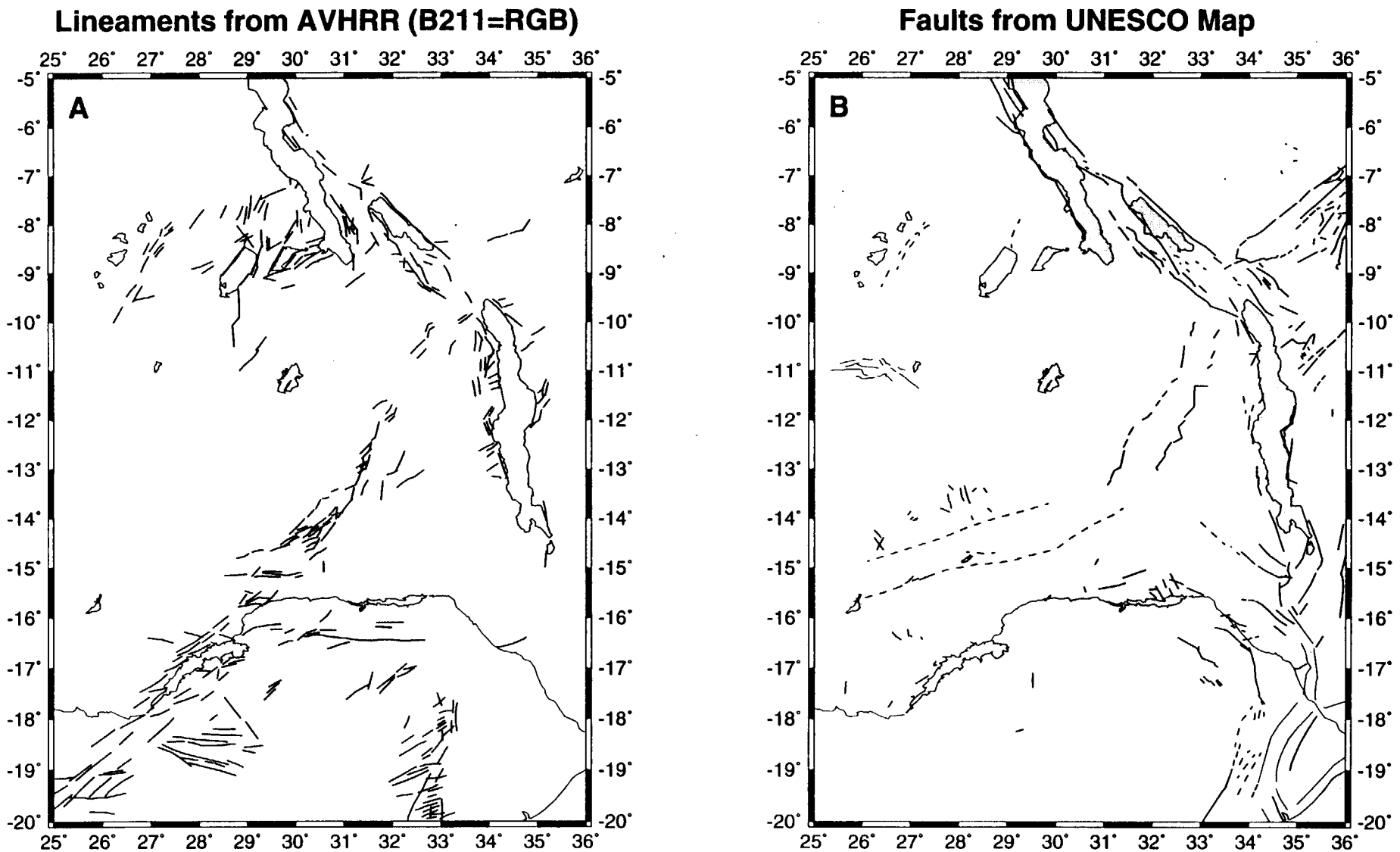

Fig. 8.3. Lineaments and Faults of the southern part of the East African Rift System. A, Lineaments mapped from AVHRR imagery; B, Faults from the UNESCO Tectonic Map (1968).

the UNESCO map indicate some of the border faults but the border faulting indicated by UNESCO between 12°S and 13°S does not allow for the incidence of the Maniamba trough (clearly seen on the topography) nor does it match the observations of Versfelt & Rosendahl (1989).

8.1.3 Topography

The topography of the Lake Malawi area is shown in figure 8.4. The rift boundaries at the north end of the Lake are clearly defined as far south as 12°S. In this northern section the highland rift flanks are clearly seen to extend up to 100 km from the rift shoulder, south of 12°S the western flank narrows to less than 50 km while the eastern flank is discontinuous. The Ruhuhu Trough is barely discernible as it meets the Lake shore at about 10.5°S while the Maniamba Trough clearly cuts the flanking rift highlands at about 12.3°S. The bifurcation of the rift at the southern end of Lake Malawi is seen on the topography and the scarp for the western branch of this is seen to the west of the Lake shore. The scarp for the eastern branch, which is in continuation with the Shire valley appears to follow the Lake shore. There is little surface evidence for the continuation of the rift along the Shire valley.

The generally NNE - SSW trending feature on the west of figure 8.4 is the Luangwa Valley. The topography shows no evidence of rifting along the valley and there are no signs of scarp slopes or faulting of any kind.

8.1.4 Seismicity and Volcanism

Seismicity (for the period of 1964 to 1991) and volcanism of the Malawi rift are shown in figure 8.5. The Malawi rift valley from the Rungwe volcanic province in the north to the Shire valley, south of the Lake, is seismically active. There is a band of epicentres along the length of the Lake although they are more numerous in the central and southern parts of the Lake. The epicentres for this period are more frequent along the western shore, and on-land from the western shore, than on the east side of the Lake. The belt of earthquakes becomes less coherent but can be traced trending south from the southern end of Lake Malawi.

Two fault plane solutions in the region of Lake Malawi are given by Shudofski (1985), see figure 1.6. One lies in the Luangwa valley to the west of the Lake and shows normal

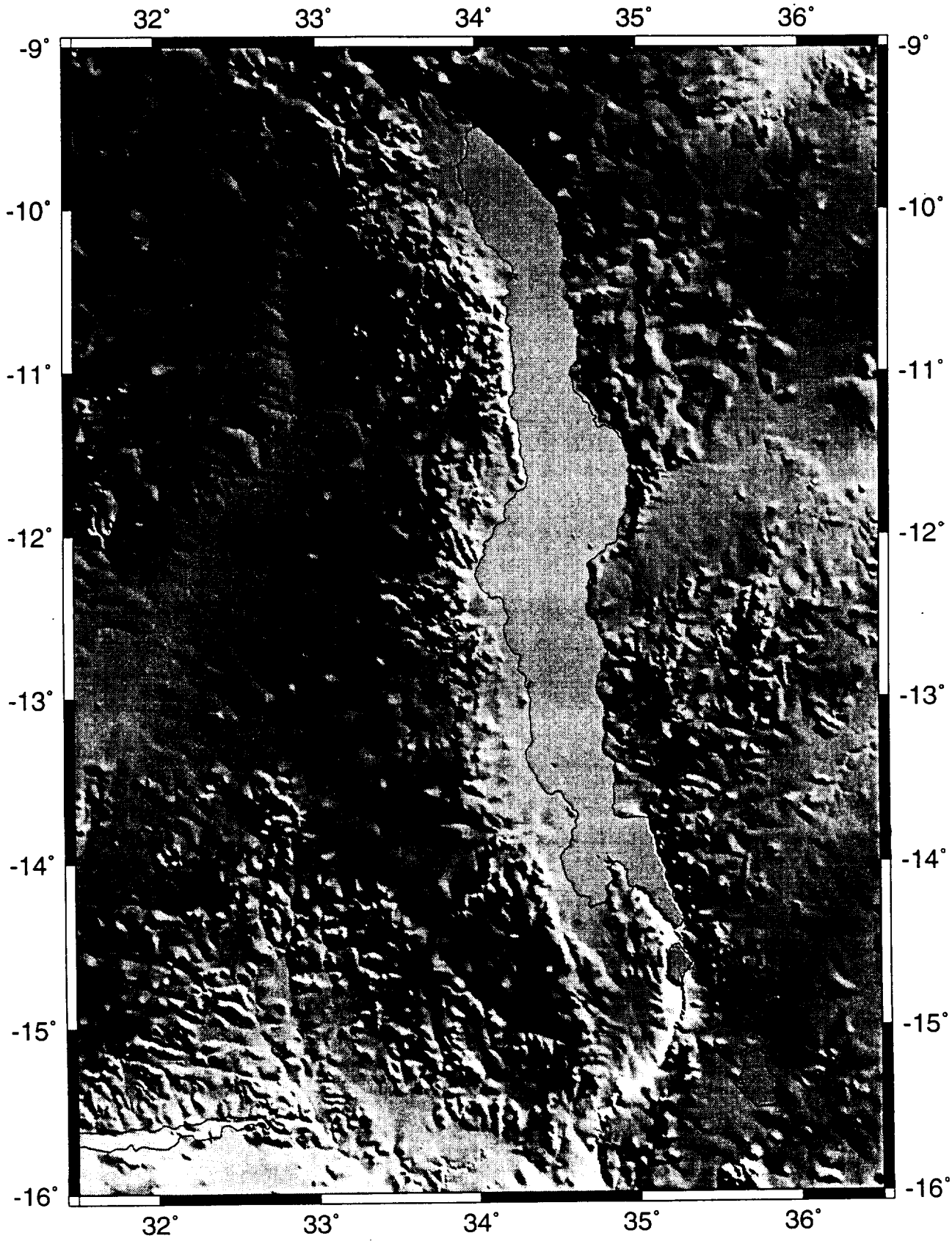

Fig. 8.4. Topography of the Lake Malawi region, illuminated from the east.

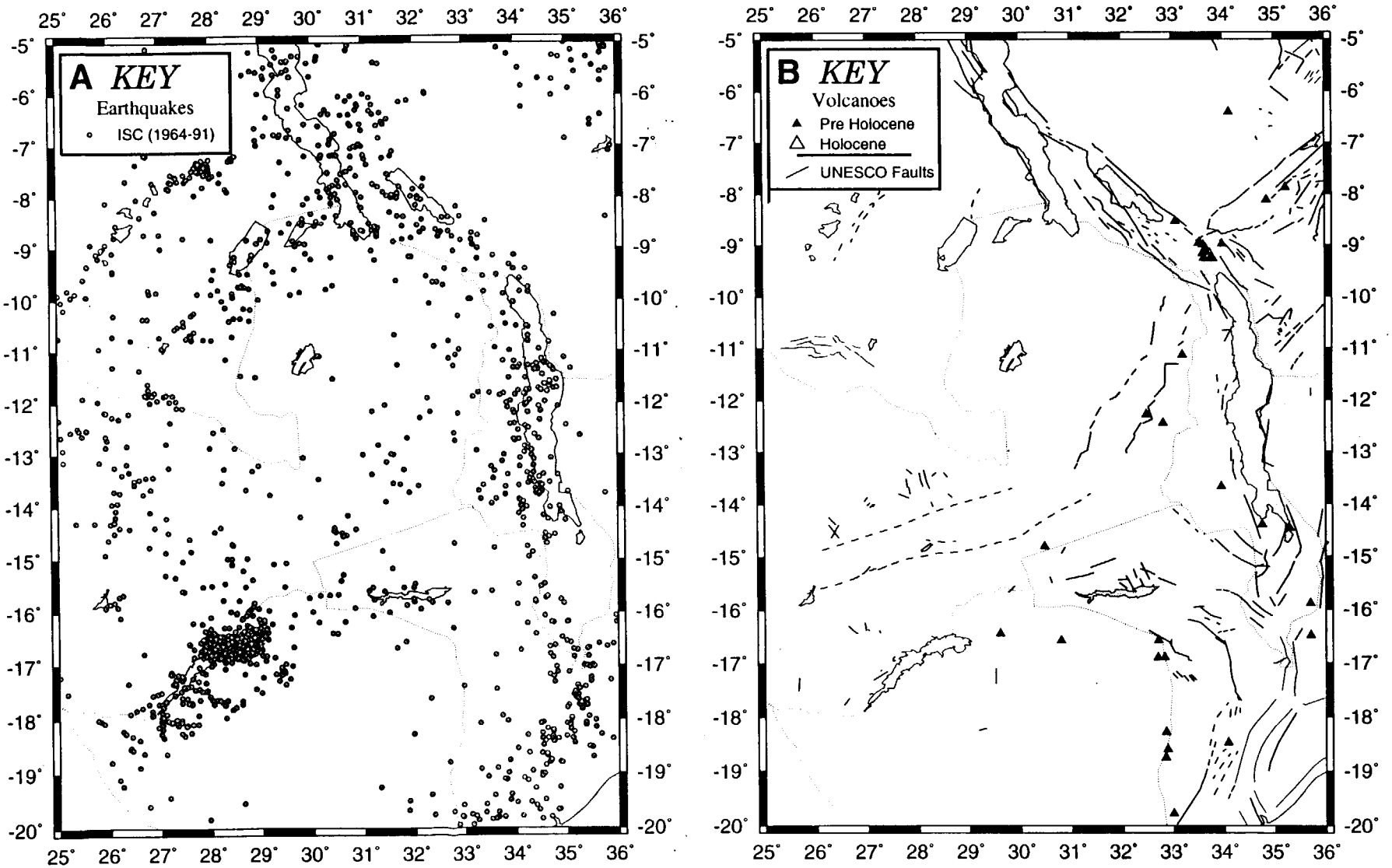

Fig. 8.5. Earthquakes and volcanoes of the Lakes Malawi and Kariba region. A. Earthquakes ftom the ISC (1964 - 1991); B. Volcanoes from Nusbaum et al (1994) and faults from UNESCO (1968).

faulting related to WNW - ESE extension. .The second mechanism, situated just to the west of the Shire River, shows normal faulting; indicating NW-SE extension. A PDE mechanism from the centre of Lake Malawi also shows normal faulting but the extension is WSW - ENE (Dzeiwonski *et al*, 1983 etc.).

Volcanism is largely confined to the Rungwe volcanic province at the north end of Lake Malawi, where the Malawi rift meets the Rukwa rift and the, Karoo age, Luangwa and Ruaha rifts. The most recent phase of volcanism was initiated at about 7 Ma (Ebinger *et al*, 1989). Activity has occurred in the Holocene and in historical times at Kieyo. Nusbaum *et al* (1994) recognised a few Pre Holocene volcanoes scattered around the Malawi rift, based on studies from satellite imagery. Many of these volcanoes may be pre-rift although the two located at the southern end of Lake Malawi would appear to be intimately related to the current rift valley.

8.2 Southwestern Rifts

The generally accepted termination of the East African Rift System is thought to lie where the Shire River joins the Zambesi (e.g. Rosendahl, 1987). However, there are a number of rifts which are pre-Tertiary in age that extend in a roughly southwesterly direction from the Western branch (e.g. McConnell, 1972; Rosendahl, 1987), see figure 1.14. Three southwesterly trending valleys are possible candidates for propagating rifts branching from the western branch: the Upemba Valley, the Mweru Valley and the Luangwa Valley. In addition the Urema Graben seems to form a southerly continuation of the Malawi-Shire rift and the Zambesi Valley is an E-W trending valley joining the south end of the Luangwa Valley and the southern end of the Malawi-Shire rift. The Kariba rift is also trending southwest in line with the Luangwa rift.

8.2.1 Geological Background

Of the three southwest trending rifts which branch from the western branch, Rosendahl (1987) indicates that only the Mweru rift has been reactivated during the Cenozoic whilst McConnell (1972) suggests that the Upemba and Luangwa rifts, may also have been reactivated. Despite the directional trend of Kariba, Rosendahl (1987) separates the valley from the Luangwa valley and instead joins it to the Zambesi rift (see figure 1.14). McConnell (1972) hints at activity in both the Kariba and Zambesi Valleys while Rosendahl (1987) assigns it to the pre-Tertiary.

The locations of the southwestern rifts, like the rest of the rifts in East Africa, generally skirt the Archean cratons. The Upemba Valley lies to the northwest of the Zambia Block along the Kibaran trend. The Luangwa Valley lies at the opposite, southeastern, side of the block along the Irumide belt. The Kariba, Zambesi and Urema rifts follow the northern limits of the Zimbabwe Shield to the northwest, north and northeast respectively. The only exception to the rule of the rifts avoiding the ancient nuclei is in the case of the Mweru Valley which is piercing the northeastern part of the Zambia block (McConnell, 1972, Hargraves, pers. comm.).

The Upemba rift has a northeast trending fault scarp of post-Miocene age and a downwarped trough to its northwest (McConnell, 1972). This trough is currently occupied by the shallow Upemba Lakes. The Luangwa Valley contains Karoo sedimentary fill deposited in a pre-Karoo valley that has undergone rejuvenation of its boundaries in the Cenozoic (McConnell, 1972).

9.2 Active and Inactive Rifts

McConnell (1972) argues for some Cenozoic rejuvenation in the southwestern rifts, however, he does not go as far as to suggest that these rifts are an integral part of a propagating East African Rift System. Whether a rift is tectonically active or dormant or 'failed' is difficult to define. Seismicity can provide evidence of activity but this can only be viewed over a short time-scale. It is likely, though not definite, that a rift exhibiting constant and frequent level of seismicity is tectonically active but the reverse is not true as a seismically quiet rift may be going through a short period of dormancy. Short of observing a major faulting episode volcanism provides the best evidence for current activity as dating of lavas can put a time-scale on faulting. Unfortunately not all rifts are volcanically active, which is certainly true for the southwestern rifts, to the south and west of the western branch.

If seismicity occurs along a rift valley it need not indicate that the rift is tectonically active and part of the Cenozoic rift system in Africa. If a rift fails, i.e. if the cause of rifting is removed, there will be a time lag before the seismic activity within that rift ceases, due to settlement of regions left unstable by the rifting as well as due to rebounding that may result. However, the magnitude of events is likely to be relatively small in a recently failed rift and will decrease further with time.

The problems outlined above make it virtually impossible to determine whether southwesterly extension of the East African Rift System is occurring or whether the activity that is seen today is simply a relic of the previous rifting episodes. Certainly studies from satellite platforms, alone, cannot resolve this problem and will simply help to delineate the rifts, whether active or failed.

8.2.3. AVHRR

The four AVHRR images are shown in plates 6A, B, C & D and the interpreted lineaments are shown in figure 8.2 with a comparison with mapped faults (UNESCO, 1968) given in figure 8.3. Lineaments in and around the southwestern rifts are more widespread on the day/night combination images than on the standard B211 and B521 scenes. A general description of the plates is given in section 8.1.2.

The day AVHRR scenes (plates 6A & B) show lineaments associated with the Upemba escarpment and indicates structure associated with the Mweru rift and the Mweru-Wantipa area. Some lineaments are seen south of Lake Mweru but few follow the southwesterly trend highlighted by the seismicity. A number of lineaments are also observed to the northwest of Lake Bangweulu and follow a similar trend to those to the northwest of them. The western scarp of the Luangwa Valley is clearly defined although the eastern side is virtually devoid of observed trends. At the southwestern end of the Luangwa Valley there is an almost east - west trending, graben type, feature centred on about 15.0°S, 29.3°E. This feature corresponds with the Luano rift (McConnell, 1972). The Kariba rift is characterised by NE - SW lineaments with a number of E - W trends also observed. The lineaments observed by the B211 image also indicate a southwestward continuation of the Kariba rifting to about 20°S. The B211 scene also indicated almost E - W lineaments within the Zimbabwe Shield, to the south of Lake Kariba. The southern scarp of the Zambesi rift is clear on all scenes while few indications are seen of the northern edge. The lower Zambesi Valley is virtually devoid of mapable lineaments with no sign of the Shire or Urema rifts. A region of dense lineaments is seen in the region of approximately 18° - 20°S, 32° - 33°E. The majority of these lineaments are either N - S or NW - SE. They lie away from any recognised rift zones (e.g. McConnell, 1972, Rosendahl, 1987) and are situated at the western edge of the Zimbabwe Shield.

The day/night combination AVHRR scenes (plates 6C & D) show far more numerous lineaments than the standard day scenes. The Upemba scarp is still observed as is the

faulting around Lake Mweru and Mweru-Wantipa. The western edge of the Luangwa valley is seen as is the Luano rift. Faulting around Lake Kariba is also comparable to the day scenes as is the southern Zambesi scarp and lineaments within the Zimbabwe shield. The only feature not observed by the day/night scenes which was seen on B211 is the southwest continuation of the Kariba rift. Despite the similarities the day/night images also indicate a number of other features. The eastern edge of the Luangwa Valley is clearly defined and a NNE - SSW trend to the east of Luangwa follows the same trend as the Luangwa Valley and is continuous with the Henga Valley on the west shores of Lake Malawi.

The most noticeable difference between the day/night scenes and the day images is the lineaments observed on and around the northern part of the Zambia Block. The lineaments seen in the Lake Mweru region on the day scenes is still observed but many more are also seen. No southwesterly trend is observed beyond Lake Mweru with this region being cut by N - S, and a distinct belt of NNW - SSE lineaments. The lineaments observed skirting around the northwest of Lake Bangweulu on the day images is still seen but with more numerous lines. A large number of lineaments is also seen to the east and southeast of Lake Bangweulu but northwest of the Luangwa Valley. These lineaments, like those at the eastern edge of the Zimbabwe Shield, appear to lack directional coherence and may be related to Precambrian orogenic belts around the ancient cratons. Indeed the lineaments to the northwest of the Luangwa Valley lie in the Irumide belt (McConnell, 1972). All scenes show the Great Dyke of Zimbabwe as a distinct linear feature running from about 30.9°E, 17.0°S to 30.3°E, 19.1°S.

Apart from the Luangwa Valley and Upemba escarpment the B211 scene shows few similarities to the UNESCO map of the area, figure 8.3, which indicates very few faults associated with any other of the southwestern rifts. The faults around 11°S, 26°E show some similarities to some mapped on the day/night combination scenes.

8.2.4. Topography

The topography, shown in figure 8.6, is a resampled version of the same topography used for other regions. The resolution, usually 30" of arc is resampled to 2' due to limits in computer processing capacity. The topography of the Kariba Valley, at full resolution, is shown in figure 8.7. The Upemba Lakes lie at about 8.5°S, 26.5°E and appear to lie in a half-graben structure with scarp on the southeast side. There is no obvious sign of the Upemba rift north of 8°S, as noted by Rosendahl, (1987). The Mweru and Mweru-Wantipa rift is only visible as far as the southern extent of the Lake with no obvious

Topography of the Southwestern Rifts

Terrain-30 Topography Data

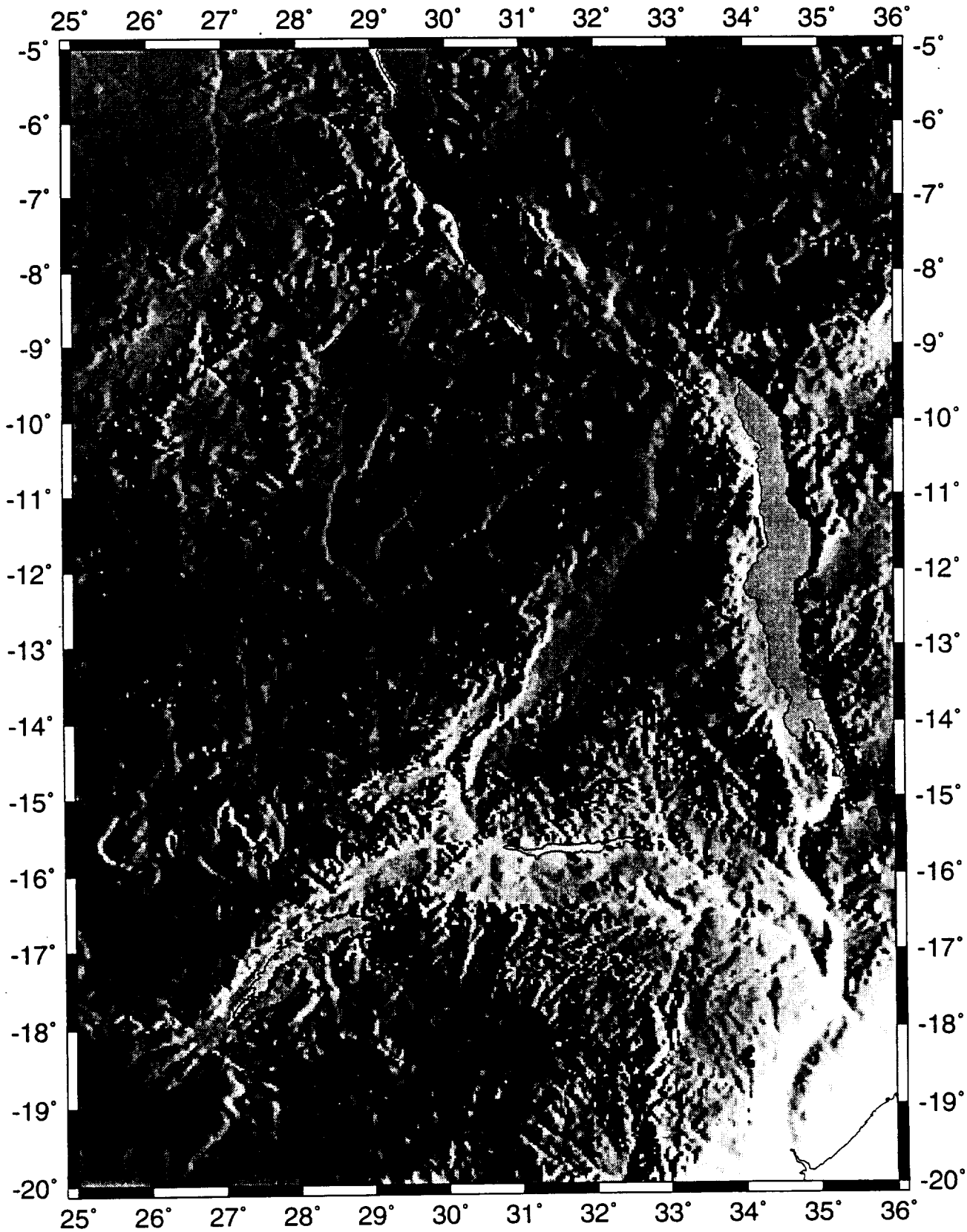

Fig. 8.6. Topography of the southwestern rifts region, illuminated from the east.

southwesterly continuation. The Luangwa Valley can be traced from the north end of Lake Malawi to the point where the Luangwa River meets the Zambesi. There is no obvious fault scarp bounding the valley north of 12°S. To the south the topography shows a western scarp. The small Luano rift (McConnell, 1972) is seen trending almost due west from 14.7°S, 30.0°E.

The Kariba and Zambesi rifts are clearly defined, in particular the southern scarp of the Zambesi Valley. The southwestern termination of the Kariba Valley appears to be at about 18.3°S with some linear trends extending to about 18.7°S. The N - S Shire Valley, south of Lake Malawi, is relatively narrow and sinuous and exhibits few rift valley traits though the steepness of the flanks and high shoulders would suggest some tectonic control. The Urema rift, south of the confluence of the Shire and Zambesi rivers continues the rift trend southwards to almost 20°S.

The topography also indicates a steep scarp-type edge to the Zimbabwe Shield running almost due north south along 33°E. The shield itself appears to be riddled with linear features. One other feature worthy of note from the topography of the area is an apparent linear trend continuous with the Maniamba rift, on the eastern shore of Lake Malawi, from the western shore at about 12.7°S, 34.2°S as far as the Luangwa/Zambesi rift at about 15.2°S, 30.1°E.

Figure 8.7 highlights the topography of the Lake Kariba region. The relatively low lying Kariba Valley is clearly seen to extend beyond the lake shores. The northwestern scarp is reasonably clearly defined but not so well as many of the western branch fault scarps. The rift shoulders are relatively narrow, only about 20 - 30 km wide. The southeastern limits of the valley are less clearly defined with a number of SSE - NNW trending lineaments visible at both the southern and eastern lake limits. The Kariba valley appears to continue to about 18.2°S although some southwestern trends continue to the southern limit of the figure.

8.2.5. Seismicity

The seismicity of the southwestern rifts is shown in figure 8.5. Trends of earthquakes can be seen following all the southwestern rifts but also occur all round the Zambia Block. A swarm of epicentres is seen around Lake Kariba, particularly at its eastern end. Some of these events are surprisingly large but most are small and recorded after a local

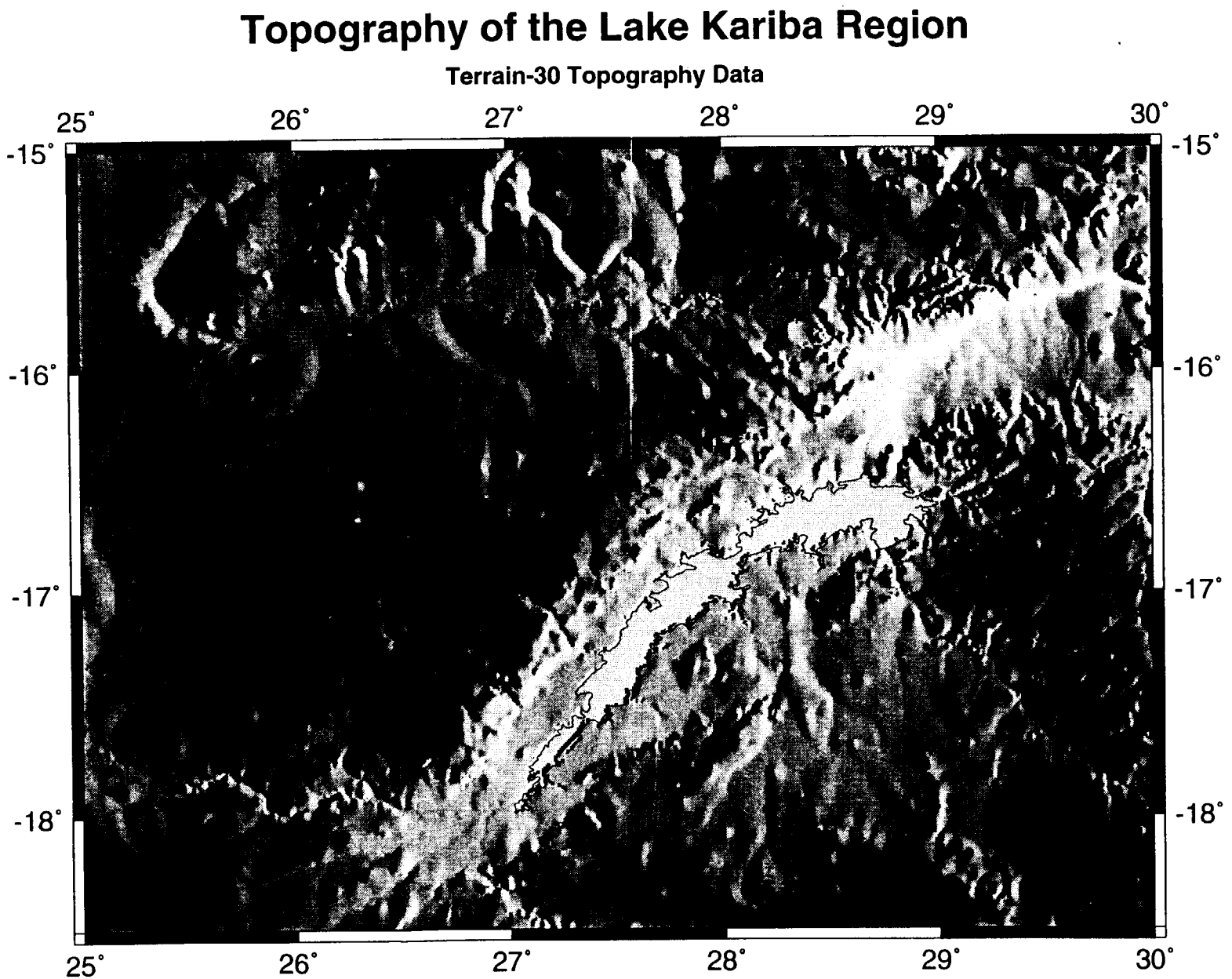

Fig. 8.7. Topography of the Lake Kariba region, illuminated from the east.

seismometer network was set up to examine activity induced by the building of the Kariba dam.

If the band of earthquakes from Lake Mweru southwestwards is indicative of propagating rifting it is cutting directly across the northwestern side of the Zambia Block. Seismicity along the Upemba Valley is narrow and confined to the valley trend while that associated with the Luangwa Valley is more diffuse and picks out the valley less clearly. The Zambesi Valley also exhibits seismicity along its length but these may be influenced by the Cahora Bassa dam. Seismicity along the southern Shire Valley and Urema fault is comparable to that observed in other parts of the western branch.

CHAPTER 9

Overview

9.1 AVHRR Studies

The biggest potential use of the AVHRR data is in providing a coherent and consistent overview of a large area; in this case the East African Rift System. It is feasible to study rift zones using higher resolution imagery (e.g. The Kenya rift zone using Landsat MSS - chapter 5) but it is helpful to put these sections together and view them in their regional context. Thus, this chapter deals with East Africa as a whole, using AVHRR imagery and other data sets such as earthquake epicentres and volcano locations.

Six AVHRR sub-scenes are used to view the East African Rift System. These are considered separately and their results combined to produce a map of lineaments for the whole of the rift system. No attempt is made to mosaic the images. It was noted in chapter 2 that it is often difficult to process individual scenes to show features at different locations to their best advantage. Mosaicing introduces the problem of trying to match scenes along their boundaries resulting in some loss of scene information. Thus, the overall compilation of lineaments has been carried out after mapping. The lineaments mapped using AVHRR B211 and B521 are shown in figures 9.1A and 9.1B respectively. Figure 9.2 shows the 1968 UNESCO fault map for comparison.

9.1.1 The Western Branch

The lineaments from AVHRR imagery show a good degree of correlation with the UNESCO map of faults associated with the East African Rift System. The region between Lakes Mobutu and Tanganyika is the most poorly mapped due to cloud cover. The scenes used to map this section had, at best, patchy cloud cover. In addition to the rift system itself, AVHRR has highlighted other zones of lineaments. If one had no prior knowledge of the area it would be reasonable to conclude that the western branch arced from Lake Tanganyika in a northeasterly direction to the western shores of Lake Victoria. This zone is the southern limit of the Karangwe-Ankole belt, a region of Kibaran orogenesis (McConnell, 1972). B211 shows this belt very distinctly while B521 shows it far less coherently.

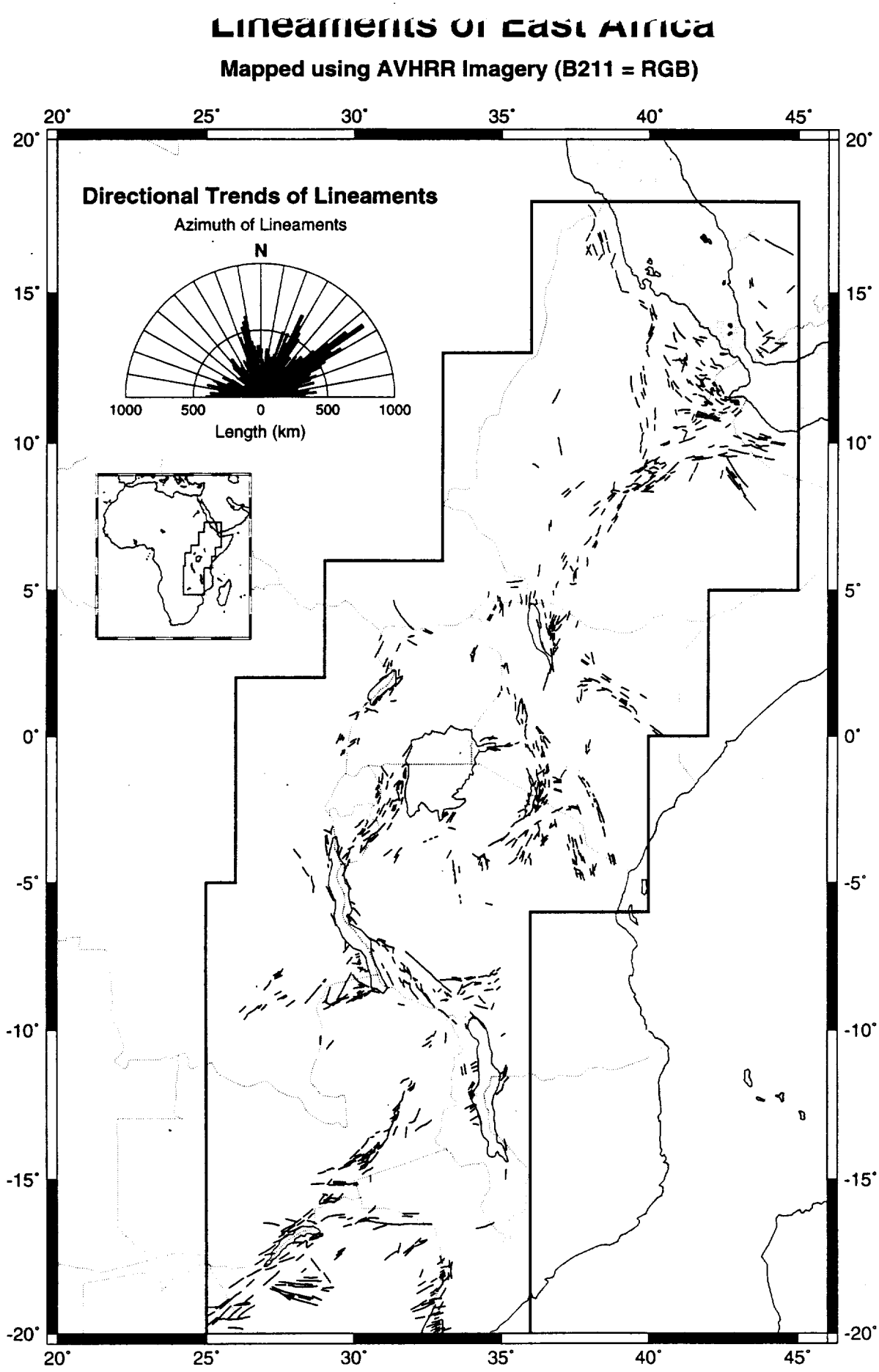

Fig 9.1A. Lineaments of East Africa as mapped from AVHRR (B211) imagery.

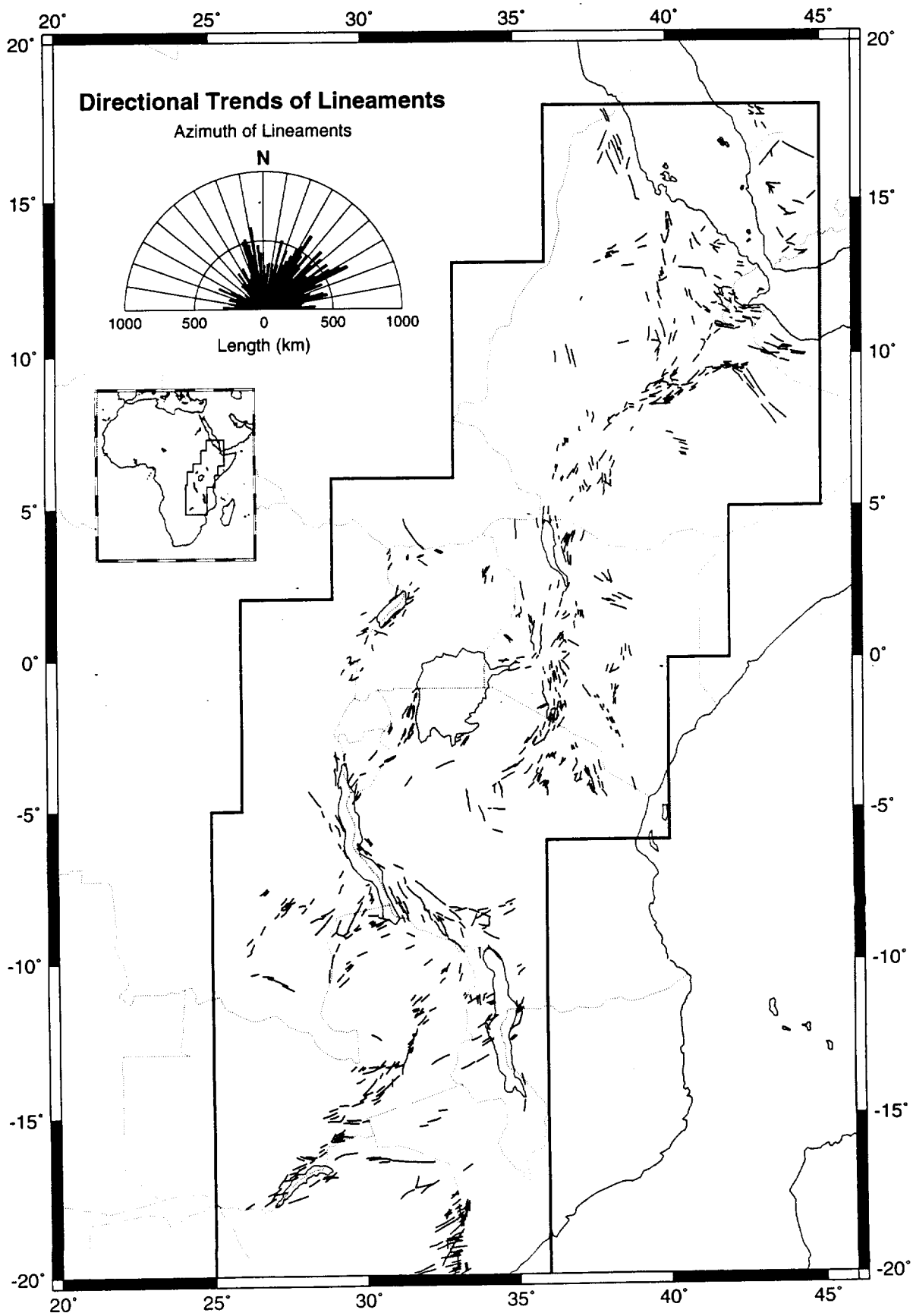

Fig 9.1B. Lineaments of East Africa as mapped from AVHRR (B521) imagery.

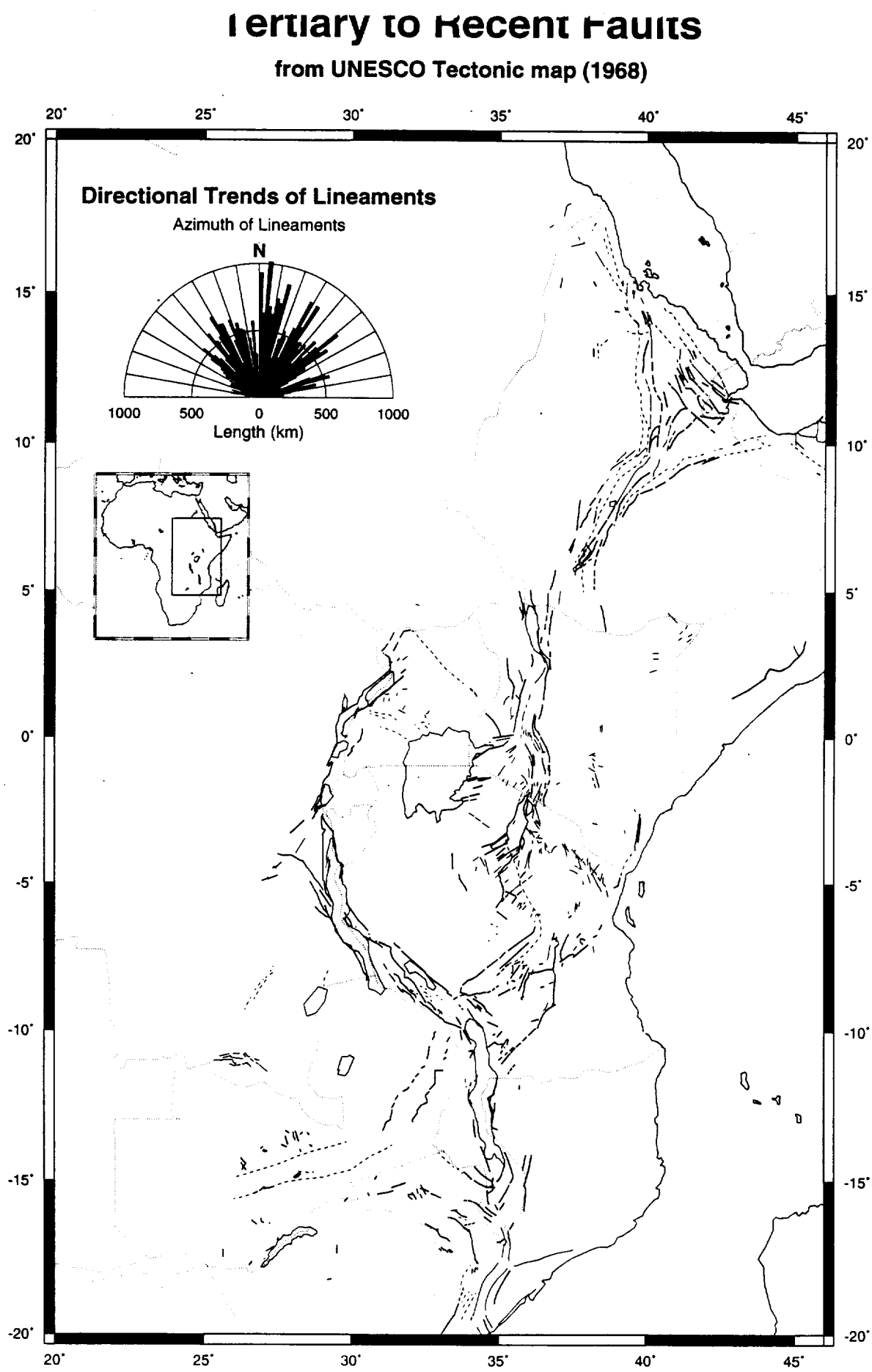

Fig 9.2. Faults of East Africa, from the UNESCO Tectonic map of Africa (1968).

At what is normally seen as the northern limit of the western branch is the Aswa Lineament. This lineament provides a good example of the variation in mapping ability. The UNESCO map shows the lineament crossing from north-central Uganda, in a NNW direction, to the Nile at Nimule. In contrast the AVHRR, both B211 and B521, has been unable to pick out this section but has highlighted the continuation in southern Sudan. This Sudanese section has the greatest topographical print of the whole lineament, see figure 6.3, and is very clearly visible on the ESC image of that area, figure 6.5. The only logical conclusion that can be drawn for the omission of the Sudan section of the Aswa Lineament, on the UNESCO map, is that mapping had been carried out in Uganda but had not been attempted in that area of southern Sudan.

In general the western branch of the rift system has been well mapped in the Lakes Tanganyika and Rukwa sections but the Lake Malawi part and the continuation of the rift southwards along the Shire valley has not been indicated. In the case of the Malawi Lake section, and to a lesser extent the Tanganyika Lake section it is likely that the presence of a large lake filling much of the rift zone has made mapping the faults problematic. Sub-lakesurface faults are, of course, not mappable and the major flank faults are probably also harder to locate near the lake edges.

The Rukwa rift section is particularly clear on AVHRR. This rift was initiated in the Karoo and continued northwestwards on what is now the western side of Lake Tanganyika. Some traces of this Karoo rift, the Luama rift, is seen on the AVHRR maps. The Upemba rift and Mweru rift are said, by Rosendahl (1987), to be Karoo in age with Tertiary to Recent reactivation in Mweru. Seismic activity exists in both of these suggesting that both may still be active. In the case of these rifts the B521 imagery has highlighted a greater number of lineaments than the B211. In addition the Ruaha and Luangwa rifts, which meet perpendicularly to the western branch at the Rungwe volcanic province are also Karoo and both are clearly traceable on the AVHRR imagery.

The rifts and other zones manifested by lineaments on AVHRR and mentioned above are generally well documented (e.g. McConnell, 1972; Rosendahl, 1987) and a reason for their existence is understood. However there is one trend which is visible on AVHRR and for which there is no obvious cause. The trend in question runs east-west from the Ruaha rift to the Lupa fault; the same east-west trend is then picked up again from the south end of Lake Tanganyika past Lake Mweru-Wantipa to the Lake Mweru rift. This is visible on both AVHRR scenes though the E-W trend is most clear on B211.

Both AVHRR scenes have highlighted a large number of lineaments on and around the Zimbabwe Block. While there is little difference between the B211 and B521 lineaments to the east of this region the west (south of Lake Kariba) is more clearly shown on B211 imagery.

9.1.2 The Eastern Branch and Afar

The eastern branch of the East African Rift System extends from Afar to northern Tanzania: the Afar region forms the link with the Red Sea and Gulf of Aden rifts. The boundary scarps of Afar are clearly defined on both B211 and B521 AVHRR imagery and indicate a boundary graben on the western scarp. The Marde fault trends in a SSE direction from the southern scarp at about 43°E (Kazmin *et al*, 1978). Faulting within the Afar triangle is separated from the scarp expressions by a region where no lineaments are observed. More lineaments are seen on the B211 imagery of Afar than with the B521 scene, while the directional trends are similar. The B521 image appears to indicate the trend of the Ethiopian rift meeting the Gulf of Aden and Red Sea trends. Both scenes suggest a gentle arcing of lineaments from an E - W trend at the end of the Gulf of Tadjoura to a NNW - SSE trend in northern Afar. The B521 image indicated more lineaments on the highland regions than B211, a situation that is seen also around Lake Bangweulu.

The Ethiopian rift is, with the exceptions of the largely cloud covered section of the western branch and the lake filled Malawi rift, the least well defined of all the rift system. The rift is seen reasonably well on the B211 imagery but much of the coherency is lost on the B521 scene. Conversely the bifurcation of the rift at its southern end around the Galana horst is better seen on B521. The Kinu-Sogo rift, joining the Kenya rift to the Ethiopian rift is seen on both band combinations though more clearly so on B211. The Kenya rift from the Sugata Trough to the Tanzania border is generally as well defined on both B211 and B521 with evidence of the Kavirondo rift and southern end of the Turkwell escarpment seen on both. The, Jurassic, Anza rift is observed very clearly on the B211 scene as it trends southeast from the south end of Lake Turkana: some lineaments associated with this rift are also seen on B521 but are limited. A dextral offset in the Ethiopian rift is seen on the AVHRR imagery at about 8.5°N.

The south end of the Kenya rift is characterised by a change in morphology from a graben type rift structure to a splayed basin and range type structure. This change in style is observed on both B211 and B521 imagery as is a hiatus in lineaments at the point at

which the change occurs, about 3°S. The Pangani Graben, trending SSE from Kilimanjaro appears to make up one of the splays, along with the Manyara and Eyasi half-grabens. A NNW - SSE trend to the east of the Kenya rift may be associated with structures in the Mozambique belt (Mosley, 1993). Neither AVHRR scene indicates the faulting which links the eastern and western branches across Tanzania.

9.1.3 Directional Trends

Directional trends of AVHRR mapped lineaments are given by means of rose diagrams on figures 9.1A and B. The trends seen on B211 show a distinct tri-directional tendency, these being approximately: N10°W, N27°E and N55°E. The N55°E direction being the most common. The mean azimuth is N43°E based on 33 400 km of lineaments. The B521 lineaments show a similar three directional trending. In this case the mean azimuth is N37°E based on 30 200 km of lineaments. The three trends observed using B521 lineaments are less distinct than those observed with B211 lineaments.

The majority of faults within East Africa are normal and will therefore be perpendicular to the direction of extension. Arguments over the direction of extension have mostly suggested E-W (e.g. Morley, 1988a) or NW-SE (e.g. Chorowicz & Mukonki, 1979) orientations. However, many of the studies have concentrated on sections of the rift rather than the entire system. The directional trends observed from AVHRR lineaments for the entire rift system in continental east Africa would suggest an almost NW-SE extension direction.

9.1.4 Comparison of AVHRR Lineaments and Faults

Comparisons of the lineaments mapped from AVHRR imagery and faults from the UNESCO (1968) tectonic map are shown in figure 9.3. In order to match lineaments a buffer zone of 5 km was chosen around the B211 lineaments; lineaments from B521 imagery falling within this buffer were considered to match. Matches between lineaments and faults were done in a similar way.

Figure 9.3A shows the lineaments common to the interpretations of B211 and B521 imagery. Much of the East African Rift System is clearly defined, in particular: Afa; the northern part of the Ethiopia rift; the southern sector of the Kenya rift; the Rukwa rift

Lineaments Common to AVHRR interpretations and UNESCO map

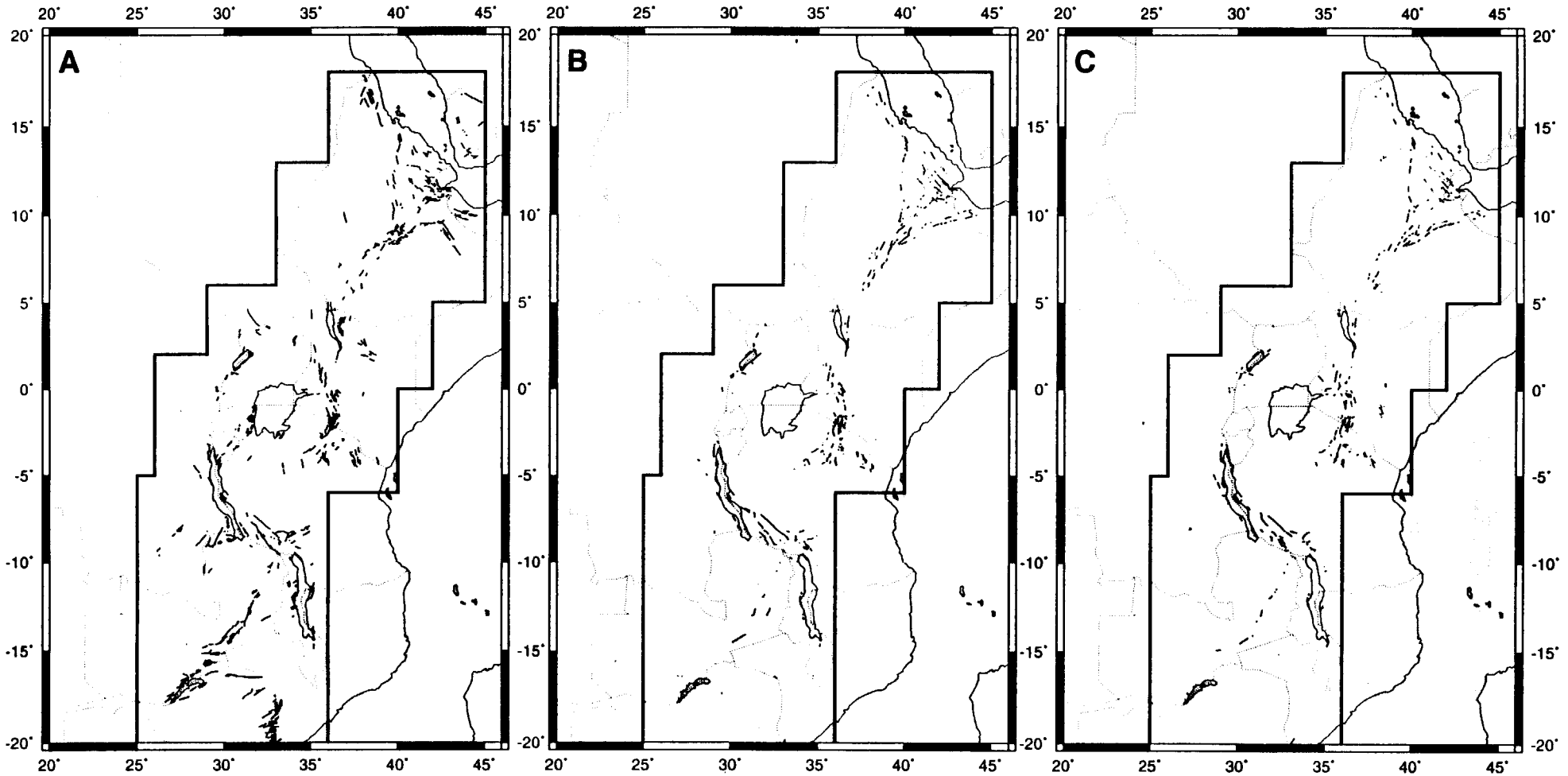

Fig 9.3. Lineaments common to: A, B211 and B521 AVHRR imagery; B, B211 & UNESCO (1968) map, and C, B521 and UNESCO.

and the Luangwa and Kariba rifts. The total length of overlapping lineaments was 19000 km, which corresponds to 57% of the B211 or 63% of the B521 lineaments.

Figure 9.3B shows the linear features common to AVHRR B211 and the UNESCO (1968) tectonic map. Figure 9.3C is a similar comparison of AVHRR B521 and the UNESCO mapped faults. Both comparisons between AVHRR lineaments and faults are very similar and show the eastern branch and Rukwa rifts reasonably well. 21% of the B211 lineaments overlapped faults and 22% of the B521 lineaments overlapped with faults.

In conclusion, the comparisons show that it is clearly worthwhile to use the two AVHRR band combinations (B211 and B521) to get the most comprehensive view of the East African Rift System.

9.2 Other Imagery

Figure 9.4 shows the lineaments mapped using 13 Landsat MSS scenes and 2 Landsat TM scenes. The area covered by these scenes is only a small portion of the rift system and only a fraction of the area covered by the AVHRR imagery. Taken on this scale the differences between AVHRR and these higher resolution imagery become less obvious. Individual faults mapped on MSS and TM are not discernible and tend to meld into the fault zones that are mapped using AVHRR.

One feature that was mapped using TM which can now be set in its regional, rather than local, context is an E-W feature trending from the Lupa fault on the northeast side of Lake Rukwa. This feature matches with the roughly E-W trending zone which stretches from the Ruaha rift to Lake Mweru.

The ESC scenes cover too small an area to be useful for studies of continental or even regional features. The single SPOT scene also covers only a tiny area and is also not considered for anything other than local studies.

9.3 Earthquakes and Volcanism

The comparisons between earthquakes and volcanism can offer some insight into the processes occurring within the East African Rift System. Figure 9.5 shows the location

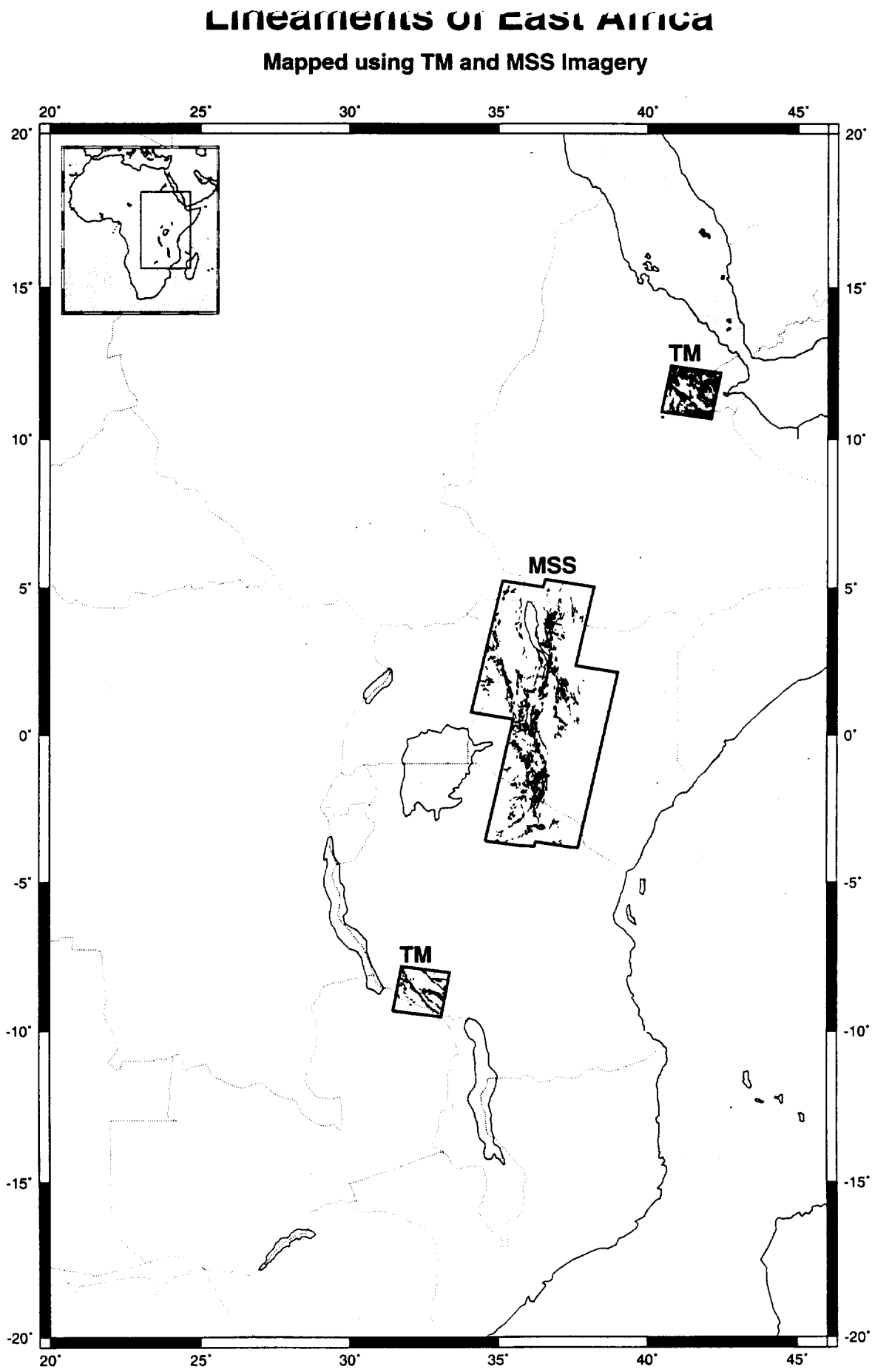

Fig 9.4. Lineaments of East Africa as mapped from TM and MSS imagery.

Earthquakes and Volcanoes of East Africa

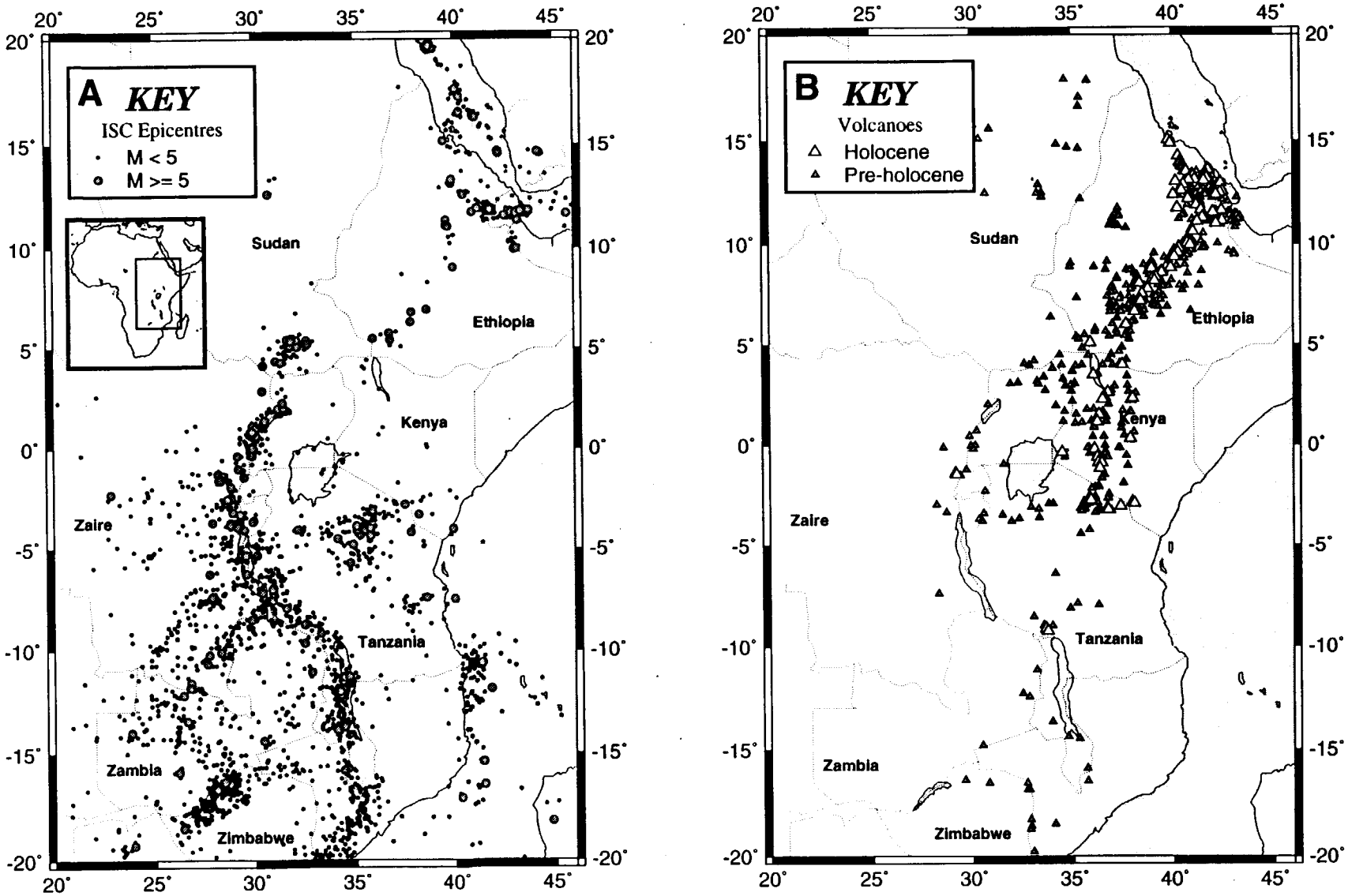

Fig. 9.5. Earthquake epicentres and volcanoes of east African: A. ISC epicentres (1964 - 1991) B. volcanoes, from Nusbaum et al (1994)

of earthquakes and volcanism of the East African Rift System. The earthquakes shown are those catalogued by the ISC from 1964 to 1991 with the emphasis given to events where $m_b \geq 5.0$. The distribution of earthquakes recorded by the ISC is not greatly different from the distribution of events since 1906 and as the accuracy of these older events is often poor only the ISC events are shown.

The assumption that the epicentre distribution and frequency of events has remained similar over the last 10 000 years (Holocene) is perhaps not valid as the view we have is of only the last 90 years at best. However, it is necessary to make this assumption if any comparison is to be drawn from the location of earthquakes and volcanoes in East Africa.

The spreading axes of the Gulf of Aden and Red Sea are clearly observed from the seismicity, however surveys in the Gulf of Aden are insufficiently detailed to indicate the presence, or absence, of volcanoes along its ridge (Nusbaum *et al*, 1994). The volcanic islands in the southern Red Sea (Gass *et al*, 1965) shows this section to be volcanically active. The directional trend of the Red Sea is preserved in a line of epicentres to the west of the Danakil horst, in Afar. This line also marks the axis of the Erte'Ale line of Holocene volcanoes, clearly visible on all satellite imagery of the area, see chapter 1. Other zones of seismicity in Afar are associated with the on-land extension of the Gulf of Aden and the western scarp of Afar.

Seismic activity is observed along the Ethiopia rift but not to the same extent as seen in much of the western branch; it does, however, show an almost continuous line of Holocene volcanoes along the valley floor. The distinct band of volcanoes, medium level of seismicity and distinct band of faulting along the valley floor (Mohr & Wood, 1976) make this section of the rift system most like an accreting margin of a mid-ocean rift. The distinct central line of volcanoes dies out at about 6°N.

The junction of the Ethiopia rift and Kenya rift is not clearly defined with small rift sections such as the Kinu-Sogo rift and Stefanie rifts bridging part of the gap. Neither seismicity nor Holocene volcanism are able to fully complete the join although pre-Holocene volcanoes are continuous throughout the Kenya and Ethiopia rifts, forming a broad swath across both rifts. The Kenya rift, from the south end of Lake Turkana to about 3°S is virtually devoid of earthquake epicentres. This same region of the Kenya rift is, like the Ethiopian rift, characterised by a distinct band of axial volcanoes. Where the rift valley breaks down into a basin and range morphology of splaying half-grabens, at about 3°S, the rift volcanoes stop and teleseismicity is observed south of this line. An

east-west line of volcanoes and a corresponding line of epicentres occur at 3°S. The seismicity south of 3°S is not continuous with the seismicity observed in the western branch.

The western branch is almost the direct opposite to the Kenya rift. The rift is characterised by a broad band of earthquake epicentres but has few volcanoes, of either Holocene or Pre-Holocene. While epicentres are largely associated with the rift valleys of the western branch there are a number of distinct trends which follow the southwestern rifts. These bands of epicentres trend in a southwest direction from about 6 °S, 7.5°S and 10°S and are associated with the Upemba, Mweru and Luangwa rifts.

The Mweru line of epicentres appears to extend southwest as far as 15°S. A bridging NW - SE line of epicentres joins the southern end of the Mweru line with the Kariba rift and appears to cause the Bangweulu Block to be completely surrounded. In addition to this, the Mweru line is the only southwestern trend which has a significant number of events with $m_b \geq 5.0$. Two fault plane solutions exist for events along the Mweru line, figure 1.6, and both show normal mechanisms with extension approximately NW - SE. While the Upemba, Luangwa and Kariba rifts are justifiable from lineament mapping and topography the Mweru line appears to show little or no surface expression south of Lake Mweru. Indeed lineaments mapped in this region were often perpendicular to this epicentre line, see chapter 8. The line also cuts across the northwestern part of the Zambia Archean craton and if it were a rift zone would be the only section of the East African Rift System to cut across such a craton, see figure 1.18.

CHAPTER 10

Conclusions

10.1 Conclusions Concerning Remote Sensing Imagery

10.1.1 AVHRR

Low resolution imagery, such as AVHRR, should be most useful as a first step in studying large regions. Once important or interesting features are located using this imagery higher resolution data can be used to study the areas in more detail.

Assuming cloud-free scenes are available, AVHRR imagery can be useful in mapping geological structures. The low resolution of AVHRR means that small faults are not resolved and only the larger lineaments are mapped. This mapping of only the larger features is useful in providing an overview of the tectonics of a large region. A further advantage is that the quantity of data required to cover such a large area is also low.

Of the two band combinations considered for the East African Rift System, AVHRR B211, highlighted about 33400 km of lineaments i.e. about 10% more than the B521 scene. This is consistent with the findings of Honey (1982).

The use of day/night combination imagery has proved useful in highlighting lineaments on the older cratonic regions. Thus complementing the use of day scenes alone. At present the day/night combinations are difficult to produce; this will be lessened with improved computer capabilities.

For some studies AVHRR imagery has too low a resolution; e.g. the Ethiopia rift contains a clear rift valley and reasonably well defined scarps but all the details, such as in the map of Baker *et al* (1972) cannot be seen. Imagery with a resolution of a few hundred metres, such as the 500 m Defense Meteorological Satellite Program (DMSP) may be able to provide better results without the need for handling huge amounts of data.

10.1.2 Galileo SSI

The Galileo SSI scene studied over Afar indicates that the narrow sensing bands are highly specific in what they are able to show. While all bands on AVHRR pick out major features to an almost equal degree the SSI image showed considerable differences between bands. Features such at the western scarp of Afar were seen most clearly on bands 1 and 2 while the Danakil basalts were distinct on all bands except band 1. The rift valley lakes marking the Ethiopia rift were only visible on band 7.

10.1.3 ESC

The ESC scenes provide a valuable extra insight into the areas they cover. There are a number of advantages of the data and mode of acquisition over more conventional satellite platforms. These include human selectivity; the small, manageable, size of the resultant data-files and the ease of obtaining the data.

10.1.4 Implications for Future Earth Observation Systems

This study has shown that low-resolution data do have a role to play in the field of Earth observation. The cost of such data can generally be much lower than higher resolution data, both financially and in terms of computer power. Thus, low resolution data provide an overview of large regions and help pinpoint areas to study in more detail.

The resolution of the Galileo SSI data used here, about 4km, was far too low to view geological features on Earth, being a significant step down from AVHRR. However, at a higher resolution the narrow bands of data could prove a valuable extra source of information about the geology of the planet. While Galileo was not designed as an Earth observing platform the technology it employed could be adapted for such a purpose.

The ESC instrument is only flown occasionally on Space Shuttle missions, while standard photographs are acquired on all missions. This study has shown that ESC scenes can provide a useful, additional, view of the areas covered and the ease of acquiring and processing the digital data leads on to suggest that the ESC should be carried and used routinely.

10.2 Scientific Conclusions

Much of the East African Rift System has been indicated from the AVHRR studies though some sections were shown better than others (e.g. the Kenya rift was clearly defined while the Ethiopia rift was less distinct). Figure 10.1 shows a map of the tectonic structures in East Africa based on the interpretation of the AVHRR B211 and B521 scenes.

In addition to showing most of the Cenozoic rifting in East Africa the AVHRR data have also indicated some older geological structures. The Karangwe-Ankole belt in Burundi and northwestern Tanzania and the Anza rift in northeast Kenya were particularly prominent belts of lineaments while the Aswa and Marde Lineaments were also shown. Additionally, an east - west trend is seen across the Rukwa rift and the southern end of Lake Tanganyika to Lake Mweru-Wantipa; this trend was also indicated by the Landsat TM scene of southern Lake Rukwa.

10.2.1 The Southwestern Rifts

The AVHRR imagery has indicated the presence of the Upemba rift and the Mweru rift as far as the southern end of the Lake. In addition the Luangwa Valley, Luamo rift, Kariba rift and Zambesi Valley have all been shown as rift like structures. The presence of earthquakes along these rifts suggests some level of contemporary activity along these Karoo rifts.

The Mweru rift is the most paradoxical of the southwestern rifts. The imagery of the area does not indicate any lineaments south of Lake Mweru, which follow the southwesterly trend of the other rifts in the region. However, the Mweru rift is the only one of the southwestern rifts which has earthquakes where $m_b \geq 5$. Fault plane mechanisms of two of these events show a NW - SE extension direction of normal faulting. This rift is also the only one of the rifts which cuts into one of the ancient nuclei in the area. All other rifts skirt the nuclei and follow belts between the ancient cratons while the Mweru rift cuts into the northern end of the Zambia Nucleus.

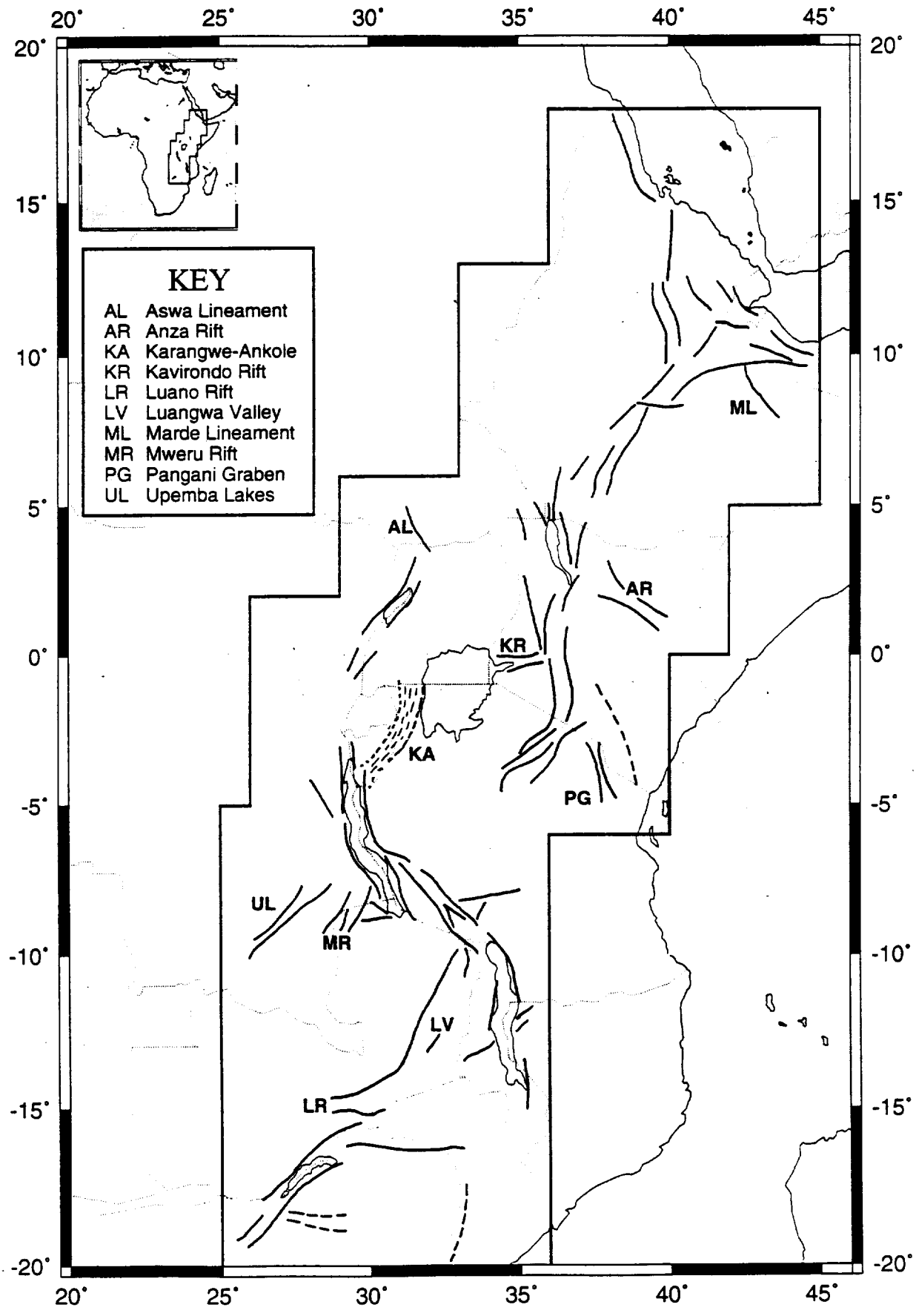

Fig 10.1. Rifting in East Africa, based on lineaments mapped from AVHRR imagery.

10.2.2 Northern Tanzania 'Leaky' Transform

The rift in Kenya indicated by AVHRR generally matched that shown from the MSS mosaic of the area. A break in faulting is indicated at about 3°S, where the morphology of the Kenya rift changes from a well defined rift valley to a basin and range type structure. This break corresponds with a line of volcanoes and a line of earthquake epicentres and adds further evidence to the suggestion of a leaky transform fault structure (Fairhead, 1980).

10.2.3 East African Stress

The mean azimuth of lineaments indicated by studies of B211 and B521 AVHRR imagery are N43°E and N37°E respectively, giving an average azimuth of N40°E. If it is assumed that all the lineaments mapped from AVHRR, are associated with normal faulting an almost NW-SE direction of extension is suggested across the rift system.

The presence of east - west offsets, most noticeably in the Ethiopian rift, suggests that either the stress direction has changed over the development of the East African Rift System or that pre-existing east - west structures affect the current stress field. The presence of a 'leaky' transform structure in northern Tanzania and the fact that the Rukwa rift has undergone extension in the SW - NE direction, with NW - SE shear would suggest a change in stress direction from a W - E direction to the current NW - SE direction.

10.2.5 Marginal Grabens of Afar

The AVHRR and topography scenes of Afar suggest a marginal graben along the western scarp of the region. The oblique views show this graben even more clearly and also suggests the presence of a similar, if less well defined, structure along part of the southern scarp. The western graben is seen to be continuous along the entire western scarp, from the northern end of the Ethiopian rift to the northern end of Afar. At its northern end the graben lessens and dips towards the Red Sea.

10.3 Suggestions for Future Work

A study using intermediate resolution data such as that from the Defense Meteorological Satellite Program (DMSP), 500 m, may help to fill the gap between 1.1 km resolution AVHRR and 80 m Landsat MSS. Studying a large area using any imagery requires much computer power and storage space; data of 500 m resolution requires four times the capacity of 1 km resolution data but this should pose fewer and fewer problems as computer capacity increases.

A study concentrating on seismicity of the East African Rift System should prove useful in determining the extent and process of rifting in the area. The application of relocation techniques to regions of specific interest, such as the southwestern rifts, should be valuable in helping to assess whether these form propagating rifts associated with the East African Rift System.

This study concentrated on the view of the entire rift system in continental East Africa. Many rift sections, such as the Kenya and Ethiopia rifts and Afar region have been well studied and mapped (e.g. Baker *et al*, 1972). Other sections such as Lake Tanganyika and Malawi have formed the basis of detailed seismic experiments (e.g. Rosendahl *et al*, 1992). Sections of the rift are still poorly mapped and would benefit from detailed studies using both satellite imagery and seismicity as well as other geophysical data where available. Sections which may benefit from such a study are the Kivu - Edward - Mobutu - Aswa rift and all the southwestern rifts.

The Mweru line of earthquake epicentres is worth further study to attempt to solve the problem of whether this forms the initial stage of a propagating rift and how it fits in to the general cratonic and tectonic framework of the area. The paradox of a distinct line of earthquake epicentres but little or no surface expression of rifting seen during this study needs more careful and detailed consideration than was possible here.

Unlike conventional satellite sensors radar satellites can obtain ground data under cloud covered regions. Where persistent cloud lingers, such as in the northern part of the western branch, radar data should prove valuable in filling the gap.

The topography data given in this study only became available in late 1994. The potential of this data-set has only been touched on here. A more detailed study of these data would probably reveal more structures associated with the East African Rift System and with other features in the area. The use of oblique views of Afar has revealed various

structural features which may otherwise have been overlooked. The potential of these oblique images as a visualisation tool could be extended to other sections of the East African Rift System as well as other parts of the world.

REFERENCES

Alsopp, H.L.. 1965. Rb:Sr and K:Ar age measurements on the Great Dyke of Southern Rhodesia, *JGR*, **70**. 977-984.

Ambraseys, N.N.. 1991a. The Rukwa earthquake of 13 December 1910 in East Africa. *Terra Nova*, **3.** 202-211.

Ambraseys, N.N.. 1991b. Earthquake hazard in the Kenya Rift: the Subukia earthquake 1928. *Geophys. J. Int.*, **105**. 253-269.

Andre, C.G. & Blodget, H.W.. 1984. Thermal Infrared Satellite Data for the Study of Tectonic Features. *Geophysical Research Letters*, **11**. 983-986.

Anon. 1876. Stanley's African Discoveries, *Nature*, **19.** 373-375.

Bagdasaryan, G.P., Gerasimovski, V.I., Polakov, A.I. & Gukasyan, R.K.. 1973. Age of volcanic rocks in the rift zones of East Africa. *Geochem. Int.*, **10**. 66-71.

Baker, B.H. & Morgan, P.. 1981. Continental Rifting: Progress and Outlook. *Eos. Trans. A. Geophys. Union*, **62**. 585-586.

Baker, B.H., & Wohlenberg, J.. 1971. Structure and evolution of the Kenya Rift Valley, *Nature*, **229**. 538-542.

Baker, B.H., Mohr, P.A. & Williams, L.A.J.. 1972. The geology of the Eastern Rift System of Africa. *Geol. Soc. Am. Spec. Pap.*, **136**, 66pp.

Baker, B.H., Williams, L.A.J., Miller, J.A. & Fitch, F.J.. 1971. Sequence and geochronology of the Kenya Rift volcanics. *Tectonophys.*, **11.** 191-215.

Belton, M.J.S., Klaasen, K., Clary, M., Anderson, J., Anger, C., Carr, M., Chapman, C., Davies, M., Greenley, R., Anderson, D., Bolef, L., Townsend, T., Greenberg, R., Head, J., Neukum, G., Pilcher, C., Veverka, J., Gierasch, P., Fanale, F., Ingersoll, A., Masursky,H., Morrison, D. & Pollack, J.. 1992. The Galileo Solid-State Imaging Experiment. *Space Science Reviews*, **60**. 413-455.

Berckhemer, H., Baier, B., Bartelsen, H., Behle, A., Burkhardt, H., Gebrande, H., Makris, J., Miller, H. & Vees, R.. 1975. Deep seismic soundings in the Afar region and on the highland of Ethiopia. *in, Afar Depression of Ethiopia, A. Pilger and A. Rösler (Eds.)*. Schweizerbart, Stuttgart. 89-107.

Bishop, W.W.. 1965. Quaternary geology and geomorphology of the Albertine Rift Valley, Uganda. In H.E. Wright Jr. and D.G. Frey eds., International studies on the Quaternary. *Geol. Soc. Am. Spec. Pub.*, **84**. 293-321.

Bosworth, W.. 1985. Geometry of propagating continental rifts. *Nature*, **316**. 625-627.

Bosworth, W.. 1987. Off-axis volcanism in the Gregory rift, East Africa: implication for models of continental rifting. *Geology*, **15**. 397-400.

Bosworth, W.. 1992. Mesozoic and early Tertiary rift tectonics in East Africa. *Tectonophysics*, **209**. 115-137.

Bosworth, W., Lambiase, J. & Keisler, R.. 1986. A New Look at Gregory's Rift: The Structural Style of Continental Rifting. *Eos*, **67**. 577, 582-583.

Bosworth, W., Strecker, M.R. & Blisniuk, P.M.. 1992. Integration of East African Paleostress and Present-Day Stress Data: Implications for Continental Stress Field Dynamics. *JGR*, **97 (B8)**. 11 851-11 865.

Brown, C. & Girdler, R.W.. 1980. Interpretation of African Gravity and its Implication for the Breakup of the Continents. *Journal of Geophysical Research*, **85** (B11). 6443- 6455.

Browne, S.E. & Fairhead, J.D.. 1983. Gravity study of the Central African Rift System: Sudan and its regional tectonic setting. *Tectonophysics*, **113**. 123-137.

Bullard, E.C.. 1936. Gravity measurements in East Africa. *Royal Soc. London. Philos. Trans. A.*, **235**. 445-531.

Burke, K. & Wilson, J.T.. 1972. Is the African Plate Stationary? *Nature*, **239**. 387-390.

Burton, R.F.. 1859. The Lake Regions of Central Equatorial Africa, with Notices of the Lunar Mountains and Sources of the Nile; being the result of an Expedition undertaken under the patronage of Her Majesty's Government and the Royal Geographical Society of London, in the years 1857-1859. *Journal of the Royal Geographical Society*, **29**. 1-454.

Cahen, L. & Snelling, N.J.. 1966. The geochronology of equatorial Africa. *Amsterdam, North Holland Publishing Co.*, pp 195.

Cahen, L., Snelling, N.J., Delhal, J. & Vail, J.R.. 1984. The Geochronology and Evolution of Africa. *Clarendon Press. Oxford.*

CEGD, 1974. Carte Geologique du Territoires Français des Afars et des Issas, feuille Easal. 1:100 000. Centre d'etudes Geologiques et des Developpement. Bordeaux.

Chorowicz, J.. 1983. Le rift est-africain: Debut de l'ouverture d'un ocean? *Bull. Centres. Rech. Explor-Production Elf Aquitaine*, **7**. 155-162.

Chorowicz, J., LeFournier, J. & Vidal, G.. 1987. A model for rift development in eastern Africa. *Geological Journal*, **22**. 495-513.

Chorowicz, J., & Mukonki, M. na B., 1980. Linéaments anciens, zones transformantes récentes et géotectonique des fossés de l'Est Africain, d'apres la microtectonique et la télédétection. *Mus. R. Afr. Centr., Tervuren (Belg.), Dépt Géol. Min. Rapp. Annu., 1979*. 143-167.

Chorowicz, J., & Sorlien, C.. 1992. Oblique extensional tectonics in the Malawi Rift, Africa. *Geol. Soc. Am. Bull.*, **104**. 1015-1023.

Clifford, T.N.. 1970. The Structural Framework of Africa, *in; Clifford, T.N. & Gass, I.G. (Eds.) African Magmatism and Tectonics: Edinburgh, Oliver & Boyd.* 1-26.

Courtillot, V.. 1982. Propagating rifts and continental breakup. *Tectonics*, **1**. 239-250.

Coussement, C., Gente , P., Rolet, J., Tiercelin, J.-J., Wafulu, M. & Buku, S.. 1994. The North Tanganyika hydrothermal fields, East African Rift system: Their tectonic control and relationship to volcanism and rift segmentation. *Tectonophysics*, **237**. 155-173.

Crane, K. & O'Connell, S.. 1983. The distribution and implications of heat flow from the Gregory Rift in Kenya. *Tectonophysics*, **94**. 253-275.

Crippen, R.E.. 1989. Selection of Landsat TM Band and Band-ratio Combinations to Maximize Lithologic Information in Color Composite Displays. *Proceedings of the International Symposium on Remote Sensing of Environment, Seventh Thematic Conference, "Remote Sensing for Exploration Geology", 2-6 October 1989.*

Dawson, J.B.. 1970. The Structural Setting of African Kimberlite Magmatism. In: African Magmatism and Tectonics. Eds. T.N. Clifford & I.G. Gass. *Oliver & Boyd, Edinburgh.* 321-335.

Dawson J.B.. 1980. Kimberlites and Their Xenoliths. *Springer-Verlag, Berlin.*

Dawson, J.B.. 1992. Neogene tectonics and volcanicity in the North Tanzania sector of the Gregory Rift Valley: contrasts with the Kenya sector. *Tectonophysics*, **204**. 81-92.

Dawson, J.B., Pinkerton, H., Pyle, D.M. & Nyamweru, C.. 1994. June 1993 eruption of Oldoinyo Lengai, Tanzania: Exceptionally viscous and large carbonatite lava flows and evidence for coexisting silicate and carbonate magmas. *Geology*, **22**. 799-802.

Delvaux, D.. 1992. Rifting in the Western Branch of the East African Rift System (Review). *Geotectonics*, **26**. 238-245.

Dypvik, M., Nesteby, M., Ruden, F., Aagaard, P., Johansson, T., Msindai, J. & Massay, C.. 1990. Upper Palaeozoic and Mesozoic sedimentationin the Rukwa-Tukuyu Region. *J. Afr. Earth Sci.*, **11**. 437-456.

Dzeiwonski, A.M., Chou, T,-A. & Woodhouse, J.H.. 1981. Determination of earthquake source parameters from waveform data for studies of global and regional seismicity. *J. Geophys. Res.*, **86**. 2825-2852.

Dzeiwonski, A.M., Franzen, J.E. & Woodhouse, J.H.. 1983. Centroid-moment tensor solutions for April-June 1983. *Phys. Earth Planet. Int.*, **33**. 243-249. and subsequent issues.

Ebinger, C.J.. 1989a. Geometric and kinematic development of border faults and accommodation zones, Kivu-Rusizi rift, Africa. *Tectonics*. **8**. 117-133.

Ebinger, C.J.. 1989b. Tectonic development of the western branch of the East African rift system. *Geol. Soc. Am. Bull.*, **101**. 885-903.

Ebinger, C.J., Rosendahl, B.R. & Reynolds, D.J.. 1987. Tectonic model of the Malawi rift, Africa. *Tectonophysics*, **141**. 215-235.

Ebinger, C.J., Deino, A., Drake, B. & Tesha, A.L.. 1989. Chronology of volcanism and rift basin propagation: Rungwe volvanic province, East Africa. *J. Geophys. Res.*, **94**. 15785-15803.

Ebinger, C.J., Crow, M.J., Rosendahl, B.R., Livingstone, D.L. & LeFournier, J.. 1984. Structural evolution of Lake Malawi, Africa. *Nature*, **308**. 627-629.

Ebinger, C.J., Yemane, T., Woldegabriel, G., Aronson, J.L. & Watler, R.C.. 1993. Late Eocene-Recent volcanism and faulting in the southern main Ethiopian rift. *J. Geol. Soc. Lond.* **150**. 99-108.

Ellis, M. & King, G.. 1991. Structural control of flank volcanism in continental rifts. *Science*, **244**. 839-842.

Fadaie, F. & Ranalli, G.. 1990. Rheology of the lithosphere in the East African Rift System. *Geophys. J. Int.*, **102**. 445-453.

Fairhead, J.D.. 1980. The structure of the cross-cutting volcanic chain of northern Tanzania and its relation to the East African Rift System. *Tectonophys.*, **65**. 193-208.

Fairhead, J.D. & Girdler, R.W.. 1970. The seismicity of the Red Sea, Gulf of Aden and Afar triangle. *Phil. Trans. Roy. Soc. Lond.* A, **267**. 49-74.

Fairhead, J.D. & Girdler, R.W.. 1971. The seismicity of Africa. *Geophys. J. r. astr. Soc.*, **24**. 271-301

Fukata, O.. 1984. Natural Gas Expected in the Lakes Originating in the Rift Valley System of East Africa, and Analogous Gas in Japan. *AAPG Memoir 40, Future Petroleum Provinces of the World.* 445-456.

Gass, I.G.. 1975. Magmatic and tectonic processes in the developmet of the Afro-Arabian Dome, *in; Afar Depression of Ethiopia, Pilger, A. (Ed.). E. Schweiz Verlagsbuchhandlung, Stutgart.* 10-18.

Geissler, P., Thompson, W.R., Greenberg, R., Moersch, J., McEwen, A. & Sagan, C.. 1995. Galileo Multispectral Imaging of Earth. *JGR*, **100**. 16 895 - 16 906

Geothermal Reconnaissance study of Selected Sites of the Ethiopian Rift System. 1987. *Ethiopian Institute of Geological Surveys.*

Gibson, I.L. & Tazieff, H.. 1970. The structure of Afar and the northern part of the Ethiopian Rift. *Phil. Trans. Roy. Soc. Lond. A.*, **267**. 331-338.

Girdler, R.W. & McConnell, D.A.. 1994. The southern Sudan earthquake sequence of May 1990. *Science*,

Girdler, R.W., Fairhead, J.D., Searle, R.C. & Sowerbutts, W.T.C.. 1969. The evolution of rifting in Africa. *Nature*, **224**. 1178-1182.

Gouin, P. & Mohr, P.A.. 1967. Recent effects possibly due to tensional separation in the Ethiopian rift system. *Bull. Geophys. Obs. Addis Ababa.* **10**. 69-78.

Gregory, J.W.. 1896. The Great Rift Valley. *John Murray, London.* pp 424.

Gregory, J.W.. 1921. The Rift Valleys and Geology of East Africa. *Seely Service, London.* pp 479.

Gutenberg, B. & Richter, C.F.. 1954. Seismicity of the Earth, Second Ed. *Princeton University Press.*

Hackman. B.D., Charsley, T.J., Key, R.M. & Wilkinson, A.F.. 1990. The development of the East African Rift system in north-central Kenya. *Tectonophysics*, **184**. 189-211.

Hecky, R.E. & Degens, E.T.. 1973. Late pleistocene-Holocene chemical stratigraphy and palaeolimnology of the rift valley lakes in central Africa. *Tech. Rep. WHOI.* pp93.

Holmes, A. 1944. Principles of Physical Geology. *Thomas Nelson & Sons, Edinburgh.*

Honey, F.R.. 1982. Application of NOAA AVHRR Data to Geological Mapping. *Proceedings of the International Symposium on Remote Sensing of Environment, Second Thematic Conference, "Remote Sensing for Exploration Geology", 6-10 December 1982.* **2**. 519-525.

Honey, F.R., Tapley, I.J. & Wilson, P.. 1984. Interpretation of Macro-scale Structural Features in Western Australia from NOAA-AVHRR Imagery. *Proceedings of the International Symposium on Remote Sensing of Environment, Third Thematic Conference, "Remote Sensing for Exploration Geology", 16-19 April 1984.* **1**. 381-394.

Huang, P.Y. & Soloman, S.C.. 1987. Centroid depths and mechanisms of mid-ocean ridge earthquakes in the Indian Ocean, Gulf of Aden and Red Sea. *J. Geophys. Res.*, **92**. 1361-1382.

Hutchinson, M.F., 1989. A new method for gridding elevation and stream line data with automatic removal of pits. *J. Hydrol.*, **106**. 211-232.

Israel, S.A.. 1992. Manned observations technology development - FY 92 Report. *LESC-30460, JSC-26032, NASA CR-185704.* 34pp

Kaz'min, V., Shifferaw, A. & Balcha, T.. 1978. The Ethiopian Basement: Stratigraphy and Possible Manner of Evolution. *Geologische Rundschau*, **67**. 531-546.

Kaz'min, V.G., Zonenshayn, L.P., Savostin, L.A., & Bershbitskaya, Ai.I.. 1987. Kinematics of the Afro-Afabian Rift System. *Geotectonics*, **21**. 452-460.

Kebede, F.. 1989. Seismotectonic studies of the East African Rift system north of 12°S to the southern Red Sea. *Seismological Dept. Upsala University. Report 1-89.* pp34.

Kebede, F. & Kulhänek. O.. 1991. Recent seismicity of the East African Rift system and its implications. *Phys. Earth Planet. Int.* **68**. 259-273.

Kidwell, K.B.. 1986. NOAA Polar Orbiter Data (Tiros-N, NOAA6, NOAA7, NOAA8, NOAA9, NOAA10, NOAA11) Users Guide. *NOAA Technical Memorandum*

Kilembe, E.A. & Rosendahl, B.R.. 1992. Structure and stratigraphy of the Rukwa rift. *Tectonophysics*, **209**. 143-158.

Legackis, R. & Pritchard, J.. 1976. Algorithm for correctiong VHRR imagery for geometric distortions due to the earth curvature, earth rotation and spacecraft roll attitude errors. *NOAA Technical Memorandum NESS 77*. 31pp.

LePichon, X. & Francheteau, J.. 1978. A plate-tectonic analysis of the Red Sea - Gulf of Aden area. *Tectonophysics*, **46**. 369-406.

Long, R.E. & Backhouse, R.W.. 1976. The Structure of the Western Flank of the Gregory Rift (Kenya). Part II. The Mantle. *Geophys. J. R. astr. Soc.*, **44.** 677-688.

MacIntyre, R.M., Mitchell, J.G. & Dawson, J.B.. 1974. Age and fault movement in Tanzania section of the East African Rift Stystem. *Nature*, **247**. 354-356

Maguire, P.K.H. & Long, R.E.. 1976. The Structure of the Western Flank of the Gregory Rift (Kenya). Part I. The Crust. *Geophys. J. R. astr. Soc.*, **44.** 661-675.

Makris, J. & Ginzburg, A.. 1987. The Afar Depression: transition between continental rifting and sea-floor spreading. *Tectonophysics*, **141**. 199-214.

McClelland, L., Simkin, T., Summers, M., Neilsen, ? & Stein, T.C.. 1989. Global Volcanism 1975-1985. *Prentice Hall, U.S.A.* pp??.

McConnell, R.B.. 1972. Geological development of the rift system of eastern Africa. *Geol. Soc. Am. Bull.*, **83**. 2549-2572.

McKenzie, D.P., Davies, D. & Molnar P.. 1970. Plate tectonics of the Red Sea and East Africa. *Nature*, **226**. 243-248.

Mitchell, A.H.G. & Garson, M.S.. 1981. Mineral Deposits and Global Tectonic Settings. *Academic Press, New York.*

Mitchell R.H.. 1986. Kimberlites; Mineralogy, Geochemistry, and Petrology. *Plenum Press, New York.*

Mohr, P.A.. 1960. Report of the geological excursions through southern Ethiopia. *Bull. Geophys. Obs. Addis Ababa.* **3**. 9-20.

Mohr, P.A.. 1962. The Ethiopian rift system. *Bull. Geophys. Obs. Addis Ababa.* No **5**. 33-62.

Mohr, P.A.. 1971. Outline tectonics of Ethiopia. *in*, Tectonics of Africa. *UNESCO.* 447-457.

Mohr, P.A.. 1974. Mapping of the major structures of the African rift system. *NASA/Smithsonian Institution* contract NAS 5-21748. pp70.

Mohr, P.A.. 1987. Structural style of continental rifting in Ethiopia: Reverse décollements. *EOS, Trans. of the American. Geophys. Union,* **68**. 721-726.

Mohr, P.A.. 1989. The nature of the crust under Afar: new igneous, not stretched continental. *Tectonophysics*, **167**. 1-11.

Mohr, P.A.. 1992. Nature of Crust beneath magmatically active continental rifts. *Tectonophysics*, **213**. 269-284.

Mohr, P.A. & Wood, C.A.. 1976. Volcano spacing and lithosphere attenuation in the eastern rift of Africa. *Earth Planet. Sci. Lett.*, **33**. 126-144.

Mohr, P.A. Mitchell, J.G. & Raynolds, R.G.H.. 1980. Quaternary volcanism and faulting at O'A Caldera, Central Ethiopia Rift. *Bull. Volcan.*, **43**. 173-189.

Mondeguer, A., Ravenne, C., Masse, P. & Tiercelin, J.-J.. 1989. Sedimentary basins in an extension and strike-slip background: the "South Tanganyika troughs complex", East African Rift. *Bull. Soc. géol. France*, **8**. 501-522.

Moore, J.M. & Davidson, A.. 1978. Rift structure in southern Ethiopia. *Tectonophysics*, **46**. 159-173.

Morley, C.K.. 1988. Variable extension in Lake Tanganyika. *Tectonics*, **7**. 785-801.

Morley, C.K.. 1988. Comment on "Off-axis volcanism in the Gregory Rift, East Africa: Implications for models of continental rifting". *Journal of the Geological Society*, **149**. 333-348.

Morley, C.K., Cunningham, S.M., Harper, R.M. & Westcott, W.A.. 1992. Geology and Geophysics of the Rukwa Rift, East Africa. *Tectonics*, **11**. 69-81.

Mosley, P.N.. 1993. Geological evolution of the late Proterozoic "Mozambique Belt" of Kenya. *Tectonophysics*, **221**. 223-250.

Nicolaysen, L.O.. 1962. Stratigraphic interpretation of age measurements in southern Africa, *in; Engel, A.E.J., James, H.L. & Leonnard, B.F. (Eds.) Petrologic Studies: A volume in honour of A.F. Buddington. Geol. Soc. America.* 569-598.

Nusbaum, R.L., Girdler, R.W., Heirtzler, J.R., Hutt, D.J., Green, D., Millings, V.E., Schmoll, B.S. & Shapiro, J.. 1994. The distribution of earthquakes and volcanoes along the East African Rift System. *Episodes*, **16**. 427-432.

O'Leary, D.W., Friedman, J.D., & Pohn, H.A.. 1976. Lineament, linear, lineation: Some proposed new standards for old terms. *Geol. Soc. Am. Bull.*, **87**. 1463-1469.

Pasteels, P., Villeneuve, M., De Paepe, P. & Klerkx, J.. 1989. Timing of the volcanism of the southern Kivu province: implications for the evolution of the western branch of the East African Rift system. *Earth Planet. Sci. Lett.*, **94**. 353-363.

Pavoni, N.. 1985. Pacific/anti-Pacific bipolarityin the structure of the Earth's mantle. *EOS Trans. Am. Geophys. Union*. **66**. 497.

Pavoni, N.. 1992. Rifting of Africa and pattern of mantle convection beneath the African plate. *Tectonophysics*, **215**. 35-53.

PCI Inc., 1993. Using PCI Software, *PCI Inc., Toronto*. 2 volumes.

Peirce, J.W., & Lipkov, L.. 1988. Structural interpretation of the Rukwa Rift, Tanzania. *Geophysics*, **53**. 824-836.

Pointing, A.J., Maguire, P.K.H., Kahn, M.A., Francis, D.J., Swain, C.J., Shah, E.R. & Griffiths, D.H.. 1985. Seismicity of the northern part of the Kenya Rift valley. *Journal of Geodynamics*, **3.** 23-37.

Pulfrey, W.. 1969. The Geology and Mineral Resources of Kenya. Second Revision, revised by J. Walsh. *Geology Survey of Kenya, Bulletin no. 9.* pp34.

Reeves, C.V., Karanja, F.M. & MacLeod, I.N.. 1987. Geophysical evidence for a failed Jurassic rift and triple junction in Kenya. *Earth and Planet. Sci. Lett.*, **81**. 299-311.

Richard, J.J. & Neuman Van Padang, M.. 1957. Catalogue of the active volcanoes of the worldincluding solfatara fields, Part IV, Africa and the Red Sea. *International Association of Volcanology*. 31-118.

Rosendahl, B.R.. 1987. Architecture of continental rifts with special reference to East Africa. *Ann. Rev. Earth Planet. Sci.*, **15**. 445-503.

Rosendahl, B.R., Kilembe, E., & Kaczmarick, K.. 1992. Comparison of the Tanganyika, Malawi, Rukwa and Turkana Rift zones from analyses of seismic reflection data. *Tectonophysics*, **213**. 235-256.

Rosendahl, B.R., Burgess, C.F., Sander, S. & Lambiasse, J.. 1986. Structural symptoms of continental rifting. *AAPG Bulletin*, **70**. 641.

Ruegg, J.-C., Gasse, F. & Briole, P.. 1990. Mouvements du sol holocènes dans le rift d'Asal à Djibouti. *C.R. Acad. Sci. Paris*. **310 Series II**. 1687-1694.

Rykounov, L.N., Sedov, V.V., Savrina, L.A. & Bourmin, V.Ju.. 1972. Study of microearthquakes in the rift zones of East Africa. *Tectonophysics*, **15**. 123-130.

Sander, S. & Rosendahl, B.R.. 1989. The geometry or rifting in Lake Tanganyika, East Africa. *J. Arf. Earth Sci.*, **8**. 255-382.

Schull, T.J.. 1988. Rift basins of interior Sudan: petroleum exploration and discovery. *Am. Soc. Petrol. Geol. Bull.*, **72**. 1128-1142.

Scott, D.L., Rosendahl, B.R., Burgess, C.F. & Sander, S.. 1989. Comments on "variable extension in Lake Tanganyika" By C.K. Morley. *Tectonics, 8.* 647-650.

SEAN (Seismic Event Alert Network). Various. *Bulletin Smithsonian Instituton.*

Searl, R.C. & Gouin, P.. 1972. A gravity survey of the central part of the Ethiopian rift valley. *Tectonophysics*, **15**. 41-52.

Shackleton, R.M., 1951. A contribution to the geology of the Kavirondo rift valley. *Q. J. Geol. Soc. Lond.*, **106**. 345-392.

Shackleton, . 1967. Quoted in Mohr, 1994 but not referenced.

Shudofsky, G.N.. 1985. Source mechanisms and focal depths of East African earthquakes using Rayleigh-wave inversion and body-wave modelling. *Geophys. J. R. astr. Soc.*, **83.** 563-614.

Shudofsky, G.N., Cloetingh, S., Stein, S. & Wortel, R.. 1987. Unusually deep earthquakes in East Africa: constraints on the thermo-mechanical structure of a continental rift system. *Geophys. Res. Lett.*, **14**. 741-744.

Simkin, T., Siebert, L., McClelland, L., Bridge, D., Newhall, C. & Latter, J.H.. 1981. Volcanoes of the World: A Regional Directory Gazetteer and Chronology of Volcanism During the last 10 000 years. *Hutchinson Ross, U.S.A.*

Slack, P.D., Davis, P.M. & The KRISP working group. 1994. Attenuation and velocity of P-waves in the mantle beneath the East African Rift, Kenya. *Tectonophysics*. **236**. 331-358.

Smith, M. & Mosley, P.N.. 1993. Crustal hetrogeneity and basementinfluense on the development of the Kenya Rift, East Africa. *Tectonics*, **12**. 591-606

Snyder, J.P., 1987. Map Projections - A Working Manual. *U.S.G.S. professional paper 1395. U.S. Government Printing Office, Washington.*

Specht, T.D. & Rosendahl, B.R.. 1989. Architecture of the Lake Malawi Rift, East Africa. *J. Afr. Earth Sci.*, **8**. 355-382.

Strecker, M.R., Blisnuik, P.M. & Eisbacher, G.H.. 1990. Rotation of extension directionin the central Kenya Rift. *Geology*, **18**. 299-302.

Suess, E.. 1891. Die Brüche des östlichen Afrika, in Beitrage zur geologischen Kentniss des östlichen Africa. *Denkscriften Keiserlichen Akademie der Wissenschaften, Wien, Mathematisch-Naturwissen Klasse,* **58**. 555-584.

Swain, C.J., Maguire, P.K.H. & Kahn, M.A.. 1994. Geophysical experiments and models of the Kenya Rift before 1989. *Tectonophysics*, **263**. 23-32.

Tapley, I.J.. 1988. The Reconstruction of Palaeodrainage and Regional Geologic Structures in Australia's Canning and Officer Basins Using NOAA-AVHRR Satellite Imagery. *Earth-Sci. Rev.*, **25**. 409-425.

Thomson, J.. 1880. Notes on the Geology of East-Central Africa. *Nature*, **23**. 102-104

Times Atlas of the World, 1956, Southern Europe and Africa. **IV**.

Tiercelin, J.J., Chorowicz, J., Bellon, H., Richert, J.P., Mwanbene, J.T., & Walgenwitz, F.. 1988. East African Rift System: onset, age and tectonic significance of the Tanganyika-Rukwa-Malawi intracontinental transcurrent fault zone. *Tectonophysics*, **148**. 241-252.

Tongue, J.A., Maguire, P.K.H. & Young, P.A.V.. 1992. Seismicity distribution from temporary earthquake recording networks in Kenya. *Tectonophysics*, 204. 71-79.

Truckle, P.H.. 1976. Geology and late Cainozoic lake sediments of the Sugata Trough, Kenya. *Nature*, **263**. 380-383.

UNESCO. 1968. Carte Tectonique Internationale de l'Afrique. 1:5 000 000. United Nations Educational Scientific and Cultural Organisation.

United States Geological Survey. 1992. LAS Land Analysis System, version 5. *USGS, EROS Data Center, Sioux Falls*. 4 volumes.

United States Geological Survey. 1994. Terrain-30; 'readme' supplied with digital data.

Vail, J.R. & Dodson, M.H.. 1969. Geochronology of Rhodesia: *Geol. Soc. South Africa Trans. and Proc.*, **72**. 79-113.

Vening Mainesz, F.A.. 1950. Les grabens africains, résultat de compression ou de tension dans la croûte terrestre? *Bull. des Séances, Inst. Roy. Collonial Belge*. **21**. 539-552.

Versfelt, J. & Rosendahl, B.R.. 1989. Relationships between pre-rift structures and rift architecture in Lakes Tanganyika and Malawi, East Africa. *Nature*, **337**. 354-357.

Wegener, A.. 1912a. Die Entstehung der Kontinente. *Petermanns Geogr. Mitt.*, **58**. 185-195, 253-256, 305-308.

Wegener, A.. 1912b. Die Entstehung der Kontinente. *Geol. Rundsch.*, **3**. 276-292.

Wessel, P. & Smith, W.H.F.. 1993. The GMT System v. 2.1.4. technical reference & cookbook. SOEST/NOAA. 59pp.

Westcott, W.A., Krebs, W.N., Englehardt, D.W. & Cunningham, S.M.. 1991. Biostratigraphic age dates from the Lake Rukwa Rift Basin in Western Tanzania. *AAPG Bull.*, **75**. 1255-1263.

Williams, L.A.J.. 1970. The Volcanics of the Gregory Rift Valley, East Africa. *Bull. Volcanol.*, **34**. 439-465.

Williams, L.A.J.. 1972. The Kenya Rift volcanics: a note on the volumes and chemical composition. *Tectonophysics*, **15**. 83-96.

Willis, B.. 1936. East African plateaus and rift valleys. *Carnegie Inst. Washington Pub.*, **470**. pp358.

Young, P.A.V., Maguire, P.K.H., Laffoley, N.d'A. & Evans, J.R.. 1991. Implications of the distribution of seismicity near Lake Bogoria in the Kenya Rift. *Geophys. J. Int.*, **105**. 665-674

Zana, N., Kamba, M., Katsongo, S. & Janssen, Th.. 1989. Recent seismic activity of the Kivu Province, Western Rift Valley of Africa. *Phys. Earth Planet. Int.* **58**. 52-60.

Zoback, M.L.. 1992. First and second order patterns of stresses in the lithosphere: The World Stress Map Project. *JGR*, **97** (B8). 11 703-11 729.

APPENDIX A

Acronyms

Acronyms used in the Text

Frequent use of acronyms has been made throughout the text. The first occurrence is usually accompanied by the full, unabridged, version of the article or organisation, however, for them to be effective further appearences are not. The majority of acronyms are thus given below.

AVHRR	Advanced Very High Resolution Radiometer
BCIS	Bureau Central International de Séismologie
CEGD	Centre d'Etudes Geologique at de Developpement
DCW	Digital Chart of the World
DEM	Digital Elevation Model
DMA	Defense Mapping Agency *(USA)*
DMSP	Defense Meteorological Satellite Program
ERTS	*Former name of Landsat*
ESC	Electronic Still Camera *(flown on Space Shuttle missions)*
GAC	Global Area Coverage
GCP	Ground Control Point
GMT	Generic Mapping Tools *(graphics package)*
ISC	International Seismological Centre
ISS	International Seimological Summary
LAC	Local Area Coverage
LAS	Land Analysis System *(Image processing system)*
MSS	Multi-Spectral Scanner *(on the Landsat satellite)*
NASA	National Aeronautics and Space Administration *(USA)*
NASA GSFC	NASA Goddard Space Flight Center
NASA JSC	NASA Johnson Space Center
NEIS	National Earthquake Information Service *(USGS)*
NOAA	National Oceanographic and Atmospheric Administration *(USA)*
ONC	Operational Navigation Chart
PCI	*No full version. Image processing package*
RGB	Red, Green, Blue.
SPOT	Satellite Probatoire Pour l'Observation de la Terre

SSI	Solid State Imaging *(on Galileo)*
STS	Space Transport Systems *(Space Shuttle)*
TM	Thematic Mapper *(on the Landsat satellite)*
TRM	Tanganyika - Rukwa - Malawi *(transcurrent fault zone)*
UNESCO	United Nations Educational, Scientific and Cultural Organisation
USGS	United States Geological Survey
WWSSN	World-Wide Standard Seismograph Net

APPENDIX B

Geographical Nomenclature

Geographical Names

One of the problems with the African continent is the changes of names of various features, both physical and political, which have occured within the region. A list of some of the more common alternatives is given below.

Name used	Other names appearing in the literature
Djibouti	Territoire des Afars et des Issas
Karirondo Rift	Nyanza Rift
Lake Bogoria	Lake Hannington
Lake Edward	Lake Amin, Lake Rutanzige
Lake Malawi	Lake Nyassa
Lake Mobutu	Lake Albert
Lake Mweru	Lake Moero
Lake Turkana	Lake Rudolf
Zimbabwe	Rhodesia

Eritrea

Since this project was started the country of Eritrea has gained independence from Ethiopia. The coastline and country boundaries used on most diagrams was included with the software used to create them, GMT; thus, the figures still show the old boundary of Ethiopia and omit Eritrea.

APPENDIX C

Image Processing Software and Hardware

Image Processing of satellite data was carried out in the Laboratory for Terrestrial Physics at NASA Goddard Space Flight Center (GSFC). Two software packages were used for the processing of the digital satellite imagery. Land Analysis System (LAS) was used for reading the Advanced Very High Resolution Data (AVHRR) from tape, applying the correction for earth distortion and converting the 10 bit data to 8 bit. PCI EASI/PACE was used for all other processing steps for AVHRR data and for the complete processing of Landsat Thematic Mapper (TM) data.

C.1 The LAS software

LAS was designed at the NASA GSFC and is supported by the United States Geological Survey (USGS). Only two routines within the LAS software were used, these being *LACIN* and *MAP*. The LAS software has largely been superseded by the PCI package in the Laboratory for Terrestrial Physics at NASA GSFC, however, the *LACIN* routine in LAS was used for reading uncorrected AVHRR data as it applies a correction for Earth curvature, a process not available in PCI.

LACIN This procedure reads in the uncorrected AVHRR data and applies the correction for Earth curvature. Earth rotation and satellite attitude are not corrected at this stage.

MAP The *MAP* routine allows the original 10 bit AVHRR data to be converted to the more versatile 8 bit format. This routine is essentially designed to apply stretches to data but can also be used to compress data into a shorter range. The conversion to 8 bit data was required for loading into PCI.

C.2 The PCI Image Processing Package

The PCI system was written by PCI Inc., Toronto, Canada (PCI, 1993). The software is the major image processing package used in the Laboratory for Terrestrial Physics at

NASA GSFC. In addition to image processing the software contains Geographical Information System (GIS) and visualisation capabilities. The software runs on a number of platforms including personal computers and UNIX workstations.

The PCI EASI/PACE system operates at a number of levels: at its most basic it allows processing of imagery through a series of keyboard entered commands; at a higher level the process becomes an interactive, menu and screen driven, system. For the most part PCI was used on Silicon Graphics' Iris workstations. This allowed all processing steps to be viewed and assessed throughout the procedure. A number of PCI routines were used in processing the data of which *GCIT, CIM, GEOSET, REG, FSHARP, STR* and *LUT* are the most important. Details of their application are given in chapter 2.

GCIT This routine allows the interactive choosing of ground control points (GCPs) on the uncorrected image. These GCPs are then usable for image rectification using *REG*.

CIM *CIM* is used to create blank 'image' files. The size of file, in pixels, and the number of bands required are defined before creating the file.

GEOSET Prior to registration a blank destination file needs to be created with the correct dimensions and co-ordinate bounds. *GEOSET* allows the user to set the limits of the destination file before carrying out the registration procedure.

REG *REG* is used to carry out the registration process. It allows a specific region to be chosen (as defined in the destination file by *GEOSET*) and a certain order of registration to be used, see section 4.1.3.

FSHARP The application of an edge enhancement filter on the image is done using the routine *FSHARP*, see section 4.1.4.

STR *STR* is used to compile 'look-up tables' which are then used to apply linear stretches to the data using *LUT*.

LUT The *LUT* routine uses the look up tables defined by *STR* to apply stretches to chosen bands.

APPENDIX D

Rose Diagram Programs

Length, Azimith Calculator for Rose Diagrams

```
      PROGRAM ROSE
C
C program to produce azimuth and length segments of lineaments
C output formatted for GMT psrose command.
C delimiter between separate lines = 999.999  999.999
C
      REAL    X,Y,X2,Y2,LENGTH,DIFX,DIFY,ANGLE,AVY,LONGSC,LATSC
      CHARACTER IPNAME*12,OPNAME*12
C
      WRITE(6,*) 'ENTER INPUT FILENAME'
      READ(5,'(A12)') IPNAME
      WRITE(6,*) 'ENTER OUTPUT FILENAME'
      READ(5,'(A12)') OPNAME
      OPEN (10,FILE=IPNAME,STATUS='OLD')
      OPEN (12,FILE=OPNAME,STATUS='NEW')

C read first point, free format
   4  READ(10,*,END=250)X,Y
C read second point, free format
   5  READ(10,*,END=250)X2,Y2
C check for line delimiter
      IF (X2 .EQ. 999.999) GOTO 4
C calculate length and azimuth of segment
      DIFX = (X2 - X)
      DIFY = (Y2 - Y)
      AVY = ((Y + Y2)/2)
      LONGSC = (111.3 * COS(AVY*(3.141593/180)))
      LATSC = 110.6
      LENGTH = SQRT(((DIFX*LONGSC)**2)+((DIFY*LATSC)**2))
      IF (LENGTH .EQ. 0) GOTO 6
      IF (DIFY .EQ. 0) THEN
      ANGLE = 90
      GOTO 99
      ENDIF
      ANGLE = ATAN(DIFX/DIFY)
      ANGLE = (180/3.141593)*ANGLE
 99   WRITE (12,180)LENGTH,ANGLE
180   FORMAT(F7.3,2X,F6.1)
  6   X = X2
      Y = Y2
      GOTO 5
250   CONTINUE
      STOP
      END
```

APPENDIX E

Algorithm for Earth Curvature Correction for AVHRR

From Legakis & Pritchard (1976)

The VHRR [forerunner of AVHRR] infrared and visible data are collected as discrete samples by the combined effect of the radiometer's scan rate and the forward motion of the satellite in its orbital plane. Since the VHRR scan rate (ω) is constant, equal increments (Δa) of the scan angle subtend unequal distances along a scan line. Since the data sampling rate (S) is also constant, these geometric distortions appear in all standard VHRR images as a contraction of the Earth's features at increasing distance from nadir.

To remove these geometric distortions from the imagery, we apply an algorithm which redistributes the original data samples (M) on the photographic film so that each new sample (N) represents an equal distance ($D = R.\Delta\phi$) on the image within the limits of the assumption and interpolation errors. ... each scan line is symmetric about the nadir. Furthermore, each scan line can be treated independently so that the cylindrical coordinates ... can be applied. Therefore, it is only necessary to derive the algorithm for one half of a line and repeat it for any number of lines desired.

The basic equation required to accomplish the interpolation scheme was suggested by Gower (pers. comm.) and is given by:

$$\tan(\alpha) = \frac{\sin\alpha}{(r/R) - \cos\phi} \qquad (1)$$

where $r = R + H_0$

...

First note that, at nadir, the distance (L) between two successive scan lines is given by:

$$L = (V_0 + U_2)/\omega \qquad (2)$$

where $V_0 = 2\pi.R/P$

$$U = [2\pi.T\cos\theta]/T$$

$$U_2 = U\cos\varepsilon$$

[for the discussion of the speed component U_2 see Legakis & Pritchard (1976) section 6]

Since the Earth scene will be displayed on a photographic product with a vertical aspect ratio (F) and a horizontal aspect ratio (G), we will define the desired image aspect ratio (A) as:

$$\mathbf{A = LF} \qquad (3)$$

and the horizontal aspect ratio as:

$$\mathbf{B = GD} \qquad (4)$$

To make the image represent an "equal area" projection of the original data we require that:

$$\mathbf{A = B} \qquad (5)$$

and solving for the distance (D) between the new samples gives:

$$\mathbf{D = L\,(F/G)} \qquad (6)$$

Since by definition the distance D subtends equal increments of the Earth center angle $\Delta\phi$ we have...

$$\mathbf{\Delta\phi = D/R} \qquad (7)$$

and since N is the number of any new sample from nadir, the angle ϕ is:

$$\mathbf{\phi = \Delta\phi.N = DN/R} \qquad (8)$$

Next, note that the increments ($\Delta\alpha$) of the Earth scan angle are defined by the VHRR scan rate (ω) and the sampling rate (S) as:

$$\Delta\alpha = \omega/S \qquad (9)$$

and since I is the number of an original sample from nadir, the scan angle is:

$$\alpha = \Delta\alpha.\mathbf{I} = \mathbf{I}\omega/\mathbf{S} \qquad (10)$$

Substituting (7) through (10) into (1), the value of the original sample I fro an integer value of the new sample N is:

$$\tan\left(\frac{I\omega}{S}\right) = \frac{\sin\left(DN/R\right)}{Y} \qquad (11)$$

where: $$Y = \left(\frac{r}{R}\right) - \cos\left(\frac{DN}{R}\right)$$

$\mathbf{N} = 0,1,2...$

Definition of Terms

A	Vertical aspect ratio of image (km/cm).
B	Horizontal aspect ratio of image (km/cm).
D	Distance between samples on image after geometric corrections.
F	Vertical aspect ratio of image display device (lines/cm).
G	Horizontal aspect ratio of image display device (lines/cm).
H	Distance from the radiometer to an arbitrary Earth scene along a scan line (km).
H_0	Altitude of radiometer (km).
I	Original sample number starting at center of scan line. ($\mathbf{I = H - H_0}$).
L	Distance between scan lines at nadir (Z = 0) after correction for Earth's rotation (km).
M	Original sample numbers starting with the first sample on a scan line.
N	New sample numbers starting from the center of the scan line after the curvature distortion is corrected.
r	Sum of the Earth's radius R and the satellite altitude H_0 (km).
R	Radius of the Earth (km).
S	Sampling rate of radiometer (samples per second).
T	Period of rotation of the Earth (hr).
U	Speed of the Earth's surface at nadir, tangent to a latitudinal plane and relative to inertial space (km/s).
U_2	Component of U parallel to satellites orbital plane (km/s).
V	Satellites ground speed relative to rotating Earth (km/s).

ω Radiometer scan rate (rpm).

α Radiometer scan angle ($\alpha = 0$ at nadir).

$\Delta\alpha$ Increment of scan angle between two original samples along a scan line.

ϕ Earth center angle ($\phi = 0$ at nadir).

$\Delta\phi$ Increment of Earth center angle which subtends equal distances along the Earth's curved surface.

θ Angle of latitude

ε Angle between the instantaneous intersection of the orbital plane and a latitudinal plane.

APPENDIX F

Method of Acquisition and Cost of AVHRR Data

The information given below is correct of 20th September 1995.

Ordering Data

AVHRR Data can be acquired as either Photographic or Computer Products. Orders and inquiries should be made to:

National Climate Data Center
151 Patton Avenue, Room 120.
Asheville, North Carolina. 28801-5001.

Tel: +1-704-271-4800
Fax: +1-704-271-4876
E-Mail: satorder@ncdc.noaa.gov

Prices

Computer Compatible Tapes:	$80 per input tape (data-set)
	$11 per output tape (9 track or EXAbyte)
Handling Charge	$11 per order
Shipping	$10 for non US orders
Data Searches	$35 per hour (min $35)

These prices are subject to change without notice.

Various specifications are required when ordering data. Further details of these are available from the above address.

COLOUR PLATES

Plate 1A. The Afar region; AVHRR B211 = RGB. 2nd February 1987.

Plate 1B. The Afar region; AVHRR B521 = RGB. 2nd February 1987.

Plate 2A. The Ethiopia rift; AVHRR B211 = RGB. 30th December 1986.

Plate 2B. The Ethiopia rift; AVHRR B521 = RGB. 30th December 1986.

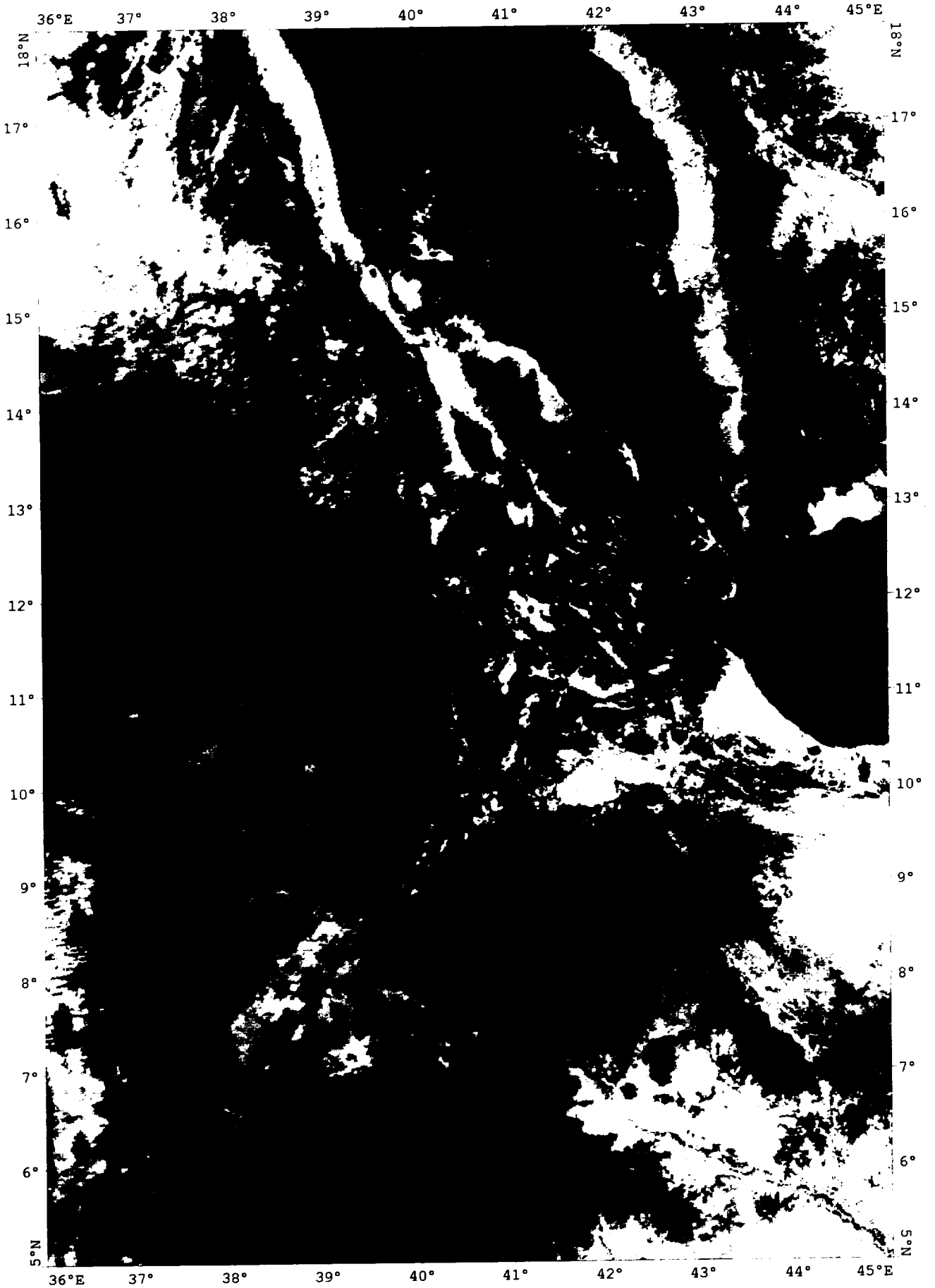

AVHRR: Afar

PCI

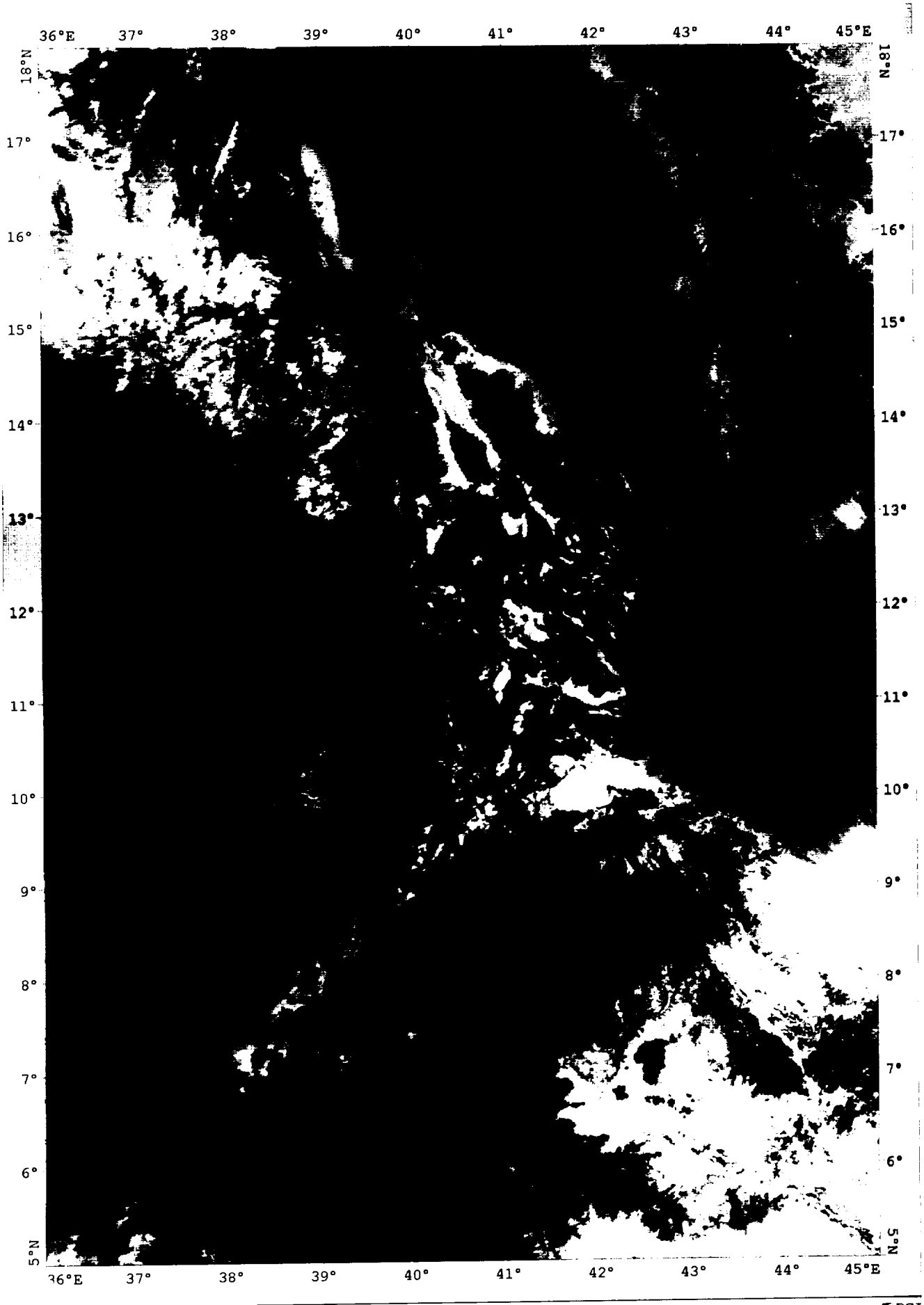

AVHRR: Afar

PCI

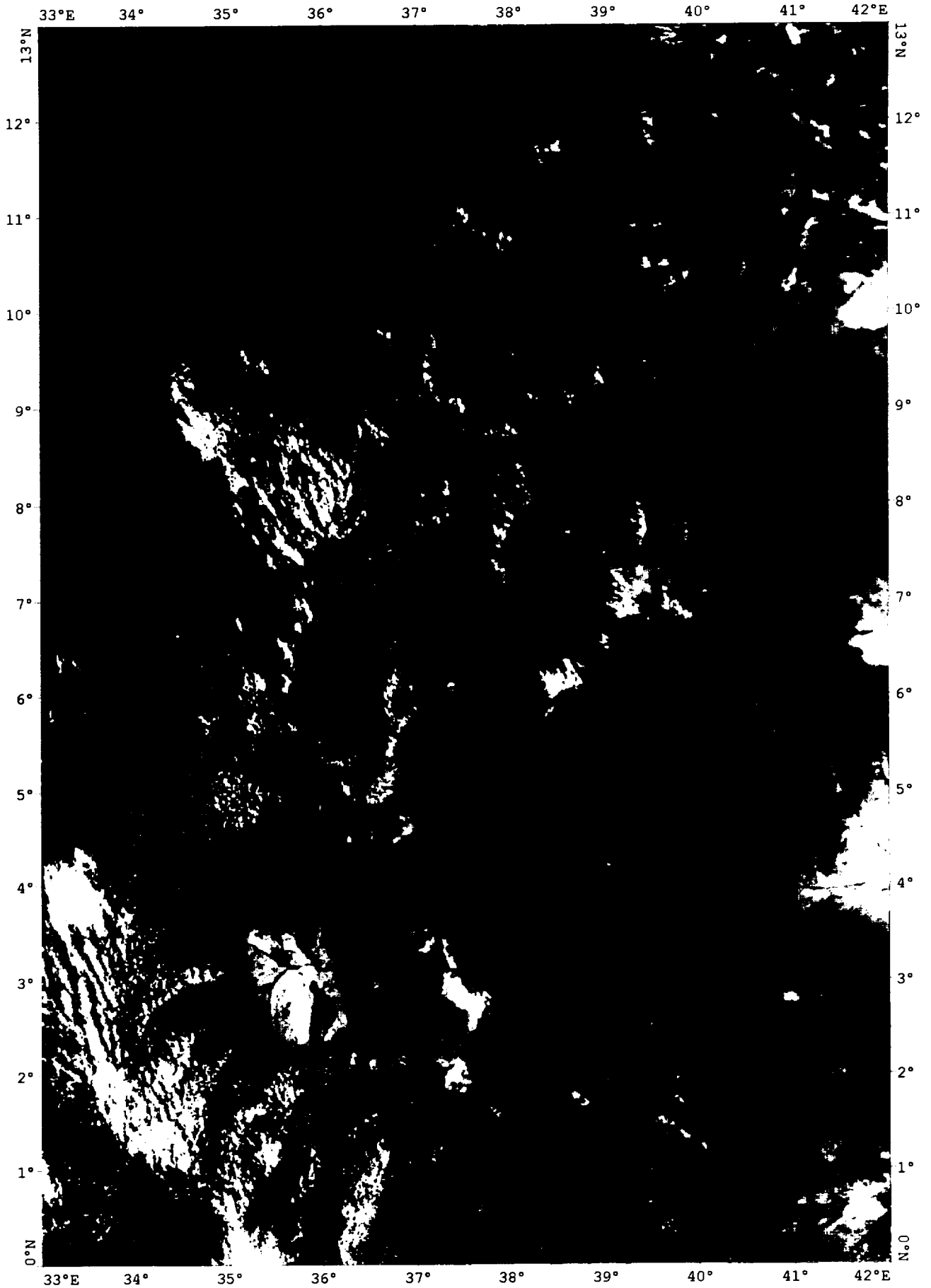

AVHRR: Ethiopian Rift

PCI

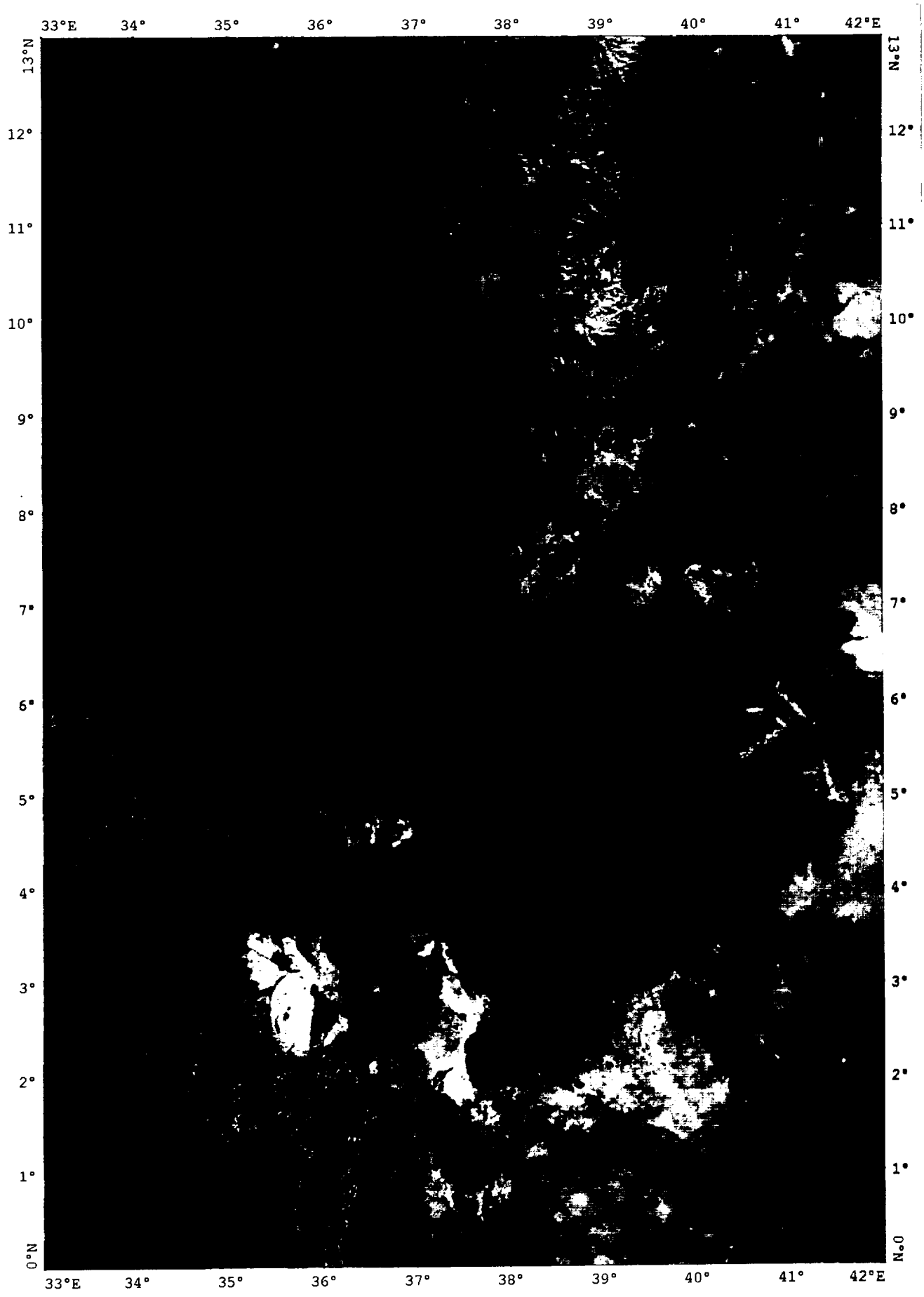

AVHRR: Ethiopian Rift

PCI

Plate 3A. The Kenya rift; AVHRR B211 = RGB. 1st March 1987.

Plate 3B. The Kenya rift; AVHRR B521 = RGB. 1st March 1987.

Plate 4A. The Mobutu rift (northern part of the western branch of the East African Rift System); AVHRR B211 = RGB. 9th January 1989.

Plate 4B. The Mobutu rift (northern part of the western branch of the East African Rift System); AVHRR B521 = RGB. 9th January 1989.

AVHRR: Kenya Rift

1st March 1987

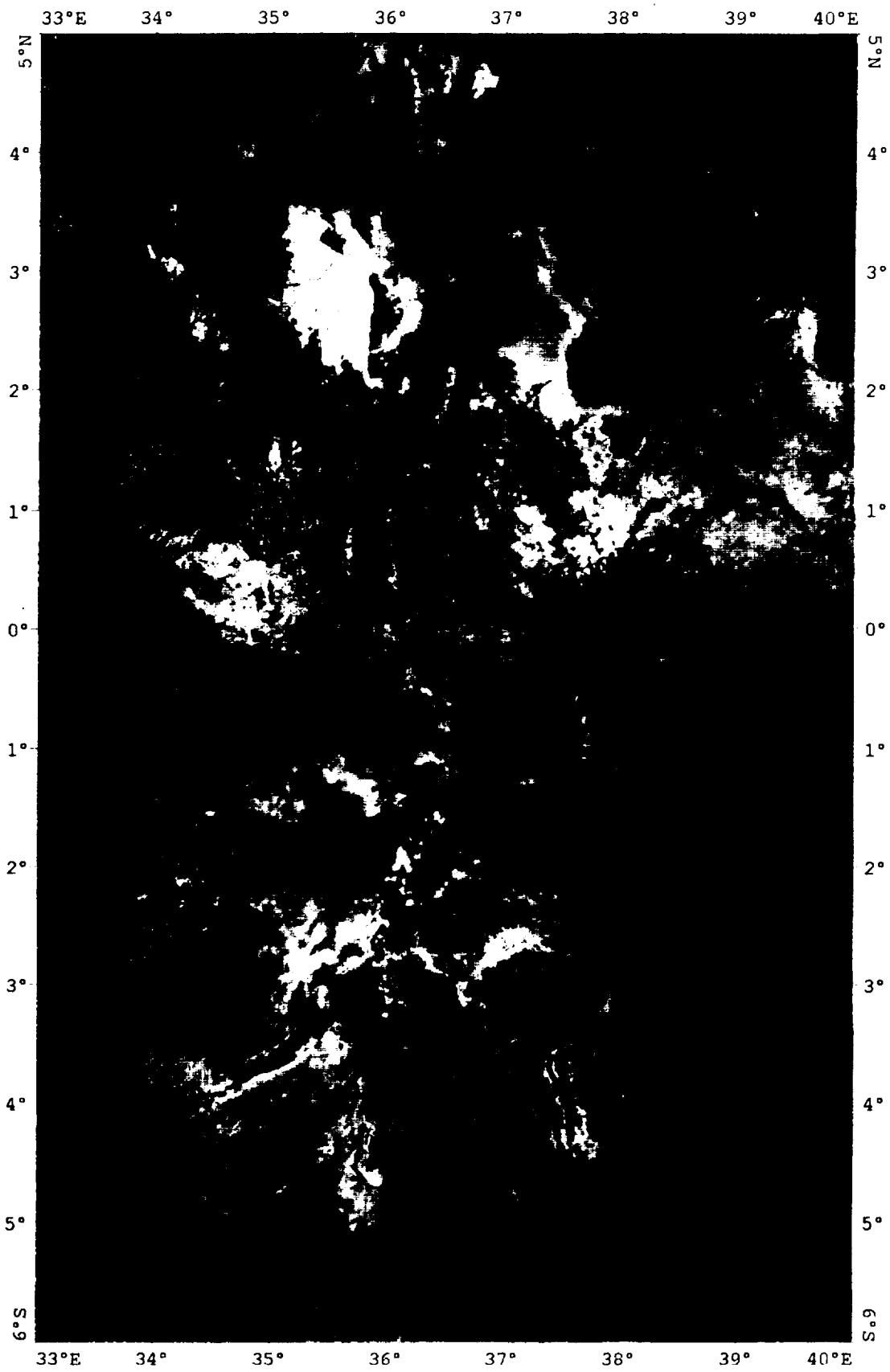

AVHRR: Kenya Rift

1st March 1987

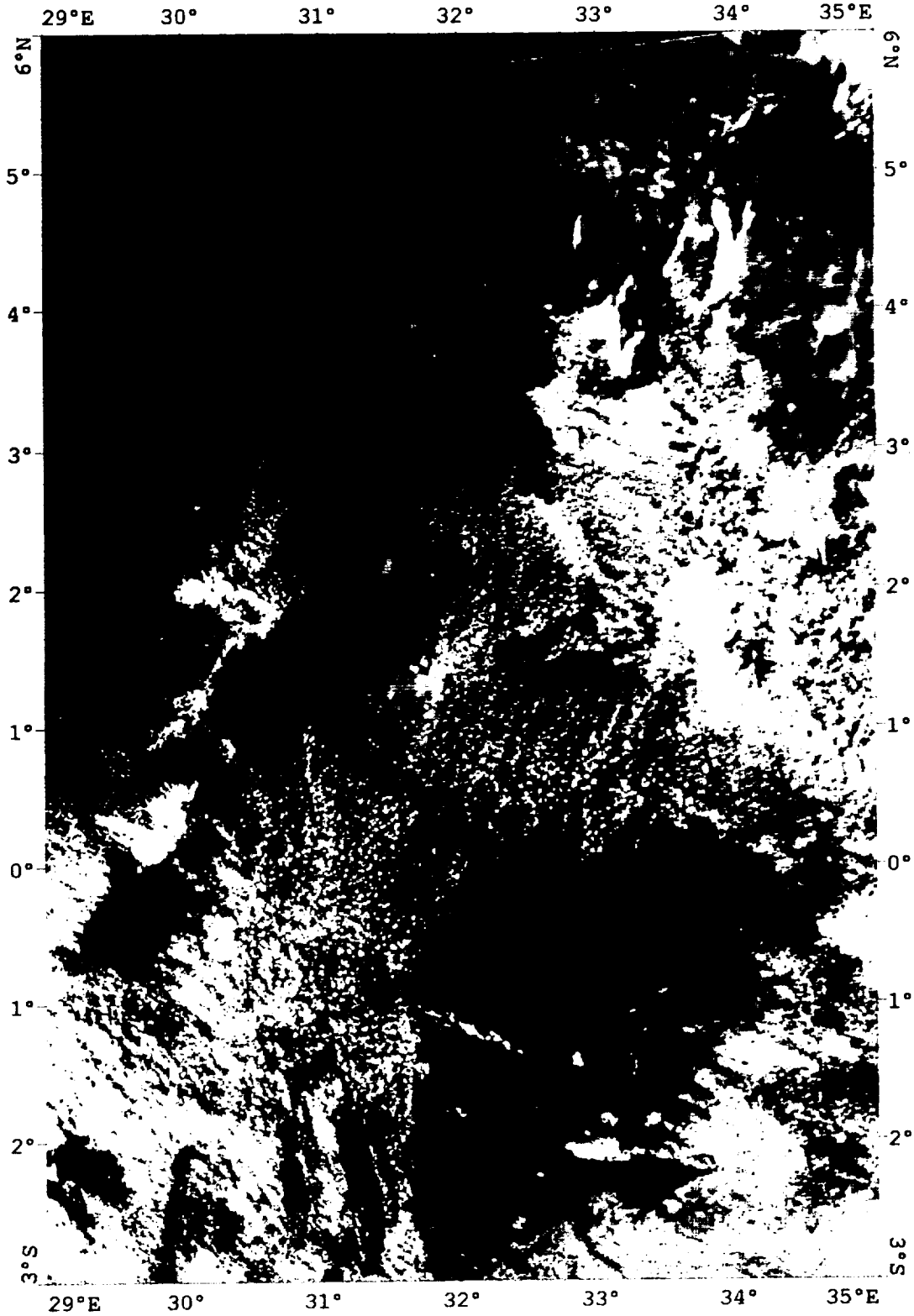

AVHRR: Northern part of the Western Branch

9th January 1989

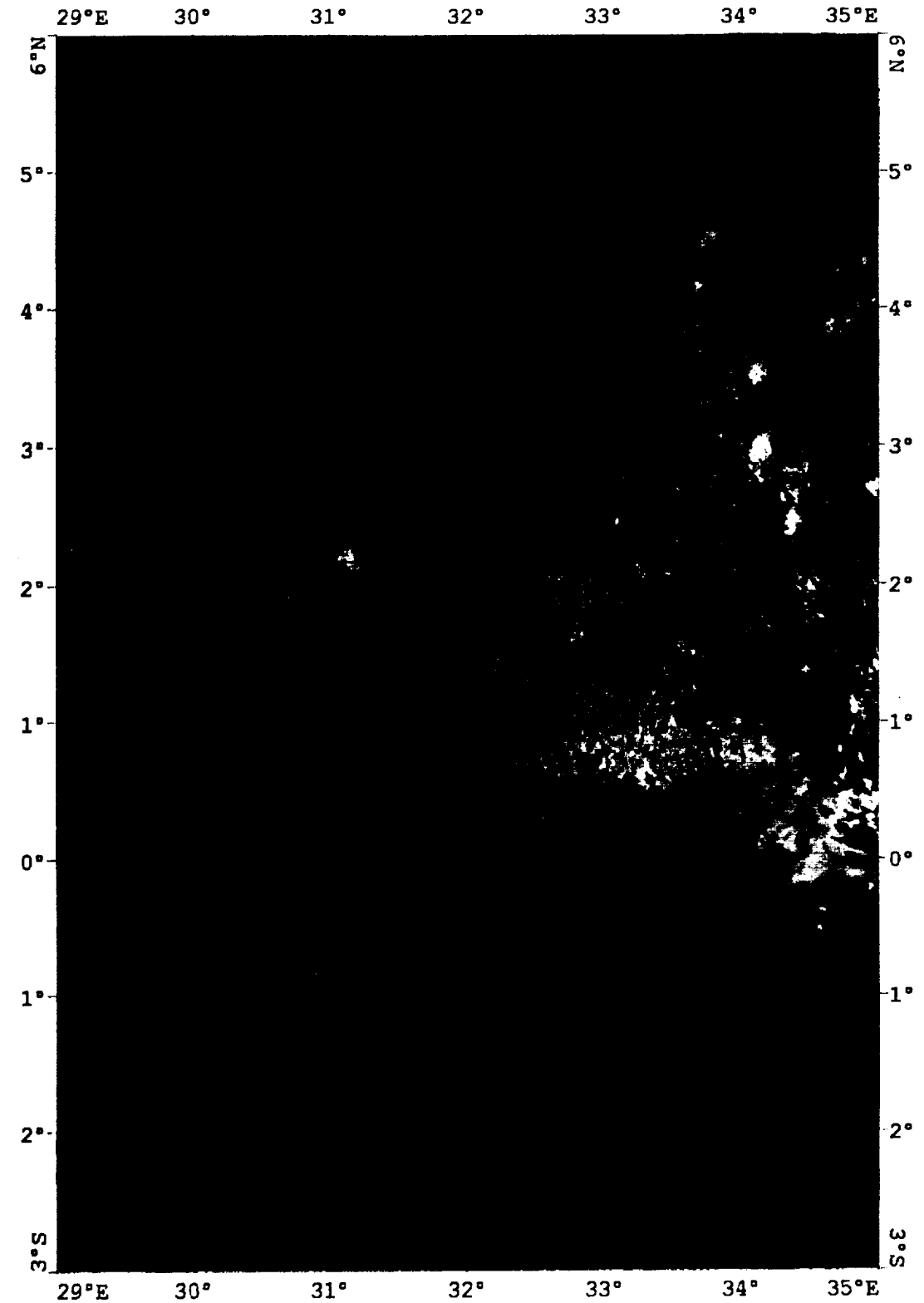

AVHRR: Northern part of the Western Branch

9th January 1989

Plate 5A. The Tanganyika and Rukwa rifts (central part of the western branch of the East African Rift System); AVHRR B211 = RGB. 24th July 1989.

Plate 5B. The Tanganyika and Rukwa rifts (central part of the western branch of the East African Rift System); AVHRR B521 = RGB. 24th July 1989.

AVHRR: Western Branch of the East African Rift System

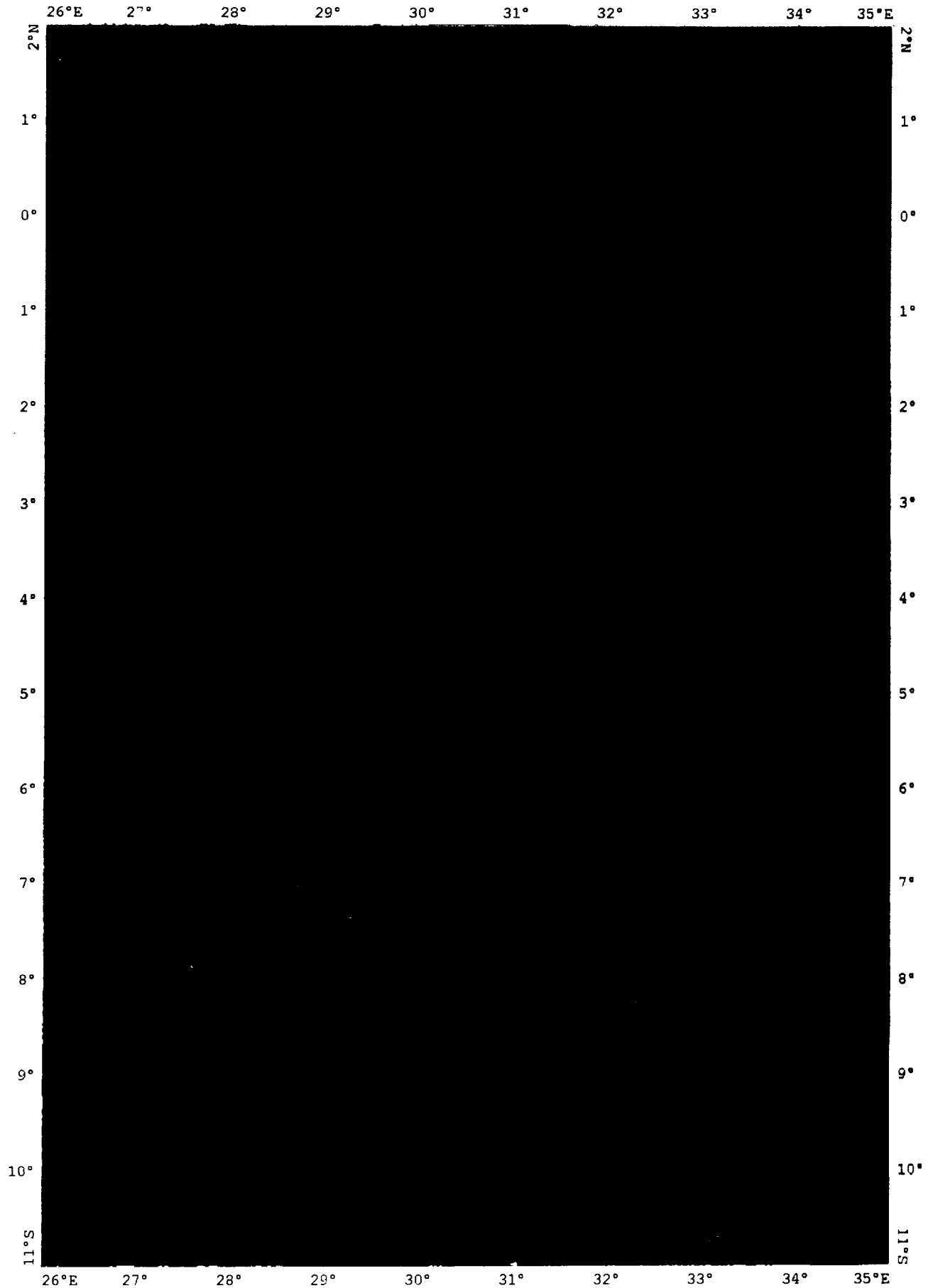

AVHRR: Western Branch of the East African Rift System

PCI

Plate 6A. The Malawi and Southwestern rifts (southern part of the western branch of the East African Rift System); AVHRR B[d2][d1][d1] = RGB. 8th August 1988.

Plate 6B. The Malawi and Southwestern rifts (southern part of the western branch of the East African Rift System); AVHRR B[d5][d2][d1] = RGB. 8th August 1988.

Plate 6C. The Malawi and Southwestern rifts (southern part of the western branch of the East African Rift System); AVHRR B[d5/n5][d4/n4][d3/n3] = RGB. 8th August 1988.

Plate 6D. The Malawi and Southwestern rifts (southern part of the western branch of the East African Rift System); AVHRR B[d5][n5][d5/n5] = RGB. 8th August 1988.

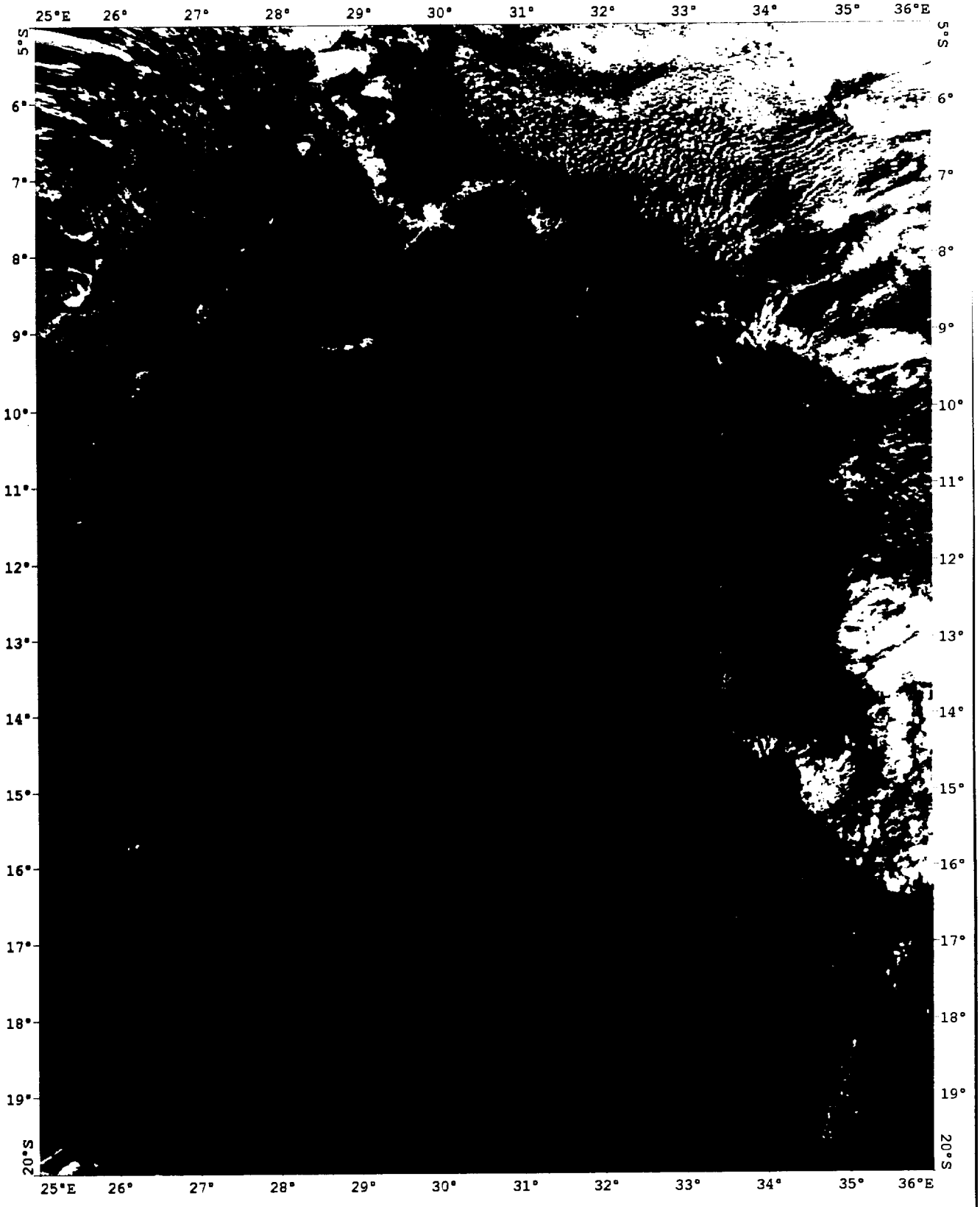

AVHRR: Southern part of the Western Branch

8th August 1988

PCI

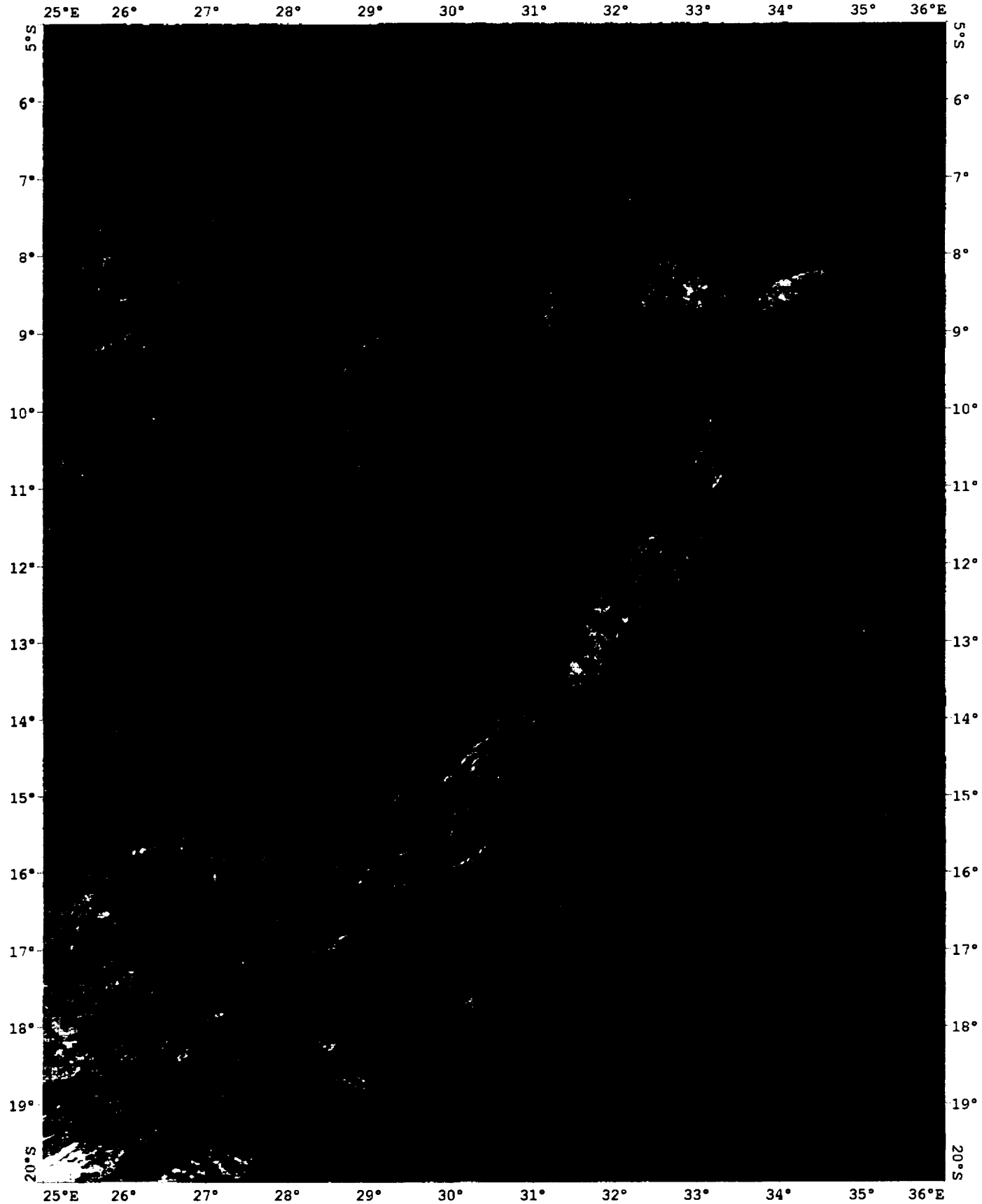

AVHRR: Southern part of the Western Branch

8th August 1988. B521 = RGB

PCI

AVHRR: Day night ratio (Bands 5, 4 & 3)

8th August 1988

PCI

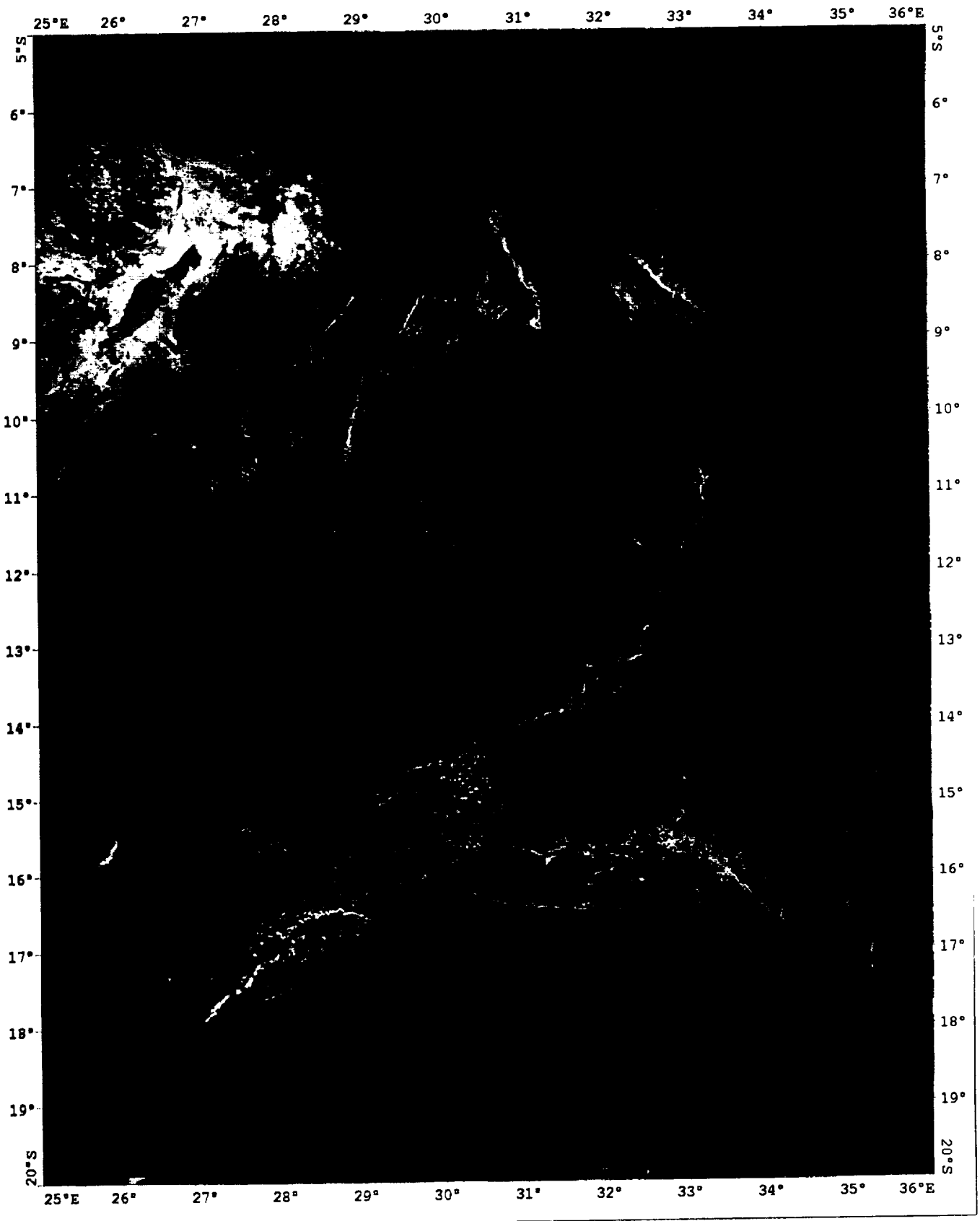

AVHRR: Southern part of the Western Branch

8th August 1988. [day5][night5][day5/night5] = RGB

REPORT DOCUMENTATION PAGE

Form Approved
OMB No. 0704-0188

1. AGENCY USE ONLY *(Leave blank)*	2. REPORT DATE	3. REPORT TYPE AND DATES COVERED
	February 1996	Technical Memorandum

4. TITLE AND SUBTITLE

Tectonics and Volcanism of East Africa as Seen Using Remote Sensing Imagery

5. FUNDING NUMBERS

Code 920

6. AUTHOR(S)

Duncan John Hutt

7. PERFORMING ORGANIZATION NAME(S) AND ADDRESS(ES)

Goddard Space Flight Center
Greenbelt, Maryland 20771

8. PERFORMING ORGANIZATION REPORT NUMBER

96B00037

9. SPONSORING/MONITORING AGENCY NAME(S) AND ADDRESS(ES)

NASA Aeronautics and Space Administration
Washington, D.C. 20546-0001

10. SPONSORING/MONITORING AGENCY REPORT NUMBER

NASA TM-104628

11. SUPPLEMENTARY NOTES

Duncan John Hutt: The University of Newcastle upon Tyne, Newcastle, England

12a. DISTRIBUTION/AVAILABILITY STATEMENT

Unclassified-Unlimited
Subject Category: 43
Report available from the NASA Center for AeroSpace Information,
800 Elkridge Landing Road, Linthicum Heights, MD 21090; (301) 621-0390.

12b. DISTRIBUTION CODE

13. ABSTRACT *(Maximum 200 words)*

The East African Rift is the largest area of active continental geology. The tectonics of this area has been studied with remote sensing data, including AVHRR, Landsat MSS and TM, SPOT, and Electronic Still Camera from Shuttle. Lineation trends have been compared to centers of volcanic and earthquake activity as well as the trends shown on existing geologic maps. Remote sensing data can be used effectively to reveal and analyze significant tectonic features in this area.

14. SUBJECT TERMS

East African Rift; remote sensing; tectonics

15. NUMBER OF PAGES

165

16. PRICE CODE

17. SECURITY CLASSIFICATION OF REPORT	18. SECURITY CLASSIFICATION OF THIS PAGE	19. SECURITY CLASSIFICATION OF ABSTRACT	20. LIMITATION OF ABSTRACT
Unclassified	Unclassified	Unclassified	Unlimited

This publication is available from the NASA Center for AeroSpace Information,
800 Elkridge Landing Road, Linthicum Heights, MD 21090-2934, (301) 621-0390.

National Aeronautics and
Space Administration

Goddard Space Flight Center
Greenbelt, Maryland 20771

POSTMASTER: If Undeliverable (Section 158, Postal Manual) Do Not Return